New Neurons for the Inner Ear: Neurogenesis in the Zebrafish Statoacoustic Ganglion during Growth, Homeostasis and Regeneration

DISSERTATION

Zur Erlangung des akademischen Grades

Doctor rerum naturalium (Dr. rer. nat.)

vorgelegt der Fakultät Mathematik und Naturwissenschaften
der Technischen Universität Dresden

von

Simone Schwarzer, M.Sc.

Eingereicht am 12. Mai 2023

Die Dissertation wurde in der Zeit von Februar 2015 bis Mai 2023
an der Professur für Molekulare Entwicklungsgenetik der TU Dresden angefertigt.

TECHNISCHE UNIVERSITÄT DRESDEN

CRTD
Center for Regenerative Therapies TU Dresden

Reviewer

Prof. Dr. rer. nat. habil. Michael Brand
Professur für Molekulare Entwicklungsgenetik
Biologische Fakultät, Medizinische Fakultät „Carl Gustav Carus“
Technische Universität Dresden, Germany
Center for Molecular and Cellular Bioengineering (CMCB)
Center for Regenerative Therapies Dresden (CRTD)

Prof. Cristina Pujades, PhD
Research Group Neurodevelopmental Dynamics
Department of Medicine and Life Sciences
Universitat Pompeu Fabra Barcelona

For Q.

Summary

The vertebrate inner ear is a remarkable sensory organ, harboring two different senses: the auditory system, responsible for hearing, and the vestibular system, responsible for balance. Even though the anatomical structure of the vertebrate inner ear is very complex, only three different cell types are mainly involved on a cellular level in the perception of sound as well as balance and movement: sensory hair cells that are surrounded by supporting cells receive the stimulus and transfer it via sensory neurons to the brain.

Worldwide, millions of people suffer from sensorineural hearing loss, caused by the loss of sensory hair cells and/or their innervating neurons within the inner ear. In mammals, including humans, both cell types are only produced during fetal stages making loss of these cells and the resulting consequences irreversible. In contrast, it is known that zebrafish produce sensory hair cells throughout life and additionally possess the remarkable capacity to regenerate them upon lesion. However, it is unknown whether new sensory neurons are also formed throughout life in the zebrafish statoacoustic ganglion (SAG), which transduces signals from the inner ear to the brain. Moreover, it is unknown whether sensory neurons are replaced upon loss.

Hence, the first aim of this study was to investigate whether new sensory neurons are produced beyond larval stages. To this end, analysis of different transgenic lines combined with immunohistochemistry against known markers for neuronal stem and progenitor cells, neurons, glia and myelinating cells as well as markers for proliferation were used to identify distinct cell populations and anatomical landmarks in the juvenile and adult SAG. In the juvenile SAG, a pool of highly proliferating Neurod/Nestin-positive neuronal progenitors produces large amounts of new sensory neurons. In contrast, at adult stages this neurogenic niche transitions to a quiescent state, in which Neurod/Nestin-positive neuronal progenitor cells are no longer proliferating and the neurogenesis rate is very low. Moreover, BrdU pulse chase experiments revealed the existence of a proliferative but otherwise marker-negative cell population that replenishes the Neurod/Nestin-positive progenitor pool throughout life, indicating a neural stem cell-like cell population upstream of the neuronal progenitor cell pool. Additionally, expression of glia markers and a switch in the myelination pattern was found to mark the peripheral and central nervous system transitional zone (PCTZ) as a prominent landmark of the SAG.

To further study the nature of the proliferating but otherwise unknown stem cell-like cell population replenishing the Neurod/Nestin-positive neuronal progenitor pool, the transcriptome of proliferating cells and their progeny of the juvenile and adult SAG was analyzed via single cell RNA-sequencing using the Smart-Seq2 technology. Therefore, a pipeline including preparation of the SAG as well as cell dissociation followed by fluorescence-activated cell sorting was established to obtain

single cells from the SAG. The fluorescent reporters *Tg(pcna:GFP)* and *Tg(nestin:mCherry-CreER^{T2})* were used to label proliferating cells (GFP-only positive), proliferating progenitors (GFP/mCherry-double positive as well as non-proliferating progenitor cells (mCherry-positive). Additionally, based on the perdurance of the fluorophores in the progeny of the cells expressing the reporter constructs, this sorting strategy also enables to sort the progeny of proliferating cells differentiating into neuronal progenitor cells (GFP/mCherry-double positive but not expressing *pcna*) to trace back the putative stem cell-like cell population replenishing the Neurod/Nestin-positive progenitor population. Similar, the sorting strategy also included newborn neurons as the progeny of neuronal progenitors (mCherry-positive but not expressing *nestin*). In the transcriptome data obtained from the juvenile SAG, the majority of the analyzed cells could be assigned to the neuronal lineage, reflecting the neuronal differentiation trajectory from neuronal progenitor cells transitioning to newborn neurons and even further differentiating into mature neurons. Additionally, two different putative neuronal stem cell-like cell clusters were identified which are currently under validation. In contrast, in the adult transcriptome data the majority of cells were identified as cells from the sensory lineage, including cells expressing markers specific for hair cells and the sensory epithelium. Only a minority of cells came from the neuronal lineage, with the group of newborn and differentiating neurons clustering together in one cluster. Very few cells were identified as neuronal progenitor cells and did not cluster together, whereas both putative stem cell-like cell populations could be identified as distinct cluster. However, validation of the putative stem cell population remains subject to further studies.

The second aim of this thesis was to investigate the regenerative capacity of the adult SAG and to study whether the neurogenic progenitor cell niche can be reactivated and to give rise to new sensory neurons upon damage. Therefore, a lesion paradigm using unilateral injections into the otic capsule was established. Upon lesion, mature SAG neurons undergo apoptosis and a massive infiltration with immune cells was found. Importantly, the Neurod-positive progenitor cells re-entered the cell cycle displaying a peak in proliferation at 8 days post lesion before they returned to homeostatic levels at 57 days post lesion. In parallel to reactive proliferation, an increase in neurogenesis from the Neurod-positive progenitor pool was observed. Reactive neurogenesis started at around 4 days post lesion, peaked at 8 days post lesion decreased again to low homeostatic levels at 57 days post lesion. The administration of the thymidine analog BrdU to label proliferating cells and their progeny revealed the generation of new sensory neurons from proliferating neuronal progenitor cells within 19 days post lesion. Interestingly, reactive proliferation as well as an increased neurogenesis rate were also detected in the unlesioned SAG, revealing a systemic effect of the unilateral lesions.

Taken together, this study is the first to show that neurogenesis in the zebrafish SAG persists way beyond larval stages. New neurons descend from a

population of Neurod/Nestin-positive neuronal progenitor cells that is highly proliferative during juvenile stages but turn quiescent at adulthood. Nevertheless, this neuronal progenitor cell pool is replenished throughout life by a currently unknown neuronal stem cell-like cell population. Additional this study reveals the regenerative capacity of the adult SAG: upon lesion Neurod/Nestin-positive progenitor cells are reactivated to re-enter the cell cycle, proliferate and give rise to new neurons leading to an increased neurogenesis rate to replace lost mature neurons. Studying the underlying genes and pathways in zebrafish compared to mammalian species will hopefully provide valuable insights that will help developing cures for auditory and vestibular neuropathies in the future.

List of publications

The work described in chapter 4.1 and chapter 4.3 of the present doctoral thesis was (in parts) published in:

Reactivation of the Neurogenic Niche in the Adult Zebrafish Statoacoustic Ganglion Following a Mechanical Lesion. **Schwarzer S**, Rekhade DR, Machate A, Spieß S, Geffarth M, Ezhkova D, Hans S. *Front Cell Dev Biol.* 2022 Mar 15;10:850624. doi: 10.3389/fcell.2022.850624. eCollection 2022.

Neurogenesis in the inner ear: the zebrafish statoacoustic ganglion provides new neurons from a Neurod/Nestin-positive progenitor pool well into adulthood. **Schwarzer S**, Asokan N, Bludau O, Chae J, Kuscha V, Kaslin J, Hans S. *Development*. 2020 May 4:147(9):dev191775. doi: 10.1242/dev.191775.

Contributions to other projects that were not part of this doctoral thesis:

Transcriptome analysis reveals an Atoh1b-dependent gene set downstream of Dlx3b/4b during early inner ear development in zebrafish. Ezhkova D*, **Schwarzer S***, Spieß S, Geffarth M, Machate A, Zöller D, Stucke J, Alexopoulou D, Lesche M, Dahl A, Hans S. *Biol Open. accepted manuscript;* * contributed equally

Dlx3b/4b is required for early-born but not later-forming sensory hair cells during zebrafish inner ear development. **Schwarzer S**, Spieß S, Brand M, Hans S. *Biol Open.* 2017 Sep 15;6(9):1270-1278. Doi: 10.1242/bio.026211.

Table of contents

Summary ..... **VII**
List of publications ..... **X**
Table of contents ..... **XI**
List of figures ..... **XV**
List of tables ..... **XVIII**
List of abbreviations ..... **XIX**
1. Introduction **1**

1.1 Deafness – an emerging health problem for an ageing society 1
1.2 Sensorineural hearing loss is the main cause of deafness 2
1.3 Vestibular disorders: when the world starts spinning 3
1.4 The vertebrate ear: one of the most intricate anatomical structures 5
1.5 Zebrafish: a perfect model organism to study the vertebrate inner ear 7
1.6 Development of the zebrafish inner ear 8
1.7 Zebrafish: a master of regeneration 9
1.8 Mammalian models of sensorineural hearing loss 11
1.9 Replacing what is lost: new neurons for the mammalian inner ear 13
1.10 Single cell transcriptome analysis – unraveling a cell's identity and state 14

2. Aims of this study **16**
3. Material and methods **17**

3.1 Material 17
3.1.1 Technical equipment 17
3.1.2 Transgenic fish lines 17
3.1.3 Kits 18
3.1.4 Buffer and reagents 18
3.1.5 Antibodies 20
3.1.6 Cell dyes 21
3.1.7 *In situ* hybridization probes 21
3.1.8 PCR primers 22

3.2 Methods 23
3.2.1 Zebrafish husbandry and lines 23
3.2.2 Lesion of the statoacoustic ganglion via injection into the otic capsule 23
3.2.3 Bromodesoxyuridine (BrdU) pulse chase experiment 24
3.2.4 Long term lineage tracing 24
3.2.5 H&E Staining 24
3.2.6 Tissue preparation for immunohistochemistry 25
3.2.7 Immunohistochemistry 25
3.2.8 TUNEL assay 27
3.2.9 *In situ* hybridization 27
3.2.10 Image acquisition 27
3.2.11 Quantification and statistical analysis 28
3.2.12 SAG dissection to obtain single cells 29

3.2.13 Cell dissociation 30
3.2.14 FACS of cells derived from the SAG 31
3.2.15 Analysis of genes expression in *neurod*:GFP-positive cells 31
3.2.16 Transcriptome analysis via scRNAseq 32

4. Results 35

4.1 Characterisation of the juvenile and adult zebrafish statoacoustic ganglion (SAG) 35
4.1.1 Anatomy of the statoacoustic ganglion (SAG) in adult zebrafish 35
4.1.2 Sensory neurons in the adult zebrafish SAG 37
4.1.3 Amount and density of neurons decrease during growth of the SAG 39
4.1.4 *neurod*:GFP-expressing cells form dispersed islets in the anterior and posterior SAG in juvenile and adult zebrafish 41
4.1.5 The neurogenic niche is highly active in the juvenile SAG but turns quiescent over time resulting in non-proliferating neuronal progenitors and a very low neurogenesis rate in the adult SAG 44
4.1.6 *neurod*:GFP-positive neuronal progenitor cells are proliferating and can give rise to new neurons within a week at juvenile stages 47
4.1.7 Proliferating but marker-negative cell population replenishes the *neurod*:GFP-positive cell pool at adult stages and contributes to adult neurogenesis 50
4.1.8 Nestin also marks neuronal progenitors in the neurogenic niche 53
4.1.9 Long-term lineage tracing: larval *nestin*:mCherryCreER^{T2}-positive cells give rise to mature neurons in the adult SAG 55
4.1.10 Distribution of glia cells and myelination pattern label the peripheral-central nervous system transitional zone (PCTZ) in the juvenile and adult SAG 58
4.1.11 Summary 62

4.2 Transcriptome analysis of proliferating stem cell-like and progenitor cells in the juvenile and adult zebrafish SAG 64
4.2.1 Establishment of an experimental pipeline to obtain single cells from the SAG for transcriptome analysis via single-cell RNA sequencing 64
4.2.2 Transcriptome analysis of proliferating cells in the juvenile SAG using single cell RNA sequencing 66
4.2.3 Identification of 12 different cell clusters in the transcriptome data set obtained from the juvenile SAG 68
4.2.4 Expression profile eliminates cluster 10, 11 and 12 as potential stem cell-like cell clusters in the juvenile SAG 69
4.2.5 Identification of cells from the sensory epithelium (cluster 1), oligodendrocyte precursor cells (cluster 2) and myelinating cells (cluster 3) as distinct clusters in the juvenile SAG 71
4.2.6 scRNAseq revealed that *nestin* is only expressed in a subpopulation of *neurod*-expressing neuronal progenitor cells in the juvenile SAG 73
4.2.7 scRNAseq identifies a cluster of newborn neurons (cluster 8) 77
4.2.8 scRNAseq identifies a cluster of differentiating neurons (cluster 9) 79

4.2.9 scRNAseq of the juvenile SAG reveals two clusters (4 and 6) as candidates for the presumptive neuronal stem cell-like cell population 80
4.2.10 Only the cluster progenitor cells 1 and stem cell-like 2 express proliferation markers ... 83
4.2.11 scRNAseq identifies six cell populations associated with the neuronal lineage in the juvenile SAG ... 84
4.2.12 Transcriptome analysis of proliferating cells in the adult SAG using scRNAseq ... 85
4.2.13 Identification of 11 different cell clusters in the transcriptome data set obtained from the adult SAG ... 85
4.2.14 Identification of cluster 8, 9 and 10 as immune cell cluster and cluster 11 as endothelial cell/lymphathic vessel cluster in the adult SAG ... 88
4.2.15 Majority of cells in the transcriptomic data of the adult SAG identify as cells from the sensory epithelium including hair cells ... 90
4.2.16 Identification of myelinating cells (cluster 5) as a distinct cluster in the adult SAG ... 93
4.2.17 scRNAseq identifies only two populations associated with the neuronal lineage in the adult SAG ... 94

4.3 Regeneration in the adult zebrafish SAG ... 98
4.3.1 Establishment of a suitable lesion paradigm to target sensory neurons in the adult SAG ... 98
4.3.2 The chosen injection side is suitable to target the SAG ... 100
4.3.3 Emergence of apoptotic sensory neurons in the adult zebrafish SAG ... 101
4.3.4 Accumulation of leukocytes in the adult SAG persists beyond 16 days post lesion ... 105
4.3.5 Reactive proliferation in the neurogenic niche of the adult zebrafish SAG peaks at 8 days post lesion ... 107
4.3.6 Lesion-induced reactive neurogenesis in the neurogenic niche of the adult SAG ... 112
4.3.7 Sensory neurons derived from reactive proliferating mature within 19 days post lesion. ... 114
4.3.8 Summary ... 116

5. Discussion ... 117

5.1 Characterization of the zebrafish SAG during growth and homeostasis focusing on juvenile and adult neurogenesis ... 117
5.1.1 Cellular composition and landmarks in the SAG ... 117
5.1.2 Neurod/Nestin-positive progenitor cells in the neurogenic niche act as a source for lifelong neurogenesis in the SAG ... 119
5.1.3 Finding the presumptive stem cell-like cell population maintaining the pool of neuronal progenitor cells ... 127

5.2 Regenerative capacity of the adult zebrafish SAG ... 130
5.2.1 Establishment of a suitable lesion model to study neuronal regeneration in the adult zebrafish SAG ... 131

5.2.2 Reactivation of the neurogenic niche upon lesion results in reactive proliferation and reactive neurogenesis 133
5.2.3 Future goal: investigating underlying mediators of regenerative response 135
5.2.4 Generation of more precise lesion paradigms for future studies 136

6. Conclusion & Outlook 139
Supplements XX
References XXXI
Acknowledgement LI
Erklärung entsprechend §5.5 der Promotionsordnung LIII

List of figures

Figure 1.1 The complex structure of the vertebrate inner ear is highly conserved. 6

Figure 1.2 Development of the zebrafish statoacoustic ganglion. 9

Figure 1.3 Mouse model for auditory neuropathy: Ouabain-induced cochlear nerve degeneration. 12

Figure 4.1 Anatomy of the adult zebrafish statoacoustic ganglion (SAG). 36

Figure 4.2 Localisation of sensory neurons and sensory hair cells in the VIIIth cranial nerve of adult zebrafish. 38

Figure 4.3 Number and density of HuC/D-positive neurons decrease during growth of the SAG. 40

Figure 4.4 *neurod*:GFP expression in the anterior and posterior SAG of adult and juvenile zebrafish. 42

Figure 4.5 *Tg(neurod:GFP)* line faithfully recapitulates endogenous neurod expression in the zebrafish SAG 43

Figure 4.6 Proliferation and neurogenesis rapidly decrease at juvenile stages and are severely reduced in the adult zebrafish SAG. 45

Figure 4.7 Quantification of proliferation and neurogenesis the SAG reveals that the neurogenic niche is highly active at juvenile stages but turns almost quiescent in the adult zebrafish SAG 46

Figure 4.8 *neurod*:GFP-positive cells are proliferating and give rise to new neurons at juvenile stages. 48

Figure 4.9 Quantification of proliferation and neurogenesis in the *neurod*:GFP-positive neuronal progenitor cell pool upon BrdU treatment in the juvenile SAG 49

Figure 4.10 A proliferating but marker-negative stem cell-like cell population replenishes the *neurod*:GFP-positive cell pool at adult stages and contributes to adult neurogenesis. 51

Figure 4.11 Quantification of proliferation and neurogenesis in the neurod:GFP-positive neuronal progenitor cell pool upon BrdU treatment in the adult SAG. 52

Figure 4.12 Nestin is expressed in the neurogenic niche and overlaps largely with *neurod*:GFP expression at juvenile and adult stages. 54

Figure 4.13 Larval *nestin*:mCherryCreER^{T2}-positive cells give rise to half of the mature neurons present in the adult SAG 56

Figure 4.14 Sox2-positive cells reside along a line outside the Neurod/Nestin-positive progenitor pool in the SAG. 58

Figure 4.15 Expression of glia marker GFAP in the medial part of the SAG in close proximity of Sox2 expressing cells 59

Figure 4.16 Expression of glia marker *her4.3*:GFP shows similar expression pattern to GFAP/Zrf1. 60

Figure 4.17 Expression of Sox2, the glia marker GFAP and differences in myelination patterns mark the peripheral and central nervous system transitional zone (PCTZ) in the SAG. 61

Figure 4.18 Expression of neurod and nestin in cells isolated from the adult SAG of *neurod*:GFP transgenic fish to demonstrate suitability of the established single cell isolation pipeline. 65

Figure 4.19 Experimental workflow to find novel marker genes for neuronal stem and progenitor cells in the juvenile SAG..... 67

Figure 4.20 scRNAseq identifies 12 different cell populations in the juvenile SAG. 68

Figure 4.21 UMAP depicting the distribution of cells sorted as GFP-positive or GFP/mCherry-positive in the transcriptome data set from the juvenile SAG. 69

Figure 4.22 scRNAseq identifies cell clusters containing endothelial cells/lymphatic vessels and immune cell populations. 70

Figure 4.23 Cluster 1 expresses markers associated with the sensory epithelium. 72

Figure 4.24 scRNAseq identifies two clusters involved in myelination. 73

Figure 4.25 Neuronal progenitor cells of the progenitor cell 1 (cluster 5) co-express nestin and neurod1..... 75

Figure 4.26 Neuronal progenitor cells of the progenitor cell 2 cluster (cluster 7) express neurod1 as well as markers associated with glutamatergic synapses. 76

Figure 4.27 scRNAseq identifies cluster 8 as newborn neurons. 78

Figure 4.28 scRNAseq identifies a cluster of differentiating neurons (cluster 9). 79

Figure 4.29 The stem cell-like 1 cluster (cluster 4) is characterized by the exclusive expression of *rbp4*. 80

Figure 4.30 Cluster 6, stem cell-like 2, is characterized by the expression of *fabp7a* and other glia marker. 81

Figure 4.31 Expression of proliferation marker *mki67*, *mcm5* and *pcna* in cluster 5 (progenitor cells 1), 6 (stem cell-like 2) and 7 (progenitor cells 2)..... 83

Figure 4.32 scRNAseq identifies six clusters associated with the neuronal lineage. 84

Figure 4.33 scRNAseq identifies 11 different cell populations in the adult SAG. 86

Figure 4.34 UMAP depicting the distribution of cells sorted as GFP-positive, GFP/mCherry-positive or mCherry-positive in the transcriptome data set from the adult SAG. 87

Figure 4.35 scRNAseq identifies cell clusters containing different immune cell populations and endothelial cells/lymphatic vessels. 89

Figure 4.36 Cluster 2 and 3 contain cells from the sensory epithelium. 90

Figure 4.37 scRNAseq identifies cluster 4 as hair cell progenitors. 91

Figure 4.38 Hair cells (cluster 6) form the biggest cell population in the transcriptome data set from the adult SAG..... 92

Figure 4.39 scRNAseq identifies one cluster of myelinating cells. 93

Figure 4.40 scRNAseq identifies cluster 7 as newborn/differentiating neurons..... 95

Figure 4.41 scRNAseq identifies a *rbp4*-expressing stem cell-like cluster (cluster 1) similar to the juvenile stem cell-like 1 cluster in the adult SAG. 96

Figure 4.42 *fabp7a*-expressing cells still present in the adult SAG..... 97

Figure 4.43 Establishment of a lesion paradigm for the adult zebrafish SAG. 99

Figure 4.44 CellTracker Red injection shows suitability of injection side to target neurons in the SAG. 100

Figure 4.45 Presence of phospholipid phosphatidylserines marked by *ubiq*:secAnnexinV-mVenus in the distal part of the SAG upon lesion. 102

Figure 4.46 Expression of *ubiq*:secAnnexinV-mVenus reveals signs of apoptosis in neurites upon lesion. 103

Figure 4.47 TUNEL staining reveals apoptotic neurons upon lesion. 104

Figure 4.48 Accumulation of leukocytes in the adult zebrafish SAG upon lesion. 106

Figure 4.49 Reactive proliferation of *neurod*:GFP-positive progenitors in the adult zebrafish SAG upon lesion. 109

Figure 4.50 Quantification of reactive proliferation of *neurod*:GFP-positive progenitors. . 111

Figure 4.51 Generation of new sensory neurons from the *neurod*:GFP-positive progenitor pool upon lesion. 113

Figure 4.52 Quantification of reactive neurogenesis upon lesion. 114

Figure 4.53 Sensory neurons derived from reactive proliferating mature within 19 days post lesion. 115

Figure 5.1 Cellular composition of the zebrafish SAG. 118

Figure 5.2 Neurod/Nestin-expressing neuronal progenitor cells act as a source for lifelong neurogenesis in the SAG. 120

Figure 5.3 Temporal dynamics of the regenerative response in the adult zebrafish SAG upon lesion. 134

Figure S.1 Expression of glia marker S100B shows similar expression pattern to GFAP. . XX

Figure S.2 Heatmap showing the expression of selected marker genes in all cell clusters from the transcriptome data set obtained from the juvenile SAG. XXI

Figure S.3 *r3hdm1* expression can be observed in proliferating and non-proliferating cells of the neurogenic niche in the juvenile SAG. XXII

Figure S.4 *r3hdm1* is expressed in cells of the neurogenic niche as well as in mature neurons in the juvenile SAG. XXIII

Figure S.5 Expression of *tubb5* is confined to the *neurod*:GFP-positive neurogenic niche. XXIV

Figure S.6 *gap43*:GFP labels axonal projections of newborn neuron. XXV

Figure S.7 Expression of *rbp4* in a small cell population medial to the neurogenic niche. XXVI

Figure S.8 *fabp7a* is expressed in the PCTZ and throughout the neurogenic niche in the juvenile SAG. XXVII

Figure S.9 Heatmap showing the expression of selected marker genes in all cell clusters from the transcriptome data set obtained from the adult SAG. XXVIII

Figure S.10 Reactive proliferation in the neurogenic niche and the utricular macula. XXIX

Figure S.11 Expression of *rbp4*, *cyp26b1*, *aldh1a2* and *aldh1a3* in the transcriptome obtained from cells in the juvenile SAG. XXX

List of tables

Table 3.1 Technical equipment 17
Table 3.2 Trangenic fish lines 17
Table 3.3 Kits 18
Table 3.4 Buffers and reagents 18
Table 3.5 Primary antibodies 20
Table 3.6 Secondary antibodies 20
Table 3.7 Cell dyes 21
Table 3.8 *In situ* hybridization probes 21
Table 3.9 Primers used for PCR 22

List of abbreviations

°C	degree Celsius
µg	microgram
µl	microliter
µM	micromolar
bHLH	basic helix-loop-helix
BL	body length
bp	base pairs
CNS	central nervous system
DAPI	4',6-diamidino-2-phenylindole
DMSO	dimethyl sulfoxide
DNA	deoxyribonucleic acid
dNTP	deoxynucleotide triphosphate
dpf	days post fertilization
dpi	days post injection
dpl	days post lesion
dpp	days post BrdU pulse
e.g.	*exempli gratia*, for example
EGFP	enhanced green fluorescent protein
et al.	et aliter
FACS	fluorescent-activated cell sorting
EtOH	ethanol
FISH	fluorescent *in situ* hybridization
GFAP	glial fibrillary acidic protein
HE	Hematoxilin Eosin
IHC	immunohistochemistry
ISH	*in situ* hybridization
MeOH	methanol
MESAB	ethyl-m-aminobenzoate methansulfphonate
mM	millimolar
MTZ	metronidazole
NaOH	sodium hydroxide
NTR	nitroreductase
PBS	phosphate buffered saline
PCR	polymerase chain reaction
PCTZ	peripheral and central nervous system transitional zone
PNS	peripheral nervous system
qPCR	quantitative PCR
RNA	ribonucleic acid
ROI	region of interest
RT	room temperature
SAG	statoacoustic ganglion
scRNAseq	single-cell RNA sequencing
SD	standard deviation
TAE	tris-acetate ethylenediamine tetraacetic acid
Tg	transgenic
Tris-HCl	tris-hydrochloride buffer
TUNEL	TdT-mediated dUTP-biotin nick end labeling
US	United States
WT	wildtype

1. Introduction

1.1 Deafness – an emerging health problem for an ageing society

According to the World Health Organization, over 5 % of the world's population which corresponds to roughly 466 million people are affected by hearing impairment or deafness. In the next two decades this number will rise to nearly 2.5 billion, corresponding to 1 out of every 10 people, and at least one quarter of the affected individuals will require hearing rehabilitation (www.who.int/news-room/fact-sheets, 2023). Since the prevalence of hearing loss increases with age, with one quarter of every person older than 60 years being affected, the number of people affected by hearing disabilities will increase in our over-ageing society. Additionally, hearing loss cases caused by exposure to loud noise are rising. In particular amongst young people, over 1 billion individuals worldwide are at risk of hearing loss due to unsafe listening practices (Dillard *et al.*, 2022). Unaddressed hearing loss impacts several aspects of personal life, including communication and speech, mental cognition, social interactions as well as education (which children with hearing loss and deafness do often not receive in developing countries) and employment. As estimated by the WHO, the annual global costs of US$ 980 billion for health care, educational support, loss of productivity and societal costs are immense. Hence, as the life expectancy rises and also more young people suffer from hearing impairment, there is a pressing need to develop new therapies restoring hearing abilities.

Hearing impairment and loss are caused by a number of different factors such as genetics, birth trauma, exposure to loud noise, trauma to the ear or the head, infectious diseases and particularly ageing, and can be present from birth (congenital) or acquired at any time afterwards. In general hearing loss can be divided into three categories based on the affected area: conductive, sensorineural and central hearing loss (Zahnert, 2011). Conductive hearing loss affects the outer and/or middle ear and includes conditions that can be well cured by medical or surgical treatment. Common examples for conductive hearing loss are the presence of foreign bodies in the auditory canal or the perforation of the tympanic membrane caused for instance by an otitis media infection which often heals without medical care (Wright, 2015; Berger *et al.*, 1997). In patients suffering from conductive hearing loss, the sensory hair cells in the inner ear, which are responsible for receiving the sensory stimulus and translating it into an electrical signal, and the sensory neurons forming the VIIIth cranial nerve, which transduce these electrical signals to brain, are still intact. Therefore, even if the cause of the conductive hearing loss is not reversible, hearing aids offer a satisfactory alternative for patients to cope with the hearing impairment (Kozlowski *et al.*, 2017).

The majority of hearing impaired or deaf patients, however, suffer from sensorineural (or mixed) hearing loss which effects the sensory hairs cells and/or the sensory neurons in the inner ear. Central hearing loss, sometimes also classified as a subtype of sensorineural hearing loss, originates from a malfunction of neurons in the auditory pathways and/or auditory cortex in the brain.

1.2 Sensorineural hearing loss is the main cause of deafness

Sensorineural hearing loss is a type of hearing impairment that occurs as a consequence of damage to cells in the inner ear, in most cases to the sensory hair cells and/or sensory neurons. As the mature sensory tissue exhibits a limited capacity to repair damage and cannot replace lost hair cells or sensory neurons, sensorineural hearing loss is in the majority of cases permanent and irreversible. There are several known causes for sensorineural hearing loss that can be subcategorized into external, such as loud noise, ototoxic drugs and traumatic injury of the inner ear/head, and internal causes, like ageing, genetical disorders or virus infections.

Among these, noise induced hearing loss due to long-term continuous or single/repeated sudden noise exposure, is the most common and preventable cause of sensorineural hearing loss (Le *et al.*, 2017). Additionally, ototoxicity is reported as one of the five most frequent adverse drug reactions (Tanoshima *et al.*, 2019). Known ototoxic drugs include a variety of pharmaceutical medications out of which cis-platinum-based chemotherapeutics agents and aminoglycoside antibiotics can cause irreversible damage primarily to sensory hair cells (reviewed in Schacht, Talaska and Rybak, 2012). However, also commonly used, over the counter available nonsteroidal anti-inflammatory drugs such as ibuprofen were linked to sensorineural hearing loss in several studies (as reviewed in Kyle, Wang and Shin, 2015). In animal models, multiple studies have shown that loss of hair cells can occur within hours after exposure to noise or ototoxic drugs whereas the degeneration of sensory neurons in the spiral ganglion is only detectable after weeks to months or even years after injury, suggesting hair cells to be the most vulnerable element in the cochlea (Bohne and Harding, 2000; Suzuki, Ushio and Yamasoba, 2008). However, this long-standing dogma of hair cells being the primary target of acoustic overexposure and ototoxic drug while sensory neurons being lost only secondarily upon a lack of neurotrophic support and sensory input from the damaged/missing hair cells, has already been overturned more than a decade ago (Kujawa and Liberman, 2006; Kujawa and Liberman, 2009; (Zilberstein, Liberman and Corfas, 2012). Studies in mammalian models revealed the existence of noise-induced cochlear synaptopathy and neuronal degeneration without previous hair cell loss. In these cases, noise exposure can cause a moderate but completely reversible damage

of hair cells in the inner ear while inducing a loss of afferent nerve fiber terminals followed by primary neurodegeneration of spiral ganglion neurons (Kujawa and Liberman, 2009). Similar, ototoxic drugs can directly target sensory neurons inducing a swelling and subsequent rupturing of afferent synapses prior or even without damaging the inner hair cells (IHC) in the cochlea (Wang, Ding and Salvi, 2003). A study by Zilberstein et al., using a transgenic mouse model in which a dietary thiamine restriction specifically induces a rapid, widespread loss of the IHCs, showed that sensory neurons survive for months after IHC loss. This further confirms the theory, that IHCs are not necessary for the survival of sensory neurons and that most likely supporting cells of the organ of Corti provide survival factors for the sensory neurons (Zilberstein, Liberman and Corfas, 2012).

In addition to acoustic overexposure and usage of ototoxic drugs, ageing is another major cause for sensorineural hearing loss, affecting approx. two-third of adults older than 70 years (Goman and Lin, 2016). In general, age-related hearing loss, defined as the gradual, progressive hearing loss occurring in individuals as they age, exhibits multifarious underlying pathophysiological processes. Besides genetic predisposition, vascular pathology and other causes, chronic noise overexposure throughout life is one of the risk factors for age-relating hearing loss (Wu *et al.*, 2020). More than a decade ago, a contribution of age-related hearing loss to cognitive decline in the elderly has been proposed (Lin *et al.*, 2013; Wayne and Johnsrude, 2015). Recent cohort studies could show, that hearing loss is one of the individual risk factors that has the biggest impact on whether someone develops dementia (Livingston *et al.*, 2017; Chern and Golub, 2019).

Taken together, sensorineural hearing loss is a pathology with an increasing prevalence that affects billions of people worldwide. The risk to develop sensorineural hearing loss can be lowered since some of the causes are preventable, such as acoustic overexposure or can be minimized, for example by a restricted, more controlled usage of ototoxic drugs. Nevertheless, once developed, sensorineural hearing loss is in most cases permanent and irreversible due to the fact that the mammalian inner ear is extremely limited in its ability to replace damaged or lost hair cells and sensory neurons after birth. Over decades, multiple studies suggested sensory hair cells as the main target of damage resulting in sensorineural hearing loss. However, in the past years this view has changed and more evidence for a critical role of damaged sensory neurons in developing sensorineuronal hearing loss was found. This reveals the urgent need to study sensory neurogenesis and the potential capacity and limitations of neuronal regeneration in the inner ear in greater detail.

1.3 Vestibular disorders: when the world starts spinning

Among all sensory organs, the inner ear is unique, harboring not only the sense of hearing but also a second sensory organ: the vestibular system. The

vestibular system is responsible for the sense of balance, spatial orientation and detection of movement and is of high importance for postural reflexes and coordinating eye movement. The information generated by the vestibular system is integrated with the information of two other sensory system, the sense of vision and proprioception (the sense of self-movement and relative body-position mediated through mechanosensory neurons in muscles, tendons and joints). This multimodal integration enables complex behaviors to remain stable and upright and the compensatory response to unexpected self-movement (Cullen, 2019). Even though information from the visual system and proprioception can compensate the loss of sensory input from the vestibular system to a certain degree, affected individuals exhibit a reduced sense of balance. Vestibular dysfunction has a high prevalence and several recent epidemiological studies have shown that they affect more than 35 % of all US adults aged 40 and older are. Additionally, vertigo, dizziness or imbalance rank among the most common complaints in medicine and account for approx. 12 % of neurological consultations in the emergency room (Royl *et al.*, 2010).

Vestibular disorders include a variety of different pathologies and are categorized into two classes based on their origin: central vestibular disorders, originating in the central nervous system (CNS), and peripheral vestibular disorders, originating in the vestibular system (semicircular canals and the otolithic organs) and the VIIIth cranial nerve innervating the inner ear (Brandt and DIeterich, 2017). Central vestibular disorders include for instance vertebrobasilar ischemic stroke, caused by a reduced blood supply of the brain stem, cerebellum and inner ear by the vertebrobasilar system, or migraine-associated dizziness. The majority of vestibular dysfunction, however, origin in the inner ear, hence belong to the group of peripheral vestibular disorders. These include for example benign paroxysomal positional vertigo, Meniere's syndrome, vestibular neuronitis, labyrinthitis or vestibular schwannoma. Among these, the benign paroxysomal positional vertigo has the highest prevalence and is caused by free-floating densities stimulating sensory hair cells in the semicircular canals thus creating the sensation of vertigo. The second most common cause for vestibular vertigo is vestibular neuronitis in which a (in most cases) viral infection of the vestibular nerve lead to nerve degeneration (reviewed in Thompson and Amedee, 2009). Similar to the auditory system, ototoxic drugs as well as ageing also damage hair cells and/or sensory neurons in the vestibular system thus resulting in a loss of vestibular function.

Altogether, this shows that besides individuals suffering from hearing impairment also people affected by vestibular diseases will benefit from a deeper scientific knowledge of the mechanisms involved in inner ear development as well as regeneration.

1.4 The vertebrate ear: one of the most intricate anatomical structures

The vertebrate ear is a highly complex structure that can be composed of up to three different parts: the outer, middle and inner ear. The outer ear, which includes the visible part of the ear and the ear canal, is a unique feature of mammals and is lacking all other vertebrates. The middle ear, an air-filled cavity containing up to three ossicles responsible for transmitting and amplifying sound to allow animals to hear in an aerial environment, is also present in mammals and additionally also in amniotes and most amphibians (Mallo, 2001). However, the core of the vertebrate ear, which every vertebrate possesses, is the inner ear. It contains the auditory and vestibular system and is responsible for receiving and transducing the sensory in-put into electrical signals that are subsequently transferred to the brain.

The complex anatomical structure of the inner ear is highly conserved among vertebrates (Waterman and Bell, 1984; Haddon and Lewis, 1996)(Figure 1.1A). It consists of three semicircular canals: the posterior and superior semicircular canal that fuse at their non-ampullated end forming the crus commune, as well as the horizontal semicircular canal. Additionally, the inner ear harbors two otolithic organs, the utricle and the sacculus. During evolution, mammals have developed the cochlea containing the organ of Corti as the auditory system. In contrast, teleosts such as zebrafish possess a third otolithic organ, the lagena, which is not homologous to the cochlea. Although lacking the cochlea, zebrafish can still receive auditory stimuli. As part of the Otophysi, zebrafish possess Weberian ossicles, four small bones connecting the swim bladder to the inner ear, that transferring sound to the inner ear (reviewed in Whitfield, 2002; Bang, Sewell and Malicki, 2001). In zebrafish, the lagenar macula and the saccular macula are involved in sound perception (Fay and Popper, 2000; Lu and Desmidt, 2013; Leitner, 2014).

One a cellular level, the auditory and vestibular system rely on the same three cell types, despite being two different senses: mechanosensory hair cells, supporting cells and sensory neurons (Figure 1.1B).

Mechanosensory hair cells

Mechanosensory hair cells are the stimulus receiving cells. Their main characteristic is the stereocilia, also known as auditory hair bundles, that are arranged on the apical surface of the cells. The stereocilia are formed by an array of F-actin and exist in different heights and are arranged in an uprising order on each hair cell. The sensory mechanoelectrical transduction channel near the tip of one stereocilium is linked through a filament to the next higher, neighboring stereocilia. Depending on the direction of the mechanical stimulus, the probability of the mechanoelectrical transduction channel to be open increases or decreases, thereby

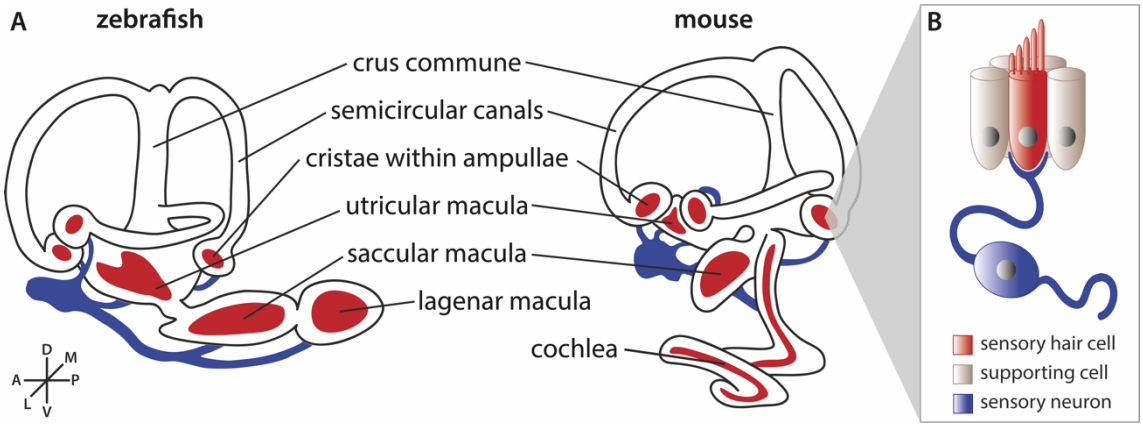

Figure 1.1 The complex structure of the vertebrate inner ear is highly conserved. (**A**) Scheme illustrating the zebrafish and the mouse inner ear, showing the high similarity of inner ears of different vertebrate species; zebrafish and mouse possess three semicircular canals harboring the three different cristae, and the otolithic organs utricular macula and saccular macula. In contrast, the mammalian cochlea which harbors the receptor organ of hearing, the organ of Corti, is not homologous to the lagenar macula, the third otolithic organ present in teleosts such as zebrafish (modified after Whitfield and Hammond, 2007). (**B**) Scheme of the cellular composition of the vertebrate inner ear: sensory neurons connect the sensory hair cells, which are surrounded by supporting cells in the sensory epithelium, to the brain.

changing the electrical property of the hair cells (Schwander, Kachar and Müller, 2010, Qiu and Müller, 2018)

In the organ of Corti, the mammalian auditory system, a second anatomically and functionally different type of hair cells, the outer hair cells, can be distinguished. In contrast to the inner hair cells (IHC), which are receive the sound and transduce it to an electrical signal as described above, the function of the OHC is to amplify the acoustic stimulus by converting the varying receptor potentials created by the stimulus to active vibrations of the cell body, thus enhancing the initial stimulus (Ashmore, 2008; Ashmore *et al.*, 2010) .

Supporting cells

Mechanosensory hair cells are surrounded by the supporting cells, together forming the sensory epithelium. For a long time, supporting cells have been considered to primarily play a role in structural and homeostatic function (Ramírez-Camacho *et al.*, 2006). As reviewed by Wan et al., more and more functions of supporting cells have been discovered in the last decades, such as modulation of the extracellular matrices important for the formation and maintenance of acellular structures in for example the organ of Corti. Interestingly, supporting cells also play an important role in context of inner ear trauma and regeneration and are crucial to maintain the health and structure of the sensory epithelium upon damage and loss of sensory hair cells. Additionally, it has been shown that supporting cells act as a source of new sensory neurons in the non-mammalian inner ear and possess the capacity to replace lost hair cells, suggesting supporting cells as a valuable and

potent target for hair cell regeneration also in the mammalian inner ear (as reviewed in Wan, Corfas and Stone, 2013).

Sensory neurons

Sensory neurons in the inner ear form the VIIIth cranial nerve, also known as vestibulocochlear nerve or statoacoustic ganglion (SAG), and are responsible for transmitting the electrical signal from the sensory hair cells in the vestibular and auditory system to the brain. They from specialized synapses, that use the neurotransmitter glutamate and are characterized by the presence of a large presynaptic organelle, the synaptic ribbon, with hair cells to enable a fast transmission of the signal (Nouvian *et al.*, 2006). In mammals, neurons in the organ of Corti can be assorted to two different pathways. Neurons of the afferent pathway innervate the sensory hair cells to transmit the auditory information to the brain and are further sub-categorized into type I and type II sensory neurons. Type I neurons are large, myelinated, bipolar neurons that innervate IHCs, whereas smaller, pseudo-unipolar type II neurons are only partly-myelinated and innervate OHCs. Neurons from the efferent pathway descend from the cortex to the OHCs and are responsible for improving sound detection and function of the OHCs as well as to protecting the cochlea from acoustic damage (Pavlinkova, 2021). As in all cranial ganglia and nerve roots in vertebrates, the axonal projections of the sensory neurons enter the CNS and thereby cross the PNS-CNS interface. The area, in which these axonal projections are surrounded by cells from the CNS, is called the PNS-CNS transitional zone (PCTZ), and is characterized by CNS-derived, oligodendrocyte-mediated myelination in contrast to the Schwann cell-mediated myelination present in the rest of the nerve (Fraher and Delanty, 1987; Fraher, Smiddy and O'Sullican, 1988; Wang *et al.*, 2013; Bojrab *et al.*, 2017).

1.5 Zebrafish: a perfect model organism to study the vertebrate inner ear

After being established as new research model organism by George Streisinger half a century ago, the zebrafish (*Danio rerio*) has turned into an excellent model to study development and regeneration in vertebrates (Varga, 2018). As reviewed by Tanya Whitfield, besides the general advantages of using zebrafish as a model organism, such as the high number of offspring, the rather low-cost and simple maintenance as well as the availability of classical forward and reverse genetic approaches and genomic tools to study gene function, zebrafish is a particularly great model to study the vertebrate inner ear (Whitfield, 2002). First, zebrafish develop externally and are optically transparent during the first stages of development and even beyond when treated with a chemical compound to suppress the development of pigmentation. This enables to observe the development of the

inner ear inside the living embryo. Furthermore, like other aquatic animals, zebrafish possess an additional sensory organ on the body surface: the lateral line. The lateral line consists of multiple neuromasts that rely on hair cells as the stimulus receiving cells and are highly similar to the sensory patches in the inner ear regarding structure and function. In the zebrafish larva, neuromasts are not enclosed in canals which makes them easily assessable for manipulations to study hair cells. Last but not least, the genetic mechanisms of otic development and the anatomical and physiological structure of the inner ear is highly conserved among vertebrates and zebrafish possess a typical vertebrate inner ear, turning zebrafish into an ideal model for hearing and deafness (Whitfield, 2002; Fritzsch and Beisel, 2001).

1.6 Development of the zebrafish inner ear

Since the first anatomical characterization of the teleost inner ear was published as early as 1872 by Gustav Retzius, the zebrafish inner ear was subject to detailed studies, providing comprehensive descriptions for embryonic and larval development (Bever and Fekete, 2002; Haddon and Lewis, 1996; Waterman and Bell, 1984). The inner ear originates from a zone of ectoderm surrounding the anterior boarder of the neural plate, the pre-placodal region (PPR). As development continues, the PPR gives rise to the otic/epibranchial precursor domain (OEPD), which subsequently forms a transient thickening, the otic placode (Barald and Kelley, 2004). The otic placode then cavitates to form the otic vesicle, a hollow ball of epithelium, that gives rise to nearly all cell types in the inner ear. The fate decision for neurogenic (sensory neurons) vs. non-neurogenic (hair cells) cells is made already in the otic placode and is dependent on the expression of a subset of genes such as *fox1* and *neurog1* for the neuronal lineage and *dlx3b/4b* and *atoh1a/b* for the sensory lineage (Andermann, Ungos and Raible, 2002; Fritzsch, Eberl and Beisel, 2010; Whitfield, 2015).

The generation of sensory neurons begins as early as 16 hpf with the specification of SAG neuroblasts by the expression of *neurog1* on the ventral side of the otic placode (Andermann, Ungos and Raible, 2002) (Figure 1.2A). By 17 hpf, neuroblasts start to delaminate from the otic vesicle which is accompanied by the downregulation of *neurog1* expression and the initiation of the expression of the transcription factor *neurod1*, a member of the bHLH gene family. *neurod1*-expressing cells enter a phase of transient amplification. The pool of transit-amplifying *neurod1*-expressing cells exists at least until 4 dpf and stays relatively constant in size over time. First *neurod1*-expressing precursor cells exit the cell cycle, downregulate the expression of *neurod1* and start to differentiate into mature neurons as early as 20 hpf. Newborn neurons almost immediately start to extend their axons toward the developing sensory patch and the CNS (Vemaraju *et al.*, 2012). As a result, within two days after the first appearance of mature neurons, the

SAG has already started to form. At that stage, the SAG can be divided into an anterior part innervating the anterior and lateral cristae as well as the utricular macula and a posterior part, innervating the posterior crista and the saccular macula in 3 dpf old zebrafish larvae (Sapède and Pujades, 2010a) (Figure 1.2B).

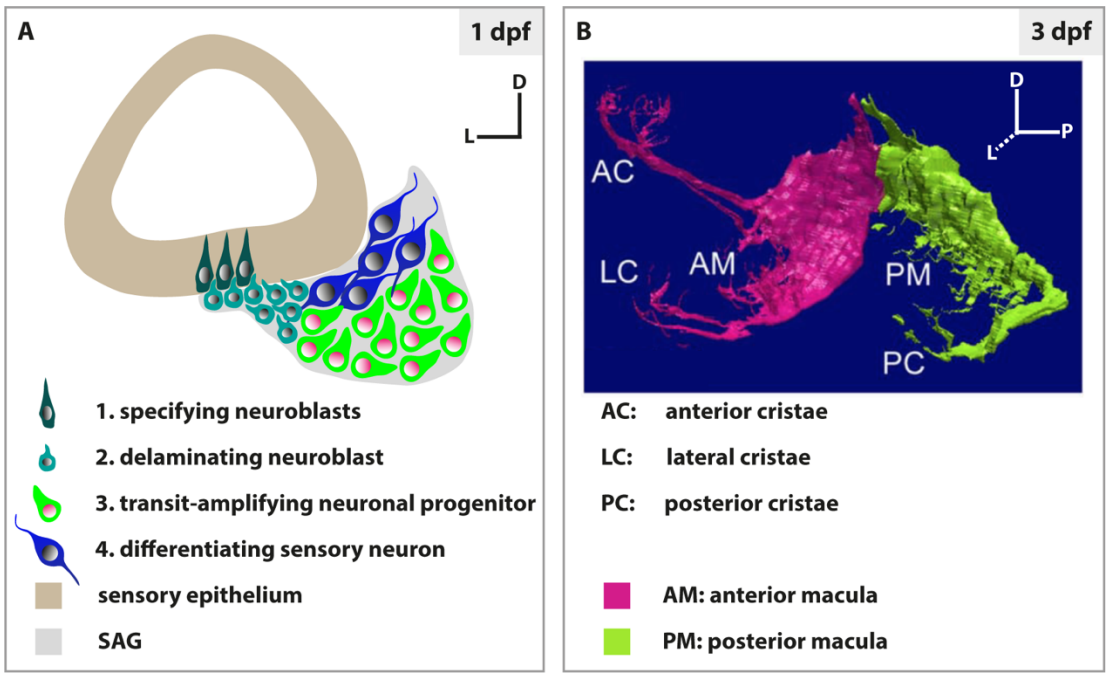

Figure 1.2 Development of the zebrafish statoacoustic ganglion.
(**A**) Scheme illustrating the various stages of SAG development. Neuronal precurors (neuroblasts) are (1.) specified and (2.) delaminated from the floor of the otic vesicle. Neuroblasts undergo a phase of (3.) transit-amplification wherein they migrate to a position between the otic vesicle and the hindbrain as the continue to delaminate. Neuroblasts finally (4.) differentiate into mature neurons (adapted from Vemaraju et al., 2012). (**B**) 3D-model of the topological organization of the SAG in 3 dpf larvae, performed with BioVis 3D software (modified from Sapède and Pujades, 2010)

1.7 Zebrafish: a master of regeneration

Regeneration describes the ability to replace damaged or lost tissue and organs to restore their function. During the course of evolution, the regenerative potential has declined, leaving mammalian vertebrates with an extremely limited regenerative potential (Julier *et al.*, 2017; Maden, 2018). In contrast, zebrafish possess a remarkable capacity to regenerate several different tissues and organs upon lesion, such as fin, heart, liver but also brain, retina and spinal cord as well as sensory hair cells (Gemberling *et al.*, 2013; Marques, Lupi and Mercader, 2019).

CNS regeneration

In mammals, the loss of neurons due to traumatic injury, stroke or neurodegenerative diseases cannot be repaired and often leads to a strong gliotic response preventing neuronal regeneration (Buffo *et al.*, 2008). In comparison, zebrafish can fully recover severe injuries of the retina, brain, and spinal cord. In the damaged zebrafish retina, Müller glia are the source of new neurons. Upon lesion, Müller glia are activated, dedifferentiate and re-enter the cell cycle to produce multipotent neuronal progenitor cells that subsequently replace the lost cells (Raymond *et al.*, 2006). During the course of regeneration, the gene expression profile of neuronal progenitor cells resembles in parts the program of retina development (Lahne *et al.*, 2021; Celotto, 2022). In the zebrafish telencephalon, radial glia cells in the ventricular zone serve as neuronal progenitors that replace lost neurons upon stab lesion(Kroehne *et al.*, 2011; Kizil *et al.*, 2012). Similar, regeneration of neurons in the zebrafish spinal cord depends on the corresponding radial glia cell in the spinal cord (Reimer *et al.*, 2008). The question whether neuronal regeneration also occurs in the zebrafish PNS, for example in the SAG of the inner ear, and which cells would be the source of newly generated sensory neurons remains to be investigated.

Hair cell regeneration

In contrast to mammals, zebrafish exhibit continuous formation of new hair cells throughout life (Higgs *et al.*, 2002). Moreover, hair cell regeneration after trauma has been described in the vestibular and auditory parts of the inner ear in zebrafish and also in other non-mammalian vertebrate species (Corwin and Cotanche, 1988; Ryals and Westbrook, 1990; Schuck, Julie B, Smith, 2009; Stone and Rubel, 2000). Additionally, hair cell regeneration in zebrafish occurs also in the neuromasts of the lateral line (Lush, Mark E, Piotrowski, 2013). In general, hair cell regeneration is mediated by the supporting cells surrounding sensory hair cells in the sensory epithelium. In the chicken and amphibian sensory epithelium, two different mechanisms for hair cell regeneration have been described: new hair cells derive either through mitotic regeneration, whereby a proliferating supporting cell gives rise to two daughter cells and one or both of them differentiate into new hair cells, or via direct transdifferentiation, a phenomenon in which the supporting cell differentiates into a hair cell without previous proliferation (Stone and Cotanche, 2007; Burns and Corwin, 2013). In contrast to that, hair cell regeneration in the zebrafish lateral line relies on mitotic regeneration and cannot occur when proliferation is blocked (Mackenzie and Raible, 2012). However, whether the robust regeneration of hair cells in zebrafish is accompanied by the generation of new sensory neurons to connect the newly generated hair cells to the central auditory system has not been studied yet.

1.8 Mammalian models of sensorineural hearing loss

Animal models for specific diseases aim to provide a better understanding of a given pathology with the overall goal to develop new medical treatments to improve the life of affected individuals. Considering that deafness and hearing impairment as well as vestibular diseases are pathologies with a high prevalence especially in an ageing society (chapter 1.1, 1.2 and 1.3), animal models resembling these diseases are a valuable platform to investigate the benefits and limitations of potential treatments. As of now, several mammalian models have been established to study sensorineural hearing loss caused either by the loss of hair cells and/or the sensory neurons.

Noise-induced lesion paradigms

Mammalian models for hearing loss based on a noise-induced lesion have been used already more than half a century ago (Eldredge, Covell and Gannon, 1959). A variety of rodent model organisms such as rat, mice and chinchilla have been used to study noise-induced hearing loss, all coming with certain advantageous and disadvantageous such as similarities or differences in the hearing ranges or there susceptibility to acoustic trauma (Escabi *et al.*, 2019; Clifford, Hertzano and Ohlemiller, 2019; Trevino *et al.*, 2019).

Ototoxic lesion paradigms

Besides noise-induced and age-related hearing impairment, the usage of ototoxic drugs is a common cause for sensorineural hearing loss. Exposure of model organisms to ototoxic drugs is a common method to study ototoxicity (Lin *et al.*, 2021). Several ototoxic lesion paradigms are based on the application ototoxic drugs that are commonly prescribed like the chemotherapeutic agent cisplatin or aminoglycosides such as kanamycin or gentamycin, sometimes even combined with other drugs known to increase their ototoxicity (Abbas and Rivolta, 2015; Wang *et al.*, 2015; Gibaja *et al.*, 2022). These lesion models have the benefit of studying the pathology of sensorineural hearing loss induced by these ototoxic drugs as well as searching for strategies to prevent or minimize the ototoxic effect.

Application of the neurotoxin Ouabain, a cardiac glycoside specifically blocking the Na^+/K^+-ATPase, to the round window of the cochlea is another established model of auditory neuropathy in mice, rats and gerbils (Schmiedt *et al.*, 2002; Lang, Schulte and Schmiedt, 2005; Fu *et al.*, 2012; Yuan *et al.*, 2014; Wakizono *et al.*, 2021). Upon short-term Ouabain application, Schmiedt *et al.* showed, that apoptosis in in spiral ganglion cells was present one to three days post treatment (Schmiedt *et al.*, 2002). Similarly, a study by Yuan *et al.* in mice revealed that Ouabain-application selectively destroys type I spiral ganglion cells while sparing type II spiral ganglion cells and inner and outer hair cells, suggesting this a suitable

model for cochlear nerve degeneration and auditory neuropathy in mouse (Yuan *et al.*, 2014) (Figure 1.3).

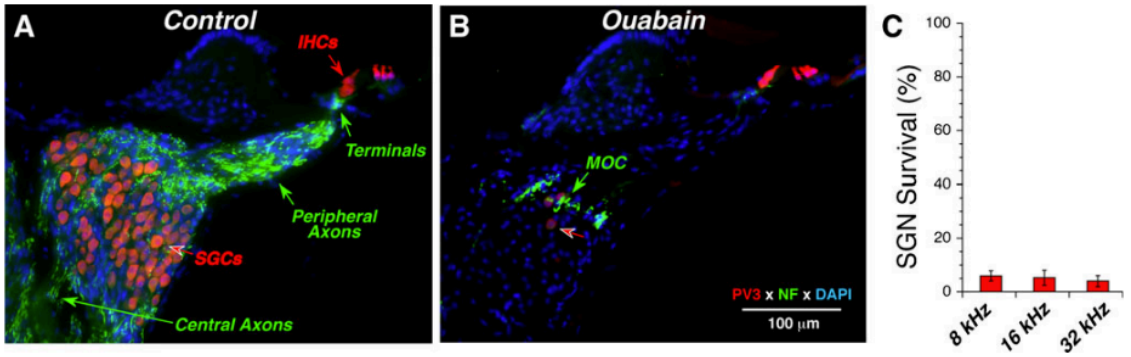

Figure 1.3 Mouse model for auditory neuropathy: Ouabain-induced cochlear nerve degeneration.
Ouabain treatment can eliminate 95 % of spiral ganglion cells while leaving the inner and outer hair cells intact. (**A-B**) Antibody staining against parvalbumin3 (PV3), labeling spiral ganglion cells (SGCs) and hair cells, and anti-neurofilament (anti-NF), labeling auditory nerve fibers in untreated, control ears (**A**) and Ouabain-treated ears one week post treatment (**B**). In untreated control ears, anti-NF shows myelinated central and peripheral axons of auditory nerve fibers as well as unmyelinated terminals below the inner hair cells. In contrast, in Ouabain-treated ears, only a few spiral ganglion cells remained (red arrow). (MOC: medial olivocochlear neuron of the efferent system). (**C**) Quantification of spiral ganglion neuron survival in Ouabain-treated ears (n=6) normalized to place-matched counts from control ears (n=6) reveals a survival rate of roughly 5 %. (from: Yuan *et al.,* 2014)

Pharmacogenetic lesion paradigms

In principle, pharmacogenetic lesion paradigms allow for the targeted ablation of specific cell types, for instance to study whether the loss of hair cells cause a secondary degeneration of sensory neurons. The Cre-LoxP system enables conditional gene expression that can be controlled in a spatial and temporal manner (Kim *et al.*, 2018). In mice, the transgenic Cre-inducible diphtheria toxin receptor (*iDTR*$^{+/+}$) is a powerful tool to specifically ablate a cell type of interest. When crossed to the spiral ganglion-specific Cre driver line, the diphtheria toxin receptor is expressed exclusively in spiral ganglion cells which leads to cell death of spiral ganglion cells upon diphtheria toxin application (Pan *et al.*, 2017; Hu *et al.*, 2021).

Mutant animal models resembling age-related hearing loss

Several mouse models have been generated to study ageing and age-related diseases (Schriner *et al.*, 2005; Lindsten *et al.*, 2000; Martinou *et al.*, 1994). Some of these mouse models also exhibited age-related sensorineural hearing loss, turning them into valuable tools to study the development and progression of age-related hearing loss (Han and Someya, 2013).

1.9 Replacing what is lost: new neurons for the mammalian inner ear

In mammalian species, hair cells and sensory neurons are only produced during fetal stages. To compensate for a loss of neuronal cells in the inner ear during later stages of development or even adulthood, several approaches can be considered: the direct reprogramming of resident cells, the reactivation of potential stem cell-like cells or the transplantation of exogenous stem/progenitor cells.

The prerequisite for the first approach is to find a suitable resident cell to target for direct reprogramming. In the zebrafish retina, Müller glia serve as a neural stem cell and the key players in regeneration: upon injury, Müller glia get reactivated and replace lost neurons, indicating the potential of glial-like cells to serve as precursor cells for neurons (Lenkowski and Raymond, 2014). Interestingly, recent studies have also demonstrated the potential of glial cells of the CNS to be targeted and reprogrammed into functional neurons with high efficiency *in vitro* and *in vivo* (Meas, Zhang and Dabdoub, 2018). Similarly, glia cells closely associated with the neurons of the inner ear can be reprogrammed *in vitro* into neuron-like cells that display a transcriptome profile resembling that of endogenous inner ear neurons (Noda *et al.*, 2018), suggesting glia cells to be a potential target for direct reprogramming also *in vivo*.

Besides using glial-like cells for direct reprogramming, reactivation of quiescent, resident stem cell-like cells could be used to replace lost neurons. Indeed, several studies revealed, that neurosensory stem cells exist in the adult mammalian inner ear (Bermingham *et al.*, 1999; Li *et al.*, 2003; Ma *et al.*, 1998). Using sphere-forming assays, Diensthuber et al, showed, that the early postnatal spiral ganglion contains cells capable of forming neurospheres similar to those obtained from the brain. These neurospheres kept their proliferative capacity and stem/progenitor status after propagation which allowed to maintain and even expand these cells *in vitro* (Diensthuber *et al.*, 2014).

Efforts are made to target these neurosensory stem cells *in vivo* to proliferate and give rise to new neurons. However, these cells are also a valuable source for obtaining cells for transplantations. Additionally, also various other types of stem cells such as embryonic stem cells, induced pluripotent stem cells or mesenchymal stem cells have been tested for their potential to replace lost neurons via cell transplantation (Shi and Edge, 2013; Reyes *et al.*, 2008). Besides the source, also the maturation state of the transplanted cell can influence the success of the transplantation: the used stem cell can either be directly transplanted or differentiated into neuronal precursor cells or neurons prior to transplantation. Recently, Chang et al. could show that transplanted embryonic stem cells survive and migrate to the cochlea after an Ouabain mediated loss of neurons in the inner ear of mice. Furthermore, the transplanted embryonic stem cells increased the auditory connection to the central auditory pathway (Chang *et al.*, 2021). Other

studies suggest to transplant embryonic stem cells after differentiating them to neural progenitors or even more mature neurons to avoid the risk of teratoma formation by the transplanted embryonic stem cell. In this context, Shi et al showed, that the transplantation of neural progenitor cells to be more successful than the transplantation of differentiated neurons, which are more prone to undergo apoptosis when transplanted in a suspension (Shi *et al.*, 2007).

However, if reprogramming of inner ear glia into neurons or the transplantation of exogenous stem/progenitor cells are successful *in vivo*, the cellular properties of the reprogrammed cells to ensure functional restoration have yet to be studied. Hence, an in-depth characterization of genes and pathways involved in successful neuronal regeneration can help to increase/optimize the outcome of cell replacement therapies.

1.10 Single cell transcriptome analysis – unraveling a cell's identity and state

Transcriptome analyses have excel at unraveling genes and signaling pathway that play a role in the context of regeneration (Bideau *et al.*, 2021). In recent years, single cell RNA sequencing (scRNAseq) technologies have revolutionized the field of genomics and became the key technology to investigate cell heterogeneity, developmental biology and regeneration (Chen, Ning and Shi, 2019). In contrast to previously used methods such as bulk RNA sequencing or microarray, scRNAseq allows to analyze gene expression patterns on a single cell level to identify different cell types and cell states in the given sample. Currently, 10x Genomics Chromium and Smart-Seq2 are the most popular platforms for scRNAseq (Wang *et al.*, 2021). 10x Genomics Chromium is a droplet-based scRNAseq approach that can analyze thousands of cells at once, which enables to detect also rare cell populations. In contrast, Smart-seq2 is a plate-based technique, hence analyzing only a finite number of cells but with a higher sequencing depth.

The subsequent bioinformatical analysis of transcriptomic data set obtained from scRNAseq identifies the transcriptional similarities and differences between single cells. Especially differentially expressed genes are used to define certain cell populations and cell states. To visualize these multidimensional matrices of thousands of gene expression levels in a 2D dimensional map, dimensionality reduction tools such as principal component analysis (Pearson, 1901), t-distributed stochastic neighbor embedding, t-SNE (Kobak and Berens, 2019) and Uniform Approximation and Projection (UMAP) (McInnes *et al.*, 2018) are applied. In these transcriptomic maps, cells with similar transcriptomic profiles are located closer to each other than cells with a different transcriptomic profile. Additionally, more advanced bioinformatical analysis tools such as RNA velocity or pseudo-temporal ordering offer a more in-depth understanding of cell differentiation trajectories and

dynamic biological processes (La Manno *et al.*, 2018; Herring *et al.*, 2018; Campbell and Yau, 2018).

2. Aims of this study

Sensorineural hearing loss is caused by the loss of hair cells and/or their innervating sensory neurons in the inner ear and affects millions of people worldwide. Since both cell types are only produced during fetal stages in mammals, including humans, a loss of these cell types and the resulting consequence are irreversible. Zebrafish, however, exhibit a lifelong generation of hair cells. However, whether this constant generation of hair cells is accompanied by adult neurogenesis in the zebrafish statoacoustic ganglion (SAG) remains unknown.

Additionally, in contrast to mammals, zebrafish possess a remarkable regenerative capacity and are able to repair a variety of complex organs and tissues upon damage, including neuronal tissue in the CNS and hair cells in the inner ear and lateral line. Again, how the adult SAG reacts upon lesion and whether it is able to generate new sensory neurons to connect regenerated hair cells to the brain and replace lost neurons has not been studied to date.

Therefore, this study aims to identify and characterize a potential neurogenic niche within the juvenile and adult SAG and investigate its potential regenerative capacity using a suitable lesion paradigm. To address these aims, this thesis was divided into two main parts:

(I) Characterization of the zebrafish SAG during growth and homeostasis

(a) extensive histological analysis using different transgenic reporterlines and immunohistochemistry to identify different cell populations and landmarks in the juvenile and adult SAG
(b) transcriptome analysis using single cell RNA sequencing to identify novel marker genes for neuronal stem and progenitor cell populations in the juvenile and adult SAG

(II) Exploring the regenerative capacity of the adult zebrafish SAG

(a) establishing a suitable auditory/vestibular neuropathy model for the adult zebrafish SAG
(b) analysis of the regenerative response upon lesion focusing on potential reactive proliferation and reactive neurogenesis

3. Material and methods

3.1 Material

3.1.1 Technical equipment

Table 3.1 Technical equipment

Equipment	Manufacturer
AxioCam MRC	Zeiss AG
Axio Imager.Z1 with Apotome.2	Zeiss AG
BD FACS Aria III	BD Bioscience
BD Microlance™ 3 30 G ½"	Beckton Dickinson
fluorescent lamp	Olympus K.K.
HM 650 Kryostat	Microm
MACS SmartStrainers 70 µm	Miltenyi Biotec
Mastercycler PCR machine	Eppendorf SE
Microliter™ #75 syringe	Hamilton
Nx70 Kryostat	Thermo Fisher Scientific
stereomicroscope SZX10/16/MVX10	Olympus K.K.
STP 420 Paraffin-Infiltration-Processor	Thermo Fisher Scientific
swan neck lamp, KL 1500 LCD	Olympus K.K.
thermocycler	Eppendorf comfort
thermomixer	Eppendorf comfort
tube rotator MACSmix	Miltenyi Biotec

3.1.2 Transgenic fish lines

Table 3.2 Trangenic fish lines

Line	referred to as	Publication
TgBAC(neurod1:EGFP)nl1	*neurod*:GFP	(Obholzer *et al.*, 2008)
Tg(pou4f3:GAP-GFP)s356	*pou4f3*:GFP	(Xiao *et al.*, 2005)
Tg(her4.3:GFP)y83	*her4.3*:GFP	(Yeo *et al.*, 2007)
TgBAC(nes:EGFP)tud100	*nestin*:GFP	(Kaslin *et al.*, 2009)
Tg(hsp70l:loxP-DsRed2-loxP-nlsEGFP)tud9	*hsp70l*:loxP-DsRed2-loxP-nlsEGFP	(Knopf *et al.*, 2011)
Tg(nestin:mCherry-T2A-CreER^{T2})tud45	*nestin*:mCherry-T2A-CreER^{T2}	(Schwarzer *et al.*, 2020)
Tg(sox2:sox2-P2a-GFP)stl84	*sox2*:GFP	(Shin *et al.*, 2014)
Tg(pcna:EGFP)	*pcna:GFP*	(Celotto, 2022)
Tg(-3.5ubb:SECHsa.ANXA5-mVenus,cryaa:mCherry)	*ubiq*:secAnnexinV-mVenus	(Morsch *et al.*, 2015)
Tg(elavl3:EGFP)	*elavl3*:GFP	(Park *et al.*, 2000)

3.1.3 Kits

Table 3.3 Kits

Purpose	Kit	Company
cell death detection (TUNEL assay)	ApopTag Red In Situ Apoptosis Detection Kit	Millipore
cell dissociation	Neural Tissue Dissociation Kit (P)	Miltenyi Biotec
fluorescent ISH	TSA Plus Cy3/Cy5 kit	Perkin-Elmer

3.1.4 Buffer and reagents

All chemicals were purchased from Applichem, Merck, Roth, Thermo Fischer Scientific and Sigma-Aldrich if not stated otherwise.

Table 3.4 Buffers and reagents

Buffer/reagent	Composition and preparation
10x salt	195 mM NaCl, 89 mM Tris-HCl, 11 mM Trizma 50 mM $NaH_2PO_4H_2O$, 50 mM EDTA
2 % agarose gel	2 g agarose in 100 ml 1x TAE buffer, add 1 µl ethidium bromide after dissolving in microwave
2 % DIG-blocking reagent	2 % Digoxigenin Blocking Reagent in MABT
20x SSC	SSC: 3 M NaCl, 0.3 M Na_3Citrate2xH_2O, adjust to pH 6.0 with 1 M citric acid SSCT: add 0.01 % Tween-20 (w/v) to 1x SSC
4 % PFA	dilute 16 % Formaldehyde solution (Thermo Fisher Scientific) 1:4 with 0.1 M phosphate buffer
50x TAE buffer	242 g Trizma base, 57.1 ml acetic acid, 100 ml 0.5 M EDTA, 1 l H_2O (pH 8.5)
DEPC H_2O	1 ml diethylpyrocarbonate in 1 l H_2O, autoclave
E3 medium	5 mM NaCl, 0.17 mM KaCl, 0.33 mM $CaCl_2$ x H_2O, 0.33 mM $MgSO_4$ x 7 H_2O, 0.0002 % methylene blue (pH 6.5)
gelatin/sucrose buffer	7.5 g gelatin, 20 g sucrose, fill up to 100 ml with 0.1 M phosphate buffer; dissolve via heating
Glycerol (80 %)	80 % (v/v) Glycerol in PBS
HEPES buffer	for 500ml: dissolve 119,5 g HEPES ($C_8H_{17}N_2NaO_4S$) in 400-450 ml ddH_2O for 30-

	60 min (no heat), adjust pH to 7,4 with 2-5 M NaOH, fill up to 500 ml
hybridization buffer	Hyb-: 50 % deionized formamide, 1x salt, 10 % dextran sulphate, 1x Denhardts, mix in this order to dissolve Hyb+: add 0.5 mg torula yeast RNA and 50 µg heparin to Hyb- buffer
maleic acid buffer (MAB)/MABT	MAB: 100 mM maleic acid, 150 mM NaCl, adjust to pH 7.5 with NaOH pellets, sterile filter MABT: add 0.1 % Tween-20 (w/v) to 1x MAB
MS222 / Tricaine (Mesab)	2 g Ethyl 3 aminobenzoate methansulfate salt, 5 g Na_2HPO_4 x H_2O, 500 ml H_2O
Ouabain octahydrate	Sigma
Phosphate buffered saline (PBS)	1.7 mM KH_2PO_4, 5.2 mM Na_2HPO_4, 150 mM NaCl
PBST	add 0.1 % Tween-20 (w/v) to 1x PBS
PBSTx	add 0.3 % Triton-X (w/v) to 1x PBS
phosphate buffer	0.1 M: 100 ml 1 M Na_2HPO_4 x $2H_2O$, 400 ml 1 M NaH_2PO_4 x $2H_2O$, fill up to 5 l with DEPC-H_2O, adjust to pH 7.4, sterile filter
Sodium citrate buffer	10 mM: 2.94 g sodium citrate (2x H_2O) in 1 l H_2O, adjust to pH 6.0 with acetic acid
Sodium tetraborate buffer	0,1 M: for 1 l: dissolve 38.137 g sodium tetraborate (decamer 10xH_2O) in 950 ml H_2O via stirring; adjust to pH 8,5 first with 37 % HCl then with 2 M HCl, fill up to 1 l
sucrose (20 % w/v)/EDTA buffer	for 2 l: dissolve 372.24 g Tritriplex III (0.5 M EDTA) in 1.5 l of 0.1 M phosphate buffer, adjust to pH 7.5 using 5 M NaOH, add 400 g sucrose, fill up to 2 l, sterile filter
Tris-HCl buffer	50 mM Trizma Base in H_2O, adjust to pH 7.5 or pH 8-8.5 with HCl
tyramid solution	amplification buffer, 1:500 tyramid Cy3
washing solution for ISH	15 ml 10x SSC, 150 ml formamide, fill up to 300 ml with DEPC-H2O

3.1.5 Antibodies

Table 3.5 Primary antibodies

Antigen	Species	Isotype	Company	Catalogue Code	Dilution
BrdU	rat	polyclonal	Abcam	ab6326	1:500
Calretinin	rabbit	polyclonal	Swant Inc.	7699/4	1:2000
ClaudinK	rat	polyclonal	non-commercial (Münzel *et al.*, 2012)		1:1000
GFP	chicken	polyclonal	Abcam	ab13970	1:2000
HuC/D	mouse	IgG2b, k	Thermo Fisher Scientific	A21271	1:500 - 1:300
L-Plastin	rabbit	polyclonal	Generated by the CRTD Antibody Facility		1:1000
Mbp	rabbit	polyclonal	non-commercial (Pinzon-Olejua *et al.*, 2017)		1:100
mCherry	mouse	IgG1	Clontech	632543	1:500
PCNA	mouse	IgG2a, k	Dako	M0879	1:500
Sox2	rabbit	polyclonal	Millipore	AB5603	1:2000 - 1:1000
Zrf1/GFAP	mouse	IgG1	Zebrafish International Resource Center (Trevarrow, Marks and Kimmel, 1990)	CM-Zrf1-OG2B96	1:100

Table 3.6 Secondary antibodies

Secondary antibody	Fluorophore	Company	Catalogue code	Dilution
Goat anti-Mouse IgG (H+L	Alexa Fluor 555	Thermo Fisher Scientific	A21424	1:500
Goat anti-Mouse IgG1	Alexa Fluor 488	Thermo Fisher Scientific	A21121	1:500
Goat anti-Mouse IgG1	Alexa Fluor 555	Thermo Fisher Scientific	A21127	1:500
Goat anti-Mouse IgG1	Alexa Fluor 633	Thermo Fisher Scientific	A21126	1:500
Goat anti-Mouse IgG2a	Alexa Fluor 488	Thermo Fisher Scientific	A21131	1:500
Goat anti-Mouse IgG2a	Alexa Fluor 555	Thermo Fisher Scientific	A21137	1:500

Goat anti-Mouse IgG2a	Alexa Fluor 633	Thermo Fisher Scientific	A21136	1:500
Goat anti-Mouse IgG2b	Alexa Fluor 488	Thermo Fisher Scientific	A21141	1:500
Goat anti-Mouse IgG2b	Alexa Fluor 555	Thermo Fisher Scientific	A21147	1:500
Goat anti-Mouse IgG2b	Alexa Fluor 633	Thermo Fisher Scientific	A21146	1:500
Goat anti-Mouse IgG2b	Alexa Fluor 647	Thermo Fisher Scientific	A21242	1:500
Goat anti-Chicken IgY (H+L)	Alexa Fluor 488	Thermo Fisher Scientific	A11039	1:500
Goat anti-Rabbit IgG (H+L)	Alexa Fluor 488	Thermo Fisher Scientific	A11034	1:500
Goat anti-Rabbit IgG (H+L)	Alexa Fluor 555	Thermo Fisher Scientific	A21428	1:500
Goat anti-Rabbit IgG (H+L)	Alexa Fluor 633	Thermo Fisher Scientific	A31576	1:500
Goat anti-Rat IgG (H+L)	Alexa Fluor 555	Thermo Fisher Scientific	A21434	1:500

3.1.6 Cell dyes

Table 3.7 Cell dyes

Dye	Company	Concentration
4',6-Diamidin-2-phenylindol (DAPI)	Thermo Fisher Scientific	1 mg/ml (use 1:5000-1:3000)
CellTracker Red CMTPX Dye	Thermo Fisher Scientific	1 µg/µl
Calcein Violet 450 AM viability dye	Thermo Fisher Scientific	2 mM (use 1:500)

3.1.7 *In situ* hybridization probes

Table 3.8 *In situ* hybridization probes

Gene	Publication
GFP	(Andermann, Ungos and Raible, 2002)
neurod	(Hans and Campos-Ortega, 2002)

3.1.8 PCR primers

Table 3.9 Primers used for PCR

Gene	Primer	Sequence	Product length
neurod	forward	5'-CGCAAGCCACACTAGACTTC-3'	177 bp
	reverse	5'-GCTGCTGTGACACTTGTCG-3'	
nestin	forward	5'-CTTCAACATCTTCAGGCCCAAG-3'	187 bp
	reverse	5'-GTGTTGGTCTGTCGATTCTCAG-3'	

3.2 Methods

3.2.1 Zebrafish husbandry and lines

Zebrafish were kept and bred according to standard procedures (Brand, Granato and Nüsslein-Volhard, 2002; Westerfield, 2000). All experiments were carried out using juvenile (2 and 3 months old) and adult (6 months and older) zebrafish from wild type stocks with the AB genetic background and transgenic lines as listed in Table 3.2. Besides date of birth and genotype, also sex and body length (measured from tip of the mouth to the basis of the caudal fin) of every analyzed fish was taken. For the characterization of the SAG during growth and homeostasis (see chapter 4.1) age and body length were used as a staging criteria: body length of 2 month old fish varied from 15.5 to 19 mm, body length of 3 month old fish varied from 20 to 27 mm and body length of adult fish (6 months and older) varied from 27 to 34 mm.

3.2.2 Lesion of the statoacoustic ganglion via injection into the otic capsule

To study the regenerative capacity of the zebrafish statoacoustic ganglion (SAG), we established a lesion assay based on fluid injection into the otic capsule. Fish were anaesthetized in 0.024 % Tricaine (Sigma-Aldrich) diluted in fresh fishwater. During the procedure, the anesthetized fish were placed left-sided under a stereomicroscope with dorsal to the top and rostral to the right on a tissue soaked with the Tricaine-fishwater solution laying in a petri dish. Animals were covered with a second Tricaine-fishwater soaked tissue to keep them moist. After creating a small hole in the triangular shaped bone above the gills at the height of the cerebellum using a 20 gauge needle, a Hamilton syringe was carefully inserted approx. 1 to 1,5 mm vertically along the dorsal-ventral axis to place it above the anterior part of the SAG without rupturing it. To visualize the area of injection and prove the fluid administration to the SAG, a fluorescent dye (CellTracker™ Red CMTPX Dye, Thermo Fisher Scientific) was slowly injected into the otic capsule in a first round of experimental trials. For all other experiments, three different approaches were performed, namely sham treatment, NaCl injection and Ouabain injection. For sham-treated animals, the Hamilton syringe was retracted from the otic capsule without injecting any fluid. For NaCl and Ouabain injections, 0,5-0,8 µl fluid (0.9 % NaCl solution or 100 µM Ouabain, dissolved in 0.9 % NaCl) were slowly injected into the otic capsule. Afterwards fish were transferred to cages with fresh fishwater for recovery. Around 60-90 % of all treated fish temporarily showed circular swimming behavior after regaining consciousness, which usually lasted 15-30 min and only in very rare cases longer than 1 hour. Minor bleedings at the injected side occurred in 50-75 % of all experimental fish.

3.2.3 Bromodesoxyuridine (BrdU) pulse chase experiment

To label cells in S-phase of the cell cycle, juvenile and adult transgenic *neurod*:GFP zebrafish were immersed for 24 hours in 5 mM BrdU (Sigma-Aldrich) solution (modified after Grandel *et al.*, 2006). Therefore, BrdU was dissolved in E3 medium and pH was adjusted to pH 7.2 – 7.4 using freshly prepared HEPES buffer. Depending on age and size of the fish, up to 5 fish were kept under oxygen supply in beakers containing 500 ml of the 5 mM BrdU solution. After 24 h, fish were kept in the normal fishwater for 0, 7, 15 and 28 days in case of the juvenile (3 months old) zebrafish and for 0, 7, 14 and 29 days in case of the adult (8 months old) zebrafish before fish were sacrificed for analysis.

To analyze reactive neurogenesis following reactive proliferation in the context of regeneration, transgenic *neurod*:GFP zebrafish were immersed twice in 5 mM BrdU (Sigma) solution (modified after (Grandel et al., 2006)) for each 24 hours from 2 to 3 and from 4 to 5 days post lesion with a 24 hours resting period. Again, BrdU was dissolved in E3 medium and the pH was adjusted to pH 7.2-7.4 using freshly prepared HEPES buffer. Up to 5 fish were kept under oxygen supply in beakers containing 500 ml of the 5 mM BrdU solution. After the second BrdU pulse, fish were kept in the normal fishwater for 14 days prior to analysis.

3.2.4 Long term lineage tracing

To trace nestin-derived cells in the SAG, the Cre-driver line *Tg(nestin:mCherry-T2A-CreER^{T2})tud45* was crossed to the Cre-dependent reporter line *Tg(hsp70l:loxP-DsRed2-loxP-nlsEGFP)tud9*. Subsequently, 4-hydroxy-tamoxifen (4-OHT; Sigma-Aldrich, H7904) and heat shock treatments during embryonic stages were performed as previously described (Hans et al., 2011; Hans et al., 2009). Briefly, recombination was achieved by immersing embryos from 8 to 24 hpf in 0.5 µM 4-OHT in E3 medium. At 24 hpf, embryos were heat shocked at 37 °C for 0.5 hours and GFP-positive embryos were raised. At 6 months, zebrafish were placed in a heat shock tank and heat shocked 6 times for 1 hour at 37 °C with 11 hours intervals at 27 °C between the heat shocks. Afterwards, zebrafish were sacrificed to analyze nestin-derived cells.

3.2.5 H&E Staining

Wild type zebrafish were sacrificed and the skull plate was carefully removed with forceps to enable better fixation of the otic tissue underneath the brain. Samples were fixed overnight in 4 % paraformaldehyde in 0.1 M phosphate buffer (PB), pH 7.5 at 4 °C and then incubated for 2 days in 0.5 M EDTA in 0.1 M PB, pH 7.5 at 4 °C, refreshing the solution after the first day. Afterwards, samples were

washed twice in Phosphate-buffered saline (PBS) and prepared for paraffin embedding which was done in a Paraffin-Infiltration-Processor (STP 420, Thermo Fisher Scientific) according to the following program: 3 min ddH_2O;70 min 70 % EtOH; 90 min 96 % EtOH; 70 min 96 % EtOH/ 90 min 96 % EtOH; 70 min 100 % EtOH; 90 min 100 % EtOH; 60 min Xylol; 90 min Xylol/ 2x 60 min paraffin at 60 °C; 70 min paraffin at 60 °C and 90 min Parrafin at 60 °C. After dehydration and paraffin infiltration, samples were embedded using an Embedding Center EG1160 (Leica) and cut into 10 µm thick sections using an microtome (Microtom HM 355S; Thermo Fisher Scientific/Microm). Subsequently, samples were counterstained using haematoxylin/eosin (Hematoxylin Solution, Gill No. 2, Sigma-Aldrich) and covered with Epredia™ Richard-Allan Scientific™ Mounting Medium (Thermo Fisher Scientific).

3.2.6 Tissue preparation for immunohistochemistry

Experimental animals were sacrificed and the skull plate was carefully removed with forceps to enable better fixation of the otic tissue adjacent/underneath the brain. Samples were fixed overnight in 4 % paraformaldehyde in 0.1 M phosphate buffer (PB), pH 7.5 at 4 °C and then incubated overnight in 20 % sucrose/20 % EDTA in 0.1 M PB, pH 7.5 for decalcification and cryoprotection. Subsequently, samples were embedded in 7.5 % gelatin/20 % sucrose and stored at -80 °C. Samples were cut into consecutive 12 µm thick transverse sections using a Microm HM 560 Kryostat or Thermo Scientific CryoStar NX70 Kryostat and stored at -20 °C. For all regeneration-related experiments, samples were split into two series.

3.2.7 Immunohistochemistry

For immunohistochemistry, slides were kept in the dark using washing cuvettes and humidity chambers covered with aluminum foil throughout all steps. First, sections were post-fixed for 20-30 min with 100 % ice cold methanol at room temperature under the hood until the methanol evaporated. Afterwards, sections were washed once with PBS and 3 times with PBS containing 0.3 % Triton X-100 (PBSTx 0.3 %) and were incubated at 4 °C overnight with primary antibodies in PBSTx 0.3 % (Table 3.5). Next day, sections were washed 3 times with PBSTx 0.3 % before incubation with Alexa 488-, 555-, 633- and 647-conjugated secondary antibodies (Table 3.6) in PBSTx 0.3 % for two hours at room temperature. To counterstain nuclei, 4,6-diamidino-2-phenylindole (DAPI, 1 µg/ml, Invitrogen) was added to the secondary antibody-containing solution. Sections were washed again 3 times with PBSTx 0.3 %. If DAPI was not added to the secondary antibody-mix, slides were incubated in a washing cuvette with a reusable DAPI solution (DAPI

1 µg/ml in PBSTx 0.3 %) for 15-30 min and subsequently washed for 3 times with PBSTx 0.3 %. For the final washing step slides were washed in PBS and then mounted in 80 % glycerol/PBS. Mounted samples were stored in the dark at 4 °C.

3.2.7.1 Modification for CellTracker Red dye

Samples from CellTracker Red dye-injected fish were washed 3 times in PBSTx 0.3 % for 10 min. Subsequently, samples were incubated with DAPI (1 µg/ml) diluted in PBSTx 0.3 % for 30 min to counterstain nuclei, washed again 2 times in PBSTx 0.3 % and once in PBS before mounting them in 80 % glycerol/PBS.

3.2.7.2 Modifications for PCNA and HuC/D staining

For immunohistochemistry against PCNA and/or HuC/D, an antigen retrieval was performed prior to incubation with primary antibodies. Therefore, slides were incubated in 85–95 °C preheated sodium citrate buffer, pH 6 (10 mM) for 15 min, followed by a 10 min cool down in the heated sodium citrate buffer at room temperature.

3.2.7.3 Modifications for Sox2 staining

For immunohistochemistry against Sox2, an antigen retrieval was performed prior incubation with primary antibodies. Therefore, slides were incubated in 99 °C preheated sodium citrate buffer, pH 6 (10 mM) for 10 min, followed by a 10 min cool down in the heated sodium citrate buffer at room temperature.

3.2.7.4 Modifications for BrdU staining

Since samples were co-stained for *neurod*:GFP, BrdU and HuC/D and BrdU and HuC/D both require different antigen retrieval, immunohistochemistry was performed sequentially. First, samples were stained for *neurod*:GFP and HuC/D as described above without adding DAPI while incubating with the secondary antibodies. Instead of mounting, samples were washed again with PBSTx 0.3 % and afterwards slides were incubated for 13 min at 37 °C in preheated 2 M HCl to retrieve the antigenicity of BrdU. Afterwards, slides were washed 10 min in sodium tetraborate buffer and then with PBSTx 0.3 %. Slides were incubated with primary antibody against BrdU overnight at 4 °C, washed with PBSTx 0.3 %, incubated with all secondary antibodies plus DAPI for 2 hours at room temperature, and then washed again and mounted as described above.

3.2.8 TUNEL assay

To analyze the presence of apoptotic cells, the ApopTag Red In Situ Apoptosis Detection Kit (ApopTag Chemicon S7165) was used according to the manufacturer's instructions to perform terminal deoxynucleotidyl transferase-mediated biotinylated UTP nick end labeling (TUNEL). Since the TUNEL assay was combined with a neuronal staining (*elavl3*:GFP or Calretinin), samples were washed three times in PBSTx 0.3 % after the rhodamine staining, and subsequent incubation with the primary and secondary antibodies was performed as described above.

3.2.9 *In situ* hybridization

Probe synthesis and *in situ* hybridization was essentially carried out as previously described (Westerfield, 2000). Following cDNA probes were used to detect expression: *neurod* (Andermann et al., 2002) and *gfp* (Hans and Campos-Ortega, 2002) (Table 3.8).

3.2.10 Image acquisition

Images were taken in the light microscopy facility of the CMCB technology platform with either a ZEISS Axio Imager, upright microscope with Zeiss Plan-Apochromat 10x 0.45, 20x 0.8 and 40x 0.95 korr. objectives for magnification or a Zeiss – Axiovert 200M, inverted microscope with Zeiss Plan-Neofluar 10x 0.30 and Zeiss Plan-Apochromat 20x 0.8 or 40x 0.95 korr. objectives for magnification. An Axiocam MRm (1388*1040, 6.45*6.45µm) - b/w or an Axiocam MRc (1388*1040 pixel, 6.45*6.45µm) – color was used for detection. Sequential image acquisition was used in samples co-stained with multiple fluorophores. For imaging, Z-stacks were acquired to cover the full information in all three dimensions (typically 5-25 Z-planes with an interval of 0.4-1.5 µm depending on the NA of the objective). Images were processed using ZEN blue 2012 and Fiji. Close-up images were generated from the original overview image. For overview images, a maximum projection was taken from several Z-planes, whereas only 2-3 Z-planes were used for the close-up images. Figures were assembled using Adobe Illustrator CS5 and 2021.

3.2.11 Quantification and statistical analysis

For Chapter 4.1

Quantification of HuC/D-positive neurons in juvenile (2 month) and adult (8 month) zebrafish was done at the ZEISS Axio Imager upright microscope (see chapter 4.1.3). Every HuC/D-positive cell in the entire anterior part of both SAGs as well as every section containing HuC/D-positive cells were counted on consecutive 12 µm thick sections, starting with the first section containing a HuC/D-positive cell and ending with the last section of the anterior part of the SAG. From these values the overall number of HuC/D-positive neurons, the average number of HuC/D-positive neurons per section, the section with the highest number of HuC/D-positive neurons as well as the thickness of the anterior part of the SAG containing HuC/D-positive neurons were calculated. Values from the right and from the left SAG of one fish were averaged resulting in one value per category and fish. In total, 4 fish were analyzed for both time points (n=4). For every other experiment, quantification was performed on acquired images comprising all Z-planes using the Fiji software. Therefore, one SAG per fish (either left or right side, depending on sample quality) was analyzed.

To analyze the neurogenic niche, a square covering the neurogenic area and the surrounding cells was chosen as the region of interests (see overview images in Figure 4.6, Figure 4.8, Figure 4.10: size of square: 132 mm^2).

For the proliferation analysis, cells were counted on twelve consecutive 12 µm thick sections. If a section was damaged, it was excluded from the analysis and less than twelve sections were taken into account. All values from one fish were averaged and the mean cell count/section was used for statistical analysis (in total: n=5 for the 2 months time point; n=3 for 3 months time point; n=4 for the 8 months time point).

For BrdU pulse chase experiments, cells were counted on either five or twelve consecutive 12 µm thick sections (if possible, see above). In case of all BrdU-positive cells, the average cell numbers/section for each fish, 4 fish per time point for the experiment with juvenile fish and 4-5 fish for the experiment with adult fish (time point: 0/7/14 days post treatment n=5; time point: 29 days post treatment n=4), was calculated and used for statistical analysis. For all other analysis, the average cell number/section for each fish was taken to calculate either the percentage of the specific cell group of all BrdU-positive cells (on a total of twelve sections) or the percentage of the specific cell group of all cells within that group of cell type, e.g. *neurod*:GFP/BrdU-positive cells per *neurod*:GFP-positive cells or HuC/D/BrdU-positive cells per HuC/D-positive cells, (on a total of five sections). The corresponding percentage values, one per fish and cell group, were used for further analysis.

For the *nestin* lineage tracing experiment, the number of HuC/D-positive and HuC/D/GFP-double positive cells (derived from recombined *nestin*:mCherry-T2A-CreER^{T2} cells) as well as the percentage of recombined HuC/D/GFP-double positive

cells from all HuC/D-positive cells was quantified in the whole SAG on twelve consecutive 12 µm thick sections from 3 fish (if possible, see above).

For statistical analysis the graph pad prism software was used to determine p-values with an one-way ANOVA test with a Tukey's Multiple Comparison Test for post hoc analysis. Chosen significance levels are ***p≤0.001; **p≤0.01; *p≤0.05, values above p>0.05 are not considered significant. Graphs are shown as scatter plots with bars or stacked bars with SEM.

For Chapter 4.3

Quantification was performed on acquired images comprising all Z-planes using the Fiji software. For analysis, the left and right SAG of each fish were taken: the untreated left SAG served as an internal control whereas the right SAG was treated as described above. To analyze proliferation and neurogenesis upon lesion in the neurogenic niche, a square covering the neurogenic area and the surrounding cells was chosen as the region of interests (see overview images in Figure 4.49 and Figure 4.51: size of square: 156.63 mm^2). From each individual, three section of one series of the anterior SAG showing the most *neurod*:GFP/PCNA-double positive cells were chosen for quantification. In cases with less than three sections containing *neurod*:GFP/PCNA-double positive cells in the neurogenic niche, up to three sections with the most *neurod*:GFP-positive cells were chosen. Following cell types were quantified in the region of interest: all *neurod*:GFP-positive cells, *neurod*:GFP/PCNA-double positive cells, *neurod*:GFP/HuC/D-double positive cells, *neurod*:GFP/PCNA/HuC/D-triple positive cells, only *neurod*:GFP-positive cells, all PCNA-positive cells, PCNA-positive cells in direct proximity to *neurod*:GFP-positive cells and only PCNA-positive cells. All values from one fish were averaged and the mean cell count/section was used for statistical analysis (n=3 fish for all conditions and time points; exception: NaCl-injected at 4 dpl). For statistical analysis, the graph pad prism software was used to determine p-values with a two-way ANOVA test with a Tukey's Multiple Comparison Test for post hoc analysis. Chosen significance levels are ***p≤0.001; **p≤0.01; *p≤0.05, values above p>0.05 are not considered significant. Graphs are shown as scatter plots with bars with SEM.

3.2.12 SAG dissection to obtain single cells

Prior to dissection, experimental animals were sacrificed and placed on their ventral side in a petri dish on ice. Initially, the skull plate was carefully removed using forceps. After cutting through the brain between optic tectum and cerebellum with dissection scissors, the entire anterior part of the brain including olfactory bulb, telencephalon and optic tectum was carefully removed. The cerebellum was carefully pushed to the side to localize the anterior part of SAG laying underneath the lapillus (otolith of the utricular macula). Both SAGs were cut in a 50-60° angle from the

frontal plane including the medial parts of the SAG entering the brain. Afterwards the brain was cut posterior of the brain stem and the brain was completely removed, so that also the posterior parts of the inner ear came into sight. The anterior part of the SAG attached to the utricular macula and semicircular canals, was collected using forceps to grab the otolith within the utricle and carefully lift out the utricular macula, parts of the adjacent semicircular canals and the anterior SAG. The lapillus was removed from the utricular macula either before or after taking out the anterior part of the inner ear. If possible, also parts of the posterior SAG were collected and otoliths were removed from the posterior part of the inner ear. All dissected tissue was placed into an Eppendorf tube and stored on ice.

For the establishment of the experimental pipeline (chapter 4.2.1)

In total, tissue from either eight male or eight female adult *Tg(neurod:GFP)* fish were pooled, generating two samples (male and female) with the tissue from 16 SAGs each. The whole dissection procedure did not take longer than 1:15 hours to minimize the degree of tissue degradation.

For the transcriptome analysis of the juvenile SAG (chapter 4.2.2)

In total, tissue from 12 adult double-transgenic *Tg(pcna:GFP) Tg(mCherry-T2a-CreER^{T2})* fish were pooled, generating one sample with the tissue from 24 SAGs each. The whole dissection procedure did not take longer than 1:15 hours to minimize the degree of tissue degradation.

For the transcriptome analysis of the adult SAG (chapter 4.2.12)

In total, tissue from 22 adult double-transgenic *Tg(pcna:GFP) Tg(mCherry-T2a-CreER^{T2})* fish were pooled, generating one sample with the tissue from 44 SAGs each. The whole dissection procedure did not take longer than 1:15 hours to minimize the degree of tissue degradation.

3.2.13 Cell dissociation

To dissociate the inner ear tissue including the SAG, the Neural Tissue Dissociation Kit (P) (Miltenyi Biotec, Germany) was used with some modifications to the manufacturer's protocol. After a primary enzymatic dissociation step in preheated enzyme mix 1 for 15 min at 28 °C, enzyme mix 2 was added to stop enzymatic dissociation. Subsequently, samples were further sheared mechanically by carefully pipetting samples up and down through fire-polished glass Pasteur pipettes (230 mm). Four different opening sizes were used starting with the pipette with the widest opening and additional incubation steps at 28 °C between changing

from pipette with a wide opening to one with a smaller opening. The acquired cell suspension was drop wise filtered through a Hanks´ Balanced Salt Solution (HBSS; without Ca^{2+} and Mg^{2+})-equilibrated 70 µm-cell strainer, collected in HBSS and the cell strainer was washed once with 5 ml HBSS. After centrifugation of the cell suspension for 15 min at 300 x g and 4°C, the supernatant was removed and cells where re-suspended in approx. 400 µl fresh HBSS and stored on ice.

3.2.14 FACS of cells derived from the SAG

Calcein violet with a final concentration of 8 µM was added to the cell suspension prior to fluorescence-activated cell sorting (FACS) to distinguish live from dead cells. FACS was performed with the help of Flow Cytometry Core Facility of the CMCB technology platform using a BD FACSAria III system.

3.2.14.1 For analysis of gene expression via RT-PCR

250 single living *neurod*:GFP-positive cells and 300 single living wildtype cells were sorted into PCR tubes and kept on ice.

3.2.14.2 For transcriptome analysis of the juvenile and adult SAG

Single living cells (*pnca*:GFP-positive; *pcna*:GFP/*nestin:*mCherry-T2a-CreER^{T2}-double positive and in case of the dataset generate of the adult SAG additionally also *nestin:*mCherry-T2a-CreER^{T2}-positive were sorted into 384 well plate for the following sequencing experiment via Smart-Seq2 (Illumina).

3.2.15 Analysis of genes expression in *neurod*:GFP-positive cells

To analyze gene expression of *neurod* and *nestin*, RNA isolation and cDNA synthesis (including a RNA amplification step from sorted *neurod*:GFP-positive cells as well as WT negative control) were performed by the Deep Sequencing Facility of the CMCB technology platform. Primers (see Table 3.9) were designed in a way that primers were either located in two neighboring exons (*neurod*) or that one primer was exon-junction spanning (*nestin* forward primer) and the corresponding primer was located in the neighboring exon (*nestin* reverse primer) to exclude amplification of amplicons derived from genomic DNA. Polymerase chain reaction (PCR) was performed with both samples (*neurod*:GFP-positive male, *neurod*:GFP-positive female) and genomic DNA (gDNA) sample as a negative control. Forty PCR cycles (initial denaturation step: 5 min/94 °C; 40x 30 sec/94 °C denaturation, 30 sec/59 °C annealing, 30 sec/72 °C elongation; final elongation step: 7 min/72 °C, ∞/4 °C) were used and the amplification products were separated on a 2 % agarose gel.

3.2.16 Transcriptome analysis via scRNAseq

3.2.16.1 Library preparation

The library preparation was done by the Deep Sequencing Facility (part of the DRESDEN-concept genome Center) according to the protocol described in (Willenborg *et al.*, 2022)with two modifications:

Transcriptome analysis of the juvenile SAG

Step 71, using the Vazyme TruePrep DNA Library Prep Kit V2, was used for library prep with 13 cycles for amplification.

Transcriptome analysis of the adult SAG

Step 72, using the Illumina DNA prep Tagmentation kit, was used for library prep with 15 cycles for amplification.

3.2.16.2 Bioinformatic analysis of the transcriptome data obtained via Smart-Seq2

The bioinformatic analysis of the juvenile and adult transcriptome data set was performed by Dr. Fabian Rost, member of the DRESDEN-concept Genome Center (CMCB Core Facility), according to the following protocol:

FastQC (http://www.bioinformatics.babraham.ac.uk/) was used to perform a basic quality control of the resulting sequencing data. Fragments were aligned to the zebrafish reference genome GRCz11 (+92 ERCC spike in sequences added) with support of the Ensembl 104 splice sites using the aligner gsnap (v2020-12-16) (Wu and Nacu, 2010). Counts per gene and cell were obtained based on the overlap of the uniquely mapped fragments with the same Ensembl annotation using featureCounts (v2.0.1) (Liao et al., 2014). To quantify expression of the mCherry and EGFP constructs, a fasta file containing the sequence of both constructs was created. The aligner bwa (0.7.17-r1188) was used to align the fragments to construct reference fasta file. Next, featureCounts was used to quantify the abundance of both constructs for each cell. The complete software stack for this upstream analysis is available in a singularity container under https://gitlab.hrz.tu-chemnitz.de/dcgc-bfx/singularity/singularity-base/ (tag v1.0.0). A count matrix for cells of juvenile fish, a count matrix for the cells from adult fish and a combined count matrix were created (the last one by simply merging the first two).

The count matrices generated above was further analyzed using scanpy 1.9.1 following current best practice (Wolf, Angerer and Theis, 2018; Luecken and Theis, 2019). For quality control, the cells were filtered based on the total number of counts, the number of detected genes, the percentage of counts in the 50 highest expressed genes, the percentage of mitochondrial counts, the percentage of ERCC spike-ins and

the percentage of counts that could be assigned to features (the last metric is an ouput of featureCounts). The counts were normalized with the scanpy function sc.pp.normalize_total. The normalized counts were log-transformed using the numpy function log1p. The top 5000 highly variable genes were detected using the scanpy function scanpy.pp.highly_variable_genes (n_top_genes= 5000). Cell cycle scores were computed using scanpy.tl.score_genes_cell_cycle in each sample separately. As genes associated to S-phase, the genes *mcm5, pcna, tyms, fen1, mcm2, mcm4, rrm1, unga, gins2, mcm6, cdca7a, dtl, prim1, uhrf1, si:dkey-185e18.7, hells, rfc2, rpa2, nasp, rad51ap1, gmnn, wdr76, slbp, ccne2, ubr7, pold3, msh2, atad2, rad51, rrm2, cdc45, cdc6, exo1, tipin, dscc1, blm, casp8ap2, usp1, pola1, chaf1b, brip1* and *e2f8* were used. As genes associated to G2/M phase, the genes *hmgb2a, cdk1, nusap1, ube2c, birc5a, tpx2, top2a, ndc80, cks2, nuf2, cks1b, mki67, tmpoa, cenpf, tacc3, smc4, ccnb2, ckap2l, aurkb, bub1, kif11, anp32e, tubb4b, gtse1, kif20ba, si:ch211-69g19.2, jpt1a, cdc20, ttk, kif2c, rangap1a, ncapd2, dlgap5, si:ch211-244o22.2, cdca8, ect2, kif23, hmmr, aurka, anln, lbr, ckap5, cenpe, ctcf, nek2, g2e3, gas2l3, cbx5* and *selenoh* were used. A principal component analysis (PCA) was performed on the highly variable genes (function scanpy.pp.pca using svd_solver='arpack'). For the combined count matrix, data integration was performed with harmony. A k-nearest-neighbour (knn) graph was computed using scanpy.pp.neighbors and a UMAP was computed using scanpy.tl.umap. Clustering was performed using a combination of unsupervised and supervised methods: An initial clustering was performed with scanpy.tl.leiden, with subsequent subclustering of some clusters. Next, to identify very small cell populations with less than 4 cells, gene scores were computed with scanpy.pp.score (the gene sets are shown in the heatmaps, Figure S.2 and Figure S.9) and cells with a score above 3 were assigned to the corresponding cell type. The source code for the analysis is available from Fabian Rost (fabian.rost@tu-dresden.de) upon reasonable request. The complete software stack for the downstream analysis is available as a Singularity container (https://gitlab.hrz.tu-chemnitz.de/dcgc-bfx/singularity/singularity-single-cell, tag v1.0.0).

4. Results

4.1 Characterisation of the juvenile and adult zebrafish statoacoustic ganglion (SAG)

4.1.1 Anatomy of the statoacoustic ganglion (SAG) in adult zebrafish

The vertebrate inner ear is a highly complex structure consisting of six sensory patches which are innervated by sensory neurons transferring the sensory stimulus from the sensory patches to the nuclei of the brainstem. The bipolar sensory neurons form the VIIIth cranial nerve, in zebrafish known as the statoacoustic ganglion (SAG). To study the morphological structure of the zebrafish SAG and the corresponding axonal projections of these bipolar SAG neurons, I performed H&E stainings on serial transversal sections spanning the complete inner ear of adult wild type zebrafish which reaches a size of several mm (depending on the size of the fish in the range of 3-4 mm). Consistent with 3D reconstructions of the larval SAG (Sapède and Pujades, 2010b), I found that in the adult zebrafish the axonal projections of the SAG neurons are distally a highly branched structure innervating all six sensory patches which are spread over almost the entire size of the inner ear along the rostral-caudal axis. These branches then conjoin to form a flat (in dorsal-ventral and lateral-medial dimension) and rather broad (measuring up to approx. 1 mm in rostral-caudal dimension in adult zebrafish) sheet-like structure entering the hindbrain underneath the cerebellum (Figure 4.1). As previous thin-sheet laser imaging with 3D reconstruction has shown in juvenile zebrafish (Santi *et al.*, 2009), the SAG is closely associated with the medioventral wall of the pars superior (dorsal part of the ear) containing the utricular macula as well as the anterior, lateral and posterior crista and the pars inferior (ventral part of the ear) harboring the saccular and lagenar macula.

Morphologically, the VIIIth cranial nerve can be divided into two parts:

(I) an anterior part shaped (simplified) in an elbow-like/U-like manner, entering the brain aligned along the dorsoventral axis and afterwards bending at a 90 ° angle aligned along the horizontal axis (Figure 4.1C, purple arrowhead) with an accumulation of neuronal cellbodies medioventrally of the utricular macula and

(II) a posterior part first forming a rod-like structure aligned along the dorsoventral axis when entering the brain (Figure 4.1D, purple arrowhead), then bending backwards aligning along the rostrocaudal axis and a short branch aligned along the horizontal axis with an acumulation of neuronal cellbodies mediodorsally of the saccular macula.

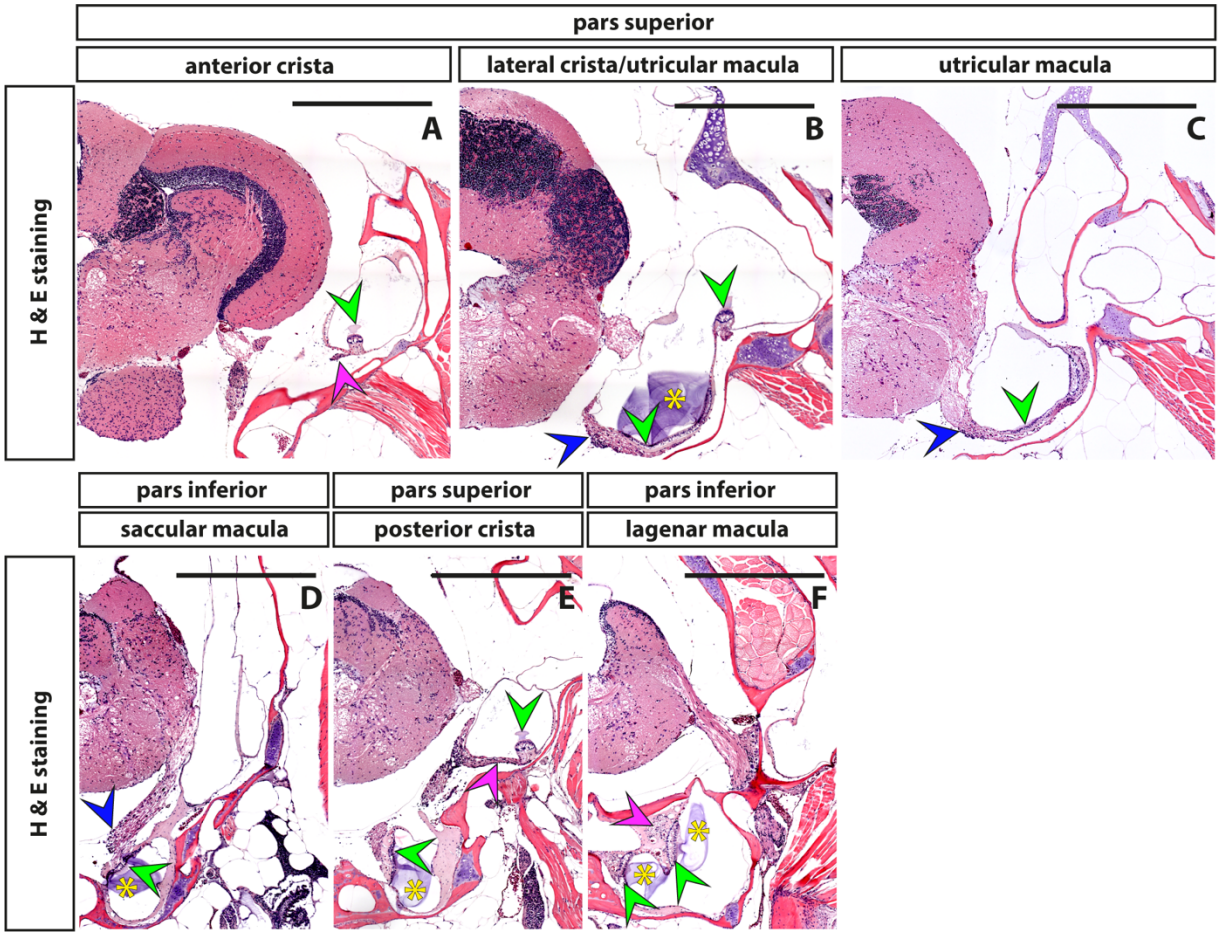

Figure 4.1 Anatomy of the adult zebrafish statoacoustic ganglion (SAG).
(**A**-**F**) Haematoxylin/eosin staining (H&E) of transversal cross sections through the entire inner ear of adult zebrafish with the six sensory patches innervated by sensory neurons of the statoacoustic ganglion (SAG) forming the VIIIth cranial nerve. The inner ear is devided in a dorsal part, the pars superior, consisting of the anterior (**A**), the lateral (**B**) and the posterior cristae (**E**) and the utricular macula (**B**,**C**), and in a ventral part, the pars inferior, including the saccular macula (**D**) and the lagenar macula (**F**). The VIIIth cranial nerve is distally highly branched to innervate all six sensory patches (green arrowheads) by axonal projections (magenta arrowheads) of SAG neurons, whereas the cellbodies of sensory neurons (dark purple, blue arrowheads) mainly reside medioventrally of the utricular macula (**B**, **C**) in the anterior part and mediodorsally of the saccular macula (**D**) in the posterior part of the SAG. The former position of the three otoliths lapillus (utricular macula), sagitta (saccular macula) and asteriscus (lagenar macula) are visible as light purple residual structures left after decalcification of the otoliths, close to the sensory patch (marked with a yellow asterisk). Scale bar: 200 µm; cross sections showing dorsal to the top and lateral to the right; distance from first section through semicircular canals till section of interest: anterior cristae (**A**) 0.5 mm; lateral cristae (**B**) 1.39 mm; utricular macula (**C**) 1.66 mm; posterior cristae (**D**) 2.53 mm; saccular macula (**E**) 3.15 mm; lagenar macula (**F**) 3.44 mm.

The anterior part lays directly underneath the utricular macula and innervates the anterior crista (Figure 4.1G), the lateral crista (Figure 4.1B,H) and the utricular macula (Figure 4.1C,I), which all belong to the pars superior. The posterior part connects the posterior crista (Figure 4.1E), both belonging to the pars inferior, to the brain.

4.1.2 Sensory neurons in the adult zebrafish SAG

To investigate the position of the neuronal cell bodies forming the SAG and their processes in reference to the brain and the six sensory patches, I performed an antibody staining labeling sensory neurons and sensory hair cells in the adult SAG on transversal cross sections covering the entire inner ear. To stain for sensory neurons, I used the pan-neuronal marker HuC/D labeling the neuronal cell soma and the calcium-binding protein Caretinin not only labeling the neuronal cell soma but also the neuronal processes in transgenic *pou4f3*:GFP animals expressing GFP in differentiated hair cells (Xiao *et al.*, 2005) (Figure 4.2). As described above, the VIIIth cranial nerve can be divided into two parts based on its orientation: the anterior part which is (simplified) aligned along the mediolateral axis, (Figure 4.2B, C) and the posterior part which is (simplified) aligned along the dorsoventral axis (Figure 4.2D) at the entrypoint of the brain on transversal sections.

Analyzed from rostral to caudal, the most anterior sensory patch innervated by SAG neurons is the anterior crista at the height of the posterior optic tectum/anterior cerebellum (Figure 4.2A). The first neuronal cell bodies of the anterior part of the SAG are present at the height of the cerebellum, where they reside ventromedially of the sensory hair cells of the utricular macula (Figure 4.2B, G). Further posterior still at the height of the utricular macula is the entry point of the neuronal processes into the brain (Figure 4.2C). The majority of neuronal cell bodies in the posterior part of the SAG innervating the saccular macula, lagenar macula and posterior crista, can be found on the first transversal sections of the posterior part of the SAG with the highest density of neuronal cell bodies at the ventral tip and fewer neuronal cell bodies scattered on the ventrodistal side of the nerve. More posterior, the nerve branches out to innervate the posterior crista and the lagenar macula, (Figure 4.2E, F).

Interestingly, HuC/D labels a subgroup of Calretinin-negative neurons mostly found ventromedial in the anterior part and ventrodistal in the posterior part of HuC/D-Calretinin-double positive neurons (Figure 4.2, H). Since sections of the anterior SAG where the nerve forms an elbow-like structure (Figure 4.2B, C) contain a high accumulation of mature neurons as well as the large sensory patch of the utricular macula and are relatively stable during tissue preparation, I primarily focused on this part for further studies.

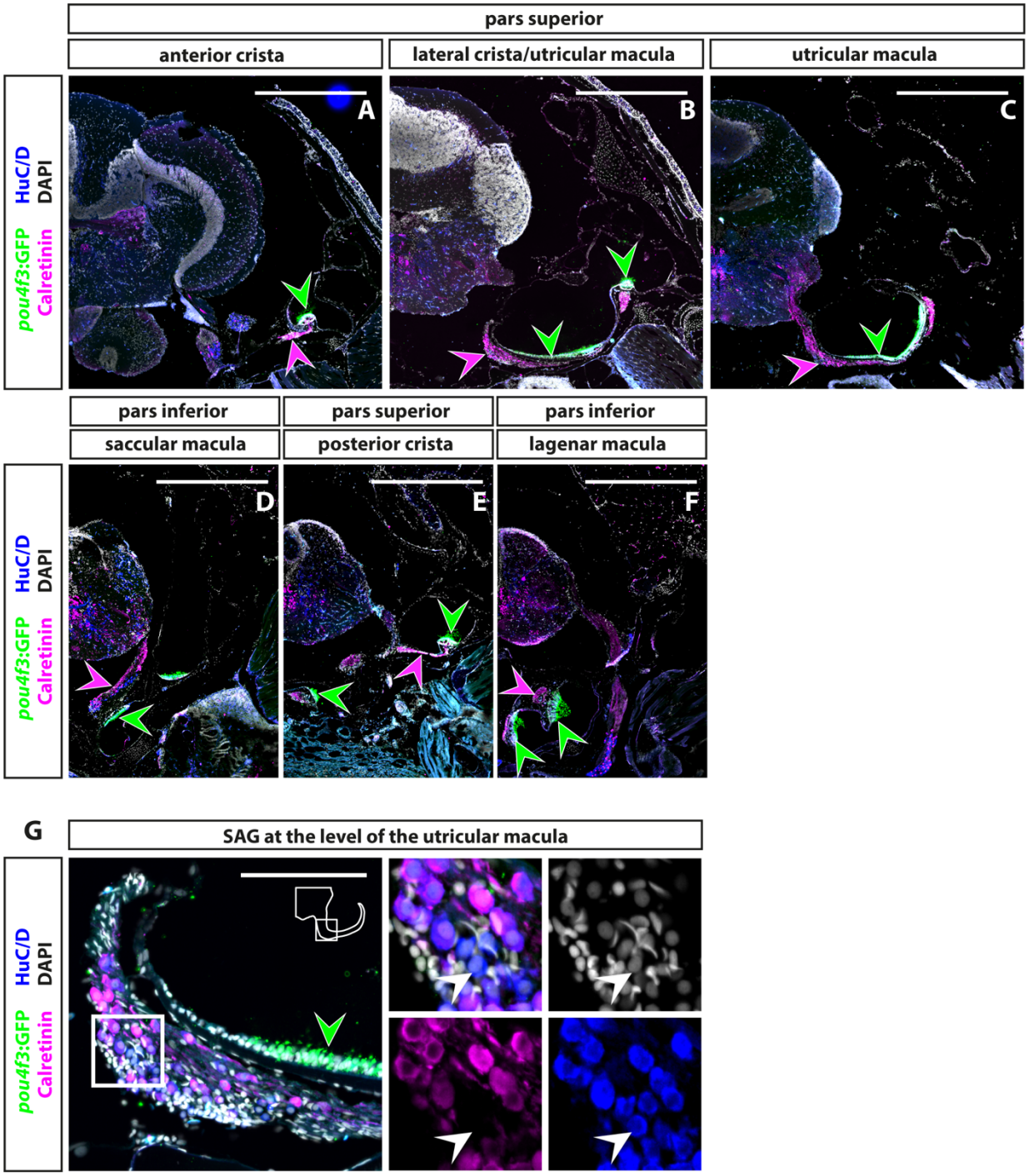

Figure 4.2 Localisation of sensory neurons and sensory hair cells in the VIIIth cranial nerve of adult zebrafish.
(**A**-**F**) Immunohistochemistry on transversal cross sections through the entire inner ear shows sensory neurons of the SAG expressing the neuronal markers HuC/D (labeling neuronal cell bodies) and Calretinin (labeling neuronal cell bodies as well as the axons; magenta arrowheads) and hair cells in the sensory patches labeled by pou4f3:GFP (green arrowheads) in adult transgenic *pou4f3*:GFP zebrafish. (**G**) Close-up of the medial part of the SAG at the level of the utricular macula; comparison of HuC/D and Calretinin reveals that the latter only labels a subpopulation of neurons in the dorso-lateral part of the SAG (white arrowhead points to HuC/D-positive but Calretinin-negative neuron). Scale bar: 200 µm for **A**-**F**; 50 µm for **G**; cross sections showing dorsal to the top and lateral to the right.

4.1.3 Amount and density of neurons decrease during growth of the SAG

Loss of neuronal cells during development and maturation of the vertebrate central and peripheral nervous system is a well-known phenomenon (Maxwell Cowan *et al.*, 1984; Oppenheim, 1991). To evaluate the growth and the amount of sensory neurons in the anterior SAG, I used the neuronal marker HuC/D labeling neuronal cell bodies to quantify all neurons in the entire anterior SAG of juvenile (2 months) and adult (8 months) zebrafish (Figure 4.3). In juveniles, cell bodies of HuC/D-positive neurons were found with a high density in the medial part of the SAG throughout all sections, whereas in adult zebrafish, cell bodies of HuC/D-positive neurons were found in the medial part of the SAG in the anterior sections but were distributed more lateral over a broader area in the posterior sections (Figure 4.3, second last section/highest density section 2 months vs. 8 months). The highest number of HuC/D-positive neurons in 2 months old fish was found in the first half of the anterior part of the SAG where neurons were densely accumulating in a relatively small region on the ventral side in the medial part of the SAG (Figure 4.3A, highest density). In contrast, the highest number of HuC/D-positive neurons in adult fish was usually located in the posterior part of the anterior SAG where neurons were spread more widely across the mediolateral axis (Figure 4.3A).

Quantification corroborates that the overall thickness of the anterior SAG calculated from the first transversal section with a HuC/D-positive neuron till the last section of the anterior SAG significantly increased with age-related growth from an average of 336 μm at 2 months to an average of 466.5 μm at 8 months (Figure 4.3). However, the density of HuC/D-positive neurons in the adult SAG analyzed by comparing highest number of HuC/D-positive neurons counted on one single section (151.13 ± 5.07 at 2 months vs. average: 97.5 ± 7.69 at 8 months) as well as the average number of HuC/D-positive neurons per section (76.13 ± 2.28 at 2 months vs. 44 ± 3.55 at 8 months) was significantly decreased compared to the juvenile SAG (Figure 4.3D). Surprisingly, I also found a significant decrease in the overall number of HuC/D-positive neurons (average: 2117.25 ± 64.47 at 2 months vs. 1692.63 ± 70.26 at 8 months).

Taken together, this data reveals that during growth HuC/D-positive neurons are lost in the anterior SAG shown by a decreased overall number and density of HuC/D-positive neurons while the overall thickness of the adult SAG increases.

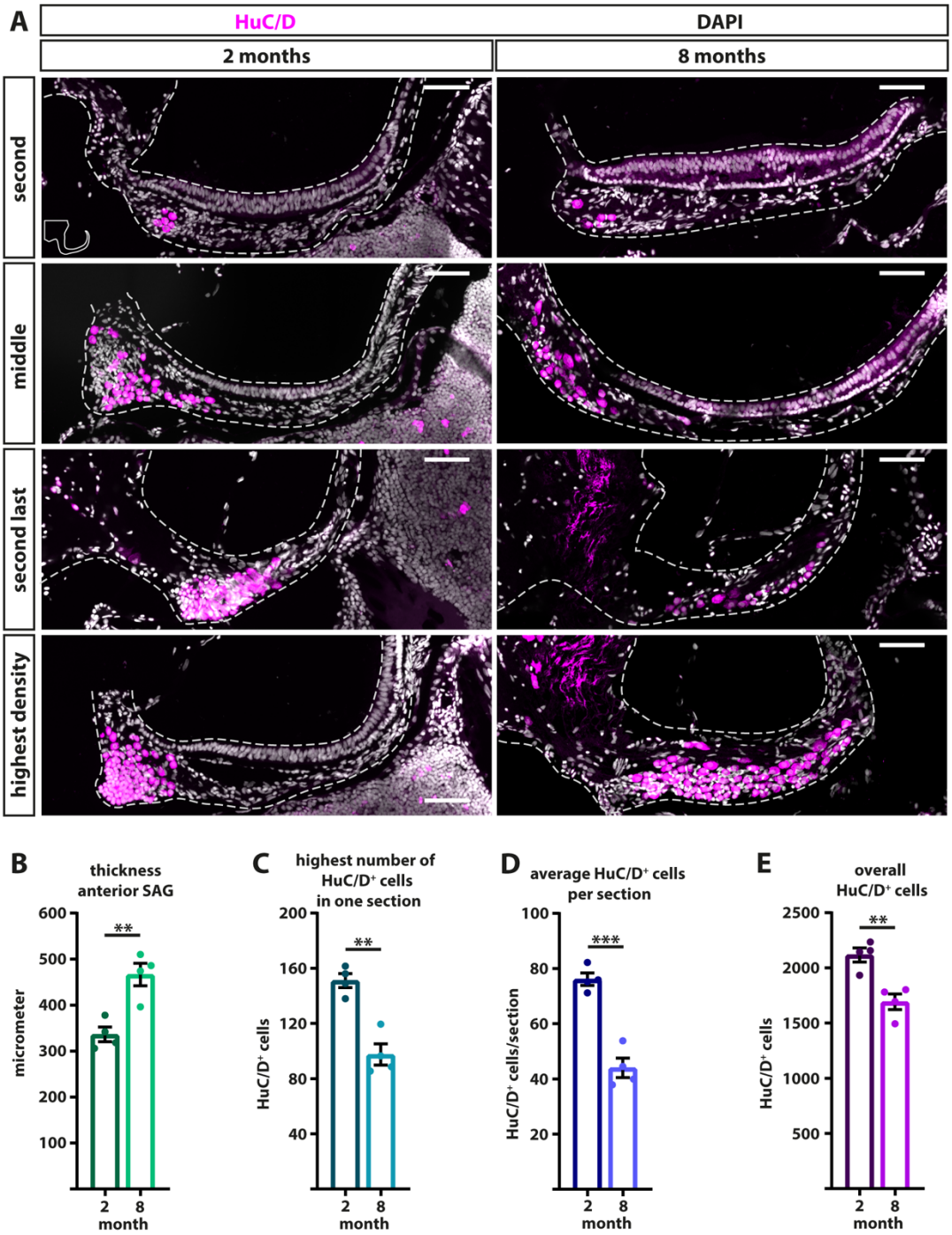

Figure 4.3 Number and density of HuC/D-positive neurons decrease during growth of the SAG.

(**A**) Antibody staining against the neuronal marker HuC/D in the SAG of 2 and 8 months old fish. The entire anterior part of the SAG was analyzed, starting with the first section containing HuC/D-positive neurons and ending with the last section of the anterior part of the SAG. Shown are the second, middle and second last section as well as the section with the highest density of HuC/D-positive cells. Note that in 2 months old fish, the section with the highest density of HuC/D-positive cells is found in the first half of the anterior SAG, whereas at 8 months, it is usually found in the last quarter of the anterior SAG. *Continued on next page*

(**B**-**E**) Quantification of HuC/D-positive neurons in the entire anterior part of the SAG: the (**B**) overall thickness of the anterior SAG along the anteroposterior axis increases while the (**C**) highest number of HuC/D-positive cells on one section, (**D**) average number of HuC/D-positive cells per section and (**E**) overall number of HuC/D-positive cells decreases during growth. Scale bar: 50 µm; cross sections showing dorsal to the top and lateral to the right. for all quantifications n=4 fish with mean values calculated of all sections of both anterior SAGs; data are presented as mean ± SEM. ***P≤0.001; **P≤0.01; *P≤0.05.

4.1.4 *neurod*:GFP-expressing cells form dispersed islets in the anterior and posterior SAG in juvenile and adult zebrafish

During inner ear development, the proneural basic helix-loop-helix transcription factor Neurod1 plays a crucial role in neurogenesis as it is required for sensory neuron differentiation and survival (Kim *et al.*, 2001; Jahan *et al.*, 2015). To investigate whether Neurod1 is still expressed in the juvenile and adult SAG, I analyzed *neurod* expression by performing immunohistochemistry against *neurod*:GFP and the neuronal marker HuC/D in juvenile and adult transgenic *Tg(neurod:GFP)* zebrafish (Obholzer *et al.*, 2008). *neurod*:GFP expressing cells were present at the ventromedial side of the juvenile and the adult SAG (Figure 4.4): in the anterior part of the SAG they resided on the ventral side near or at the bend of the elbow-like shaped VIIIth cranial nerve (representative image from adult SAG: Figure 4.4A) and in the posterior part at the ventromedial side at the tip and/or as small islets in between HuC/D-positive neurons (representative image from juvenile SAG: Figure 4.4B). Importantly, the *neurod* expressing cells did usually not form a continuous domain but appear in dispersed groups of cells along the anterio-posterior and medio-lateral axis.

To verify that the *Tg(neurod:GFP)* line reflects endogenous *neurod* expression, I used *in situ* hybridisation against *neurod* and *gfp* on consecutive sections of adult transgenic *Tg(neurod:GFP)* fish (Figure 4.5). Indeed, *neurod* (Figure 4.5A) and *gfp* (Figure 4.5B) were expressed in the same cell population, here shown on the ventromedial side of the anterior part of the SAG, corroborating that the reporter faithfully recapitulates endogenous *neurod* expression.

Taken together, this analysis shows that *neurod* expression in the inner ear is not limited to larval stages but continues livelong in the zebrafish SAG and that the *Tg(neurod:GFP)* transgenic line is a valuable tool for further investigations in this study.

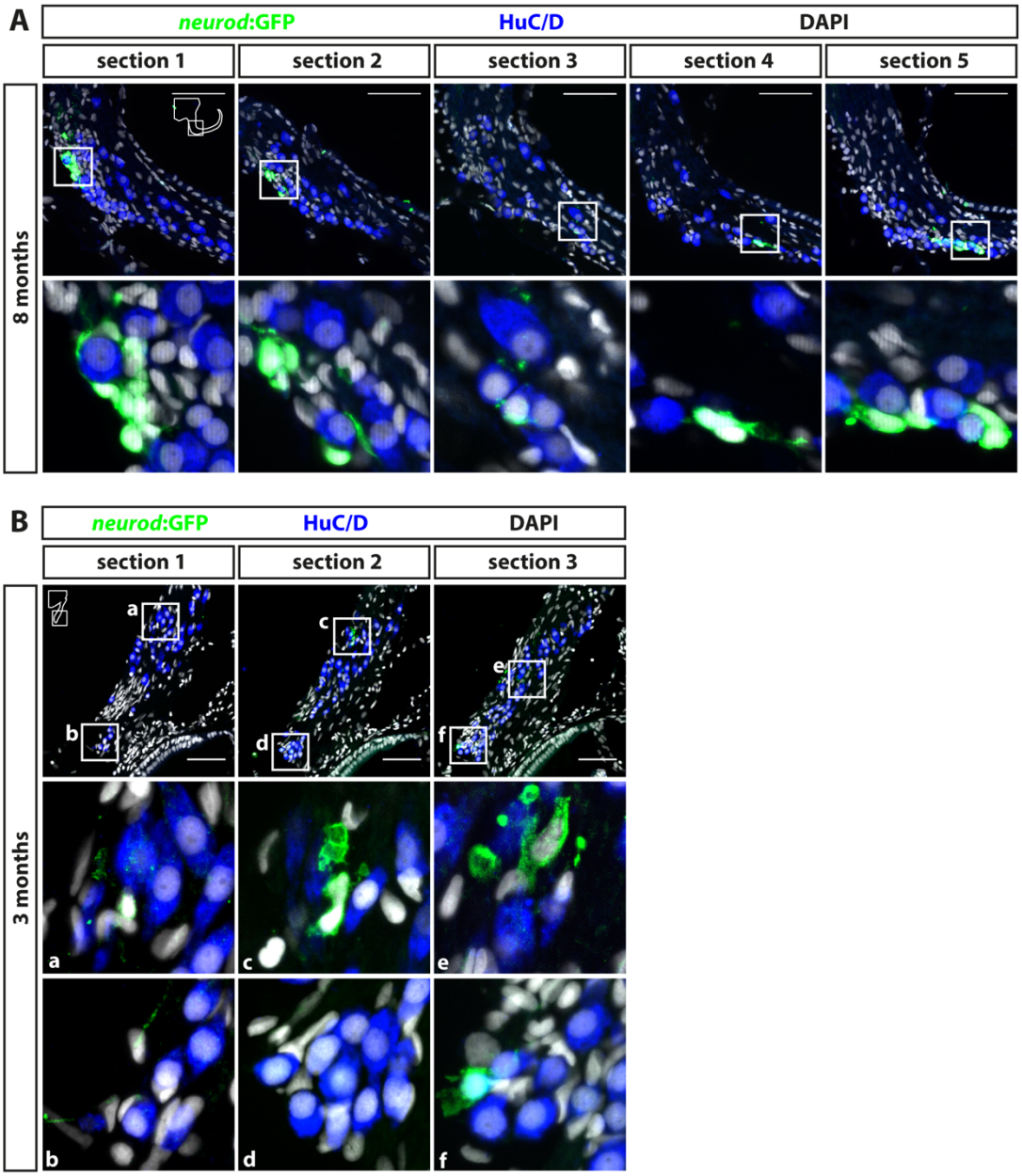

Figure 4.4 *neurod*:GFP expression in the anterior and posterior SAG of adult and juvenile zebrafish.
The representative images show that dispersed groups of *neurod*:GFP-positive cells reside at the ventromedial side in the anterior and posterior part of the zebrafish SAG. (**A**,**B**) Antibody staining against HuC/D and GFP in the *neurod*:GFP transgenic reporter line with (**A**) five consecutive sections in the anterior part of the SAG from a 8 months old fish and (**B**) three consecutive sections of the posterior part of the SAG from a 3 months old fish. The two groups of *neurod*:GFP-positive cells at different positions illustrate that the *neurod*:GFP-positive domain is not a continuous band within the SAG but rather divided into several islets located within the SAG. Scale bar: 50 µm; cross sections showing dorsal to the top and lateral to the right.

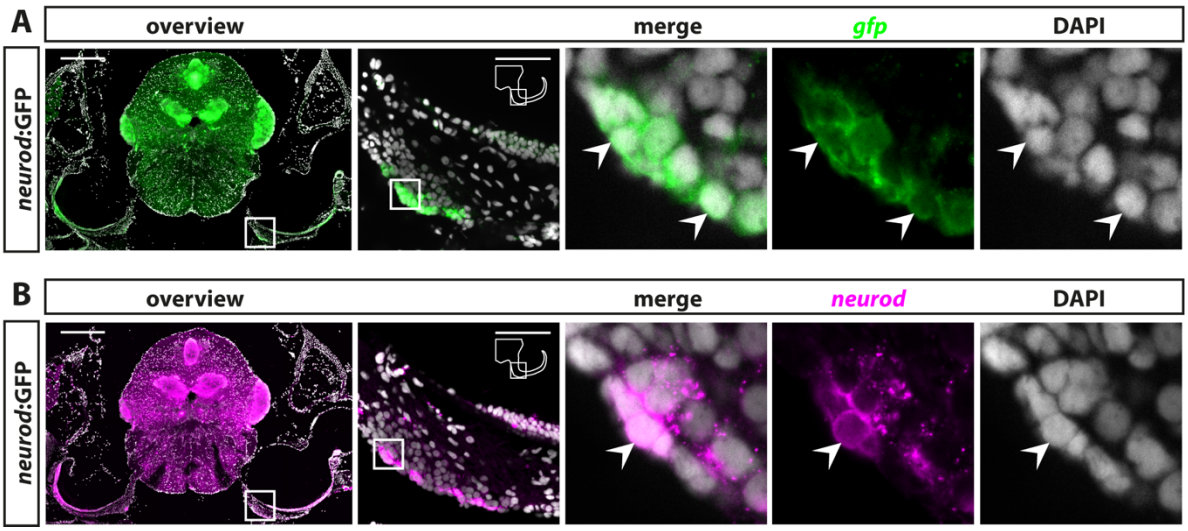

Figure 4.5 *Tg(neurod:GFP)* line faithfully recapitulates endogenous *neurod* expression in the zebrafish SAG.
(**A**,**B**) *In situ* hybridization against *gfp* (**A**) and *neurod* (**B**) on a series of transversal consecutive sections of adult, transgenic *Tg(neurod:GFP)* fish shows expression of *gfp* and *neurod* in the same cell population on the medioventral side of the anterior SAG (white arrowhead). Scale bar: overview: 200 µm; close-up: 50 µm; cross sections showing dorsal to the top and lateral to the right.

4.1.5 The neurogenic niche is highly active in the juvenile SAG but turns quiescent over time resulting in non-proliferating neuronal progenitors and a very low neurogenesis rate in the adult SAG

In contrast to mammals, zebrafish exhibit widespread adult neurogenesis and lifelong brain growth (Grandel *et al.*, 2006). Similarly, hair cells in the inner ear are continuously generated throughout life (Schuck, Julie B, Smith, 2009). During early mammalian inner ear development, the proneural transcription factor Neurod is crucial for neuronal differentiation and required to build a pool of transient-amplifying, neuronal progenitor cells (Kim *et al.*, 2001).

Neurod is also expressed in neuronal progenitors co-expressing proliferation markers in the developing zebrafish inner ear and is responsible for neuronal differentiation (Vemaraju et al., 2012). To analyze whether Neurod-positive cells present in the juvenile and adult SAG (see chapter 4.1.4) are still proliferating and also contributing to neurogenesis in the juvenile and adult SAG, I performed immunohistochemistry combining the proliferation marker PCNA and the neuronal marker HuC/D in *neurod*:GFP transgenic animals (Obholzer *et al.*, 2008). Here, persistence of GFP from the *neurod*:GFP transgene is used as a short-term lineage tracing to analyze neurogenesis from *neurod*:GFP-positive neuronal progenitor. In juvenile, 2 months old zebrafish, *neurod*:GFP-positive neuronal progenitor cells in the SAG were highly proliferative (*neurod*:GFP/PCNA-positive) and gave rise to new neurons (*neurod*:GFP/HuC/D-positive) (Figure 4.6A, 2 month). In one months older individuals, proliferation and neurogenesis in the *neurod*:GFP-positive progenitor cell pool was still present, but in lower levels (Figure 4.6A, 3 months). Additionally, there were differences in the nuclear shape of proliferating and non-proliferating *neurod*:GFP positive progenitor cells observable: whereas proliferating *neurod*:GFP-positive cells contain oblong nuclei, newborn *neurod*:GFP-positive neurons display a round-shaped nucleus similar to mature neurons. In contrast to juvenile stages, proliferating *neurod*:GFP-positive cells in the pool of *neurod*:GFP-positive progenitors were absent at adult stages (8 months) and in aged fish (20 months) (Figure 4.6A). However, newborn neurons (*neurod*:GFP/HuC/D-positive), although infrequent, were still present in the adult SAG and were mostly found in the first half of the anterior SAG. Noteworthy, proliferation was not completely absent in the adult SAG and proliferating but *neurod*:GFP-negative cells could be detected within the vicinity of *neurod*:GFP cells at all stages examined (Figure 4.6B).

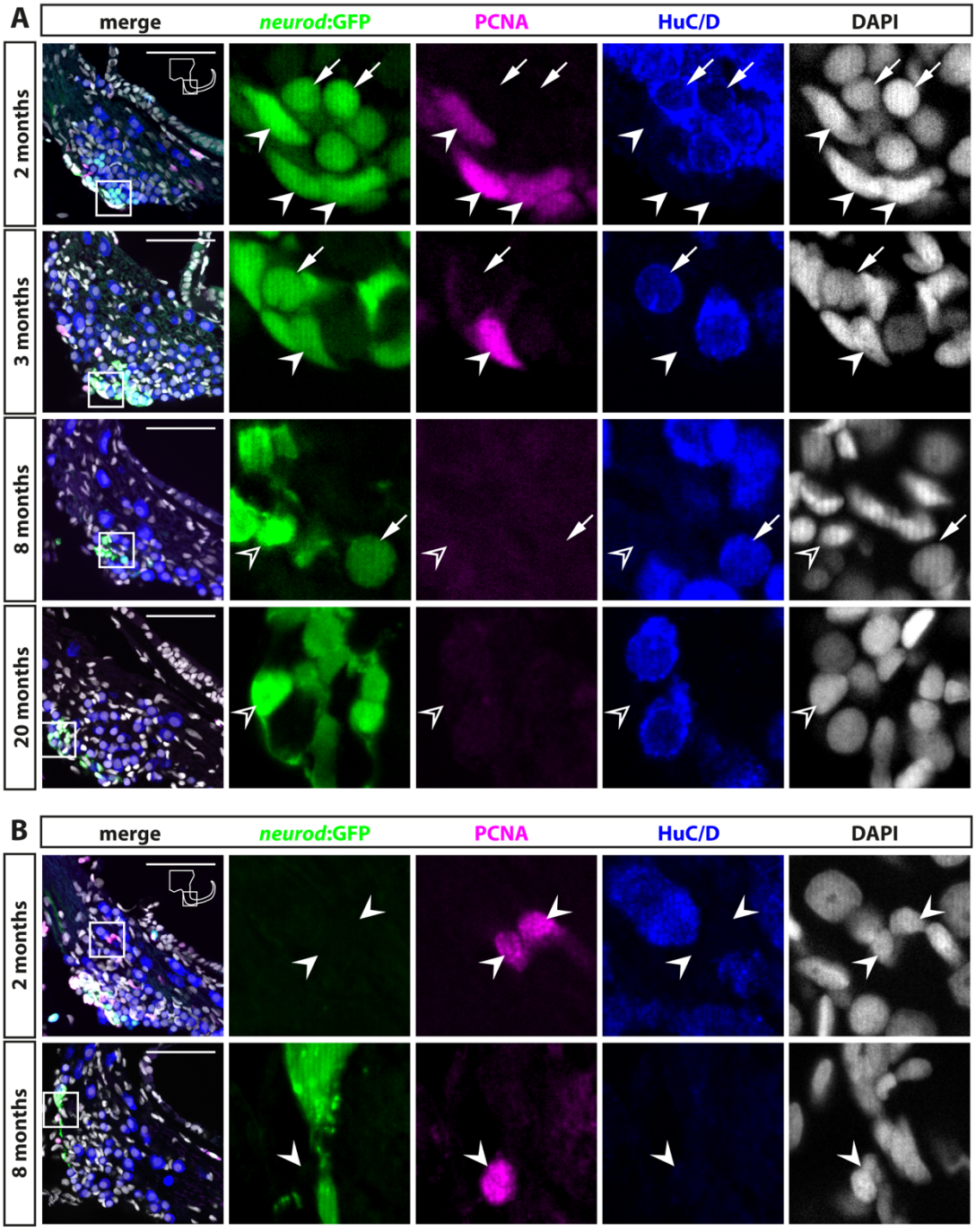

Figure 4.6 Proliferation and neurogenesis rapidly decrease at juvenile stages and are severely reduced in the adult zebrafish SAG.
(**A**,**B**) Antibody staining showing proliferation (PCNA), *neurod*:GFP-positive cells and mature neurons (HuC/D) in the SAG of juvenile (2 and 3 months) and adult (8 and 20 months) *neurod*:GFP zebrafish. (**A**) At juvenile stages, *neurod*:GFP-positive cells proliferate (*neurod*:GFP/PCNA-positive cells, arrowheads) and give rise to new neurons (*neurod*:GFP/HuC/D-positive cells, arrows). In contrast, *neurod*:GFP-positive cells (open arrowheads) are not proliferating in adult fish and *neurod*:GFP/HuC/D-positive cells are rarely found. (**B**) Proliferating PCNA-positive but *neurod*:GFP-negative cells (arrowheads) can be found in the vicinity of the *neurod*:GFP-positive population at all stages. Scale bar: 50 µm; cross sections showing dorsal to the top and lateral to the right.

Quantification of overall PCNA-positive cells in the SAG revealed a significant reduction in proliferation from 2 to 3 months (PCNA-positive cells per section: 30.03 ± 4.73 at 2 months vs. 4.69 ± 0.93 at 3 months) and a further decline to a low but steady-state level at adult stages (1.1 ± 0.25 PCNA-positive cells per section) (Figure 4.7A). Also, a significant drop in the overall number of *neurod*:GFP-positive cells from 50.23 ± 3.63 at 2 months to 20.17 ± 2.67 at 3 months was observed with only a further slight decline at adulthood (13.75 ± 1.7 *neurod*:GFP-positive cells per section at 8 month) (Figure 4.7B). Similarly, the number of proliferating *neurod*:GFP-positive cells decreased significantly during juvenile stages towards complete absence at adulthood (Figure 4.7C). Antibody staining with HuC/D revealed that around one third of *neurod*:GFP-positive cells located at the dorsal side of the *neurod*:GFP expressing cell pool are also positive for HuC/D. Additionally, they showed the characteristic round nuclei of sensory neurons, indicating that these cells are early immature neurons, differentiating from the *neurod*:GFP-positive pool into neurons still retaining the GFP label (Figure 4.7A,D).

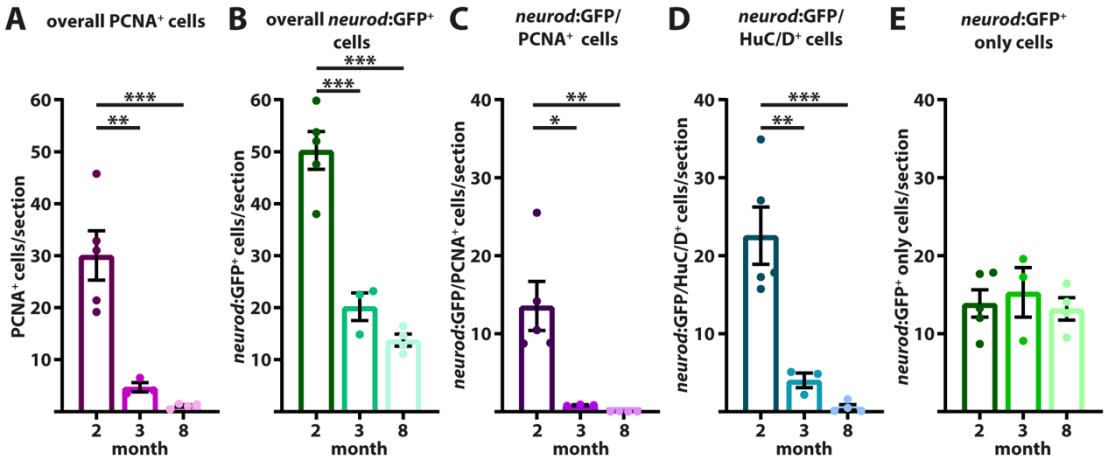

Figure 4.7 Quantification of proliferation and neurogenesis the SAG reveals that the neurogenic niche is highly active at juvenile stages but turns almost quiescent in the adult zebrafish SAG.
(**A**-**E**) Quantification of antibody staining. The (**A**) overall number of PCNA-positive cells, (**B**) overall number of *neurod*:GFP-positive cells and (**C**) *neurod*:GFP/PCNA-positive cells significantly decrease from 2 to 3 and 8 months, leaving only few PCNA-positive cells but no *neurod*:GFP/PCNA-positive cells at 8 months. (**D**) The number of newborn neurons marked by *neurod*:GFP and HuC/D decreases significantly from 2 to 3 and further from 3 to 8 months. (**E**) Number of cells in the *neurod*:GFP-positive pool that are neither proliferating nor positive for HuC/D stays constant over time. Quantifications: 2 months: n=3; 3 months: n=3; adult: n=4 (n=fish; 1 SAG/fish; 12 sections/SAG); data are presented as mean ± SEM. ***P≤0.001; **P≤0.01; *P≤0.05.

Neurogenesis significantly decreased from 2 to 3 months and a further reduction was seen from 3 to 8 months, resulting in only very few *neurod*:GFP/HuC/D-positive cell in the adult SAG (Figure 4.7D). Interestingly, the

number of *neurod*:GFP cells that neither co-express PCNA nor HuC/D (*neurod*:GFP-only cells) was constant during juvenile and adult stages (Figure 4.7E).

Taken together, the *neurod*:GFP-positive cells constitute a neuronal progenitor pool that proliferates at juvenile stages but becomes quiescent with respect to proliferation at adulthood. At the same time, neurogenesis from this *neurod*:GFP-positive progenitor pool also rapidly decreases at juvenile stages but - independent from proliferation - does not cease completely but decreases to a homeostatic baseline neurogenesis rate at adult stages.

4.1.6 *neurod*:GFP-positive neuronal progenitor cells are proliferating and can give rise to new neurons within a week at juvenile stages

Because Neurod is expressed only transiently in neuronal precursor cells in the developing zebrafish inner ear (Andermann *et al.*, 2002; Kim *et al.*, 2001), the observation of newborn neurons derived from *neurod*:GFP-positive neuronal progenitors described above is based on short-term lineage tracing due to perdurance of the fluorophore GFP. To corroborate the finding that proliferating, *neurod*-expressing neuronal progenitors differentiate into mature neurons in the juvenile SAG, I performed a pulse chase experiment using Bromodeoxyuridine (BrdU), a thymidine analogue that is incorporated during S-phase of the cell cycle and hence labels active cycling cells (Kiernan *et al.*, 2005). To this aim, 3 months old *neurod*:GFP transgenic animals were exposed to BrdU for 24 hours and kept for chase times of 0, 7, 15 and 28 days after which they were analyzed (Figure 4.8A). Consistent with the proliferation analysis at juvenile stages (Figure 4.6 & Figure 4.7), I found *neurod*:GFP-positive cells incorporating BrdU at directly after the treatment (0 days post treatment (dpt)) (Figure 4.8B). Subsequently, *neurod*:GFP-positive cells that had incorporated BrdU, differentiated into neurons already shortly after proliferation indicated by the presence of a triple positive newborn neuron (*neurod*:GFP/BrdU/HuC/D-positive) at 7 and 15 dpt. In one individual a triple positive newborn neuron was found at 0 dpt indicating an immediate neuronal differentiation after proliferation. Double positive more mature neurons that have already lost the *neurod*:GFP label (BrdU/HuC/D-positive) were observed as early as 7 dpt and at all later timepoints. Additionally, some *neurod*:GFP-positive cells that have incorporated BrdU remained in the *neurod*:GFP-positive pool beyond 28 dpt.

Quantification of overall BrdU-positive cells in the SAG revealed a significant increase of BrdU-positive cells from 0 to 15 dpt (Figure 4.9A). The percentage of *neurod*:GFP cells which incorporated BrdU (BrdU/*neurod*:GFP-positive) significantly drops from 0 dpt to the other time points (Figure 4.9B). However, the percentage of triple positive newborn neurons (BrdU/*neurod*:GFP/HuC/D-positive) increases over time to approx. 4 % at 15 dpt, revealing the exit of formerly active cycling cells from the *neurod*:GFP-positive progenitor pool to differentiate into

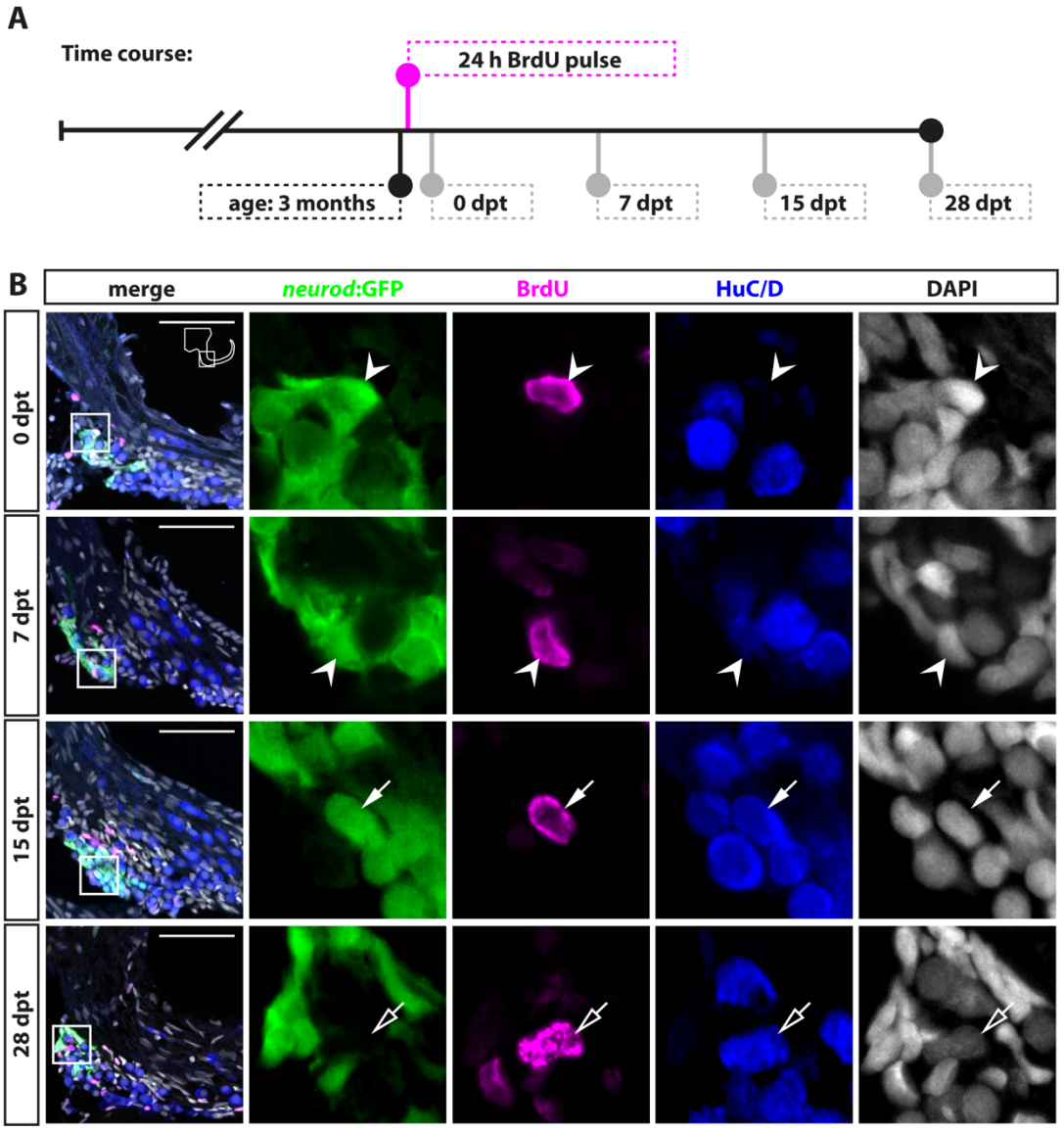

Figure 4.8 *neurod*:GFP-positive cells are proliferating and give rise to new neurons at juvenile stages.
(**A**) Time course of the BrdU pulse chase experiment. 3 months old *Tg (neurod:GFP)* zebrafish were sacrificed at 0, 7, 15 and 28 days post a 24 hour (h) long BrdU treatment (dpt). (**B**) Antibody staining shows BrdU/*neurod*:GFP-positive cells (0 and 7 dpt, arrowhead) which differentiate into BrdU/*neurod*:GFP/HuC/D-positive (15 dpt, arrow) and BrdU/HuC/D-positive neurons (28 dpt, open arrow). Scale bar: 50 µm; cross sections showing dorsal to the top and lateral to the right.

neurons (Figure 4.9C). Even though the number of newborn neurons (BrdU/HuC/D-positive) is low, the percentage of BrdU/HuC/D-positive newborn neurons increased over time (Figure 4.9D). Additionally, I also calculated the percentage of BrdU-double-positive cells in relation to the specific cell type, e.g. *neurod*:GFP-positive progenitor cell, *neurod*:GFP/HuC/D-positive immature neuron and HuC/D-positive mature neuron (Figure 4.9B'-D'). The number of BrdU/*neurod*:GFP-positive cells per *neurod*:GFP-positive cells does not change significantly during the 28 days trace.

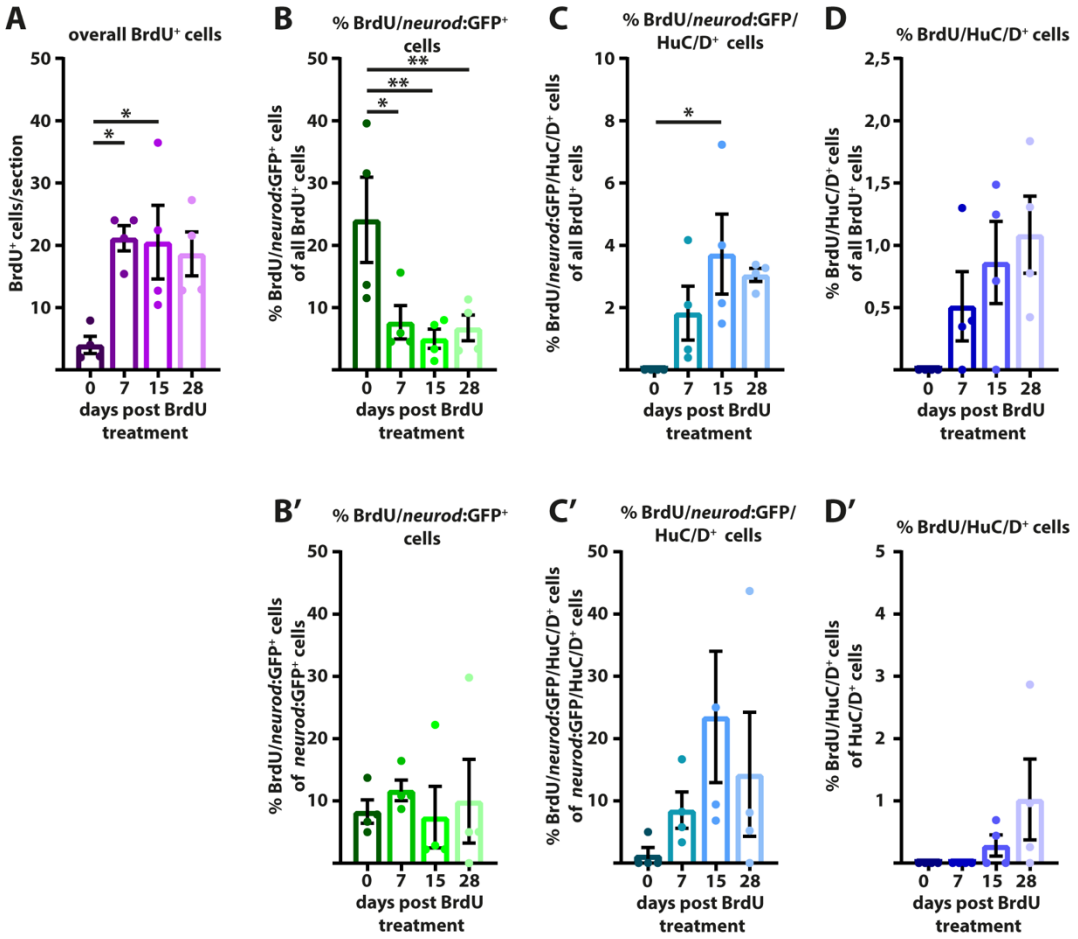

Figure 4.9 Quantification of proliferation and neurogenesis in the *neurod*:GFP-positive neuronal progenitor cell pool upon BrdU treatment in the juvenile SAG
Quantification of antibody staining shown in Figure 4.8 (**A**) The overall number of BrdU-positive cells increased from 0 dpt to later time points indicating continued proliferation of precursor cells. (**B**-**D**) Quantification of the percentage of double/triple-positive cells in relation to all BrdU-positive cells; (**B**) Percentage of BrdU/*neurod*:GFP-positive cells of all BrdU-positive cells decreased significantly from 0 dpt to later time points. (**C**) At 7 dpt, a significant amount of previously proliferaring BrdU/*neurod*:GFP-positive cells already have differentiated into immature BrdU/*neurod*:GFP/HuC/D-positive neurons. (**D**) First newborn BrdU/HuC/D-positive neurons appear as early as 7 dpt and the percentage of BrdU/HuC/D positive neurons increased over time. (**B'**-**D'**) Quantification of the percentage of double/triple-positive cells in relation to the corresponding cell type: *neurod*:GFP-positive cells (**B'**), *neurod*:GFP/HuC/D-positive cells (**C'**), HuC/D-positive cells (**D'**); (**B'**) Percentage of *neurod*:GFP/BrdU-positive cells in the pool of *neurod*:GFP-positive progenitors stayed constant over the time course of 28 days, indicating that not all recently proliferating *neurod*:GFP-positive progenitors differentiate into neurons within the same time course. (**C'**) Percentage of differentiation of previously proliferating *neurod*:GFP-positive progenitors (BrdU/*neurod*:GFP/HuC/D-positive) per all differentiating *neurod*:GFP-positive cells increased over the time course. (**D'**) Percentage of newborn neurons (BrdU/*neurod*:GFP-positive) of all neurons reached an average of 1 % newborn neurons at the latest timepoint. For all quantifications n=4 (n=fish; 1 SAG/fish; 12 sections/SAG); data are presented as mean ± SEM. **P≤0.01; *P≤0.05.

Similar to the quantifications shown above, the percentages of BrdU/*neurod*:GFP/HuC/D-positive cells per *neurod*:GFP/HuC/D-positive cells and of BrdU/HuC/D-positive cells per HuC/D-positive cells increased over time.

In summary, the data show the continued production of new inner ear neurons from proliferating neuronal *neurod*:GFP-positive progenitor cells at juvenile stages.

4.1.7 Proliferating but marker-negative cell population replenishes the *neurod*:GFP-positive cell pool at adult stages and contributes to adult neurogenesis

The PCNA-based proliferation analysis as well as the BrdU pulse chase experiment in juvenile zebrafish revealed that *neurod*:GFP-positive cells represent a progenitor pool that shows robust proliferation as well as neurogenesis at juvenile stages but not at adulthood (see chapter 4.1.5 and 4.1.6). However, a low but steady-state proliferation outside of the *neurod*:GFP-positive population was detected also at adult stages (Figure 4.6B). Hence, I repeated the BrdU pulse chase experiment at adult stages to investigate if proliferating, non-*neurod*:GFP-positive cells are able to give rise to new neurons also at this later time point (Figure 4.10A).

Consistent with the proliferation analysis using PCNA (Figure 4.6), I did not find any *neurod*:GFP-positive cell co-localizing with BrdU at 0 dpt confirming that there were no proliferating *neurod*:GFP-positive cells that could have incorporated BrdU in the adult SAG (Figure 4.10B). However, double positive cells (*neurod*:GFP/BrdU-positive) were detected at 7 dpt which indicates the presence of a proliferating, non-*neurod*:GFP-expressing (*neurod*:GFP-negative) cell population that can differentiate into *neurod*:GFP-positive cells and thus replenish the pool of *neurod*:GFP-positive cells. Furthermore, triple positive newborn neurons (*neurod*:GFP/BrdU/HuC/D-positive) as well as more mature neurons that have already lost the *neurod*:GFP label (BrdU/HuC/D-positive) were present in single individuals with chase times of more than 14 days. Interestingly, similiar to the juvenile SAG some *neurod*:GFP-positive cells derived from the recently proliferating marker-negativ presumptive neuronal stem cell still retained the BrdU label at 29 dpt, suggesting the absence of a narrow time range in which proliferating neuronal precursor cells differentiate into mature neurons.

Quantification of the overall number of BrdU-positive cells (Figure 4.11) as well as the percentage of BrdU-positive only cells, BrdU/*neurod*:GFP-positive cells and BrdU/HuC/D-positive cells per all BrdU-positive cells or per corresponding cell type (Figure 4.11) showed that neurogenesis in the adult SAG is a very rare event. A trend for an increase in the number of BrdU-positive cells from 0 dpt to 7/14/29 dpt was seen, indicating further proliferation in stem/progenitor cells (Figure 4.11A).

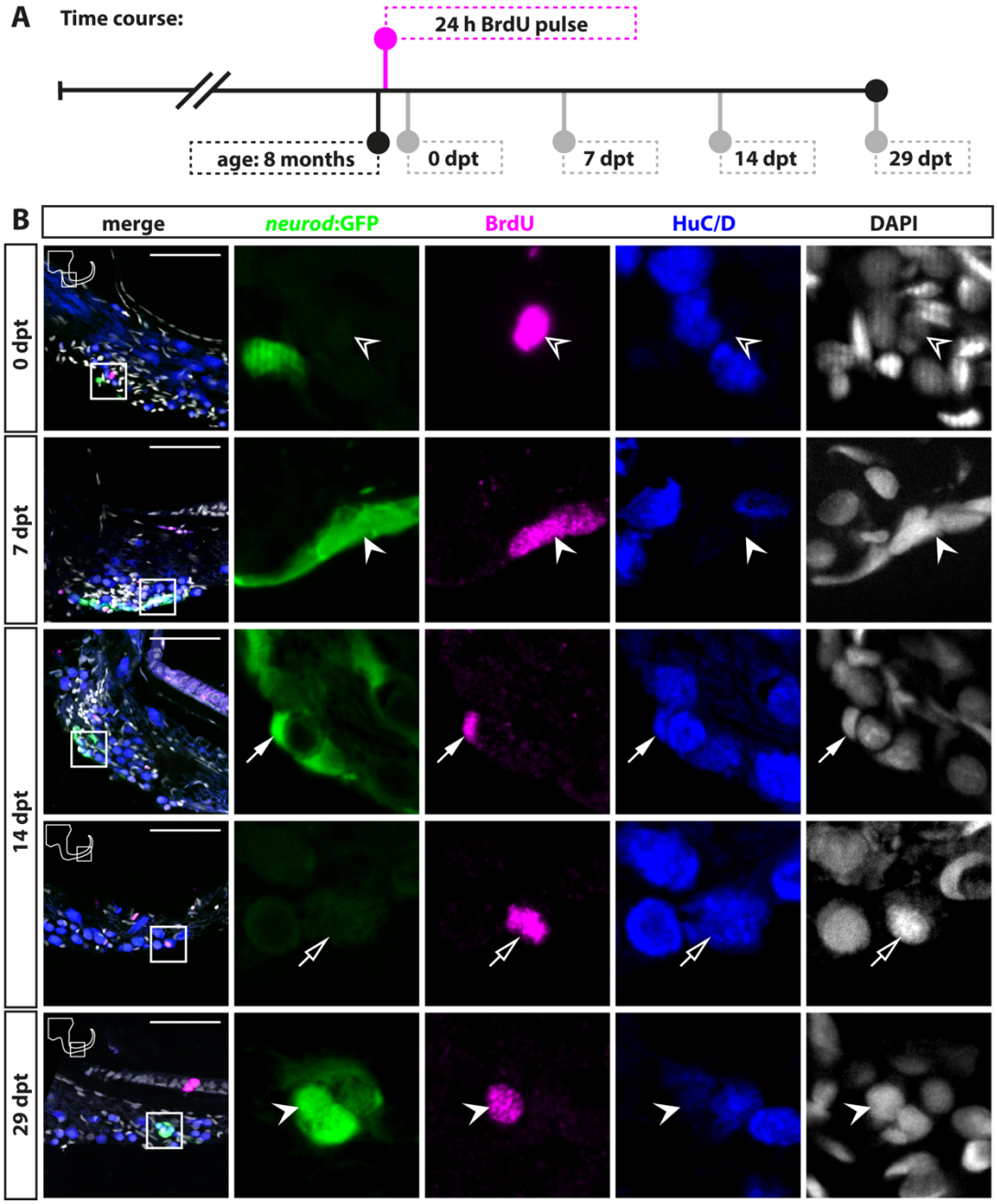

Figure 4.10 A proliferating but marker-negative stem cell-like cell population replenishes the *neurod*:GFP-positive cell pool at adult stages and contributes to adult neurogenesis.
(**A**) Time course for BrdU pulse chase experiment. 8 months old *Tg(neurod:GFP)* zebrafish were sacrificed at 0, 7, 14 and 29 days post a 24 hour (h) BrdU treatment (dpt). (**B**) Antibody staining reveals that BrdU-positive cells never co-localize with *neurod*:GFP at 0 dpt (open arrowhead). However, BrdU/*neurod*:GFP-positive cells are present at 7 dpt (arrowhead). Newly generated *neurod*:GFP-positive cells either differentiated into new neurons (BrdU/*neurod*:GFP/HuC/D-positive cells (arrow) and BrdU/HuC/D-positive cells (open arrow)) as shown as early as 14 dpt or remained in the pool of *neurod*:GFP-positive cells (arrowhead) as shown at 29 dpt. Scale bar: 50 µm; cross sections showing dorsal to the top and lateral to the right.

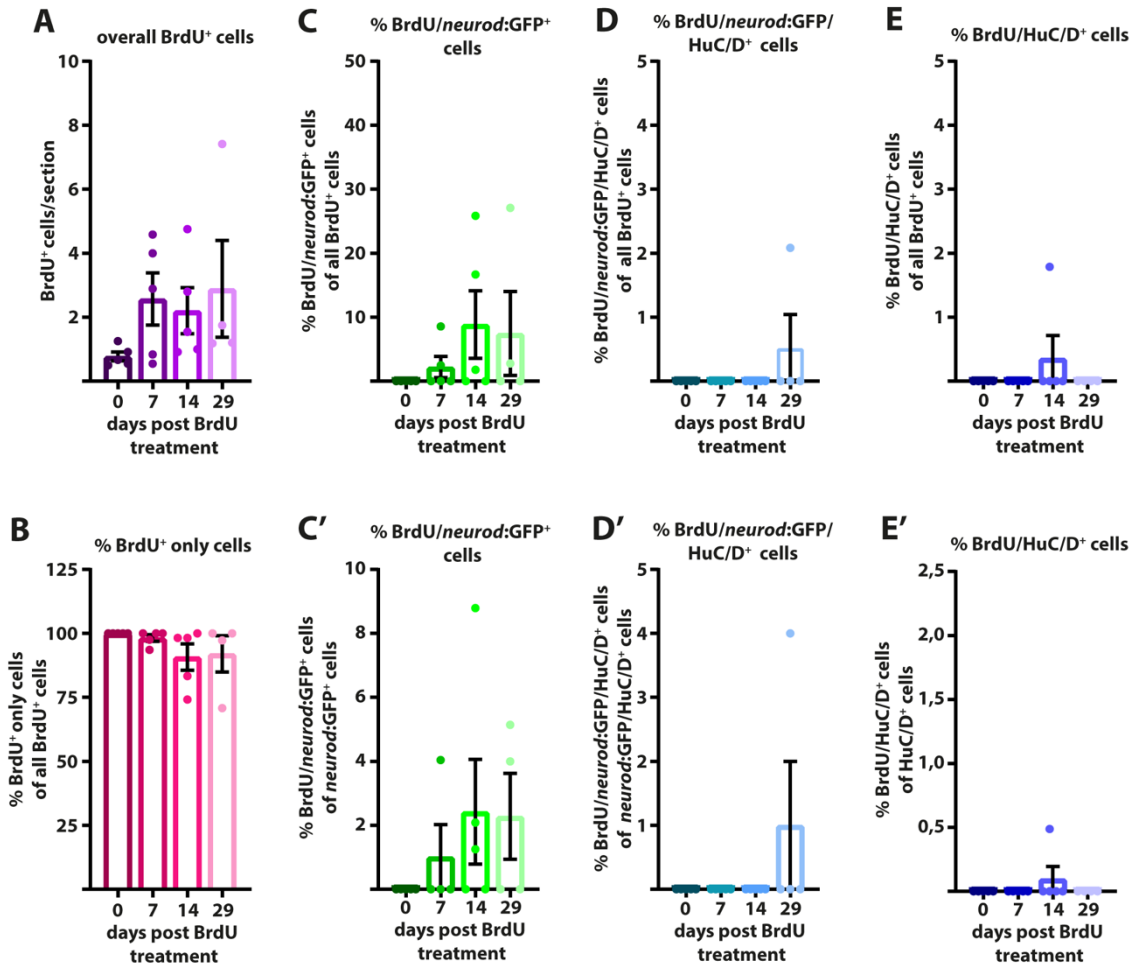

Figure 4.11 Quantification of proliferation and neurogenesis in the *neurod*:GFP-positive neuronal progenitor cell pool upon BrdU treatment in the adult SAG. Quantification of antibody staining shown in Figure 4.10. (**A**) Overall number of BrdU-positive cells increased over time, indicating multiple rounds of proliferation. (**B**-**E**) Quantification of percentage of BrdU-positive only cells (**B**), BrdU/*neurod*:GFP-positive cells (**C**), BrdU/*neurod*:GFP-positive cells (**D**) and BrdU/HuC/D-positive cells (**E**) as a fraction of all BrdU-positive cells (**B**-**E**) as well as a fraction of the corresponding cell type: *neurod*:GFP-positive cells (**C'**), *neurod*:GFP/HuC/D-positive cells (**D'**), HuC/D-positive cells (**E'**). (**B**) Percentage of only BrdU-positive cells decreased over time from 100 % to approximately 90 % only BrdU-positive cells, while the percentage of BrdU/*neurod*:GFP-positive cells increased from 0 % to an average of almost 9 % of all BrdU-positive cells (**C**) or 2,4 % of all *neurod*:GFP-positive cells (C'), proofing the presence of a proliferating stem cell replenishing the pool of *neurod*:GFP-positive progenitor cells. (*D-E'*) Adult neurogenesis from a marker-negative, proliferating stem cells occured within 14 dpt, shown by the presence of newborn (BrdU/*neurod*:GFP/HuC/D-positive, **D**/**D'**) and more mature (BrdU/HuC/D-positive **E**/**E'**) neurons. Quantifications 0/7/14 days: n=5; 29 days: n=4 (A-E) and 0/14 days: n=5; 7/29 days: n=4 (**C'**-**E'**) (n=fish; 1 SAG/fish; 12 sections/SAG); data are presented as mean ± SEM.

Importantly, at 0 dpt, all BrdU-positive cells were BrdU-positive only cells lacking expression of *neurod*:GFP or HuC/D and the vast majority of BrdU-positive cells also remained BrdU-positive only cells at later time points (Figure 4.11B). In contrast, BrdU/*neurod*:GFP-double positive cells were first seen at 7 dpt and moreover, at least one individual per timepoint displayed BrdU/*neurod*:GFP-double positive cells

in all later time points. Differentiating, BrdU/*neurod*:GFP/HuC/D-positive neuronal progenitors as well as newly formed, BrdU/HuC/D-double positive neurons were only found in one individual at 29 dpt and 14 dpt, respectively (Figure 4.11D-E'). Although the number of analyzed animals was not sufficient to reach statistical relevance, the data revealed that adult neurogenesis, even though being an extremely rare event, is present in the adult SAG and new HuC/D-positive neurons are generated during homeostasis.

Taken together, I postulate the presence of marker-negative, proliferating stem cell that adds new cells to the pool of *neurod*:GFP-positive progenitors and contributes to adult neurogenesis in the adult SAG, countervailing the loss of the neuronal *neurod*:GFP-positive progenitor pool by rare but constant differentiation of neuronal progenitors into newborn neurons over time in adulthood.

4.1.8 Nestin also marks neuronal progenitors in the neurogenic niche

The cellular composition of neural stem cell niches varies across vertebrate species and even within the very same species. However, neural stem cell niches share common characteristics and possess either a neuro-epithelial-like or radial glia identity (Lindsey et al., 2018). To address this issue, I further analyzed the cellular composition of the neurogenic niche of the SAG in more detail. One marker associated with neuro-epithelial-like stem cell identity is the class IV intermediate filament protein Nestin which is down regulated when cells differentiate and become post-mitotic (Wiese *et al.*, 2004). During zebrafish development *nestin* is expressed in proliferative zones of the central nervous system as well as in the cranial ganglia (Mahler and Driever, 2007).

To study whether *nestin* expression is still present in the SAG beyond development, I used the transgenic BAC *Tg(nestin:GFP)* line in which GFP expression is driven by *nestin* regulatory elements and recapitulates all aspects of the endogenous *nestin* mRNA expression (Kaslin *et al.,* 2009). Co-staining for proliferation (PCNA) and neurons (HuC/D) in *nestin*:GFP fish revealed the presence of *nestin*:GFP-positive cells in the region of the *neurod*:GFP-positive neurogenic niche of the juvenile SAG, which - similar to *neurod*:GFP-positive progenitor cells - were proliferating (*nestin*:GFP/PCNA-positive cells) and giving rise to newborn neurons (*nestin*:GFP/HuC/D-positive cells) (Figure 4.12A).

Since both *nestin*:GFP and *neurod*:GFP both harbor the same fluorophore, I could not use animals carrying both transgenes to corroborate my hypothesis that *nestin*:GFP and *neurod*:GFP indeed mark the same cell population. Instead, I crossed a recently in the lab generated transgenic line expressing mCherry and CreER^{T2} separated by a viral T2A peptide sequence under the control of a *nestin* promoter recapitulating the endogenous cranial *nestin* expression in larvae (Schwarzer et al., 2020) to both transgenic lines and subsequently studied mCherry

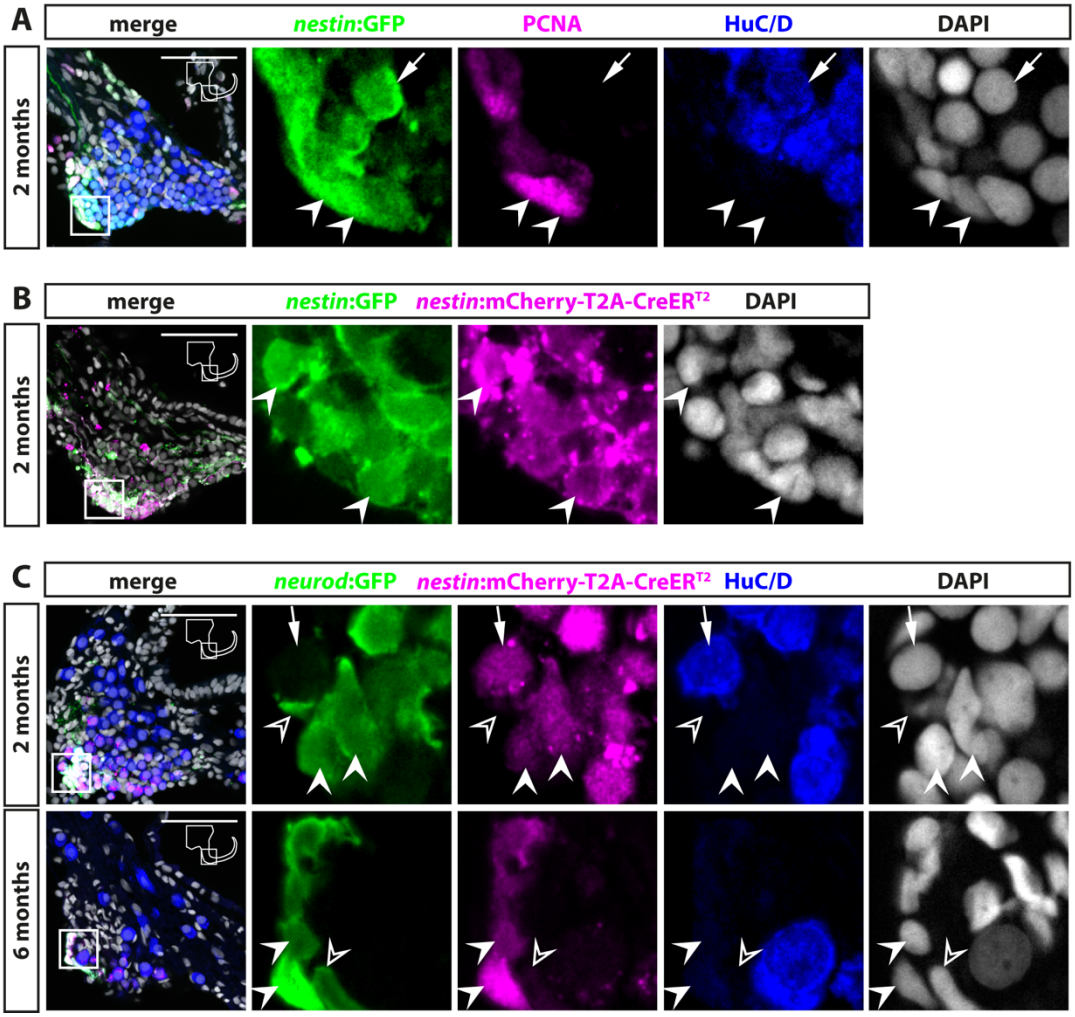

Figure 4.12 Nestin is expressed in the neurogenic niche and overlaps largely with *neurod*:GFP expression at juvenile and adult stages.
(**A**) Antibody staining showing *nestin*:GFP expression in the region of the *neurod*:GFP-positive neuronal progenitor cells. *nestin*:GFP-positive cells were proliferating (*nestin*:GFP/PCNA-positive cells, arrowhead) and differentiated into neurons (*nestin*:GFP/HuC/D-positive cells, arrow) in 2 months old zebrafish. (**B**) Co-labeling of *nestin*:GFP and *nestin*:mCherry-T2A-CreER^{T2} in 2 months old double transgenic fish showed that both transgenic lines label the same cell population in the SAG. (**C**) Antibodys staining against GFP, mCherry and HuC/D revealed that expression of *nestin*:mCherry-T2A-CreER^{T2} largely overlaps with the *neurod*:GFP-positive progenitor pool (arrowheads) in 2 and 6 months old double transgenic *neurod*:GFP/*nestin*:mCherry-T2A-CreER^{T2} zebrafish; additionally, few *neurod*:GFP-only positive progenitor cells were found (open arrowhead) and the expression of *nestin*:mCherry-T2A-CreER^{T2} persisted longer in newborn neurons than *neurod*:GFP expression (arrow). Scale bar: 50 µm; cross sections showing dorsal to the top and lateral to the right.

expression in combination with the *nestin*:GFP as well as the *neurod*:GFP transgene. Analysis of double transgenic fish harboring *nestin*:GFP and *nestin*:mCherry-T2A-CreER^{T2} proved that both transgenic lines mark the same cell population in the SAG (Figure 4.12B). Indeed, also co-staining for *neurod*:GFP, *nestin*:mCherry-T2A-CreER^{T2} and HuC/D confirmed that *neurod*:GFP and *nestin*:mCherry-T2A-CreER^{T2} are actually co-expressed in most cells in the juvenile and adult SAG (Figure 4.12C).

However, compared to *neurod*:GFP, expression of *nestin*:mCherry-T2A-CreER^{T2} persists longer in newborn neurons as shown by the presence of *nestin*:mCherry-T2A-CreER^{T2}/HuC/D-positive cells negative for *neurod*:GFP in the juvenile SAG (Figure 4.12A and C, arrow). Additionally, in rare cases *neurod*:GFP cells negative for *nestin*:mCherry-T2A-CreER^{T2} were found in the juvenile and adult SAG (Figure 4.12C, open arrowhead).

Taken together, the class IV intermediate filament protein Nestin is largely expressed in the same neuronal progenitor cell population as *neurod*:GFP at juvenile and adult stages.

4.1.9 Long-term lineage tracing: larval *nestin*:mCherryCreER^{T2}-positive cells give rise to mature neurons in the adult SAG

To estimate the degree of neurogenesis at embryonic/larval stages versus later neurogenesis, I performed long-term lineage tracing using the transgenic *nestin*:mCherry-T2A-CreER^{T2} driver line crossed to the transgenic, heat shock inducible *hsp70l*:loxP-DsRed2-loxP-nlsEGFP responder line. Upon application of 4-Hydroxytamoxifen during embryonic stages, Cre recombinase, which is expressed under the control of the *nestin* promotor, excises DsRed2 in *nestin*-expressing cells in the developing SAG. Upon heat shock, offspring of these cells recombined during early otic development express EGFP in the nucleus (Figure 4.13A).

Analysis of adult, double transgenic zebrafish recombined twice at embryonic stages by immunohistochemistry against EGFP and the neuronal marker HuC/D revealed that many but not all mature HuC/D-positive neurons populating the adult SAG were derived from the embryonic progeny of the *nestin*:mCherry-T2A-CreER^{T2}-positive cells (Figure 4.13B/C). Quantification of *nestin*:mCherry-T2A-CreER^{T2}-derived HuC/D-positive neurons showed that only approx. 57 % of all neurons in the adult zebrafish SAG are progeny of *nestin*:mCherry-T2A-CreER^{T2}-positive cells recombined at embryonic/larval stages (Figure 4.13D,E).

Taken together, this finding corroborates my previous experiments suggesting that neurogenesis is not terminated to a large extent at embryonic stages but rather takes place way beyond into juvenile and adult stages.

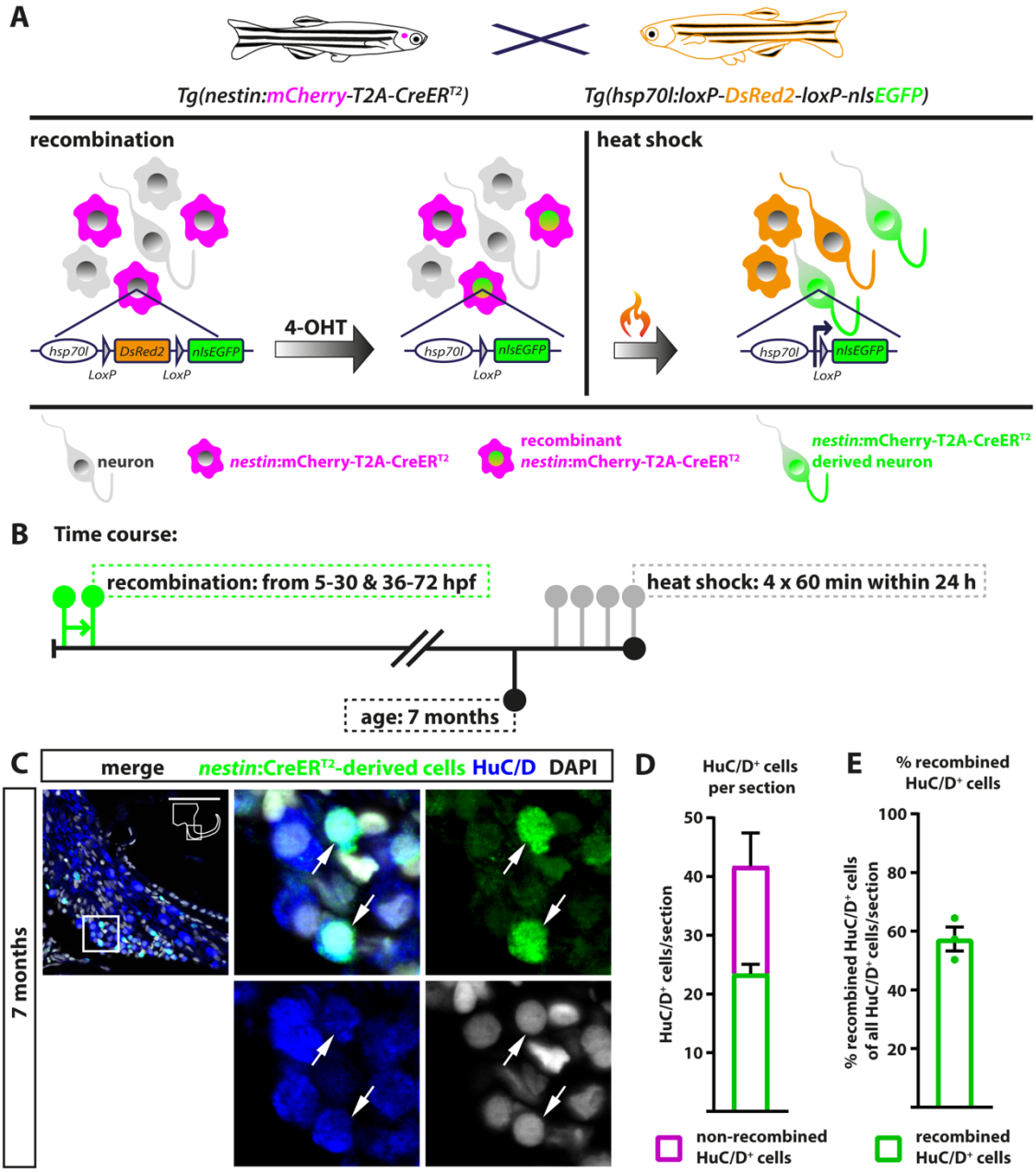

Figure 4.13 Larval *nestin*:mCherryCreER^{T2}-positive cells give rise to half of the mature neurons present in the adult SAG.

(**A**) Scheme depicting experimental set-up for long term lineage tracing experiment; *Tg(nestin:mCherry-T2A-CreER^{T2})* was crossed to the Cre-dependent reporter line *Tg(hsp70l:loxP-DsRed2-loxP-nlsEGFP)*; recombination in Cre-expressing cells is induced by application of 4-hydroxy-tamoxifen (4-OHT); upon heat shock, successfully recombined, *nestin*:mCherry-T2A-CreER^{T2}-derived cells express EGFP instead of DsRed. (**B**) Time course of *nestin*:mCherry-T2A-CreER^{T2} long term lineage tracing experiment. Recombination in *nestin*:mCherry-T2A-CreER^{T2}/*hsp70l*:loxP-DsRed2-loxP-nlsEGFP double transgenic embryos was induced from 5-30 and 36-72 hours post fertilization (hpf). At 7 months, zebrafish were heat shocked for four times within 24 hours (h) to activate the reporter and afterwards analyzed for EGFP-expressing, *nestin*:CreER^{T2}-derived cells.

Continued on next page

(**C**) Co-staining of EGFP-positive, *nestin*:CreER^{T2}-derived cells with HuC/D showed the presence of *nestin*:CreER^{T2}-derived/HuC/D-positive cells (arrow) in the adult SAG. (**D/E**) Quantification of EGFP-positive (recombined) and EGFP-negative (non-recombined) HuC/D-positive cells (**D**) and percentage of recombined HuC/D-positive cells of all HuC/D-positive neurons (**E**) in the adult SAG. Scale bar: 50 µm; cross sections showing dorsal to the top and lateral to the right; quantification n=3 (n=fish; 1 SAG/fish; 12 sections/SAG); data are presented as mean ± SEM.

4.1.10 Distribution of glia cells and myelination pattern label the peripheral-central nervous system transitional zone (PCTZ) in the juvenile and adult SAG

Sox2

The transcription factor Sox2 plays pivotal roles in the regulation and maintenance of neural stem cells (Hagey *et al.*, 2018) and it has been shown that *sox2* is expressed in the developing spiral ganglion neurons in mice and required for neurogenesis in the cochlea (Puligilla *et al.*, 2010, (Steevens *et al.*, 2017). Figure 4.14A shows the antibody staining against Sox2 in adult, wildtype zebrafish: besides presence of strong expression of Sox2 in the sensory patch of the utricular macula, Sox2-positive cells in the SAG were found arranged in a straight line in the medial part of the SAG and their nuclei exhibited a characteristic elongated shape. To analyze the whether these Sox2-positive cells reside in close proximity to the Neurod/Nestin-positive neuronal progenitor cell domain, I used 2 months old double transgenic fish harboring *sox2*:GFP and *nestin*:mCherry-T2A-CreER^{T2} and co-stained for GFP, mCherry and the mature neuronal marker Calretinin (Figure 4.14B). Again, *sox2*:GFP-positive cells were found in the medial part of the SAG,

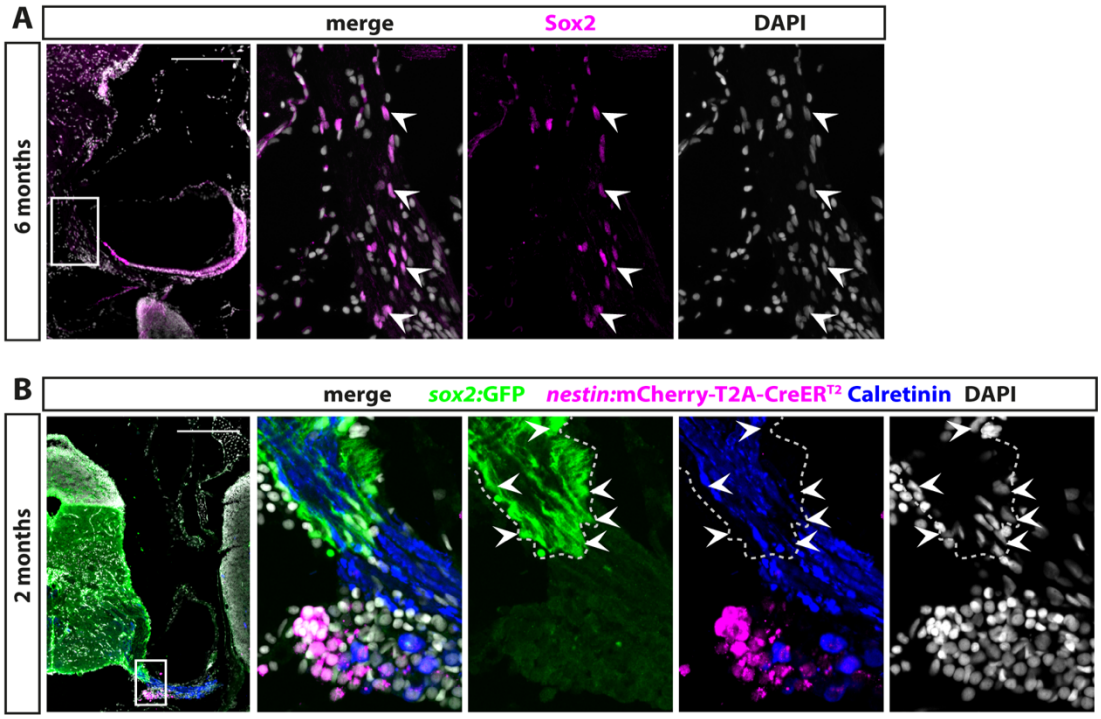

Figure 4.14 Sox2-positive cells reside along a line outside the Neurod/Nestin-positive progenitor pool in the SAG.
(**A**) Antibody staining against Sox2 revealed that Sox2-positive cells (arrowheads) were distributed along a line in the medial portion of the adult SAG. (**B**) Co-staining for *sox2*:GFP, *nestin*:mCherry-T2a-CreER^{T2} labeling the Neurod/Nestin-positive progenitor cell pool and the mature neuronal marker Calretinin showed presence of *sox2*:GFP-positive cells (arrowheads) outside of the neurogenic niche with a distance of approx. 20 µm. Scale bar: 200 µm; cross sections showing dorsal to the top and lateral to the right.

exhibited an elongated shaped nucleus and clearly reside outside of Neurod/Nestin-positive progenitor pool, which were located on the medio-ventral side of the SAG. Interestingly, the density of nuclei medial to the line of Sox2-positive cells was usually very low compared to the area lateral of Sox2-positive cells.

Glia

In the zebrafish telencephalon, radial glia expressing the filamentous proteins glial fibrillary acidic protein (GFAP/Zrf1; in the following referred to as GFAP), S100B and members of the Hairy/enhancer of split 4 (Her4) family serve as neuronal progenitor cells (Chapouton *et al.*, 2006; Ganz *et al.*, 2010; Lam *et al.*, 2009). To analyze the presence and distribution of cells with glial characteristics, I used transgenic reporter lines and marker analysis to characterize the expression of the glia markers GFAP, Her4.3 and S100B in the juvenile and adult zebrafish SAG.

Co-staining of GFAP, neuronal marker HuC/D and GFP in transgenic *neurod*:GFP zebrafish showed strong expression of GFAP in the CNS and the medial part of the SAG entering the brain with a sharp boarder not overlapping with

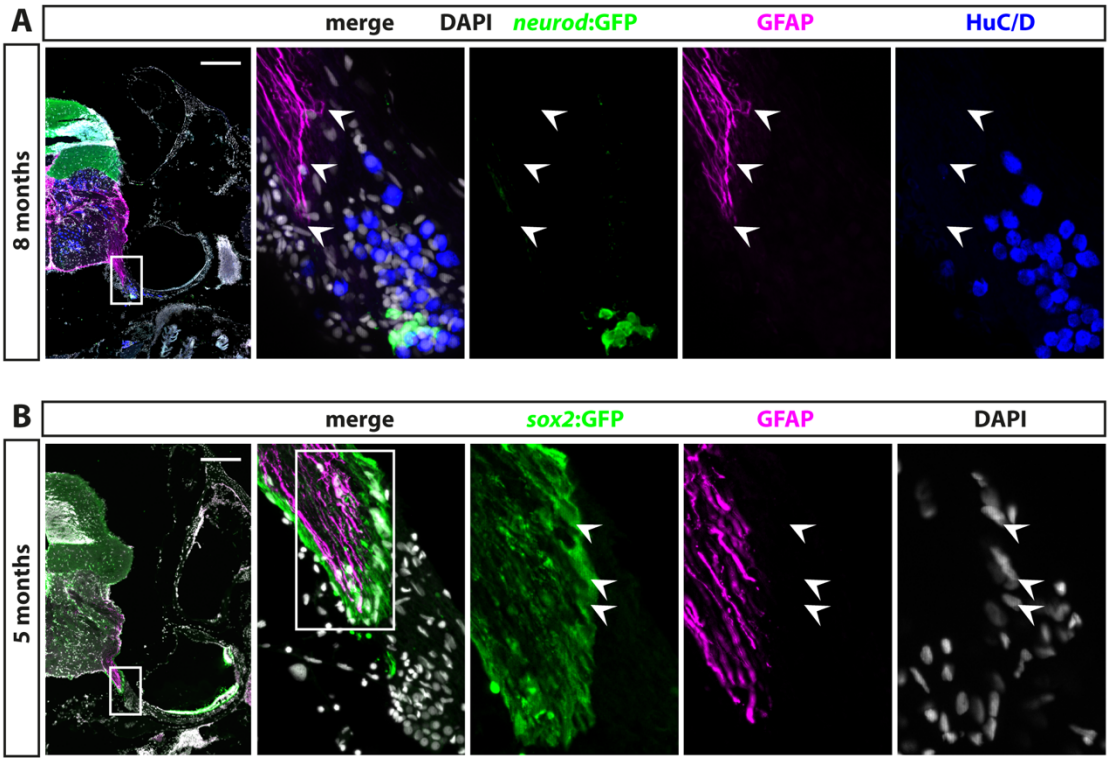

Figure 4.15 Expression of glia marker GFAP in the medial part of the SAG in close proximity of Sox2 expressing cells.
(**A**) Co-staining for GFAP and *neurod*:GFP in the adult SAG revealed presence of *neurod*:GFP-positive cells approx. 20 µm away from the GFAP-positive zone (arrowheads). (**B**) Co-staining of GFAP and *sox2*:GFP in the *sox2*:GFP line showed presence of *sox2*:GFP-positive cells (arrowheads) only a few microns lateral of the GFAP signal. Scale bar: 200 µm; cross sections showing dorsal to the top and lateral to the right.

neuronal HuC/D-positive cell bodies and separated (in this example more than 50 µm) from the more ventrolateral part of the SAG where the Neurod-positive cells of the neurogenic niche resides (Figure 4.15A). Since GFAP was expressed in the same area where also Sox2-positive cells were found, I analyzed GFAP expression in transgenic *sox2*:GFP fish and found, that *sox2*:GFP-positive cells are located only a few micrometer lateral to the GFAP domain and are not co-expressing GFAP (Figure 4.15B).

Similarily, Her4.3 (Figure 4.16) and S100B (Figure S.1) showed an identical expression pattern to GFAP, forming a sharp boarder in close proximity of Sox2 expressing cells in the medial part of the SAG, notably separated from the area where the neuronal HuC/D-positive cell bodies reside.

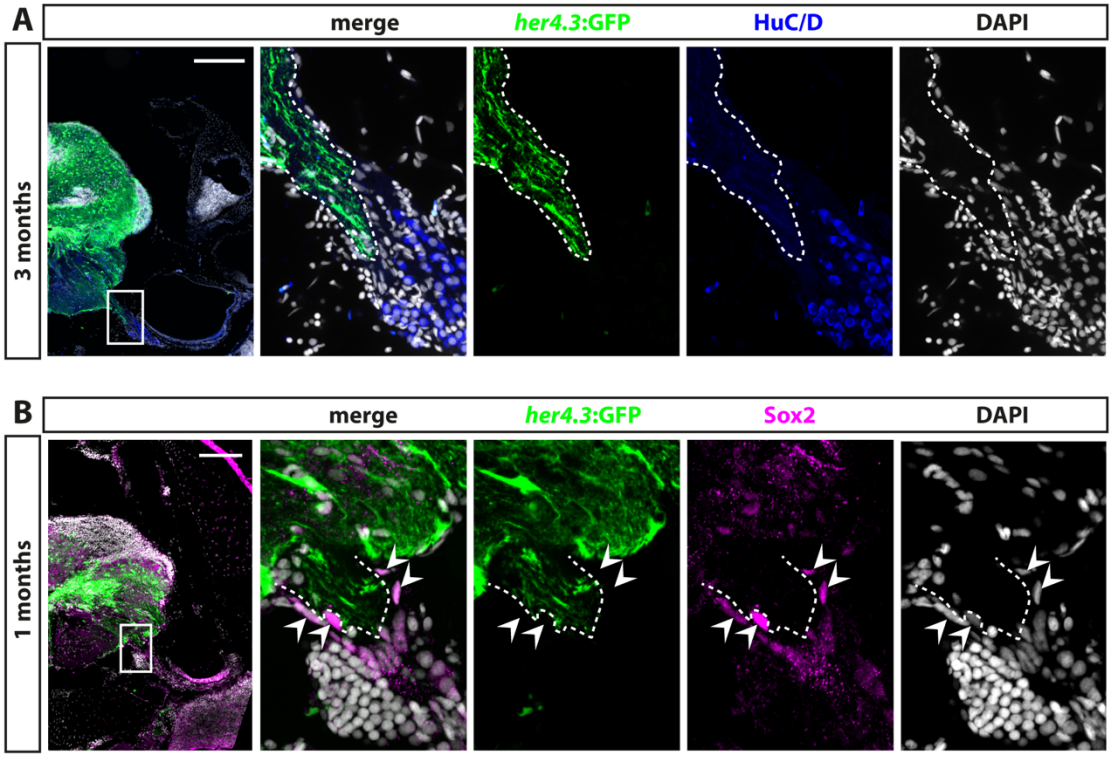

Figure 4.16 Expression of glia marker *her4.3*:GFP shows similar expression pattern to GFAP/Zrf1.
(**A**) Antibody staining against the glia marker *her4.3*:GFP and HuC/D in 3 months old zebrafish revealed expression of *her4.3*:GFP in the medial part of the SAG similar to the GFAP expression pattern (dashed line; see also Figure 4.15); HuC/D-positive neurons resided lateral from the *her4.3*:GFP expression. (**B**) Co-staining of the glia marker *her4.3*:GFP and Sox2 showed a similar expression pattern as reported in (Figure 4.15B) with expression of *her4.3*:GFP in close proximity medial of Sox2 expressing cells in the medial part of the SAG. Scale bar: (**A**) 200 µm and (**B**) 100 µm; cross sections showing dorsal to the top and lateral to the right.

Myelination

The peripheral and central nervous system transitional zone (PCTZ) is defined as the area in ganglia where the axons of the peripheral nervous system (PNS) lay within the central nervous system (CNS) and exhibits a sharp boundary at the CNS-PNS interface which is caused by the change in the myelination pattern from oligodendrocyte-mediated myelination in the CNS to Schwann cell-mediated myelination in the PNS (Bojrab *et al.*, 2017; Wang *et al.*, 2013; Fraher, 1999).

To analyze the presence and distribution of myelinating cells in the SAG, I combined antibody staining against Sox2 and the glia marker GFAP with the myelin markers ClaudinK and Mbp (Myelin basic protein). ClaudinK expression indicated strong myelination in the medial part entering the brain and low myelination in the lateral part of the juvenile SAG, resulting in a sharp boundary between both myelination levels visualizing the PCTZ as the strong myelinated zone in the medial part of the SAG (Figure 4.17A, dashed line). Co-staining with Sox2 revealed that

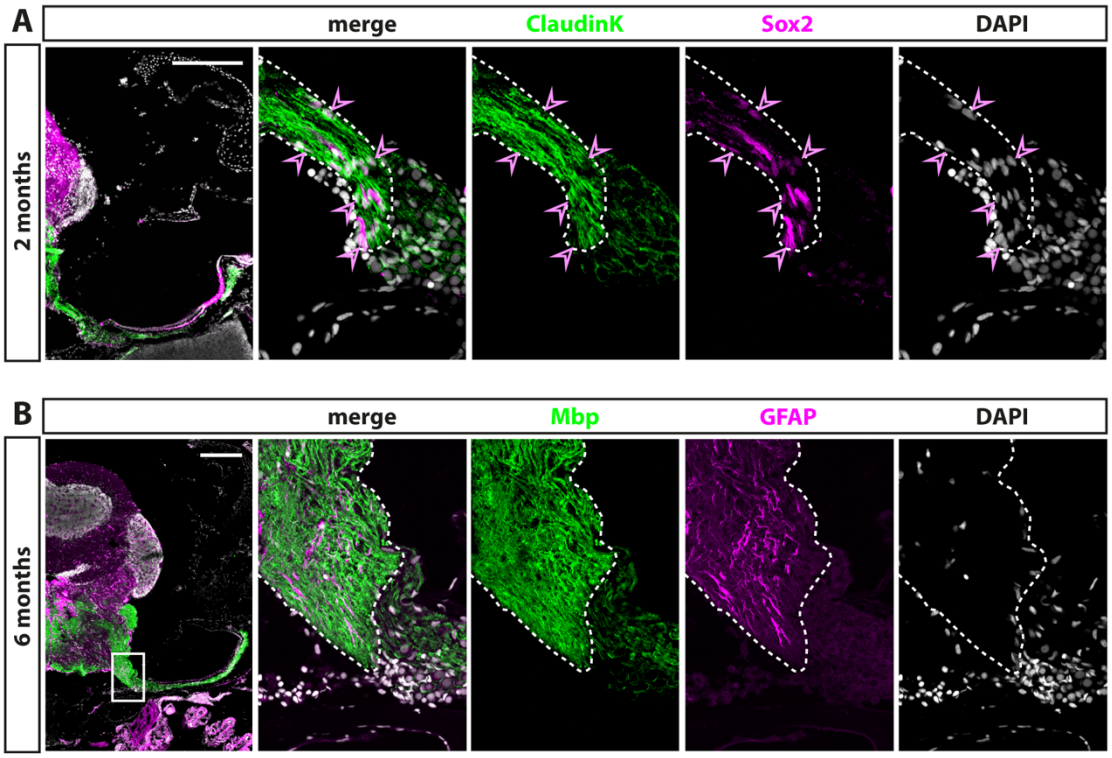

Figure 4.17 Expression of Sox2, the glia marker GFAP and differences in myelination patterns mark the peripheral and central nervous system transitional zone (PCTZ) in the SAG.
(**A**) Antibody staining against ClaudinK and Sox2 showing the CNS-PNS interface (dashed line) as a sharp boundary caused by a switch in the myelination pattern, the PCTZ (region encircled by the dashed line) as the highly myelinated area in the SAG, and Sox2-positive cells at the CNS-PNS interface in 2 months old fish. (**B**) Co-staining of the glia marker GFAP and the myelination marker Mbp shows the expression of the GFAP in the PCTZ ending a few microns medial of the CNS-PNS interface and a similar expression pattern regarding myelination as reported in (**A**) with the PCTZ marked by a change in the myelination pattern. Scale bar: 200 µm; cross sections showing dorsal to the top and lateral to the right.

Sox2-positive cells resided directly at the boarder of the CNS-PNS interface within the PCTZ (Figure 4.17, magenta arrowheads). Simultaneous labeling with the myelin marker Mbp (again showing strong signal in the medial and a weaker signal in the lateral part of the SAG (dashed line) with the glia marker GFAP revealed co-localization of GFAP-positive cells within the strongly myelinated territory in the adult SAG, hence within the PCTZ where all cells except the axonal projections of the sensory neurons from the SAG are a part of the central nervous system (Figure 4.17B). When analyzing the DAPI staining at the area of the PCTZ and in particular at the CNS-PNS interface, I found cells featuring the characteristic elongated shaped nuclei of Sox2-positive cells lateral of the GFAP stained area still within the region of strong myelination hence the PCTZ (Figure 4.17B, left of dashed line).

Comparing the nuclear DAPI staining in all samples depicted in Figure 4.14-Figure 4.17, revealed that the density of nuclei medial to the line of Sox2-positive cells in the PCTZ was usually very low in comparison to the area lateral of Sox2-positive cells. This, together with the characteristic elongated shaped nuclei of Sox2-positive cells, allows the identification of the PCTZ even on the basis of a nuclear staining such as DAPI alone. Measuring the length of the PCTZ on the ventral side of the SAG, starting at the CNS-PNS interface marked by Sox2 positive cells, expression of glia cells and/or the myelination pattern until the SAG reaches the hindbrain, revealed that the PCTZ reaches more than 100 µm (in adult examples measured here approx. 130 µm) into the SAG.

Altogether I show that the distribution of cells expressing the neuronal stem cell marker Sox2, as well as cells with glial characteristics, expressing GFAP, *her4.3*:GFP and S100B are not present in or in close proximity to the Neurod/Nestin-positive progenitor cell pool. However, I find that Sox2-positive cells, the expression pattern of glia (GFAP, *her4.3*:GFP, S100B) and myelination (ClaudinK, Mbp) marker as well as the characteristic shape and distribution of nuclei in this area mark the PCTZ in the medial part of the SAG, which is highly similar to the mammalian system (Fraher and Delanty, 1987; Hu *et al.*, 2014).

4.1.11 Summary

Taken together, the characterization of the juvenile and adult zebrafish SAG revealed that the SAG consists (simplified) of an elbow-shaped anterior and a rod-shaped posterior part, both branching laterally to innervate the six different sensory patches. Even though the overall number of sensory neurons decreases from juvenile to adult stages, the SAG exhibits lifelong neurogenesis. New sensory neurons derive from a Neurod/Nestin-positive neurogenic niche which is highly active at juvenile stages but turns quiescent during adulthood, where Neurod/Nestin-positive neuronal progenitors are no longer proliferating and only rarely give rise to new sensory neurons. Interestingly, this study indicated the existence of a presumptive,

marker-negative stem cell-like cell population that replenishes the neurogenic niche throughout life. Additionally, this thesis established the stem cell marker Sox2 to label the CNS-PNS interface at the PCTZ. The PCTZ was shown to be labeled by a strong myelination pattern and additionally by the expression of the radial glia marker GFAP, Her4.3 and S100B.

4.2 Transcriptome analysis of proliferating stem cell-like and progenitor cells in the juvenile and adult zebrafish SAG

4.2.1 Establishment of an experimental pipeline to obtain single cells from the SAG for transcriptome analysis via single-cell RNA sequencing

Since the nature of the putative stem cell-like cell population, that replenishes the pool of Neurod/Nestin-positive progenitor cells throughout life, remains unknown (see chapter 4.1.7), I aimed for an in-depth transcriptome analysis using single-cell RNA sequencing (scRNAseq). Therefore, I established an experimental pipeline to obtain single cells from the juvenile and adult SAG. Considering the size, structure and position of the SAG, the first and most difficult step in this pipeline was the dissection of the SAG, in particular when using juvenile fish, which are smaller and have softer tissue in comparison to adults (see chapter 3.2.12). When dissecting the SAG, the crucial point was to collect as much of the SAG as possible and especially of the anterior part where the neurogenic niche resides in the medial part close to the brain, while sparing the tissue of the CNS. To further increase the specificity of the analyzed samples, I used transgenic lines labeling cells of interests, such as Neurod/Nestin-positive progenitor cells and proliferating cells. To prove the suitability of the experimental pipeline, the SAG from adult transgenic *neurod*:GFP fish was dissected and dissociated to obtain single cells using the Neural Tissue Dissociation Kit (MACS, Miltenyi BIOTEC). After fluorescence activated cell sorting (FACS) for live and GFP-positive cells, samples were transferred to the Genome Center for RNA isolation and cDNA synthesis (Figure 4.18A). To analyze the obtained samples, a PCR for *neurod* and *nestin* was performed on the generated cDNA (Figure 4.18B, C). In line with the data obtained from the immunohistochemical analysis, both samples (sample F and sample M) exhibited the expected PCR products, hence confirming the expression of *neurod* and *nestin* within the neurogenic niche in the adult SAG.

Taken together, I successfully established an experimental pipeline to obtain single cells from the zebrafish SAG which can be used for further in-depth transcriptome analysis via scRNAseq.

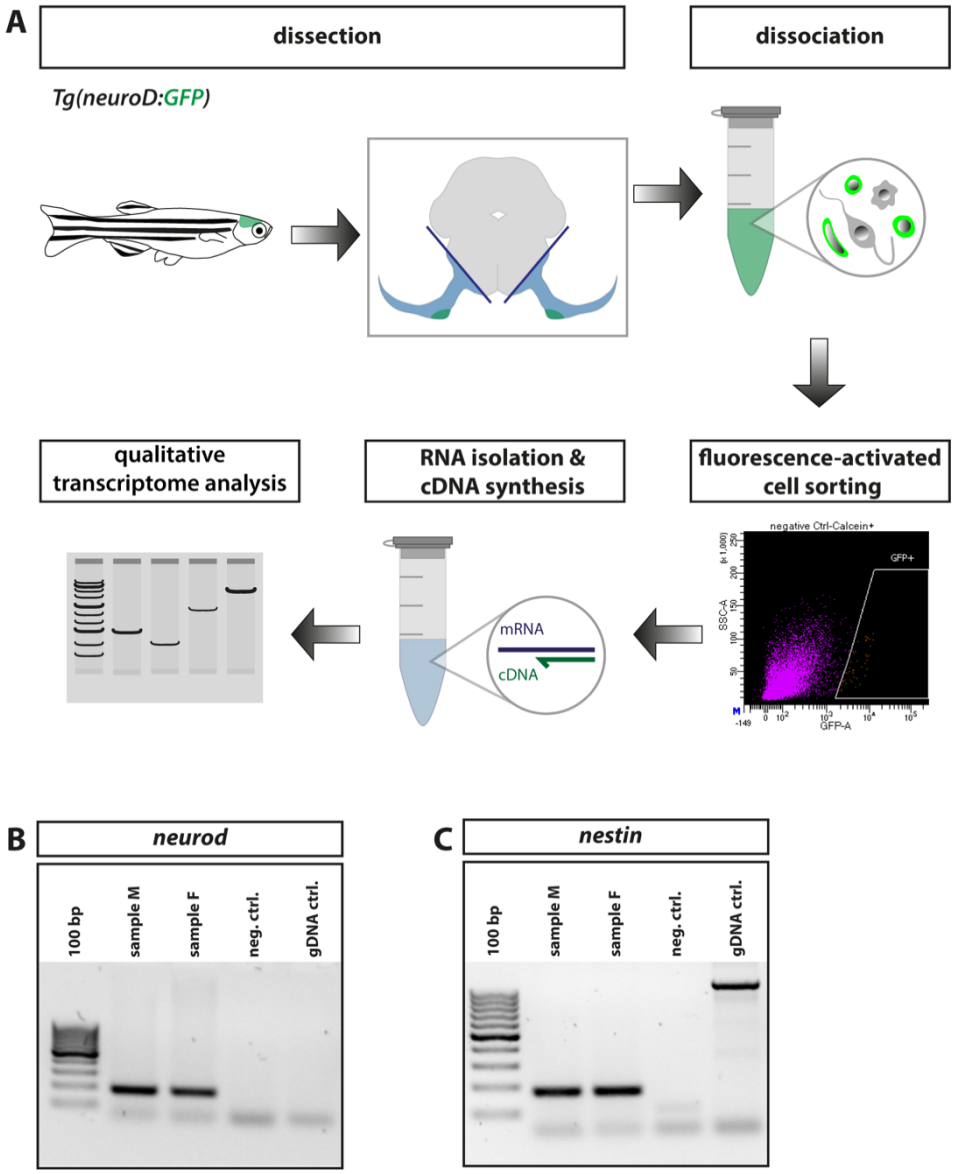

Figure 4.18 Expression of *neurod* and *nestin* in cells isolated from the adult SAG of *neurod*:GFP transgenic fish to demonstrate suitability of the established single cell isolation pipeline.
(**A**) Scheme depicting the workflow of SAG dissection, dissociation, fluorescence-activated cell sorting, RNA-isolation, cDNA synthesis and PCR to analyze the expression of *neurod* and *nestin* in the pool of *neurod*:GFP-positive progenitor cells in the SAG as a proof of principal. (**B**,**C**) PCR for *neurod* (**B**) and *nestin* (**C**) on cDNA obtain from *neurod*:GFP-positive cells isolated from the adult SAG of male (sample M) and female (sample F) *Tg(neurod:GFP)* transgenic fish further confirms expression of *neurod* and *nestin* in the adult zebrafish SAG; lanes from the left to the right: 100 base pair ladder; sample M; sample F; negative control w/o DNA; negative control with genomic DNA (gDNA).

4.2.2 Transcriptome analysis of proliferating cells in the juvenile SAG using single cell RNA sequencing

The strategy to find potential markers for the presumptive stem cell-like cells population in the SAG was based on a short-term lineage tracing approach. The double transgenic animals carried the fluorescent reporters *pcna*:GFP to label all proliferating cells in the SAG, and *nestin*:mCherry-CreER^{T2}, which was shown to label proliferating and non-proliferating neuronal progenitor cells in the juvenile SAG (see chapter 4.1.8). Based on the fluorophore perdurance in both reporter lines, sorting for *pcna*:GFP positive and *pcna*:GFP/*nestin*:mCherry-CreER^{T2} positive cells, proliferating cells outside the neurogenic niche and their progeny would be labeled by *pcna*:GFP, whereas cells sorted for *pcna*:GFP/*nestin*:mCherry-CreER^{T2}-double positive cells would include the potential progeny of the presumptive stem cell differentiating into neuronal progenitor cells, proliferating, neuronal progenitor cells and their progeny differentiating into neurons. The expression of *pcna* as well as different neuronal markers can be used to distinguish between the three latter: progeny of the presumptive stem cell niche would not express *pcna* or any neuronal marker, whereas proliferating neuronal progenitor cells would express *pcna*. Progeny of proliferating neuronal progenitor cells, however, would also not express *pcna* but in contrast to progeny from the presumptive stem cells, would express (early) neuronal markers. Additionally, the application of bioinformatic analysis tools such as pseudo-temporal ordering, sorting cells in "pseudo time" according to their differential state, or RNA velocity, predicting the future state of individual cells, could be a valuable tool to unravel the identity of the presumptive stem cells (Trapnell *et al.*, 2014; La Manno *et al.*, 2018).

Besides this, the analysis of proliferating neuronal progenitor cells would also allow to find novel markers for this cell population but would also potentially enable to investigate signaling pathways involved in regulating the proliferative capacity of neuronal progenitor cells in the SAG, for example using bioinformatic tools such as gene ontology enrichment analysis or ingenuity pathway analysis.

Nowadays, the most commonly used systems for scRNAseq are the droplet-based 10X Genomics Chromium approach and the Smart-seq2 method. In comparison to 10X Genomics Chromium, which can be used to analyze thousands of cells at once and therefore can also identify more cells clusters, the Smart-seq2 method is based on microtiter plates thus only analyzing fewer cells but with a higher sensitivity regarding the number of discovered genes (Wang *et al.*, 2021). Since the SAG is a small and very delicate anatomical structure and the potential neuronal stem cell population is a rare cell type, I decided to use the Smart-seq2 approach which relies on less cells for the analysis but has a high sequencing depth of the transcriptome.

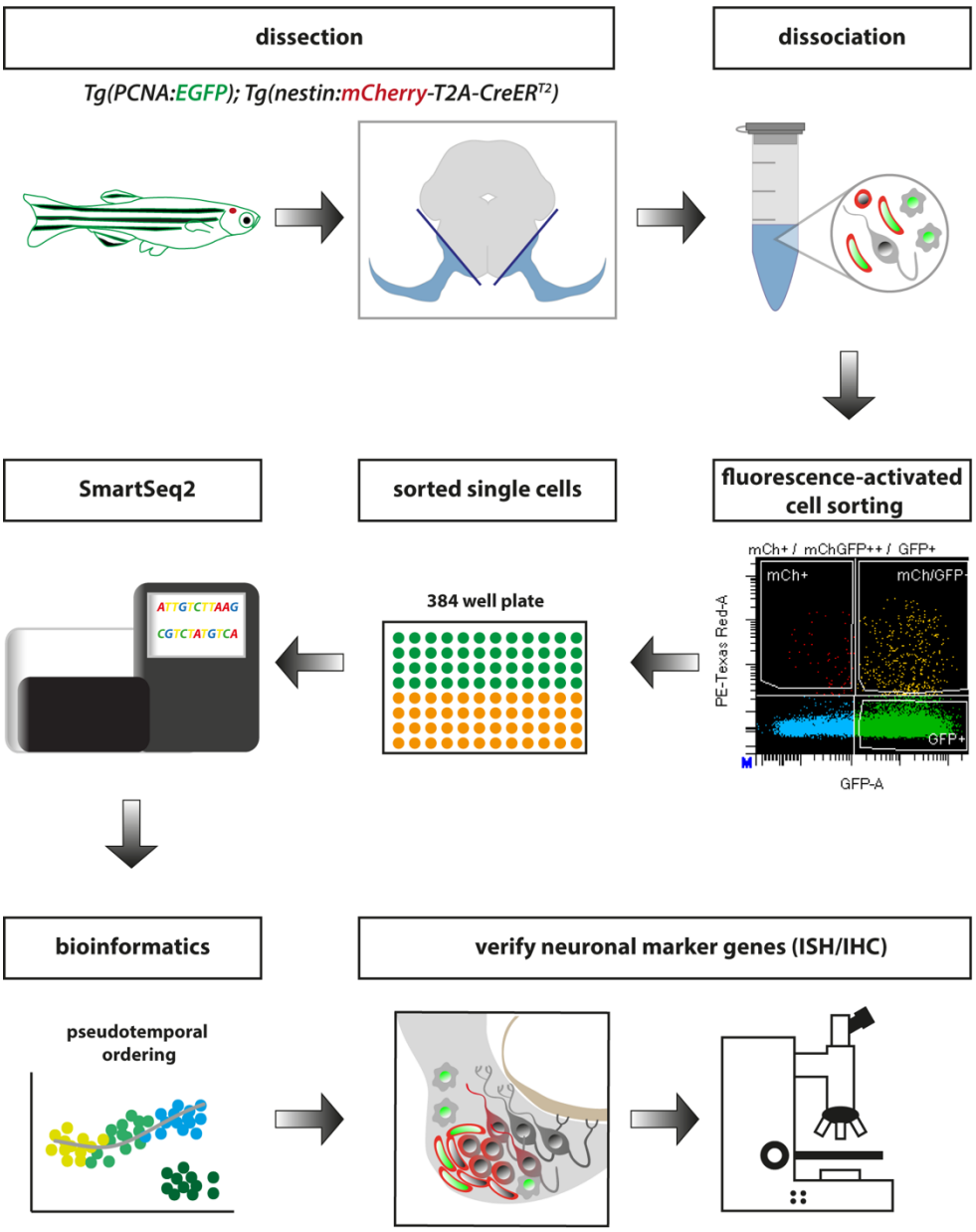

Figure 4.19 Experimental workflow to find novel marker genes for neuronal stem and progenitor cells in the juvenile SAG.
Schematic illustration of the workflow to identify novel marker genes for neuronal stem and progenitor cells using juvenile, double-transgenic *pcna*:GFP/*nestin*:mCherry-CreER^{T2} fish. in total 24 SAGs from 12 double-transgenic fish aged 8 weeks were dissected and pooled for cell dissociation. Using FACS, 144 *pcna*:GFP-positive and 205 *pcna*:GFP/*nestin*:mCherry-CreER^{T2}-double positive living cells were sorted into a 384 well-plate and handed over to the Deep Sequencing Facility (CMCB) for sequencing via the SmartSeq2 method and subsequent bioinformatic analysis. The Verification of candidate genes for potential novel neuronal stem and progenitor cell marker via ISH and IHC is still ongoing.

4.2.3 Identification of 12 different cell clusters in the transcriptome data set obtained from the juvenile SAG

For the bioinformatical analysis, out of 144 cells sorted for *pcna*:GFP and 205 cells sorted for *pcna*:GFP/*nestin*:mCherry-CreER^{T2}, 54 and 144 cells passed the quality control, respectively. In total, I annotated 12 different cell clusters in the juvenile transcriptome data set (Figure 4.20). Originally, these 198 cells were only clustered into 8 different clusters in a first analysis: the three cells of the sensory epithelium cluster were assigned to the clusters stem cell-like 1 and progenitor cells 1 and the cells from the cluster stem cell-like 2, progenitor cells 2, oligodendrocyte precursor cells and myelinating cells were grouped together into a single cluster. Identification of the 12 different clusters was done in a semi-biased approach by analyzing the most differentially expressed genes in different groups of cells as well as searching for cells expressing known marker genes for specific cell types. For every cluster a set of selected marker genes containing genes from the list of the 25 most differentially expressed genes within that clusters as well as genes serving as established marker genes for certain cell types are depicted in a heatmap (Figure S.2).

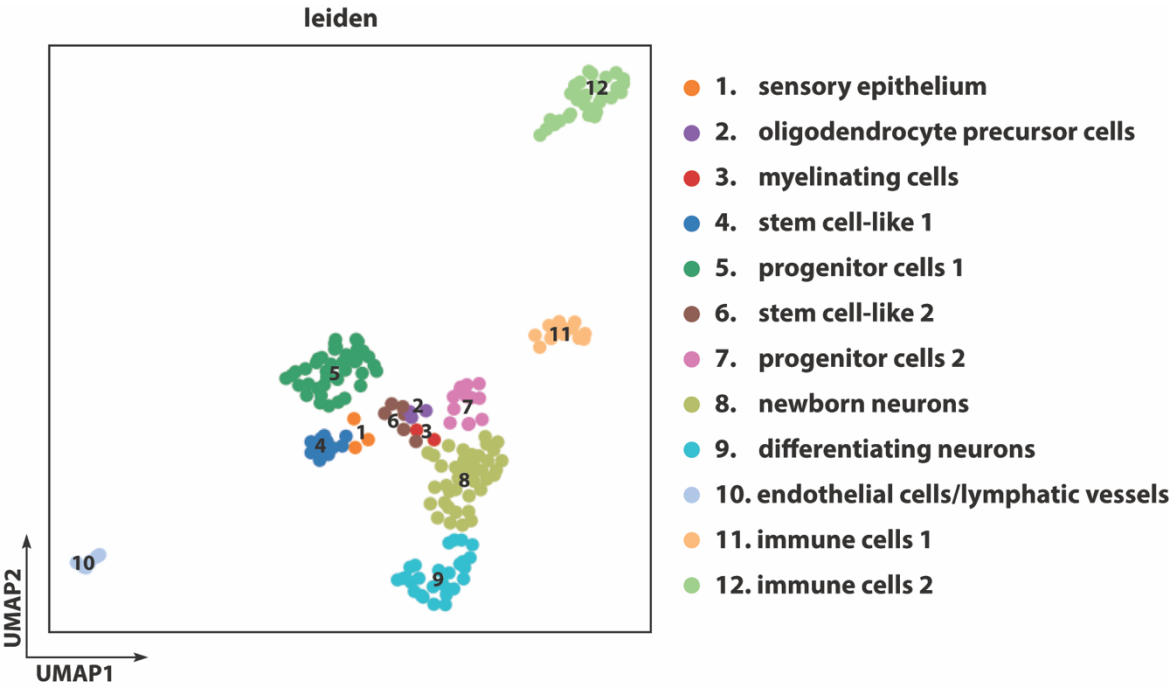

Figure 4.20 scRNAseq identifies 12 different cell populations in the juvenile SAG. The transcriptome data is depicted on the uniform manifold approximation and projection (UMAP) plot (in the following referred to as UMAP). Clusters (potentially) related to the neural lineage (sensory epithelium, oligodendrocyte precursor cells, myelinating cells, stem cell-like 1&2, progenitor cells 1&2, newborn neurons and differentiating neurons) cluster together in the center, whereas the cluster of endothelial cells and the two immune cell cluster (immune cell 1&2) are located in the periphery.

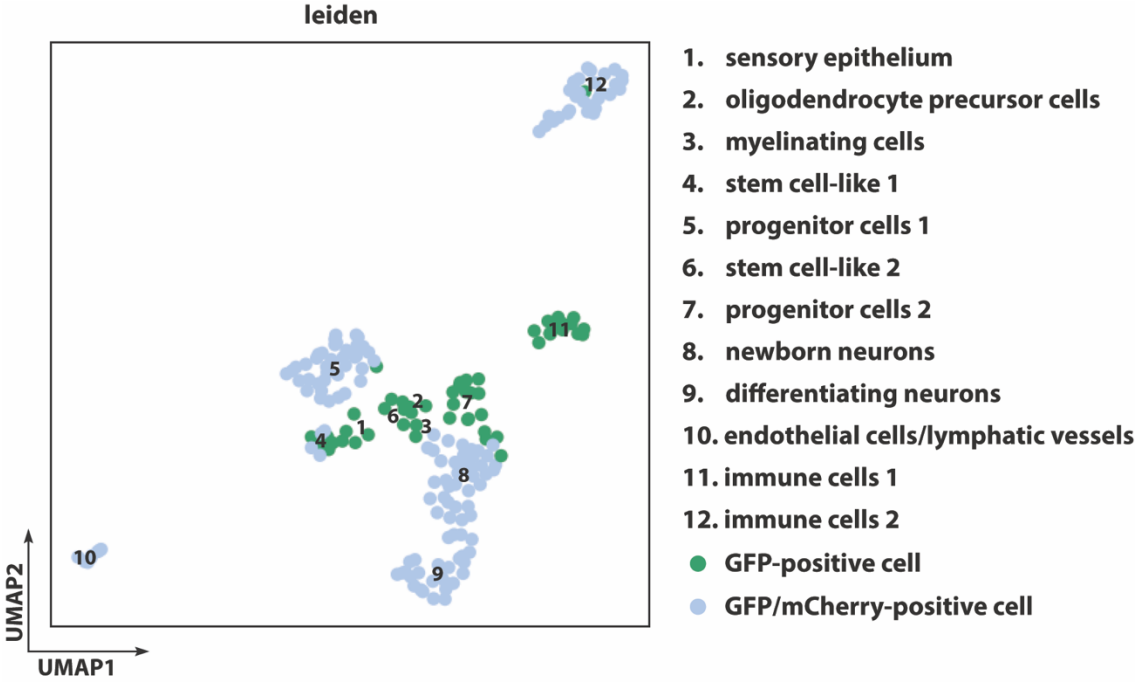

Figure 4.21 UMAP depicting the distribution of cells sorted as GFP-positive or GFP/mCherry-positive in the transcriptome data set from the juvenile SAG.
Cluster 1, 2, 6, 7, and 11 contained only cells sorted as GFP-positive. Cluster 5,8, 9, 10 and 12 contained (almost) only cells sorted as GFP/mCherry-positive. Cluster 3 and 4 contained a mix of GFP- and GFP/mCherry-positive cells.

4.2.4 Expression profile eliminates cluster 10, 11 and 12 as potential stem cell-like cell clusters in the juvenile SAG

Visualization of the juvenile transcriptome data set on a uniform manifold approximation and projection plot (UMAP), revealed that 9 of the 12 clusters were located closer together in the center of the UMAP, whereas the other 3 clusters were found in the periphery.

sqRNAseq identifies one cluster of endothelial/lymphatic vessel cells and two immune cell cluster

Gene expression analysis of cluster 10 revealed the expression of genes such as *stab2* and *flt4* which are associated with vasculogenesis and vascular endothelial cells, as well as *stab1*, involved in regulating lymphangiogenesis, hence identifying these cells as endothelial cells and cells of lymphatic vessels (Kuan *et al.*, 2009; Stoll, Bartsch and Kroll, 2013) (Figure 4.22A).

Cells of cluster 11 and 12 were identified as immune cells (Figure 4.22B/C). Based on the expression of genes associated with T cell development (e.g., *rag1* and *ccr9a*; Figure 4.22B), cells of cluster 11 are most likely immune cells of the lymphoid lineage (Willett *et al.*, 1997; Huang *et al.*, 2019) (Figure 4.22B). Cells of cluster 12 expressed markers known to label macrophages such as *mpeg1.1* and *cxcr4b*, suggesting these cluster to also contain immune cells (Rougeot *et al.*, 2019) (Figure 4.22C).

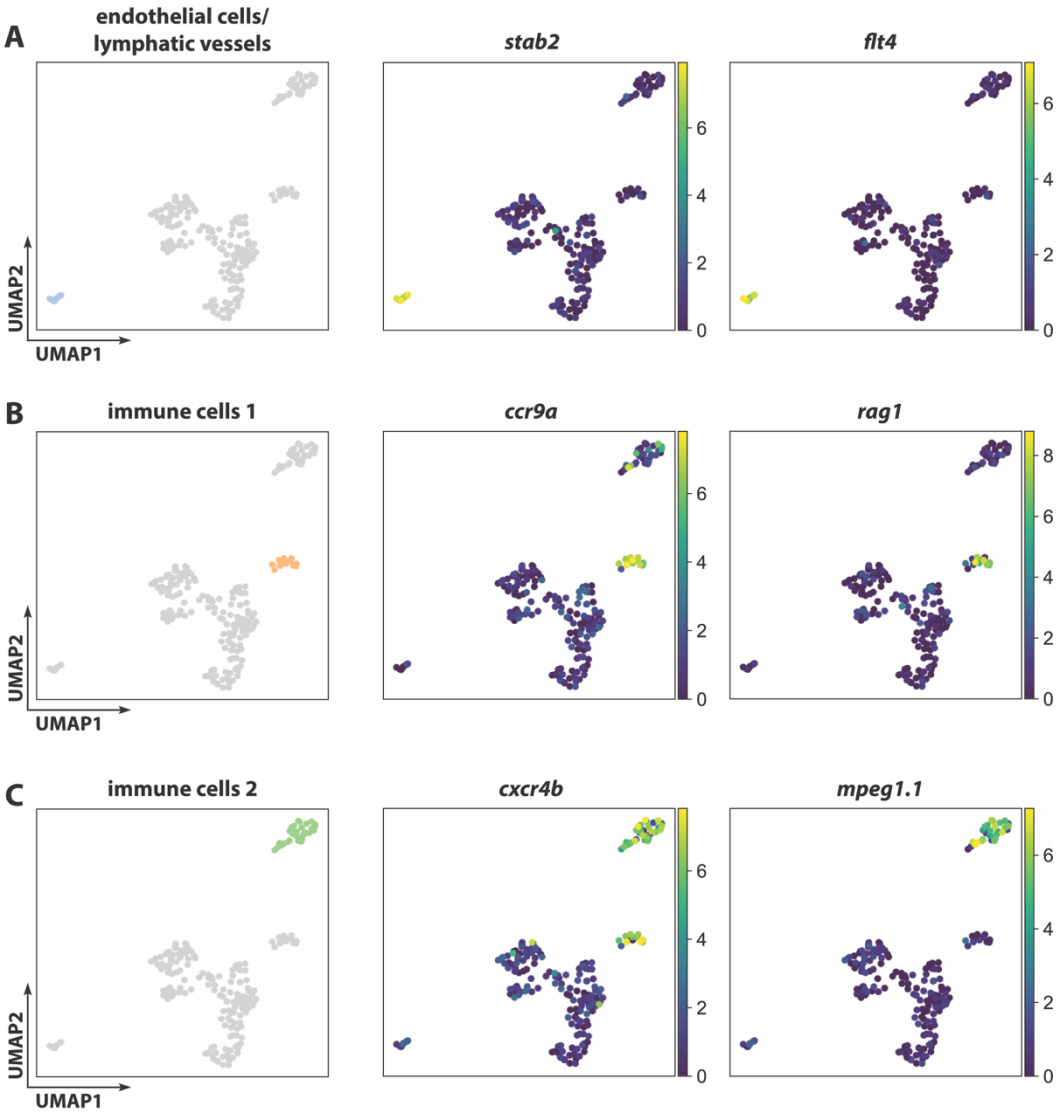

Figure 4.22 scRNAseq identifies cell clusters containing endothelial cells/lymphatic vessels and immune cell populations.
(**A**) UMAPs depicting the expression of the genes *stab2* and *flt4*, both associated with vasculogenesis, in cluster 10, identifying it as a cluster of endothelial cells/lymphatic vessels. (**B**-**C**) Identification of cluster 11 and cluster 12 as two immune cell cluster based on the expression of *ccr9a* and *rag1* associated with the lymphoid lineage (cluster 11, immune cells 1) and *cxcr4b* and *mpeg1.1* associated with the macrophages myeloid lineage (cluster 12, immune cells 2).

Interestingly, only cells from cluster 11 were sorted as *pcna*:GFP-positive, whereas cells from cluster 10 and 12 were selected as being *pcna*:GFP/*nestin*:mCherry-CreER^{T2}-double positive. Based on their expression profile, however, cluster 10, 11 and 12 were not considered as clusters containing the presumptive neuronal stem cell-like cell population.

4.2.5 Identification of cells from the sensory epithelium (cluster 1), oligodendrocyte precursor cells (cluster 2) and myelinating cells (cluster 3) as distinct clusters in the juvenile SAG

Searching for the expression of known marker genes for different cell types in combination with the analysis of differentially expressed genes in a fraction of cells from one cluster of the originally 8 annotated clusters enabled to identify small subclusters. Even though these subclusters, which were all sorted as *pcna*:GFP-positive cells, only consisted out of 2-3 cells they still featured a unique expression pattern identifying them as a separate cell population.

Cluster 1 contains cells from the sensory epithelium

Cluster 1 as well as the neighboring cluster 2 expressed *coch*, orthologous to the human gene COCH which is implicated to be involved in autosomal dominant non-syndromic hearing loss (Usami *et al.*, 2003). Additionally, cells from cluster 1 exclusively expressed markers of the otic epithelium and genes involved in otolith formation and tethering such as *stm*, *cldnb*, *epcam* and *otomp*, identifying cells from this cluster as sensory epithelium (Söllner *et al.*, 2003; Han *et al.*, 2011; Slanchev *et al.*, 2009; Murayama *et al.*, 2005) (Figure 4.23).

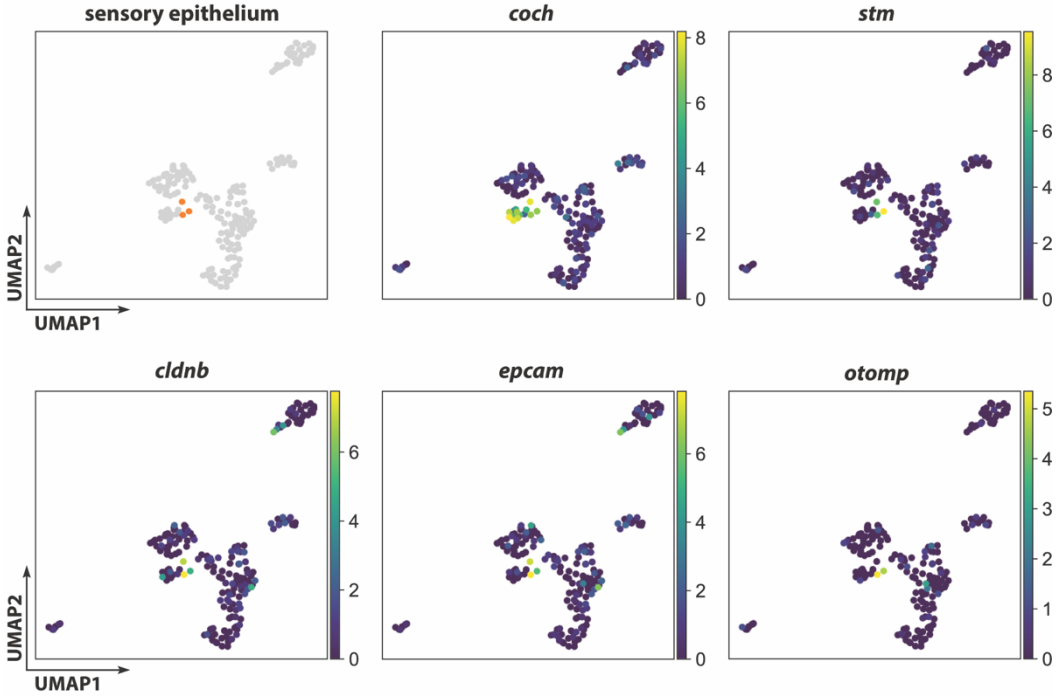

Figure 4.23 Cluster 1 expresses markers associated with the sensory epithelium. *coch* is expressed in cluster 1 as well as the neighboring cluster 2. Genes associated with the otic epithelium as well as genes involved in otolith formation and tethering such as *stm cldnb*, *epcam* and *otomp* are exclusively expressed in the three cells of cluster 1, identifying them as cells from the sensory epithelium.

Cluster 2 and 3 contain cells associated with myelination

Cluster 2 and cluster 3 were identified as clusters containing cells involved in myelination. Cells in cluster 2 expressed marker genes of oligodendrocyte precursor cells such as *olig1*, *olig2*, *sox10* and *slc1a1* as well as pre-myelinating oligodendrocytes like *nkx2.2a* (Ackerman and Monk, 2016; Bianchi *et al.*, 2014) (Figure 4.24A). Transcriptome analysis of cluster 3 revealed that these cells correspond to myelinating cells expressing marker genes like *cldnk* (*claudin k*) and *mbpb* (*myelin basic protein b*), which have been both already used in this study to analyze the myelination pattern in the SAG (Figure 4.24B; see also chapter 4.1.10) (Münzel et al., 2012).

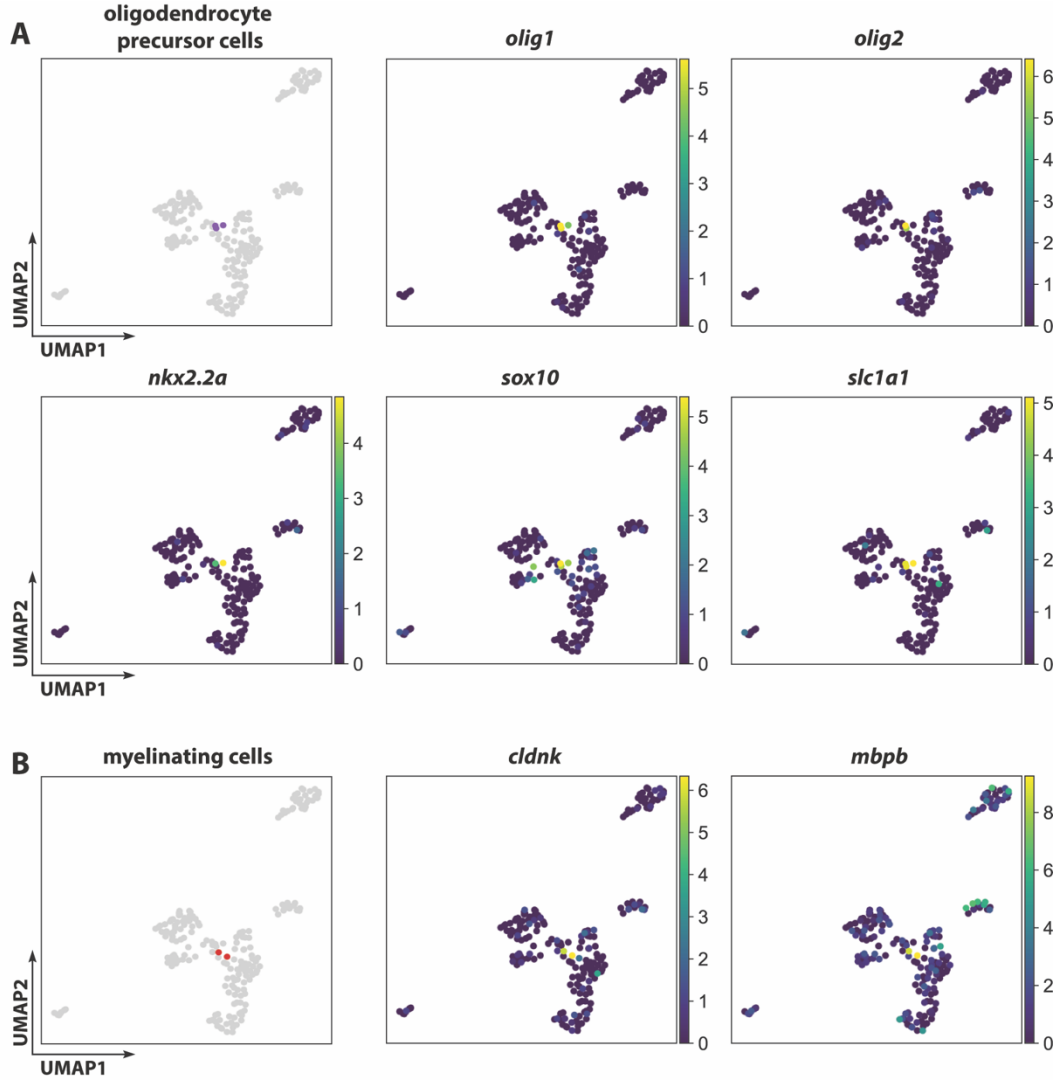

Figure 4.24 scRNAseq identifies two clusters involved in myelination.
(**A**) Cells in cluster 2 express marker genes for oligodendrocyte precursor cells like *olig1*, *olig2*, *nkx2.2a*, *sox10* and slc1a1. (**B**) The adjacent cluster 3 expresses genes involved in myelination such as *cldnk* and *mbpb* (both also used as myelination markers in Figure 4.17)

4.2.6 scRNAseq revealed that *nestin* is only expressed in a subpopulation of *neurod*-expressing neuronal progenitor cells in the juvenile SAG

Immunohistochemical analysis of the neuronal progenitor markers Neurod and Nestin using the transgenic lines *neurod*:GFP and *nestin:*mCherry-T2a-CreER^{T2} in the juvenile and adult SAG suggested that both are expressed mainly in the same population of neuronal progenitor cells in the neurogenic niche and can both be used to label this cell population (see also chapter 4.1.8). However, a few cells (usually located at the medioventral side of the cell population) were found to be only *neurod*:GFP positive, whereas a few newborn neurons were positive for *nestin:*mCherry-T2a-CreER^{T2} and the neuronal marker HuC/D but not *neurod*:GFP,

Interestingly, the scRNAseq revealed the presence of two distinct cluster of neuronal progenitor cells in the juvenile SAG: the larger cluster named progenitor cells 1 (cluster 5) comprising 39 *pcna*:GFP/*nestin*:mCherry-T2a-CreER^{T2}-positive cell co-expressing *nestin* and *neurod*, and the smaller named progenitor cells 2 (cluster 7) comprising 14 *pcna*:GFP-positive cells expressing *neurod* but not *nestin* (Figure 4.25, Figure 4.26).

The cluster of *nestin/neurod1*-expressing progenitor cells (progenitor cells 1) is characterized by the expression of genes encoding several ribosomal proteins as well as genes from the her-family such as *her4.2/4.3/4.4* and *her15.1/15.2* that are known to play a role in neuronal stem and progenitor cells (Figure 4.25). Additionally, cells from cluster progenitor cells 1 express genes they share with the cluster of newborn neurons that cells in the progenitor cell 2 cluster do not express: the radial glia marker *vim*, a marker for the statoacoustic ganglion called *tlx2* (Hatano *et al.*, 1997) and *sfpq*, a gene known to be involved in CNS development (Lowery, Rubin and Sive, 2007) (Figure 4.25).

In contrast to progenitor cells 1, the cluster of *neurod1*-only expressing progenitor cells (progenitor cells 2) exclusively expressed markers associated with glutamatergic synapses such as *cbln12* (known to be co-expressed with Neurod1 in granule cells in zebrafish larvae, Dohaku *et al.*, 2019) and *sh3gl2a* (www.ensemble.org; ENSDARG00000023600) as well as *olfm1a*, predicted to be involved in pre- and postsynaptic events (Nakaya, Sultana and Tomarev, 2017) (Figure 4.26). Also cells from cluster progenitor cells 2 showed expression of genes that are also expressed in the cluster of newborn and differentiating neurons but not in the other progenitor cell cluster (progenitor cells 1): *snap25a/b,* associated with the neuronal SNARE complex mediating synaptic vesicle fusion (Oyler *et al.*, 1989) and *stmn4*, critical for maintenance of neural progenitor cells during zebrafish CNS development (Lin and Lee, 2016). Interestingly, a gene called *r3hdm1*, expressed in mouse hair cells and associated with the function of hearing in mammals (Concas *et al.*, 2021), was the top 1 differentially expressed gene in the cluster of *neurod*-only expressing progenitor cells (progenitor cells 2) and is also expressed in a subset of progenitor cells 1 and in the cells from the cluster of newborn neurons nearest to cluster progenitor cells 2. This suggests *r3hdm1* as a potential marker for neuronal progenitor cells differentiating to newborn neurons.

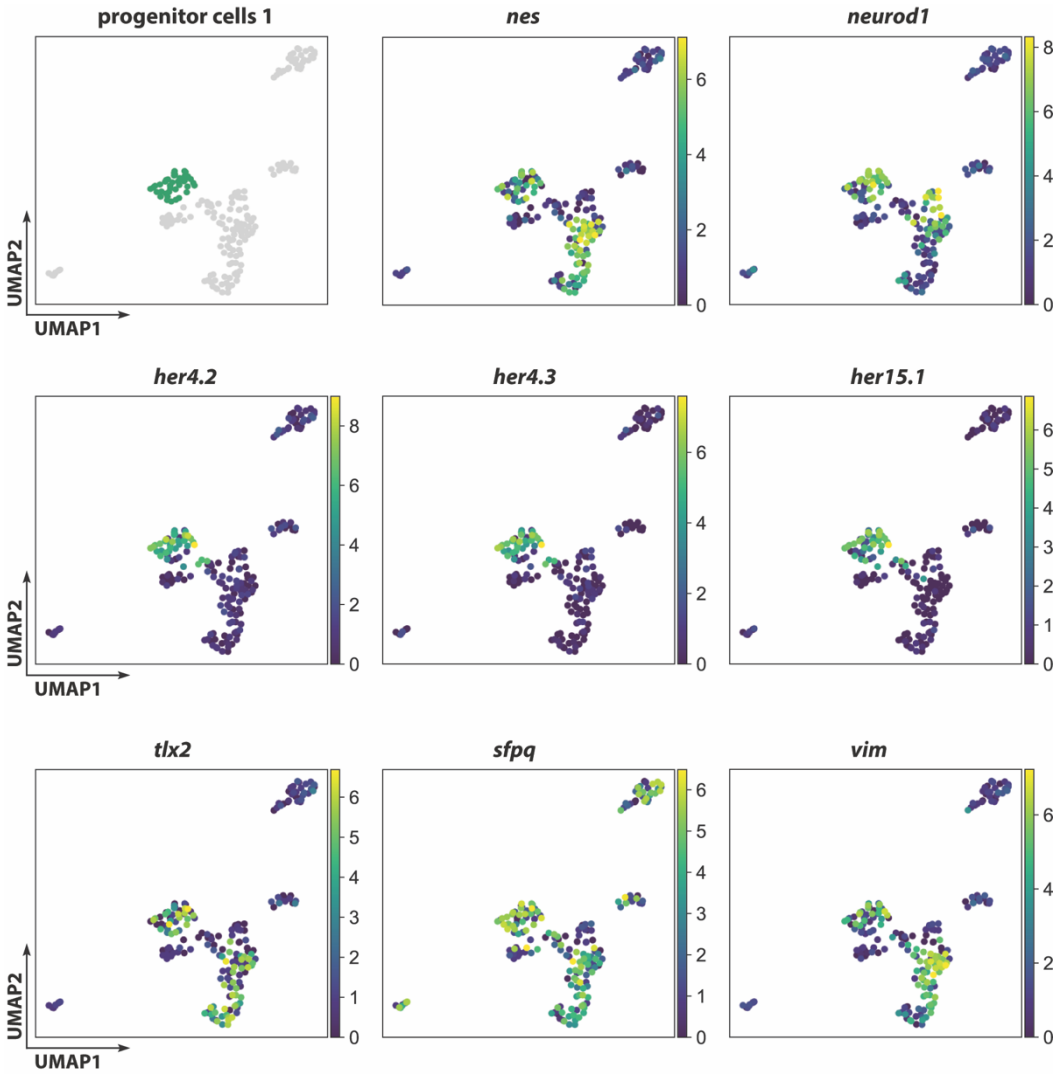

Figure 4.25 Neuronal progenitor cells of the progenitor cell 1 (cluster 5) co-express *nestin* and *neurod1*.
Cluster 5 is one out of two neuronal progenitor cell clusters, consisting of *nestin*(*nes*)/*neurod1*-positive progenitor cells (progenitor cells 1). Genes from the *her* family, here UMAPs shown for *her4.2*, *her4.3* and *her15.1*, are exclusively expressed in progenitor cells 1 and in a fraction of cells from the stem cell-like 2 cluster (cluster 6). Progenitor cells 1 share expression of *tlx2*, *sfpq* and *vim* with the cluster of newborn and differentiating neurons (cluster 8 & 9) but not with the second neuronal progenitor cell cluster (cluster 7, progenitor cells 2).

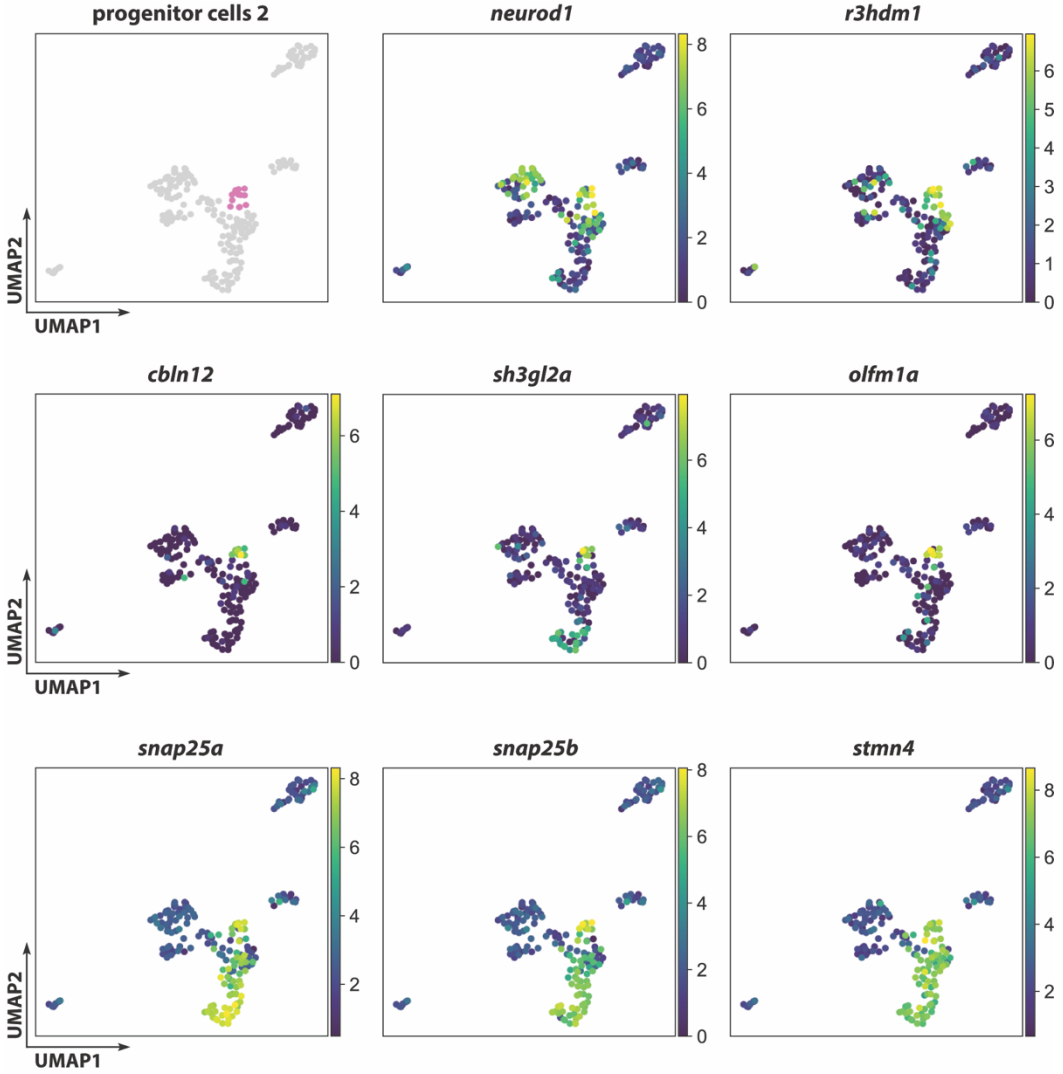

Figure 4.26 Neuronal progenitor cells of the progenitor cell 2 cluster (cluster 7) express *neurod1* as well as markers associated with glutamatergic synapses.
The second cluster of neuronal progenitor cells, progenitor cells 2 (cluster 7), expresses *neurod1* but not *nestin* (*nes*; see Figure 4.25). *r3hdm1* is the top 1 differentially expressed gene of the progenitor cells 2 cluster and is also expressed in a small fraction of cells in cluster progenitor cell 1 and newborn neurons. Progenitor cells 2 also expresses several genes associated with synapses, some of those being exclusively expressed in the cluster of progenitor cells 2 such as *cbln12*, *sh3gl2a* (also expressed at lower levels in the cluster of differentiating neurons), *olfm1a*, and others being also expressed in the clusters of newborn and differentiating neurons such as *snap25a,snap25b*. Similar, *stmn4*, involved in neuronal differentiation, is expressed throughout the clusters progenitor cells 2, newborn and differentiating neurons.

Analysis of r3hdm1 expression by in situ hybridization does not validate the transcriptome data from the juvenile SAG

To further investigate whether the expression of *r3hdm1* can be used to distinguish the two distinct neuronal progenitor cell populations, the spatial expression of *r3hdm1* was analyzed using *in situ* hybridization. To this aim, sections

of the SAG of juvenile *neurod*:GFP fish combined with antibody staining against either the proliferation marker PCNA or the neuronal marker HuC/D were used by former bachelor student Daniel Scherer (Figure S.3 and Figure S.4; Daniel Scherer, bachelor thesis, 2021). The analysis revealed that *r3hdm1* expression was present in the neurogenic niche in a fraction of the proliferating *neurod*:GFP-positive neuronal progenitor cells and the majority of *neurod*:GFP-only positive neuronal progenitor cells. Additionally, *r3hdm1* also co-localized with *neurod:*GFP/HuC/D-double positive newborn neurons and also HuC/D positive neurons which is in contrast to the scRNAseq data, where expression was limited to a few cells of cluster progenitor cells 1, the entire cluster of progenitor cells 2 and a few cells of the newborn neuron cluster. Hence, *r3hdm1* cannot be used as a marker to distinguish the two different neuronal progenitor cells.

4.2.7 scRNAseq identifies a cluster of newborn neurons (cluster 8)

HuC/D, also known as Elavl3 (HuC) and Elavl4 (HuD), is commonly used as a pan-neuronal marker. *elavl3* and *elavl4* were both expressed in cluster 8 and the adjacent cluster 9 (Figure 4.27A). As expected, both markers were also expressed in a subset of cells in both neuronal progenitor cell cluster. Interestingly, expression levels were different for *elavl3* and *elavl4* in the two progenitor cell clusters: *elavl3* was expressed at higher levels in progenitor cell 1 cluster and only in a very few cells from the progenitor cells 2 cluster, whereas *elavl4* was expressed in less cells of the progenitor cells 1 cluster (compared to *elavl3*) and in all cells from the progenitor cells 2 cluster.

Expression of (among others) *tsmb*, *tubb5* and *gap43* in the top 10 list of differentially expressed genes of cluster 8 identifies this cluster as newborn neurons: recently, Lange et al., identified *tmsb* and *tubb5* as marker genes for newborn neurons in the adult zebrafish telencephalon (Lange *et al.*, 2020). Additionally, the gene *gap43*, associated with in axonal outgrowth, is known to be expressed in post-mitotic neurons during axon elongation (Biffo *et al.*, 1990).

To confirm *tubb5* as a marker for newborn neurons in the SAG monochomic *in situ* hybridization (ISH) as well as a fluorescent *in situ* hybridization (FISH) combined with an antibody staining against GFP and PCNA in the juvenile SAG of transgenic *neurod*:GFP fish was performed by Nora Bölicke (see Nora Bölicke, lab rotation report, 2021). The monochromic *in situ* hybridization on the SAG of 4 months old WT AB zebrafish showed the expression of tubb5 in the medial part of the SAG, the area were the neurogenic niche and the cell bodies of the sensory neurons reside (Figure S.5A). FISH combined with the antibody staining revealed the expression of *tubb5* in non-proliferating *neurod*:GFP-positive progenitor cells, suggesting *tubb5* to be a marker of newborn neurons in the juvenile SAG.

The expression of *gap43* in the juvenile SAG was further investigated by antibody staining against GFP, PCNA and HuC/D in transgenic *gap43*:GFP animals. *gap43*:GFP labeled newborn neurons and their axonal projections in the area of the neurogenic niche in the medial part of the SAG (Figure 4.27B; for better display of the axonal projection see also Figure S.6). The majority of *gap43*:GFP-positive cells were co-labeling with HuC/D, a fraction of *gap43*:GFP-positive cells, however,

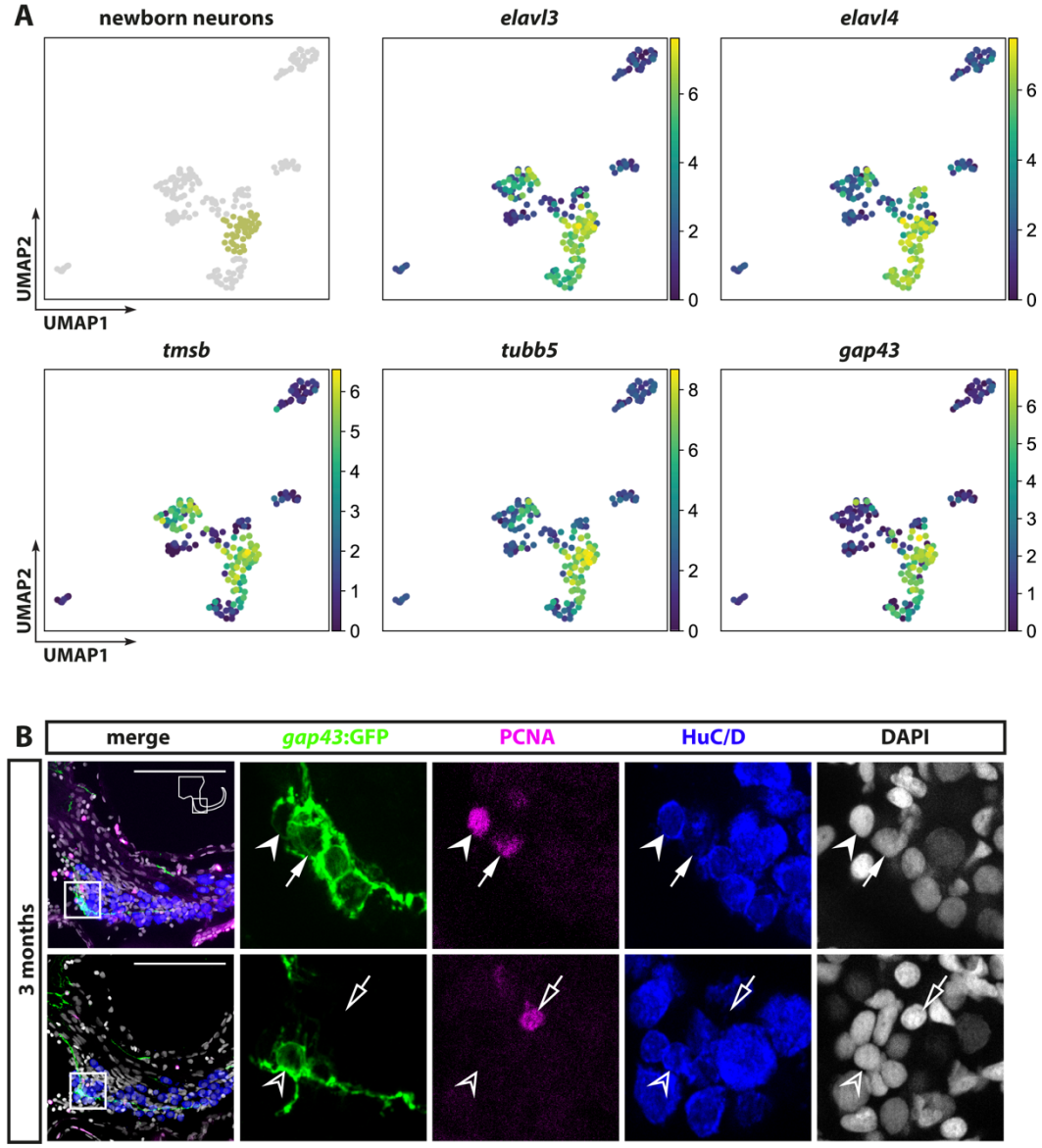

Figure 4.27 scRNAseq identifies cluster 8 as newborn neurons.
(**A**) UMAPs depicting the expression of the pan-neuronal marker *elavl3* and *elavl4* as well as the expression of *tmsb*, *tubb5* and *gap43*. (**B**) Antibody staining against GFP, PCNA and HuC/D (Elavl3/4) in the juvenile SAG from transgenic *gap43*:GFP fish reveals *gap43*:GFP-positive cells in the area of the neurogenic niche (PCNA-only positive cell marked by open arrow). *gap43*:GFP-positive cells were found to co-label with: PCNA (arrow); PCNA and HuC/D (arrowhead; found in one out of four analyzed fish); HuC/D (open arrowhead). Note the expression of *gap43*:GFP in the axons (see resized image in Figure S.6) Scale bar: 100 µm; cross sections showing dorsal to the top and lateral to the right.

stained also positive for PCNA. Surprisingly, in one individual one cell was found triple-positive for *gap43*:GFP, PCNA and HuC/D.

Taken together, scRNAseq with subsequent verification revealed *tubb5* and *gap43* as novel markers for newborn neurons in the juvenile SAG.

4.2.8 scRNAseq identifies a cluster of differentiating neurons (cluster 9)

Even though the sorting strategy aimed to sort for the presumptive stem cell population as well as proliferating neuronal progenitor cells in the neurogenic niche of the juvenile SAG, cluster 9 was identified as a cluster of differentiating neurons based on the gene expression profile (Figure 4.28). Characteristic genes expressed in cells from the differentiating neuron cluster included *nefma (neurofilament medium polypeptidea)*, associated with axonal projections (Baraban *et al.*, 2013), *atp1a3b*, expressed in neurons during zebrafish development (Doğanli *et al.*, 2013), *emb*, associated to axon guidance and dendrite self-avoidance (www.ensembl.org; ENSDARG00000059485) as well as *calb*1 and *calb2a*, the latter also known as *calretinin*, both expressed in mature neurons of the SAG (for *calb2a* expression pattern see also Figure 4.2).

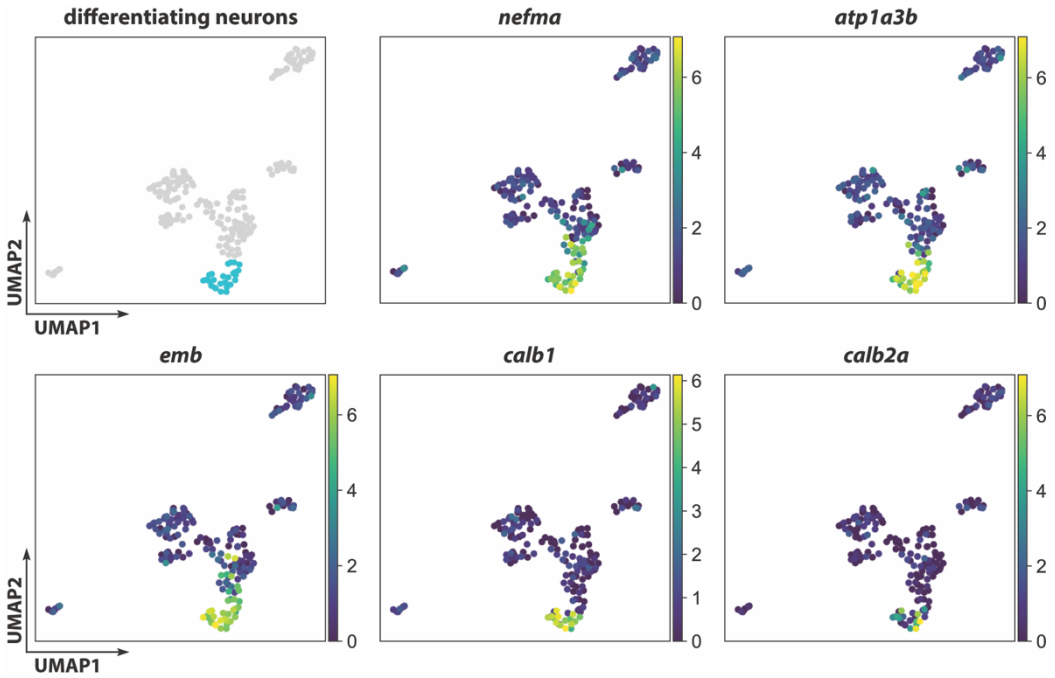

Figure 4.28 scRNAseq identifies a cluster of differentiating neurons (cluster 9). Cluster 9 was identified as differentiating neurons based on the expression of *nefma*, *atp1a3b*, *emb*, *calb1* and *calb2a* (also known as *calretinin*).

4.2.9 scRNAseq of the juvenile SAG reveals two clusters (4 and 6) as candidates for the presumptive neuronal stem cell-like cell population

The remaining two clusters 4 and 6 were located in the center of the UMAP, in close proximity to the cluster progenitor cells 1 and progenitor cells 2. Cluster 4 consisted in total of 11 cell, four sorted as *pcna*:GFP/*nestin*:mCherry-T2aCreER^{T2}-double positive cells and seven sorted as pcna:GFP-positive cells. Cluster 6 consisted of only 6 cells, all sorted as *pcna*:GFP-positive.

The gene rbp4 is exclusively expressed in cluster 4

One gene exclusively expressed in cluster 4 was *rbp4*, encoding for Retinol Binding Protein 4 (Figure 4.29). *mdka*, a gene suggested to play a role in regulating stem cell quiescence in the adult zebrafish telencephalon (Lübke *et al.*, 2022)was expressed in both stem cell-like clusters. Other genes expressed in stem cell-like 1 as well as in the neighboring progenitor cells 1 cluster, included *sparc*, *socs3a* and *sdc4*, suggesting that the stem cell-like 1 cluster might give rise to cells from the progenitor cells 1 cluster.

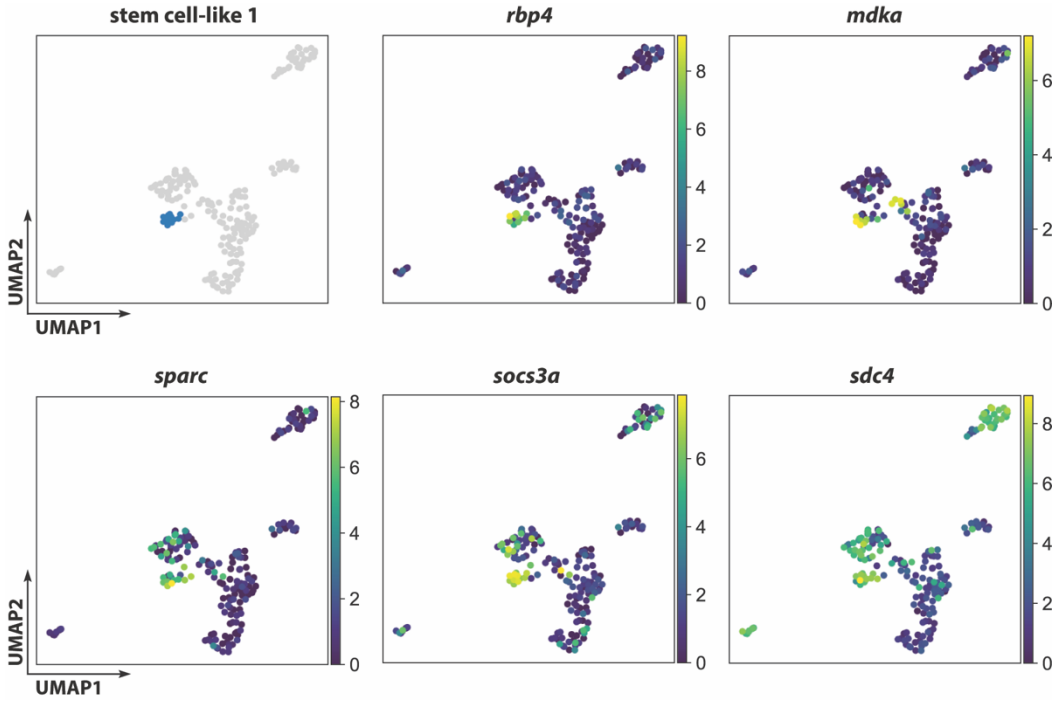

Figure 4.29 The stem cell-like 1 cluster (cluster 4) is characterized by the exclusive expression of *rbp4*.
scRNAseq revealed *rbp4* exclusively expressed in cluster 4. *mdka* was highly expressed in both stem cell-like cluster (cluster 4 and cluster 6) but not in any other cluster. *sparc*, *socs3a* and *sdc4* were expressed in cluster stem cell-like 1 as well as the neighboring cluster progenitor cell 1 (cluster 5), suggesting cells from cluster stem cell-like 1 as potential as potential precursors of the progenitor cells 1.

in situ hybridization reveals rbp4-expressing cells medial of the neurogenic niche in the juvenile SAG

To further investigate *rbp4* expressing cells as candidates for the presumptive neuronal stem cell-like cells, FISH combined with antibody staining against GFP and proliferation marker PCNA in juvenile *neurod*:GFP-positive fish was performed by former bachelor student Daniel Scherer (see also Figure S.7; Daniel Scherer, bachelor thesis, 2021). *rbp4* was found to be expressed by a small cell population medial of the neurogenic niche. In line with the absence of proliferation marker *mki67*, *mcm5* and *pcna* in the expression profile of cluster 4 based on the scRNAseq data (Figure 4.31), only very few of the *rbp4*-expressing cells were found to be positive for *pcna*. Based on the localization of the *rbp4*-expressing cell population medially to the neurogenic niche and the presence of few proliferating cells within that cell population, *rbp4* is a promising candidate for further analysis to find a marker for the presumptive stem cell niche in the SAG.

Cluster 6 is characterized by the expression of fabp7a and other glia-associated marker genes

The second candidate cluster for the presumptive stem cell-like cell is the cluster stem cell-like 2 (Figure 4.30). It was characterized by the expression of several radial glia and neuronal stem cell markers such as *fabp7a, atp1a1b*, *sox2*, *s100b*, and *cx43* (Lange *et al.*, 2020; Ito *et al.*, 2010; Liu *et al.*, 2003; Kunze *et al.*,

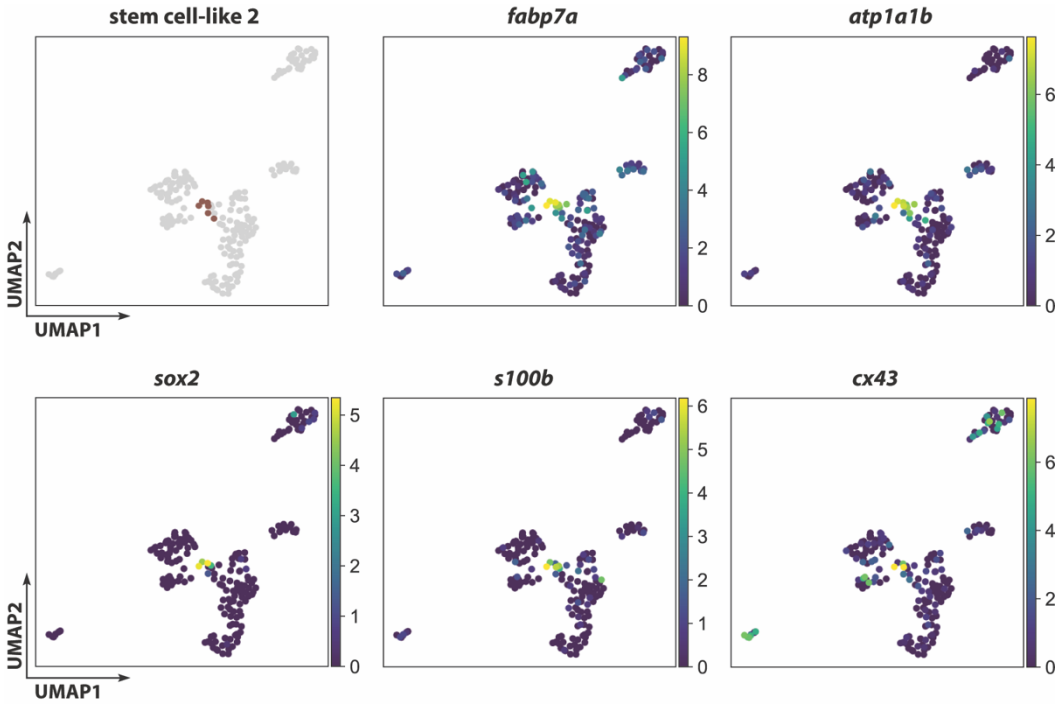

Figure 4.30 Cluster 6, stem cell-like 2, is characterized by the expression of *fabp7a* and other glia marker.
UMAPs depicting the expression several glia markers such as *fabp7a*, *atp1a1b*, *s100b* and *cx43* as well as the neuronal stem cell marker *sox2* in the cluster stem cell-like 2.

2009). In contrast to the stem cell-like 1 cluster, which did not exhibit the expression of the proliferation marker *mki67, mcm5* and *pcna*, two out of six cells from the stem cell-like 2 cluster were expressing *mcm5* and *pcna* (Figure 4.31, middle panel).

In situ hybridization reveals fabp7a to expressed in the PCTZ as well as throughout the area of the neurogenic niche in the juvenile SAG

In situ hybridization was performed to analyze the localization of *fabp7a*-expressing cells in relation to the neurogenic niche in the juvenile SAG. Therefore, FISH for *fabp7a* combined with antibody staining for GFP and PCNA in juvenile, transgenic *neurod*:GFP fish was done by Nora Bölicke (see Nora Bölicke, lab rotation report, 2021). In contrast to the expression pattern found in the transcriptome data suggesting *fabp7a* to be exclusively expressed in cells from the stem cell-like 2 cluster and not in neuronal progenitor cells, the staining revealed a broad expression of *fabp7a* in the PCTZ and the area of the neurogenic niche (Figure S.8). In the ventromedial part of the SAG, *fabp7a* was found to be expressed throughout proliferating and non-proliferating *neurod*:GFP-positive neuronal progenitor cells as well as cells adjacent to the neuronal progenitor cells, identified as newborn neurons based on their round nuclei. However, *fabp7a*-expression was also observed in proliferating cells located dorsally to and outside of the *neurod*:GFP-positive neuronal progenitor cell.

4.2.10 Only the cluster progenitor cells 1 and stem cell-like 2 express proliferation markers

Analysis of the proliferation in the clusters related to the neuronal lineage revealed that several cells in the progenitor cells 1 cluster expressed one or more of the proliferation markers *pcna*, *mki67* and *mcm5*, whereas only three cells form the progenitor cells 2 cluster were expressing *pcna* (Figure 4.31).

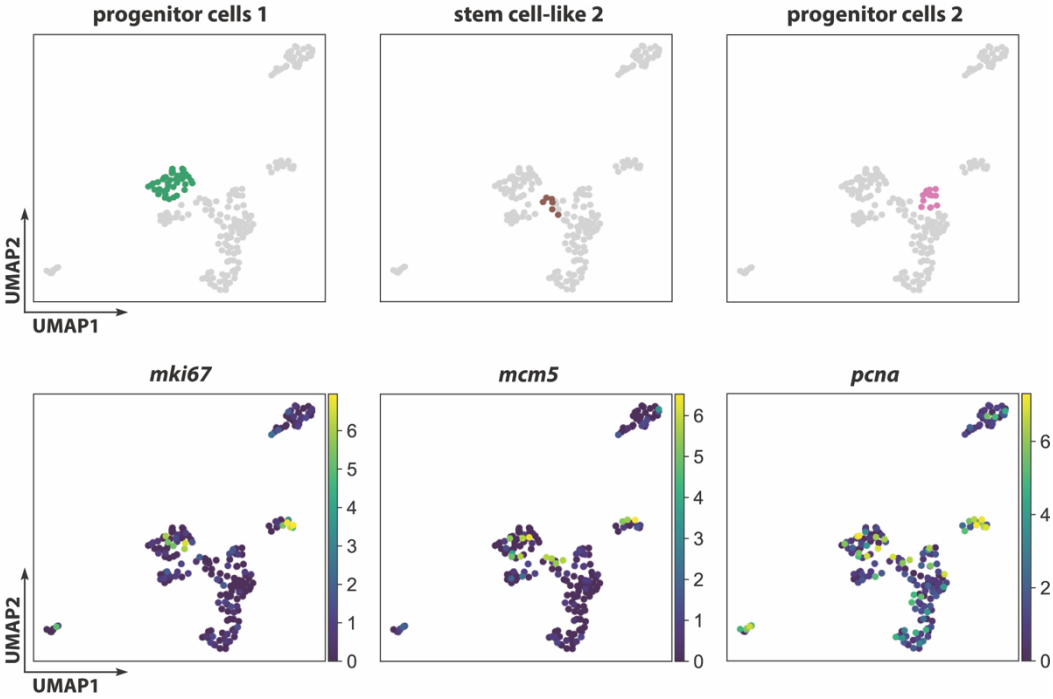

Figure 4.31 Expression of proliferation marker *mki67*, *mcm5* and *pcna* in cluster 5 (progenitor cells 1), 6 (stem cell-like 2) and 7 (progenitor cells 2).
UMAP depicting the expression of proliferation marker *mki67*, *mcm5* and *pcna*. The cluster progenitor cells 1 contained cells expressing *mki67*, *mcm5* and *pcna*. The cluster stem cell-like 2 exhibited one cell co-expressing *mcm5* and *pcna* and one cell expressing only *mcm5*, whereas in the cluster progenitor cell 2 only three cells expressed *pcna* but none of the other proliferation markers.

4.2.11 scRNAseq identifies six cell populations associated with the neuronal lineage in the juvenile SAG

Taken together, out of all 198 analyzed cells, 138 cells were identified as (potential) cells from the neuronal lineage. They clustered into two stem cell-like clusters (cluster 4 and 6), two progenitor cell clusters (cluster 5 and 7), one cluster identified as newborn neurons (cluster 8) and one cluster identified as differentiating neurons (cluster 9). To generate a heatmap of all clusters related to the neuronal lineage, 10 (in case of cluster 8: 20) genes were selected, roughly half of the genes appeared in the top 10 differentially expressed genes of each cluster and the other half being selected marker genes for neuronal stem and progenitor cells as well as neurons (Figure 4.32). Comparing the gene expression patterns between different clusters revealed marker genes exclusively expressed in a single cluster as well as markers expressed throughout several cluster, suggesting a differentiation trajectory.

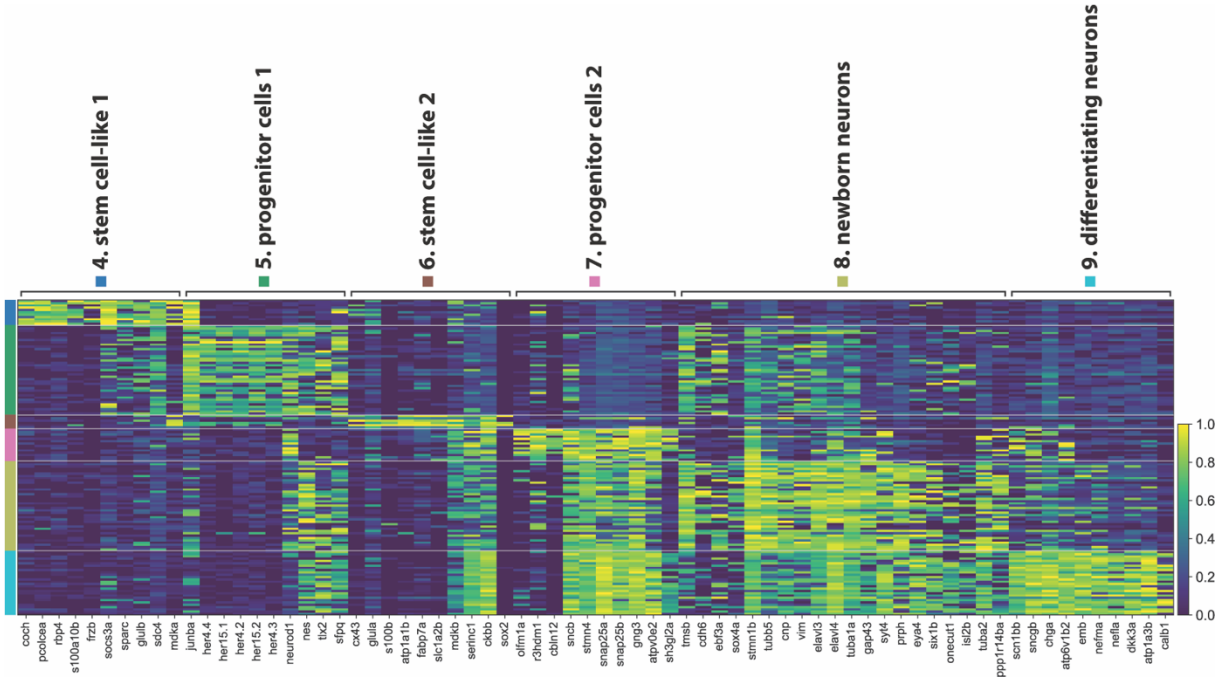

Figure 4.32 scRNAseq identifies six clusters associated with the neuronal lineage. Heatmap with 10 (in case of cluster 8, newborn neurons: 20) cluster-specific genes selected from the top 25 differentially expressed genes for each cluster as well as from known marker genes.

4.2.12 Transcriptome analysis of proliferating cells in the adult SAG using scRNAseq

To complement the transcriptomic data set from the juvenile SAG, I performed a second scRNAseq experiment using cells obtained from the adult SAG. The sorting strategy was similar to the one used for the transcriptome analysis of the juvenile SAG with one modification: in addition to sorting for *pcna*:GFP-only positive and *pcna*:GFP/*nestin*:mCherry-T2a-CreER^{T2}-double positive cells, also *nestin*:mCherry-T2a-CreER^{T2}-only positive cells were collected. In theory, this set-up would allow to analyze the following cell populations:

(I) presumptive, proliferating stem cell-like cell population (*pcna*:GFP-only positive);

(II) recent progeny of presumptive stem cell-like population that have differentiated into neuronal progenitor cells (*pcna*:GFP/*nestin*:mCherry-T2a-CreER^{T2}-double positive, not expressing *pcna*);

(III) neuronal progenitor cells (*nestin*:mCherry-T2a-CreER^{T2}-only positive, expressing *neurod1*);

(IV) and newborn neurons derived from the neuronal progenitor cells (still *nestin*:mCherry-T2a-CreER^{T2}-only positive, expressing neuronal markers).

Analysis of the transcriptomic profile of these cell population and the comparison of this transcriptome data set with the one from the juvenile SAG would provide further insights into the nature of the presumptive stem cell-like cell population. Furthermore, comparing the expression pattern found in juvenile, proliferating neuronal progenitor cells to those found in the adult, quiescent neuronal progenitor cells could help to unravel which signaling pathways and genes might regulate the switch from a proliferating to a quiescent neuronal progenitor cell population.

4.2.13 Identification of 11 different cell clusters in the transcriptome data set obtained from the adult SAG

For the bioinformatical analysis, out of 168 cells sorted for *pcna*:GFP, 141 cells sorted for *pcna*:GFP/*nestin*:mCherry-CreER^{T2} and 72 cells sorted for *nestin*:mCherry-CreER^{T2}, 60, 108 and 48 cells passed the quality control, respectively. In a first analysis, these 216 cells were clustered into 8 different clusters. Similar to the analysis of the transcriptome data obtained from the juvenile SAG, I used a semi-biased approach based on the analysis of the most differentially expressed genes in different groups of cells as well as the search for cells expressing

known marker genes for specific cell types to annotated the different cell cluster. This approach identified three additional cell clusters, resulting in 11 clusters in total (Figure 4.33).

In the first analysis, two sensory epithelium clusters, one hair cell cluster, one cluster of newborn/differentiating neurons, two immune cell clusters, one epithelium cell/lymphatic vessel cluster and one stem cell-like cell cluster were identified. The subsequent analysis revealed that one of the immune cell clusters consisted of two different immune cell populations (now annotated as cluster 8 and cluster 9) and additionally showed the presence of a small cluster of hair cell progenitors (cluster 4) previously included in cluster 3 and a small cluster of myelinating cells (cluster 6) previously included in cluster 5. For every cluster a set of selected marker genes containing genes from the list of the 25 most differentially expressed genes within that clusters as well as genes serving as established marker genes for certain cell types are depicted in a heatmap (Figure S.9).

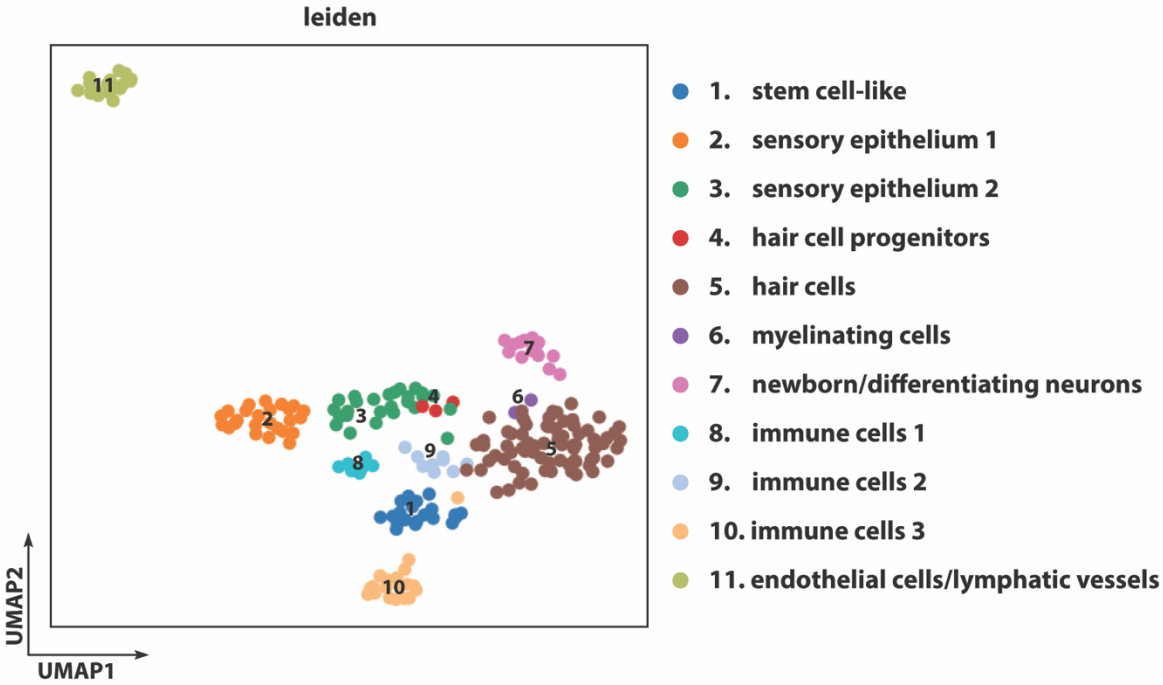

Figure 4.33 scRNAseq identifies 11 different cell populations in the adult SAG.
The transcriptome data is depicted on the uniform manifold approximation and projection (UMAP) plot (in the following referred to as UMAP). In the first analysis, cluster 8 and cluster 9 were clustering together as one immune cell cluster. Manually annotated cluster 3 (hair cell progenitors; previously part of cluster 3) and cluster 5 (myelinating cells; previously part of cluster 5) are found overlapping with their "original" cluster, whereas the rest of the clusters are more isolated. However, except cluster 11 (endothelial cells/lympathic vessels), all other cell clusters are loosely clustering together in one area.

Figure 4.34 shows a UMAP depicting the distribution of cells sorted for being GFP-positive, GFP/mCherry-positive or mCherry-positive. In contrast to the transcriptome data set obtained from the juvenile SAG, the annotated clusters in the transcriptome data set from the adult SAG consisted mostly of a mix of cells sorted for either being positive for only one of the fluorophores (GFP or mCherry-positive) or both fluorophores (GFP/mCherry-double positive). Only cluster 6, 8 and 11 contained cells sorted for the same fluorophore combination (cluster 6: GFP-positive cells; cluster 8 and 11: GFP/mCherry-double positive cells).

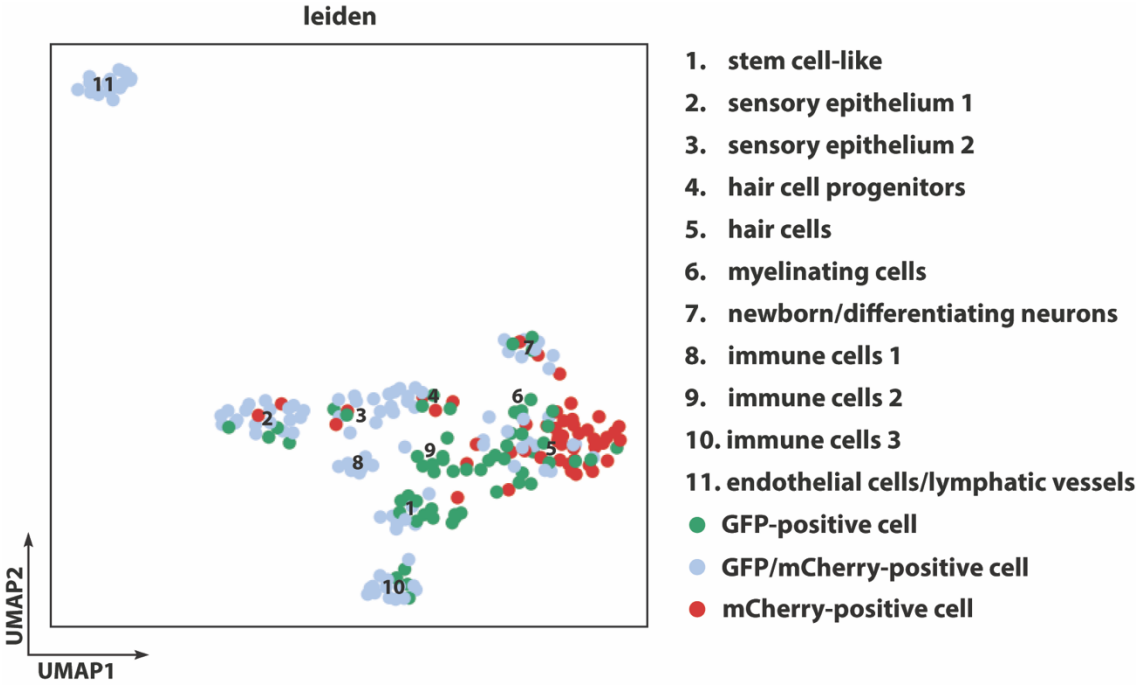

Figure 4.34 UMAP depicting the distribution of cells sorted as GFP-positive, GFP/mCherry-positive or mCherry-positive in the transcriptome data set from the adult SAG.
Only cluster 6, 8 and 11 contained exclusively GFP-only positive cells, whereas all other clusters contained a mix of GFP- and GFP/mCherry-positive cells (cluster 1, 9 and 10) or GFP/mCherry- and mCherry-positive cells (cluster 4) or even cells sorted for all three possible fluorophore combinations (cluster 2, 3, 5 and 7).

4.2.14 Identification of cluster 8, 9 and 10 as immune cell cluster and cluster 11 as endothelial cell/lymphathic vessel cluster in the adult SAG

Similar to the transcriptome data from the juvenile SAG, the applied sorting strategy also sorted cells not associated to the neuronal lineage. Cluster 8, 9 and 10 were identified as immune cells (Figure 4.35A-C). Based on the expression of *npsn* and *mpx*, cluster 8 was identified as neutrophils (Di *et al.*, 2017) (Figure 4.35A). Cluster 9 shares the expression of *cxcr4b* with the other two immune cell cluster (Figure 4.35B). Additionally, cluster 9 and cluster 10 express *cd74a* and *cd74b* which are known to be expressed in antigen presenting cells such as dendritic cells but also in the developing zebrafish inner ear (Shen *et al.*, 2012). Similar to the juvenile cluster immune cells 2 (cluster 12), cluster 10 identifies as a cluster of macrophages, based on the expression of *mpeg1.1* and *apoeb* (Leach *et al.*, 2021).

Cluster 11, the cell population with the greatest distance to all other clusters, contains endothelial cells and cells of the lymphatic vessel, characterized by the expression of *stab2* and *clic2* (Figure 4.35D).

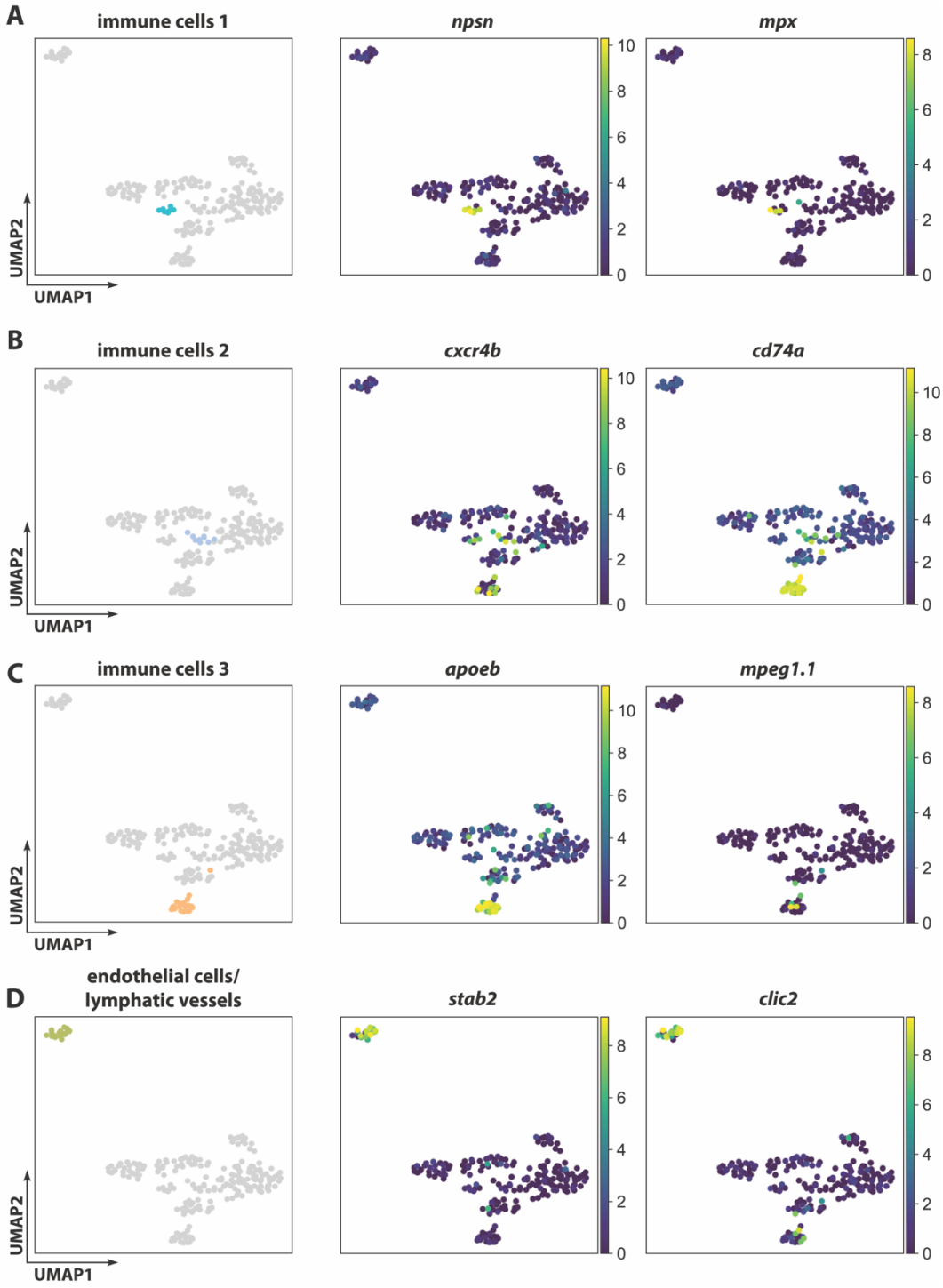

Figure 4.35 scRNAseq identifies cell clusters containing different immune cell populations and endothelial cells/lymphatic vessels.
(**A**-**C**) Identification of cluster 8, 9 and 10 as three immune cell cluster based on the expression of the immune cell markers *npsn* and *mpx* (cluster 8, immune cells 1, **A**), *cxcr4b* and *cd74a* (cluster 9, immune cells 2, **B**) and *apoeb* and *mpeg1.1* (cluster 10, immune cells 3, **C**). (**D**) UMAPs depicting the expression of the genes *stab2* and *clic2*, both associated with vasculogenesis, in cluster 11.

4.2.15 Majority of cells in the transcriptomic data of the adult SAG identify as cells from the sensory epithelium including hair cells

Cluster 2 and 3 contain cells of the sensory epithelium

Cluster 2 and 3 exhibit a similar expression profile as the sensory epithelium cluster (cluster 1, Figure 4.23) from the juvenile SAG transcriptome data set: in addition to the expression of *coch*, established marker genes for the otic sensory epithelium such as *epcam*, *stm* and *cx30.3* are expressed by cluster 2 and 3, identifying cells from these clusters as sensory epithelium (Usami *et al.*, 2003; Söllner *et al.*, 2003; Li *et al.*, 2017) (Figure 4.36).

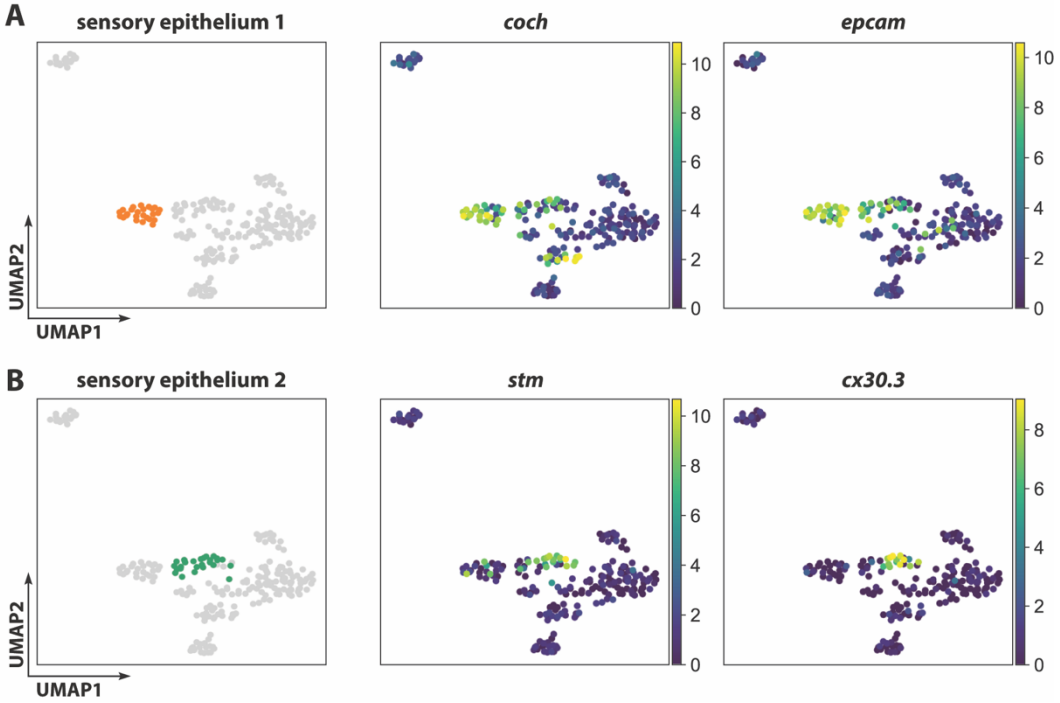

Figure 4.36 Cluster 2 and 3 contain cells from the sensory epithelium.
(**A**) Cluster 2, named sensory epithelium 1, exhibits strong expression of *coch* and *epcam*, associated with the developing inner ear epithelium. (**B**) Cluster 3 additionally expresses *stm* and *cx30.3*, both known to be expressed in the inner ear epithelium during development.

Cluster 4 identifies as hair cell progenitors related to the lineage of sensory hair cells

Three cells, that were originally part of the sensory epithelium 2 cell cluster were identified as a distinct cluster of hair cell progenitors, annotated as cluster 4 (Figure 4.37). In contrast to the transcriptome data obtained from the juvenile SAG, where members of the *her*-gene family were expressed by many cells in the neuronal progenitor cells 1 cluster, the only cells expressing *her4.2*, *her4.3* and *her4.4* in the entire transcriptome data set from the adult SAG were the three cells of cluster 4 (Figure 4.37). However, the expression of *otog* and *otogl*, genes involved in otolith formation and tethering, characterizes this cell cluster as hair cell progenitors (Lundberg *et al.*, 2015).

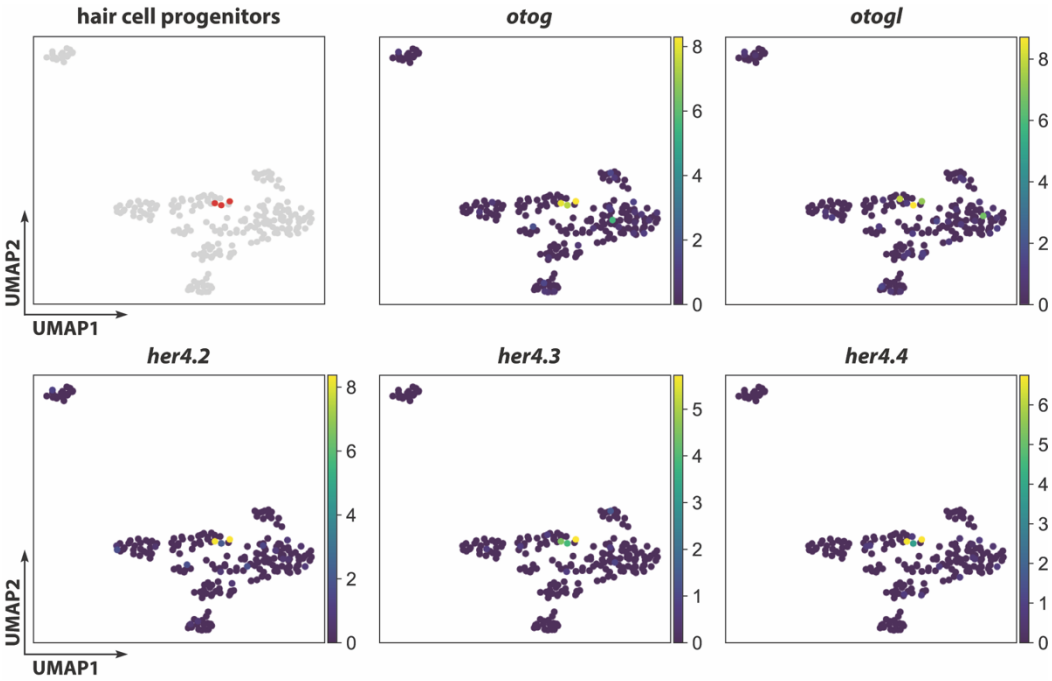

Figure 4.37 scRNAseq identifies cluster 4 as hair cell progenitors.
Besides the expression of the more general neural progenitor marker *her4.2*, *her4.3* and *her4.4*, the expression of *otog* and *otogl* identifies cluster 4 as hair cell progenitors.

Gene expression profile identifies cluster 6 as hair cells

The cluster with the highest number of cells in the transcriptome data set from the adult SAG was cluster 6. The expression of several marker genes for hair cells and the sensory epithelium such as *otofb*, *gpx2*, *s100s*, *cabp2b* and *pvalb9*, clearly identified this cluster as hair cells (Chatterjee *et al.*, 2015; Kraemer, Saraiva and Korsching, 2008; Erickson and Nicolson, 2015) (Figure 4.38). In the transcriptome data set of the juvenile SAG, the marker genes characterizing cluster 6 as hair cells, were only expressed by 1-3 cells and did not cluster together, with the exception of *gpx2*, which was also expressed by a few cells in the juvenile progenitor cells 2 cluster.

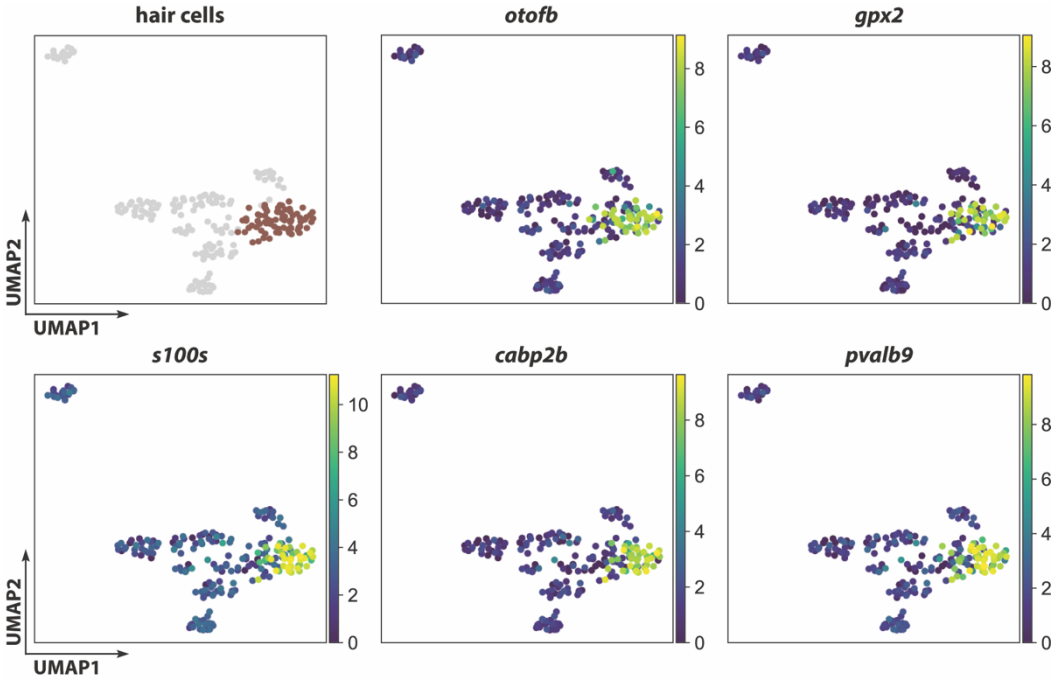

Figure 4.38 Hair cells (cluster 6) form the biggest cell population in the transcriptome data set from the adult SAG.
Expression of markers associated with hair cells and the sensory epithelium such as *otofb*, *gpx2*, *s100s*, *cabp2b* and *pvalb9* in cluster 6 identify the biggest cell population as hair cells.

4.2.16 Identification of myelinating cells (cluster 5) as a distinct cluster in the adult SAG

Searching for cells expressing marker genes for specific cell types enabled the identification of a small cluster of myelinating cells (cluster 5) in the transcriptome data of the adult SAG. The two cells within this cluster exclusively expressed genes involved in myelination such as *mpz* and *cldnk*, the latter encoding Claudin K, a marker that was also used in this study to label the myelination pattern on sections of the juvenile and adult SAG (Figure 4.39; for antibody staining against Claudin K see Figure 4.17).

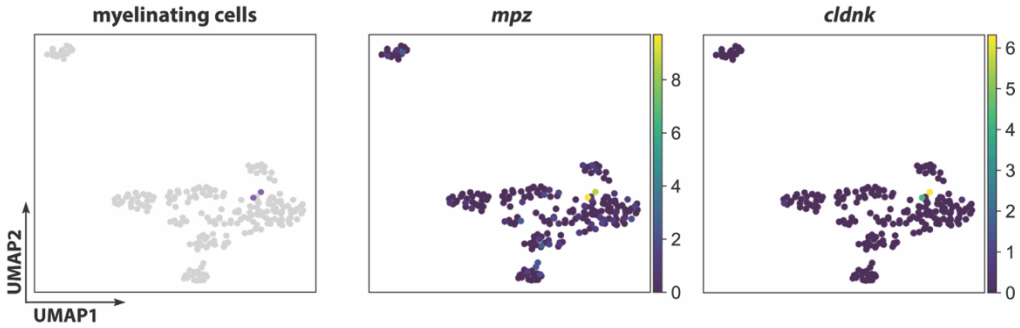

Figure 4.39 scRNAseq identifies one cluster of myelinating cells.
Originally clustered together with the hair cell cluster, cluster 5 exclusively expresses genes involved in myelination such as *mpz* and *cldnk*, identifying it as myelinating cells.

4.2.17 scRNAseq identifies only two populations associated with the neuronal lineage in the adult SAG

Out of 216 analyzed cells, only roughly 15 % were associated to the neuronal lineage. The 34 cells clustered into two different cell populations: a stem cell-like cell cluster containing 20 cells (cluster 1) and a mixed cluster consisting of 14 newborn/differentiating neurons (cluster 7).

scRNAseq clusters all neurons into a single cluster annotated as the cluster of newborn/differentiating neurons (cluster 7)

Even though 156 cells in the transcriptome data set of the adult SAG were sorted for being *nestin*:mCherry-T2a-CreER^{T2}-positive, only two cells in the entire data set were found to actually express *nestin*, both belonging to cluster 7. Similar, *neurod1*, which was expressed in around 30 % of all cells in the transcriptome data set obtained from the juvenile SAG, was only expressed in very few cells that were distributed throughout several clusters. Interestingly, expression of *r3hdm1*, which was one of the most characteristic genes for the juvenile progenitor cells 2 cluster, was not present in *neurod1*-expressing cells. Analysis of several early (*elavl3, elavl4, snap25a, stmn*4) and late (*calb2a*, also known as *calretinin*) neuronal marker revealed that cluster 7 is a mixed cell population of mainly newborn neurons and only few neuronal progenitor cells and differentiating neurons.

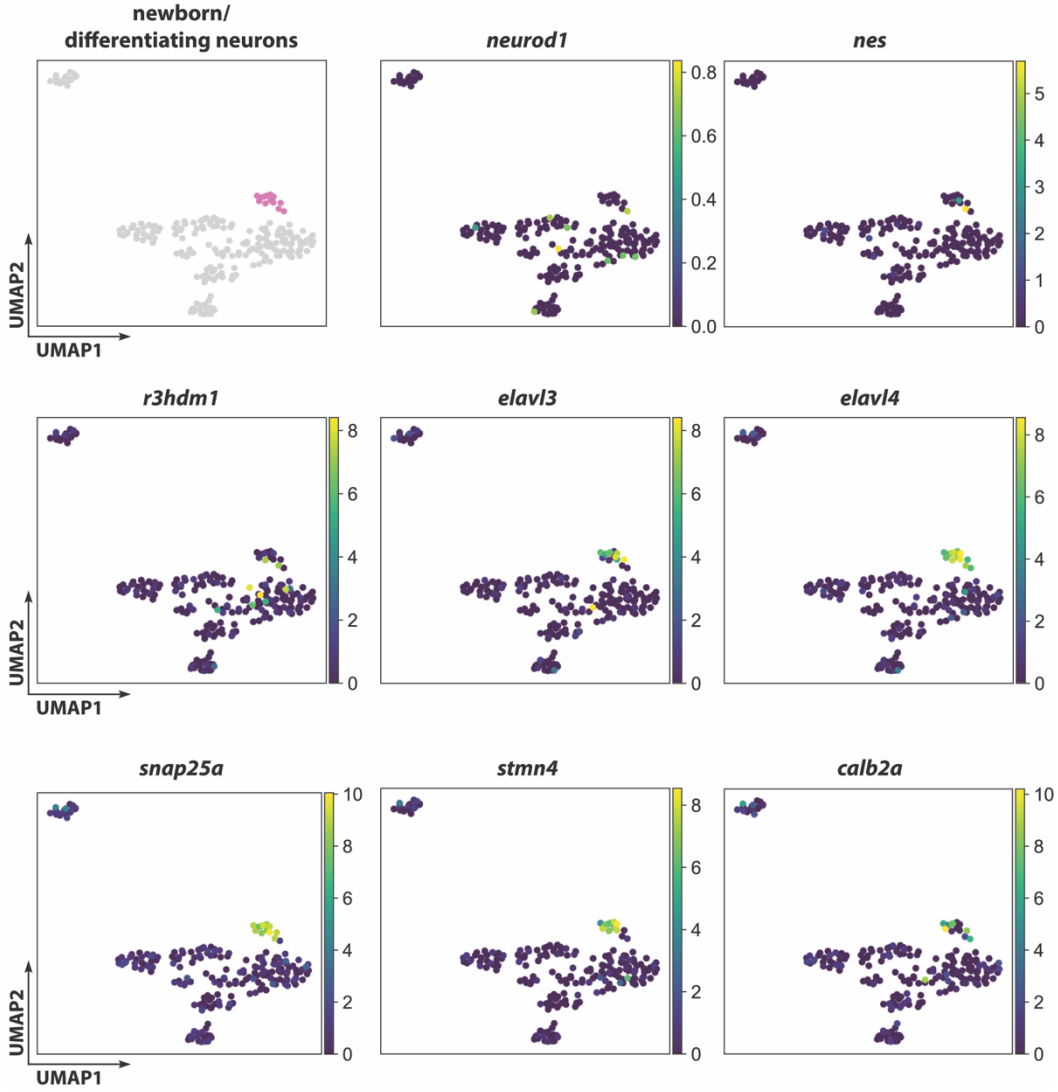

Figure 4.40 scRNAseq identifies cluster 7 as newborn/differentiating neurons. Neuronal progenitor marker *neurod1* is expressed in single, isolated cells throughout all clusters. In contrast, neuronal progenitor marker *nes* (*nestin*) ist only expressed in two cells of cluster 7. *r3hdm1*, one of the most characteristic markers for the juvenile progenitor cells 2 cluster, is also expressed in two cells of cluster 7 and in a few cells of the neighboring hair cell cluster. Expression of neuronal marker genes including very early neuronal markers such as *elavl3*, *elavl4*, *snap25a* and *stmn4* as well as markers for more mature neurons such as *calb2a* (previously known as *calretinin*; also used in this study to label mature sensory neurons on SAG sections see Figure 4.2) reveals cluster 7 to be a mixed cluster containing mostly newborn neurons but also a few neuronal progenitor cells and differentiating neurons.

scRNAseq reveals the presence of a rbp4-expressing stem cell-like cluster in the adult SAG

In contrast to the transcriptome data from the juvenile SAG, scRNAseq from the adult SAG identified only cluster 1 as a stem cell-like cluster (Figure 4.41). However, the gene expression pattern in this cluster is highly similar to the one found in the juvenile stem cell-like 1 cluster. It is characterized by the expression of *rbp4*, *frzb*, *socs3a* and *sdc4*. In additional to *rbp4*, *ccl25b* is also exclusively expressed in this cluster.

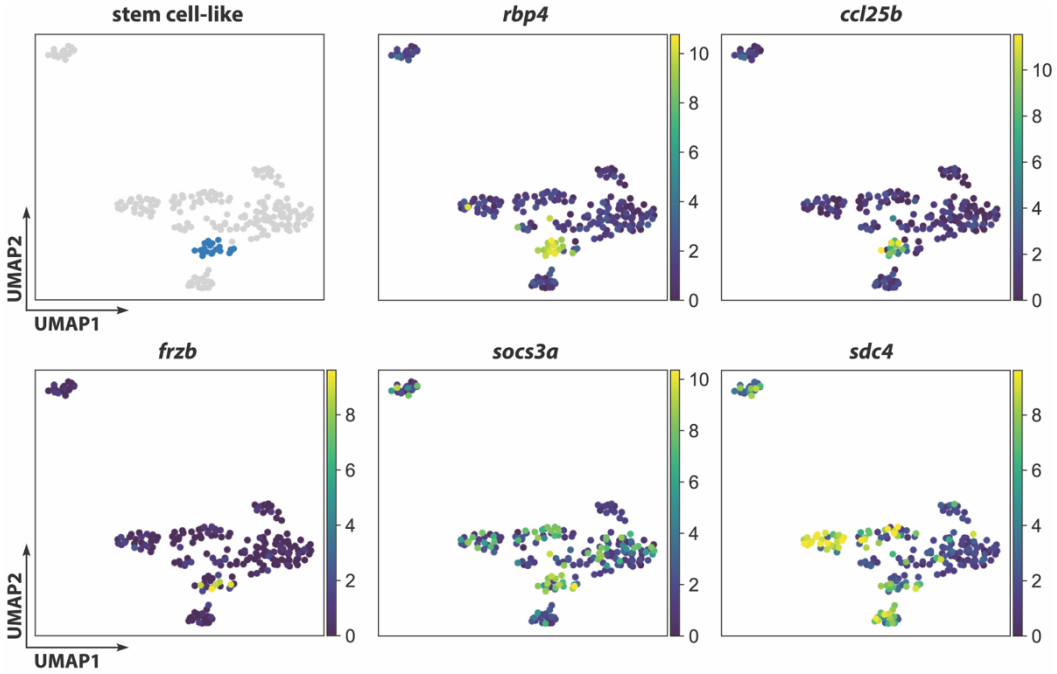

Figure 4.41 scRNAseq identifies a *rbp4*-expressing stem cell-like cluster (cluster 1) similar to the juvenile stem cell-like 1 cluster in the adult SAG.
Cluster 1 is – similar to the juvenile stem cell-like 1 cluster – characterized by the expression of *rbp4*, *frzb*, *socs3a* and *sdc4*, the two latter also showing expression in the hair cell cluster and/or both sensory epithelium clusters. Another marker that is exclusively expressed in the stem cell-like cluster is *ccl25b*.

Presence of three fabp4a-expressing cells in the transcriptome data of the adult SAG

Searching for the expression of marker genes of the second stem cell-like cluster found in the juvenile SAG revealed the presence of two *fabp7a/s100b* co-expressing cells in cluster 6 (Figure 4.42). Analysis of the proliferating markers *pcna*, *mki67* and *mcm5* revealed that (with a very few exceptions) none of the sorted cells were proliferating. Interestingly, one of the two *fabp7a/s100b* expressing cells was also expressing *pcna*. This indicates, that also the second potential stem cell-like cell population found in the juvenile SAG might persist to adulthood. However, a further characterization of the presumptive stem cell-like cell population postulated to exist in the adult SAG is necessary to proof one of the candidate populations to be the source replenishing the neuronal progenitor cell pool throughout life.

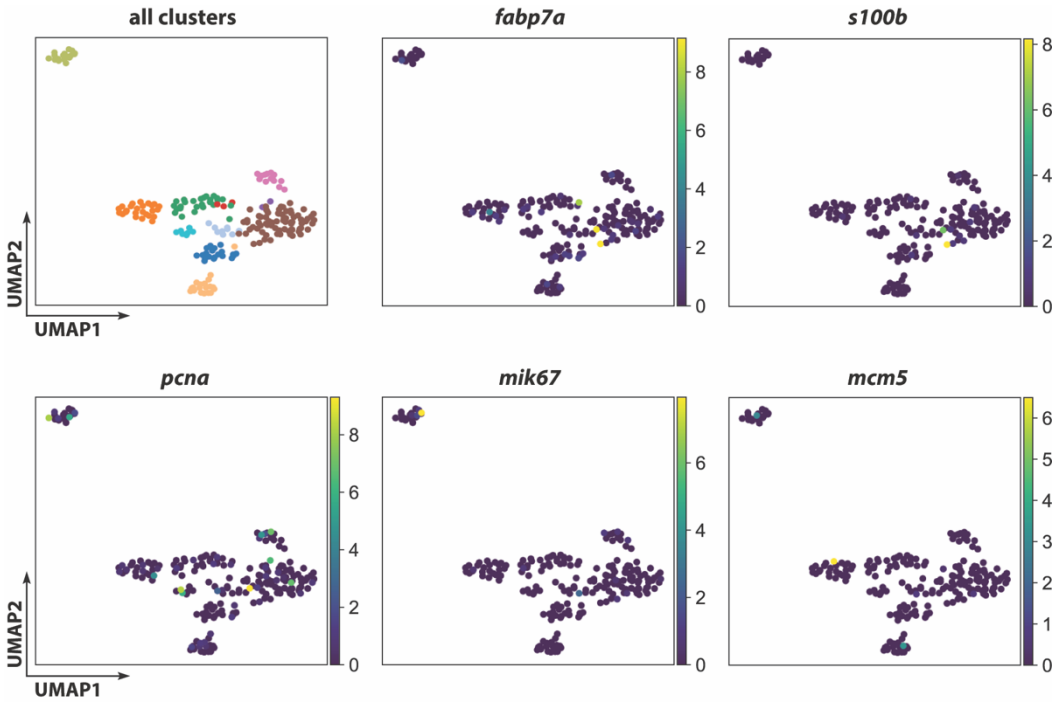

Figure 4.42 *fabp7a*-expressing cells still present in the adult SAG.
UMAPs depicting the presence of two *fabp7a/s100b* co-expressing cells in the transcriptome data from the adult SAG. The proliferation marker *pcna*, *mki67* and *mcm5* are only (if at all) expressed in very few cells, distributed throughout several clusters (*pcna*).

Taken together, the transcriptome data set of the adult SAG contained to few cells of the neuronal lineage to allow a valuable comparison between juvenile and the adult transcriptome data set. Surprisingly, more than half of the cells in the where derived from the sensory lineage, which is in contrast to the transcriptome data set of the juvenile SAG. A modification of the sorting strategy will be necessary to increase the amount of cells from the neuronal lineage for future scRNAseq experiments.

4.3 Regeneration in the adult zebrafish SAG

4.3.1 Establishment of a suitable lesion paradigm to target sensory neurons in the adult SAG

Zebrafish possess the remarkable capacity to regenerate various tissues and organs including the CNS and even hair cells in the inner ear and lateral line (Kroehne *et al.*, 2011; Lush, Mark E, Piotrowski, 2013). This raises the question whether the sensory neurons in the adult SAG can also be replaced upon lesion. After finding a lifelong maintained, but almost quiescent neurogenic niche comprising of marker-negative presumptive stem cells and Neurod-positive progenitor cells (see chapter 4.1 and 4.2) I aimed to investigate whether sensory neurons of the adult SAG can regenerate upon lesion and whether this neurogenic niche serves as the source of these newly generated sensory neurons. The first step was to establish the first lesion paradigm of the zebrafish SAG. In mammals, an established model of auditory neuropathy to specifically target sensory neurons in the spiral ganglion is the application of the neurotoxin Ouabain to the round-window membrane of the cochlea. In the Mongolian gerbil, mice and rats, this lesion paradigm induces a rapid and irreversible loss of spiral ganglion neurons while leaving the function of sensory hair cells intact (Schmiedt *et al.*, 2002; Lang, Schulte and Schmiedt, 2005; Fu *et al.*, 2012; Wakizono *et al.*, 2021). In zebrafish, injection of Ouabain into the eye is an established lesion model which is used to specifically ablate inner retinal neurons in a dose-dependent manner to study retina regeneration (Valente *et al.*, 2003; Fimbel *et al.*, 2007; Sherpa *et al.*, 2008). Based on this, I aimed to establish a lesion paradigm using the application of Ouabain to the adult SAG to specifically ablate mature sensory neurons without harming other cells within the inner ear. Since fish do not possess an outer and middle ear, application of Ouabain or any other solution needs to be administered by entering the inner ear enclosed within the skull. After extensively studying the anatomy and position of the SAG within the zebrafish skull, I identified a position to target the anterior part of the SAG, which allowed the insertion of a Hamilton syringe into the otic capsule without piercing the SAG and the sensory epithelium laying on top or the neighboring cerebellum (Figure 4.43). For the injection procedure, anesthetized animals were placed on their left side and the skull was opened (Figure 4.43B, dotted yellow circle) by punctuating the triangular shaped area above the opercle in the area of the pterotic bone using a 20 gauge needle (Figure 4.43B, blue dotted line). Then, a Hamilton syringe was inserted approx. 1.0-1.5 mm deep almost vertically along the dorsal-ventral axis into the otic capsule through the hole in the skull, without damaging the underneath located SAG as shown by H&E staining performed on sections of adult zebrafish sacrificed 30 min after applying a unilateral lesion (Figure 4.43C).

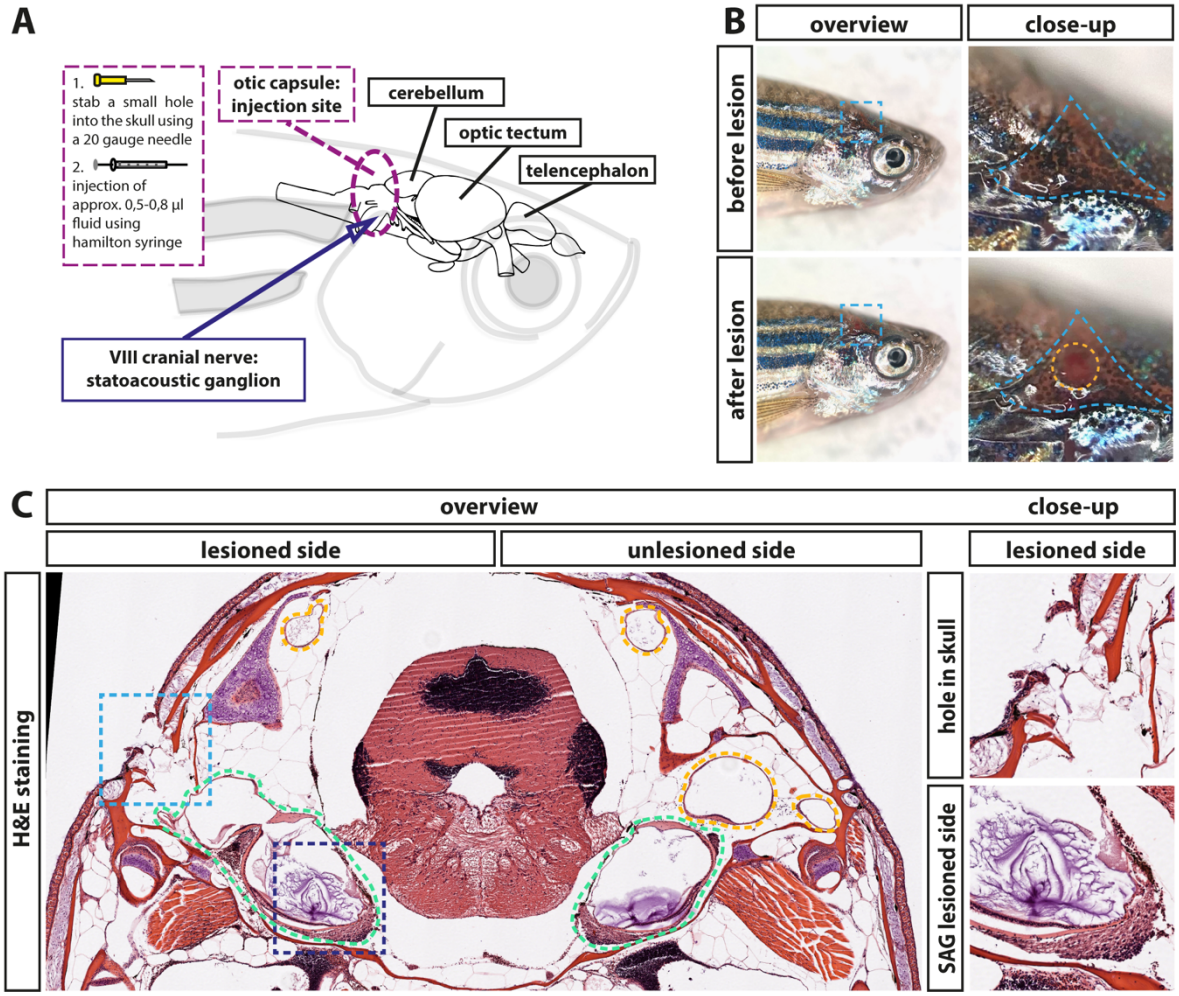

Figure 4.43 Establishment of a lesion paradigm for the adult zebrafish SAG.
(**A**) Scheme of the zebrafish head with the brain inside showing the injection position in relation to the brain and the SAG. A 20 gauge needle was used to open the skull before inserting a Hamilton syringe vertically approx. 1,0-1,5 mm deep into the skull along the dorsal-ventral axis. Subsequently, the Hamilton syringe was either removed (sham treated control) or 5-8 µl of either 0,9% NaCl or 100 µM Ouabain solution was slowly injected. (**B**) Overview of live adult zebrafish before and after injection. Close-ups of the blue dotted boxes show the injection side within the triangular bone (dotted blue line). Lower close-up shows the hole after injection (dotted yellow circle). (**C**) Haematoxylin/eosin staining (H&E) to illustrate the puncture channel on the lesioned side. Shown is a transversal cross section through the upper half of the zebrafish head at the height of the cerebellum with the semicircular canals (dotted yellow circles) and the SAG with the utricular macula (dotted green circle) 30 min post lesion; dotted close-up boxed show the hole in the skull (light blue) and the area of the neurogenic niche in the SAG (dark blue).

4.3.2 The chosen injection side is suitable to target the SAG

To test the suitability of the potential SAG lesion paradigm, unilateral injections of CellTracker Red were performed. CellTracker Red is a stable, nontoxic dye that freely passes through cell membranes into cells, where it is transformed into a cell membrane-impermeable dye that is brightly fluorescent at a physiological pH. 90 min following CellTracker Red injections, fish were sacrificed, sectioned and co-labeled with DAPI to analyze labeled structures. Analysis of the obtained section revealed that CellTracker Red was predominantly incorporated into cells within the SAG of the injected side labeling the proximal, medial and distal parts of the SAG (Figure 4.44). Importantly, almost no labeling of the neighboring cerebellum was observed. However, a striking accumulation of erythrocytes, easily recognized based on their small and condensed nuclei, was occasionally found on the injected site indicating a hemorrhage accompanying the injection procedure (Figure 4.45, Ouabain).

Taken together, the injection procedure is suitable to target the SAG specifically and can be used to apply fluids such as neurotoxins into the adult zebrafish SAG.

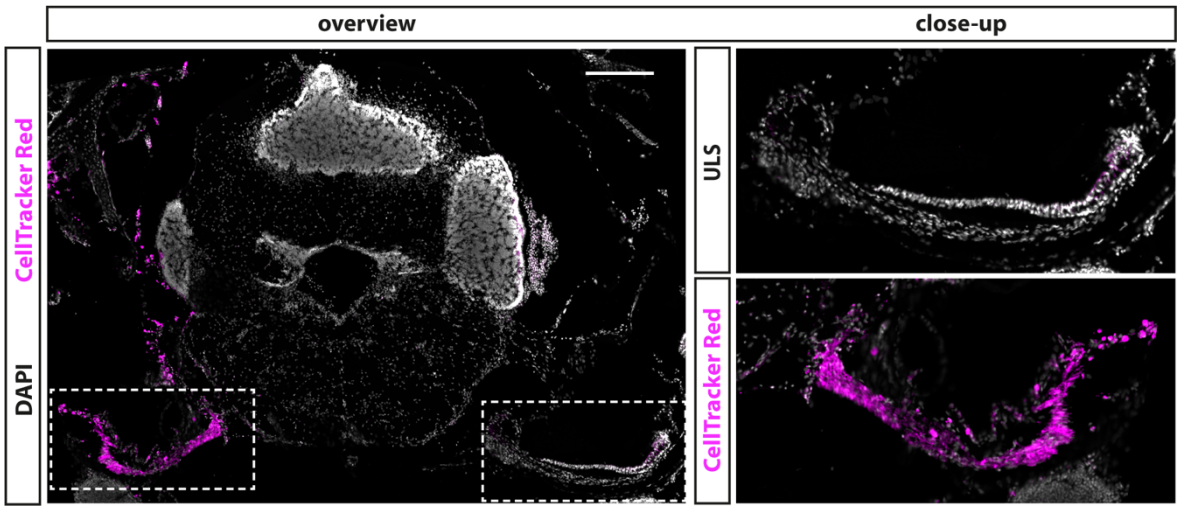

Figure 4.44 CellTracker Red injection shows suitability of injection side to target neurons in the SAG.
Immunohistochemistry of a transverse cross section at the height of the anterior SAG following CellTracker Red injection into the right inner ear showed a strong labeling of the SAG on the injected side but no labeling of the unlesioned side (ULS). Scale bar 200 µm.

4.3.3 Emergence of apoptotic sensory neurons in the adult zebrafish SAG

Following the successful establishment of the injection procedure, I set out to investigate the efficacy of Ouabain-induced lesions. To this aim, 0.5-0.8 µl of a 100 µM Ouabain solution was slowly injected into the otic capsule of the right side. As controls, I either injected the same amount of a 0,9 % NaCl solution or used sham-treated animals, in which the Hamilton syringe was inserted and removed without injecting any fluid into the otic capsule. In addition, the SAG of the uninjected side of all experimental animals was used as an unlesioned, internal control. To investigate cell death of sensory neurons in the SAG upon treatment, two approaches addressing different biochemical hallmarks of apoptosis were taken:

(I) presence of phospholipid phosphatidylserines on the outer plasma membrane of cells and

(II) the well-established TUNEL assay.

Annexin V

In the first approach, the transgenic zebrafish line *ubiq:*secAnnexinV-mVenus, which ubiquitously expresses a secreted Annexin 5 fused to mVenus was used (Morsch *et al.*, 2015). Annexin V binds phospholipid phosphatidylserines with a high affinity. Phospholipid phosphatidylserines are normally distributed asymmetrically and are only present on the inside of the cell membrane. During apoptosis however, phospholipid phosphatidylserines are redistributed to the outer plasma membrane thus enabling the detection of apoptotic cells *in vitro* and *in vivo* with Annexin V coupled to a fluorescent protein (Morsch *et al.*, 2015; Kenis *et al.*, 2005; Ham *et al.*, 2010). Immunohistochemistry against mVenus-driven from *ubiq:*secAnnexinV-mVenus combined with the neuronal marker HuC/D detected only low mVenus levels in unlesioned control sides (Figure 4.45). In the medial part of the SAG, comprising the neurogenic niche and the neuronal cell bodies, a few HuC/D-positive cells displayed a weak mVenus signal (Figure 4.45, white arrows). Besides this weak mVenus signal no strong mVenus was detectable in any part of the unlesioned SAG. In contrast, a strong mVenus signal was present in the distal part of the SAG where the neurites of the sensory neurons innervate the sensory patch in sham-treated as well as NaCl- and Ouabain-injected SAGs at 12 hours post lesion (Figure 4.45b vs. d,f,h).

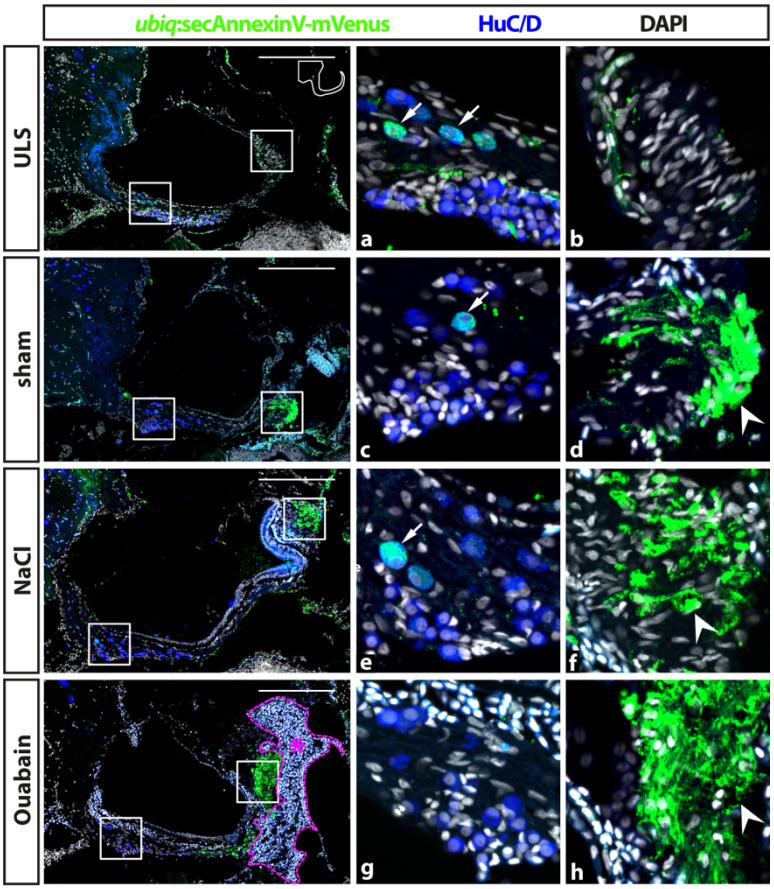

Figure 4.45 Presence of phospholipid phosphatidylserines marked by *ubiq*:secAnnexinV-mVenus in the distal part of the SAG upon lesion.
Antibody staining of the adult zebrafish SAG labeling *ubiq*:secAnnexinV-mVenus-positive cells and HuC/D-positive neurons. In contrast to unlesioned sides (ULS), a strong *ubiq*:secAnnexinV-mVenus-signal was present in the SAG following sham treatment or NaCl and Ouabain injections at 12 hours post lesion (hpl). In the medial part of the SAG, which harbors the neurogenic niche and the neuronal cell bodies, only very few HuC/D-positive cells showed a weak *ubiq*:secAnnexinV-mVenus staining in all samples (arrows in a, c, e). In the distal part of the SAG, where the neurites of the sensory neurons innervate the sensory patch, a strong *ubiq*:secAnnexinV-mVenus staining was observed in sham-treated as well as NaCl- and Ouabain-injected SAGs but almost no signal was detected in unlesioned control sides (arrowheads in d, f and h). Magenta dotted line and asterisk in Ouabain-injected SAG indicates a massive hemorrhage on the injected site. Scale bar: 200 µm; cross sections showing dorsal to the top and lateral to the right.

Combining immunohistochemistry against mVenus driven in *ubiq:*secAnnexinV-mVenus with an antibody staining against Calretinin, which labels a subset of mature neurons including their neurites, corroborated this result (Figure 4.46). Again, whereas no difference in mVenus expression was found in the medial part of the SAG (Figure 4.46a, c), a strong upregulation of mVenus co-localizing with Calretinin was observed in the distal part of the SAG in sham-injected animals in comparison to unlesioned controls (Figure 4.46b vs. d).

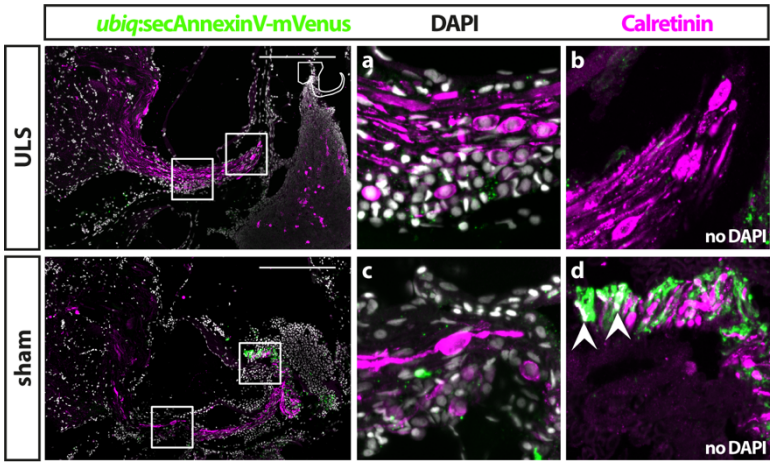

Figure 4.46 Expression of *ubiq*:secAnnexinV-mVenus reveals signs of apoptosis in neurites upon lesion.
Co-labeling of mVenus with Calretinin revealed the presence of *ubiq*:secAnnexinV-mVenus in neurites labeled by Calretinin (arrowhead in d) of sham-injected SAGs but not in unlesioned control sides. Scale bar: 200 µm; cross sections showing dorsal to the top and lateral to the right.

TUNEL-assay

To validate the presence of apoptotic sensory neurons in contrast to mere axon degeneration, the well-established TUNEL-assay, which detects nuclear DNA fragmentation, another hallmark of apoptosis, was applied. To this aim, the transgenic line *Tg(elavl3:GFP)* which drives GFP under the promoter of the *elavl3* gene (formerly known as HuC) and thereby labeling all neurons in the SAG was employed for all TUNEL-assay experiments to label apoptotic neurons (Park *et al.*, 2000). In addition to GFP and TUNEL, sections were co-stained with the neuronal marker Calretinin (Figure 4.47). In unlesioned control sides, *elavl3*:GFP/Calretinin-double positive neurons were (as expected) always present whereas no TUNEL-positive cells were ever detected within the SAG at all analyzed time points. In contrast, in addition to other, unidentified TUNEL-positive cells, TUNEL/*elavl3*:GFP/Calretinin-triple positive neurons could be found as early as 6 hpl in sham-treated as well as NaCl-injected SAGs (Figure 4.47A). At 12 hpl, apoptotic neurons were detected in all three lesion types (Figure 4.47B) and even at the latest analyzed timepoint, 24 hpl, apoptotic neurons were still present in Ouabain-injected SAGs (Figure 4.47C).

Interestingly, all TUNEL/*elavl3*:GFP/Calretinin-triple positive neurons were located on the dorsal side of the SAG closer to the sensory patch not within the area of the neurogenic niche on the ventral side of the SAG.

Taken together, analysis of apoptosis reveals that the established lesion paradigm is suitable to induce cell death in sensory neurons in the adult SAG. Notably, the insertion of a Hamilton syringe into the otic capsule already on its own induces apoptosis of sensory neurons independent of the use of a chemical neurotoxin

as the injected fluid since there were no difference observed in the apoptotic response following sham treatment, NaCl and Ouabain injections.

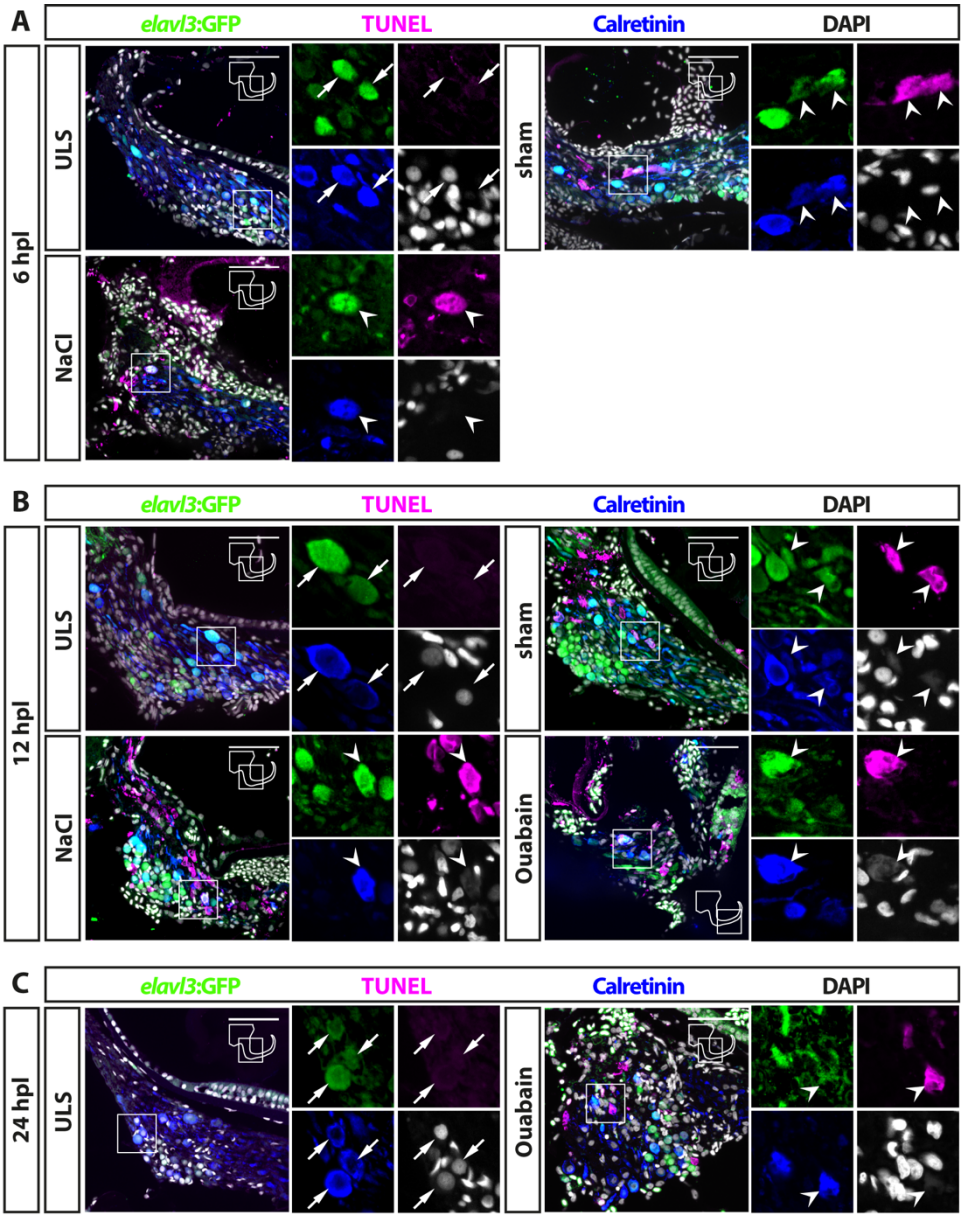

Figure 4.47 TUNEL staining reveals apoptotic neurons upon lesion.
Antibody staining labeling neurons (*elavl3*:GFP and Calretinin) combined with TUNEL-assay at 6 **(A)**, 12 **(B)** and 24 **(C)** hours post lesion (hpl). **(A)** TUNEL-assay revealed the presence of apoptotic neurons in the SAG of adult *elavl3*:GFP zebrafish as early as 6 hpl. **(B)** At 12 hpl, apoptotic neurons were found in all three lesion types. **(C)** Apoptotic neurons were still present at 24 hpl. In contrast, no TUNEL-positive neurons were found in the unlesioned control side at any analyzed time point. White arrow: *elavl3*:GFP/Calretinin-positive neuron; white arrow head: apoptotic, TUNEL/*elavl3*:GFP/Calretinin-positive neurons. Scale bars: 50 µm, cross sections showing dorsal to the top and lateral to the right.

4.3.4 Accumulation of leukocytes in the adult SAG persists beyond 16 days post lesion

The immune system plays a crucial but beneficial role in regenerative neurogenesis after injury of the zebrafish central nervous system (Kyritsis *et al.*, 2012). To address whether lesions to the SAG activate the immune system at the lesion side, I performed immunohistochemistry against the pan-leukocyte marker Lymphocyte cytosolic protein 1 (L-Plastin) on transgenic *neurod*:GFP zebrafish. Using L-Plastin antibody stainings on transgenic *neurod*:GFP fish enabled to label all myelocytes (neutrophils, eosinophiles, mast cells, dendritic cells and macrophages) and lymphocytes (T cells, B cells and natural killer cells) in relation to the *neurod*:GFP-positive neurogenic progenitor pool of lesioned SAGs at 1, 2, 4 and 16 days post lesion (Figure 4.48). Overall, I distinguished two different types of L-Plastin-positive cells: (I) cells with a ramified morphology displaying a weaker L-Plastin staining and (II) round cells with a strong L-Plastin staining. In unlesioned control sides, always only few, evenly distributed L-Plastin-positive cells displaying a ramified morphology were present within the SAG (Figure 4.48, ULS in each time point). In addition, round cells with a strong L-Plastin staining were located ventrally in close contact to the SAG at the height of the neurogenic niche labelled by *neurod*:GFP). In contrast, a massive accumulation of ramified as well as round L-Plastin-positive cells close to the neurogenic niche and throughout the SAG was found irrespective of the type of lesion at 1, 2, and 4 dpl. (Figure 4.48, sham, NaCl and Ouabain in each time point). Moreover, a massive amount of round, strongly L-Plastin-positive cells accumulated in the distal part of the SAG where the neurites of the sensory neurons innervate the sensory patch (Fig. 3, yellow asterisks). The highest density of L-Plastin-positive cells was present in those lesioned SAGs in which the sensory patch and in rare cases even the SAG itself was accidentally manually destroyed by the lesion procedure (Figure 4.48 1 dpl/4 dpl and 16 dpl Ouabain, yellow asterix). Overall, I found that the accumulation of leucocytes in the SAG is highly similar in sham-treated, NaCl- or Ouabain-injected SAGs. The pattern was already manifested

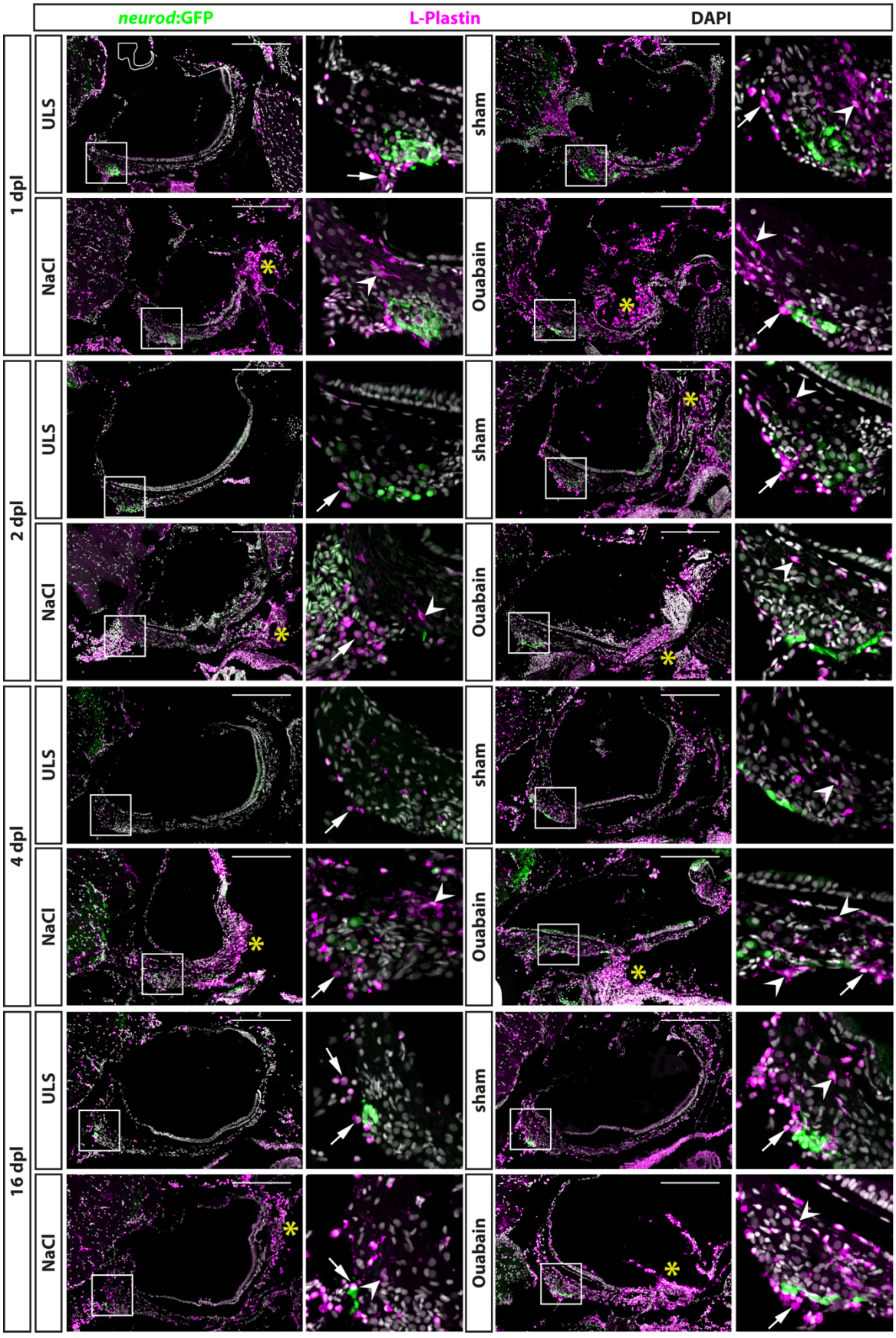

Figure 4.48 Accumulation of leukocytes in the adult zebrafish SAG upon lesion.

Continued on next page

Antibody staining against the pan-leukocyte marker L-Plastin and GFP in the SAG of transgenic *neurod*:GFP zebrafish at 1, 2, 4 and 16 days post lesion (dpl) reveals massive accumulation of leukocytes which was not resolved within 16 dpl. Shown are representative images of the SAG following sham treatment or NaCl or Ouabain injections as well as the unlesioned side (ULS) of either sham-treated, NaCl- or Ouabain-injected animal. Boxes show close-ups of the respective *neurod*:GFP-positive neurogenic niche. In the unlesioned side (ULS, upper left panel in each time point), a few ramified L-Plastin-positive cells are distributed evenly throughout the entire SAG. Some round, strongly L-Plastin-positive cells are localized in close contact to the neurogenic niche on the ventral side of the SAG (arrows). In contrast, accumulation of ramified as well as round L-Plastin-positive cells (arrowheads) is observed close to the neurogenic niche at all time points within sham-treated, NaCl- or Ouabain-injected SAGs (upper right and lower panels in each time point). In addition, density of L-Plastin-positive cells is usually the highest at the distal part of the SAG, especially when the sensory patch is massively destroyed as for example seen in 1 dpl/NaCl and Ouabain, 2 dpl/Ouabain and 16 dpl/Ouabain, irrespective of the lesion type (yellow asterisks). Scale bars: 200 µm, cross sections showing dorsal to the top and lateral to the right.

at 1 dpl, did not change much at 2 or 4 dpl and was even not resolved at 16 dpl, which constituted the end of the time course.

Taken together, the data show that sham treatment or NaCl or Ouabain injection into to the SAG results in a massive infiltration and accumulation of immune cells in the lesioned SAG, which lasts longer than 16 dpl.

4.3.5 Reactive proliferation in the neurogenic niche of the adult zebrafish SAG peaks at 8 days post lesion

As shown in chapter 4.1, the neurogenic niche in the SAG is highly proliferative and a source of new sensory neurons at juvenile stages but turns to a quiescent state with only very rare neurogenesis at adult stages. Hence, it was unknown whether the neurogenic niche can be reactivated and provide neuronal cells to compensate for the loss of sensory neurons upon lesion at adult stages. To investigate the regenerative capacity, immunohistochemistry against the proliferation marker PCNA and GFP in transgenic *neurod*:GFP zebrafish was used to check for proliferating cells in the neurogenic niche in sham-treated as well as NaCl- and Ouabain-injected animals at 2, 4, 8, 16 and 57 days post lesion (dpl). In contrast the analysis of the homeostatic adult SAG, in which proliferating Neurod-positive progenitor cells (*neurod*:GFP/PCNA-double positive) were – with extreme rare exceptions - always absent in the adult SAG during homeostasis (chapter 4.1.5), *neurod*:GFP/PCNA-double positive cells were present upon lesion under all three conditions (Figure 4.49). Following injection of Ouabain, *neurod*:GFP/PCNA-double positive cells were already present at 2 dpl and were also detected at 4, 8 and 16 dpl (Figure 4.49, Ouabain). Similar results were obtained for sham-treated and NaCl-

injected SAGs. Here, *neurod*:GFP/PCNA-double positive cells were frequently detected starting at 4 dpl and were consistently found at 8 and 16 dpl (Figure 4.49, sham and NaCl). Importantly, *neurod*:GFP/PCNA-double positive cells were also found occasionally in some SAGs of all three lesion types even at 57 dpl, which constituted the end of the time course, indicating that the neurogenic niche did not return completely to homeostatic levels after lesion at this time point. Surprisingly, *neurod*:GFP/PCNA-double positive cells were also present occasionally in SAGs of the unlesioned side of injected animals (Figure 4.49, ULS). This finding was mostly restricted to 4, 8 and 16 dpl indicating a systemic effect of the unilateral lesion.

To analyze the proliferation results in greater detail, I quantified the number of all proliferating cells in the area of the neurogenic niche (PCNA-positive, Figure 4.50A) as well as the number of proliferating neuronal progenitors (*neurod*:GFP/PCNA-double positive cells, Figure 4.50B). In order to detect subtle differences in the severity of the systemic effect provoked by the three different conditions, the data was obtained individually for the unlesioned SAG for sham-treated, NaCl-injected and Ouabain-injected fish.

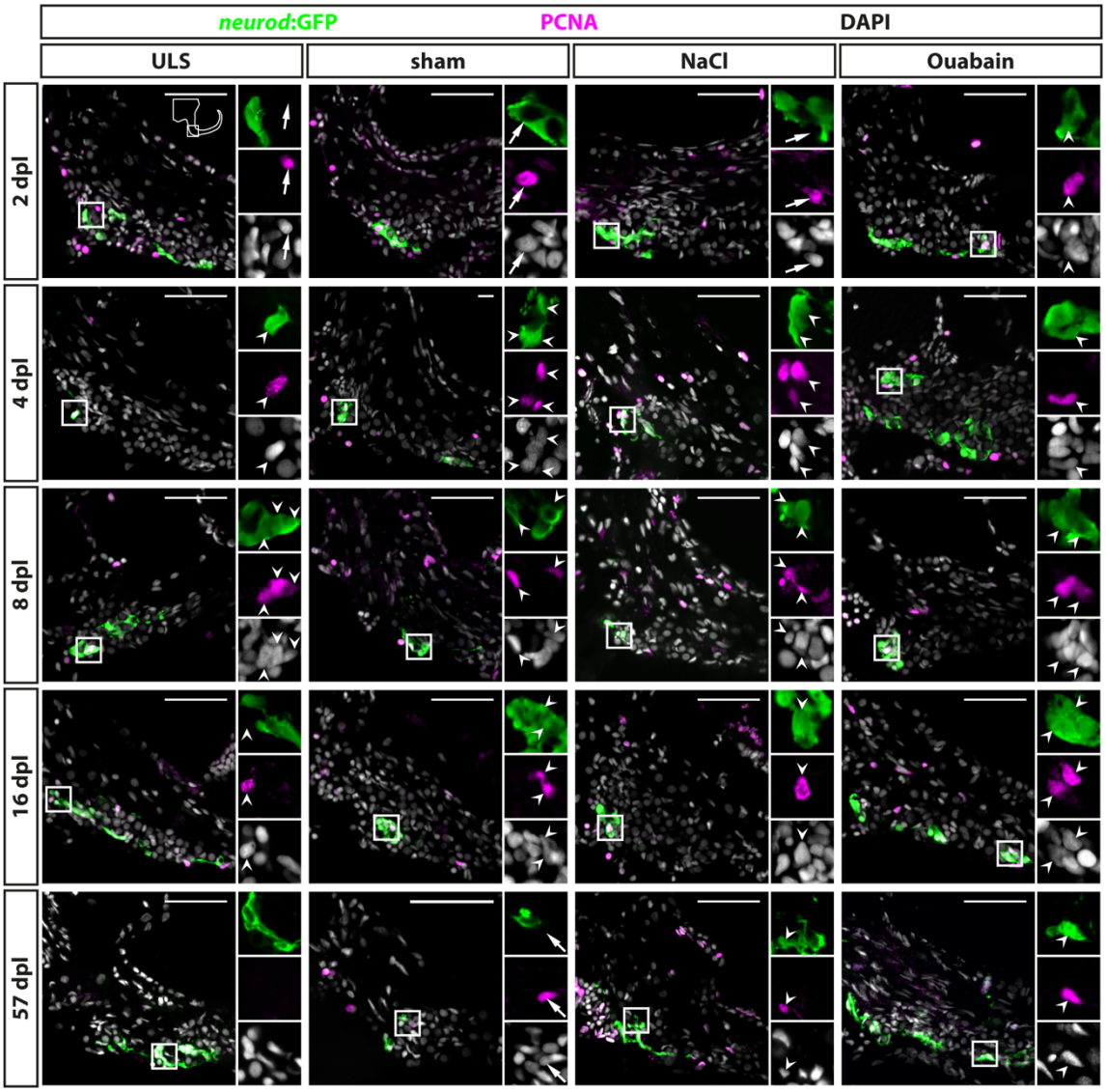

Figure 4.49 Reactive proliferation of *neurod*:GFP-positive progenitors in the adult zebrafish SAG upon lesion.
Immunohistochemistry against the proliferation marker PCNA and GFP in the SAG of *neurod*:GFP transgenic animals. Shown are representative images of the neurogenic niche of the SAG following sham treatment or NaCl or Ouabain injections as well as the unlesioned side (ULS) of either sham-treated, NaCl- or Ouabain-injected animals at 2, 4, 8, 16 and 57 days post lesion (dpl). Boxes show close-ups to visualize co-staining. Proliferating but marker-negative cells close to *neurod:*GFP-positive cells (arrows) were found frequently in unlesioned sides for example at 2 dpl and in sham-treated SAGs at 57 dpl. However, proliferating *neurod*:GFP/PCNA-double positive cells (arrowheads) were also present from 2 dpl onwards in Ouabain-injected animals (right column) and frequently from 4 dpl onwards in sham-treated and NaCl-injected animals (medial columns). Proliferating *neurod*:GFP/PCNA-double positive cells continued to be present at 8 and 16 dpl before returning to homeostatic levels at 57 dpl where the majority of sham-treated, NaCl- or Ouabain-injected animals did not show proliferating neuronal progenitors in the lesioned SAG. Interestingly, PCNA/*neurod*:GFP-double positive cells were also found occasionally in SAGs of the unlesioned side, in particular in the unlesioned sides of Ouabain-injected fish at 8 dpl. Scale bar: 50 µm, cross sections showing dorsal to the top and lateral to the right.

Quantification of all PCNA-positive cells in the area of the neurogenic niche revealed that the number of proliferating cells in the unlesioned SAG for sham-treated, NaCl-injected and Ouabain-injected animals did not change significantly over time. It varies to an average of 2 to 8 PCNA-positive cells per section with a slight increased number in unlesioned SAGs of Ouabain-injected fish (Figure 4.50A). Compared to the respective SAGs of unlesioned sides, a significant increase in proliferating cells was observed for sham-treated SAGs at 8 dpl, NaCl-injected at 2 dpl and Ouabain-injected at 4 dpl, respectively. The number of proliferating cells decreased in all three lesion types to an average of 6 PCNA-positive cells per section within 57 dpl. Comparison of the number of proliferating cells of individual time points from sham-treated, NaCl-injected or Ouabain-injected SAGs did not reveal any significant differences with one exception. At 4 dpl, the number of PCNA-positive cells was significantly increased in Ouabain-injected animals compared to sham-treated animals.

Quantification of *neurod*:GFP/PCNA-double positive cells showed that Ouabain injection led to the fastest response in the neurogenic niche, where reactive proliferation was already present at 2 dpl. In the SAG of sham-treated animals, *neurod*:GFP/PCNA-double positive cells were present as early as 4 dpl. The number of proliferating progenitor cells peaked at 8 dpl with a significantly increased number of 5-6 *neurod*:GFP/PCNA-double positive cells per section, which represents a significant difference in comparison to the unlesioned side, before returning to lower levels at 16 and 57 dpl in sham-treated and Ouabain-injected animals. A similar profile in the number of proliferating progenitors was observed in the SAGs of NaCl-injected animals, although the overall quantified numbers of *neurod*:GFP/PCNA-proliferating cells was significantly lower at 8 dpl compared to sham-treated and Ouabain-injected SAGs.

As mentioned above, reactive proliferation -surprisingly - also occurred in the unlesioned SAG under all three conditions. In sham-treated animals, proliferating neuronal progenitors in the unlesioned SAG were observed only once at 8 dpl (Figure 4.50B). In contrast, one quarter (4 out auf 14 for NaCl-injected animals) to one third (5 out auf 15 for Ouabain-injected animals) of all analyzed animals showed low level reactive proliferation in the neurogenic niche of the unlesioned SAG following NaCl and Ouabain injection, respectively.

These findings were also confirmed by a BrdU pulse chase experiment, in which I used the thymidine analog BrdU to label actively cycling cells (Kiernan *et al.*, 2005). Analysis of transgenic *neurod*:GFP fish which were lesioned and immersed in BrdU from 2 to 3 dpl and from 4 to 5 dpl and subsequently sacrificed confirmed reactive proliferation in the neurogenic niche by the presence of *neurod*:GFP/BrdU-positive cells (Figure S.10B).

Taken together, I show that neuronal progenitors in the neurogenic niche of adult zebrafish SAG indeed re-enter the cell cycle upon lesion and display a peak in reactive proliferation at 8 dpl.

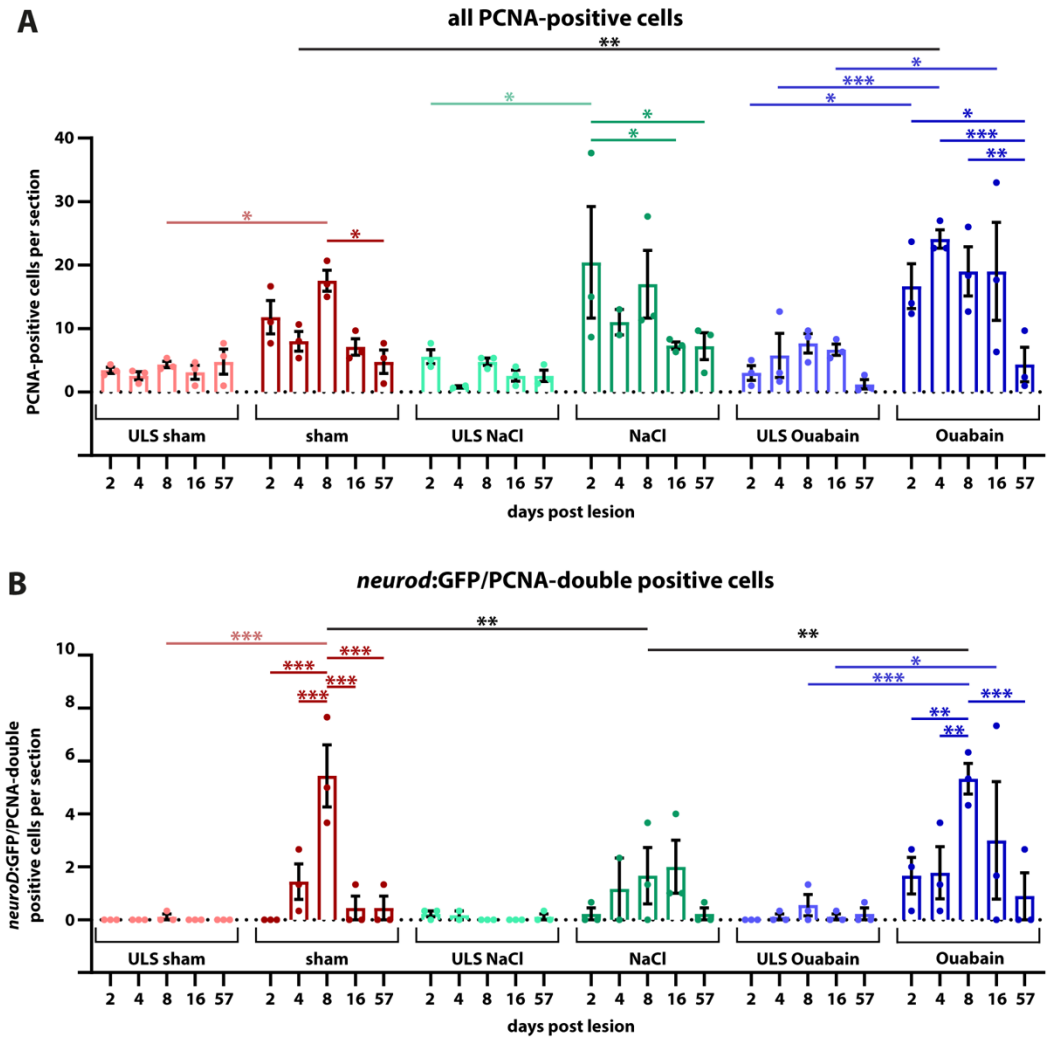

Figure 4.50 Quantification of reactive proliferation of *neurod*:GFP-positive progenitors.

(**A**) Quantification of all PCNA-positive cells. Compared to the respective SAGs of unlesioned sides (ULS sham, ULS NaCl, ULS Ouabain), the number of PCNA-positive cells per section increased following sham-treatment, NaCl- or Ouabain-injections in the first 8 days post lesion (dpl). An even significant increase compared to the unlesioned side is present at 2 dpl following NaCl injection, at 4 dpl following Ouabain injection and at 8 dpl following sham treatment, respectively. At 57 dpl, the proliferation rate in the lesioned SAG was significantly decreased to levels of the unlesioned side. (**B**) Quantification of *neurod*:GFP/PCNA-double positive cells. Compared to the respective SAGs of unlesioned sides, the number of *neurod*:GFP-positive cells per section that re-enter the cell cycle increased following sham treatment, NaCl or Ouabain injections. The significant peak of proliferation of active cycling neuronal progenitors was observed at 8 dpl and significantly decreased at 16 and 57 dpl to homeostatic levels in the majority of individuals in sham-treated and Ouabain-injected SAGs. Even though changes in the overall proliferation rate in NaCl-injected SAGs followed a similar trend, the number of proliferating *neurod*:GFP neuronal progenitors was significantly lower in NaCl-injected SAGs compared to sham-treated and Ouabain-injected SAGs at 8 dpl. Notably, *neurod*:GFP/PCNA-double positive cells were also observed in the unlesioned side, in particular in Ouabain-injected animals, in which an average of 0,5-1 *neurod*:GFP/PCNA-double positive cells per section was seen. Samples size n=3 (n=fish with 3 sections/SAG; exception: 4 dpl/NaCl: n=2); data is presented as mean±SEM. two-way ANOVA with Tukey's multiple comparisons test; ***$P \leq 0.001$; **$P \leq 0.01$; *$P \leq 0.05$.

4.3.6 Lesion-induced reactive neurogenesis in the neurogenic niche of the adult SAG

During homeostasis, neurogenesis in the zebrafish SAG decreases significantly to very low levels at adult stages (chapter 4.1.5). To investigate whether the adult SAG is capable of reactive neurogenesis upon lesion, I chose two different strategies to prove the presence of newborn neurons: (I) short-term lineage tracing using the perdurance of GFP from the *neurod*:GFP transgene in the neuronal progenitors of the neurogenic niche and (II) a pulse chase experiment using BrdU.

4.3.6.1 Reactive neurogenesis from *neurod*:GFP-positive progenitor cells in the neurogenic niche of the adult SAG peaks at 8 days post lesion

For the short-term lineage tracing, sham-treated, NaCl-injected or Ouabain-injected *neurod*:GFP transgenic zebrafish were sacrificed for analysis at 2, 4, 8, 16 and 57 dpl. Using immunohistochemistry against the neuronal marker HuC/D and GFP, I analyzed the presence of HuC/D-positive neurons carrying the GFP-label from the *neurod*:GFP transgene, which represent newborn neurons derived from the *neurod*:GFP-positive neuronal progenitor population. In contrast to the SAG of unlesioned sides, *neurod*:GFP/HuC/D-double positive cells were present in the lesioned SAG irrespective of the type of lesion (sham-treated, NaCl- or Ouabain-injected) as early as 4 dpl (Figure 4.52). At 8 dpl, *neurod*:GFP/HuC/D-double positive newborn neurons were frequently found in all three lesion types and occasionally also in the respective SAGs of the unlesioned sides. At 57 dpl, *neurod*:GFP/HuC/D-double positive cells were rarely found in lesioned as well as in unlesioned SAGs.

Quantification of *neurod*:GFP/HuC/D-double positive newborn neurons corroborated a significant increase in neurogenesis upon lesion (Figure 4.51). At 2 dpl, the number of *neurod*:GFP/HuC/D-double positive cells per section in unlesioned and lesioned SAGs of all sham-treated, NaCl- and Ouabain-injected animals is less than 0,5 *neurod*:GFP/HuC/D-double positive cells per section which lays within the range of the homeostatic baseline that was previously described in chapter 4.1.5. However, neurogenesis rates in the SAGs of all three lesion types, but not in the respective SAGs of the unlesioned sides, exceeded the values of the homeostatic baseline already at 4 dpl. The neurogenesis rate increased even further significantly and displayed a peak of 3-4 *neurod*:GFP/HuC/D-double positive cells per section at 8 dpl in the lesioned SAG after sham treatment, NaCl or Ouabain injection. Interestingly, a slight increase in neurogenesis above the homeostatic baseline was also observed in the unlesioned side of sham-treated and NaCl-injected animals at 8 dpl as well as of Ouabain-injected animals at 16 dpl. At 57 dpl, the number of newborn neurons returned to homeostatic levels in lesioned SAGs as well as in the respective unlesioned sides.

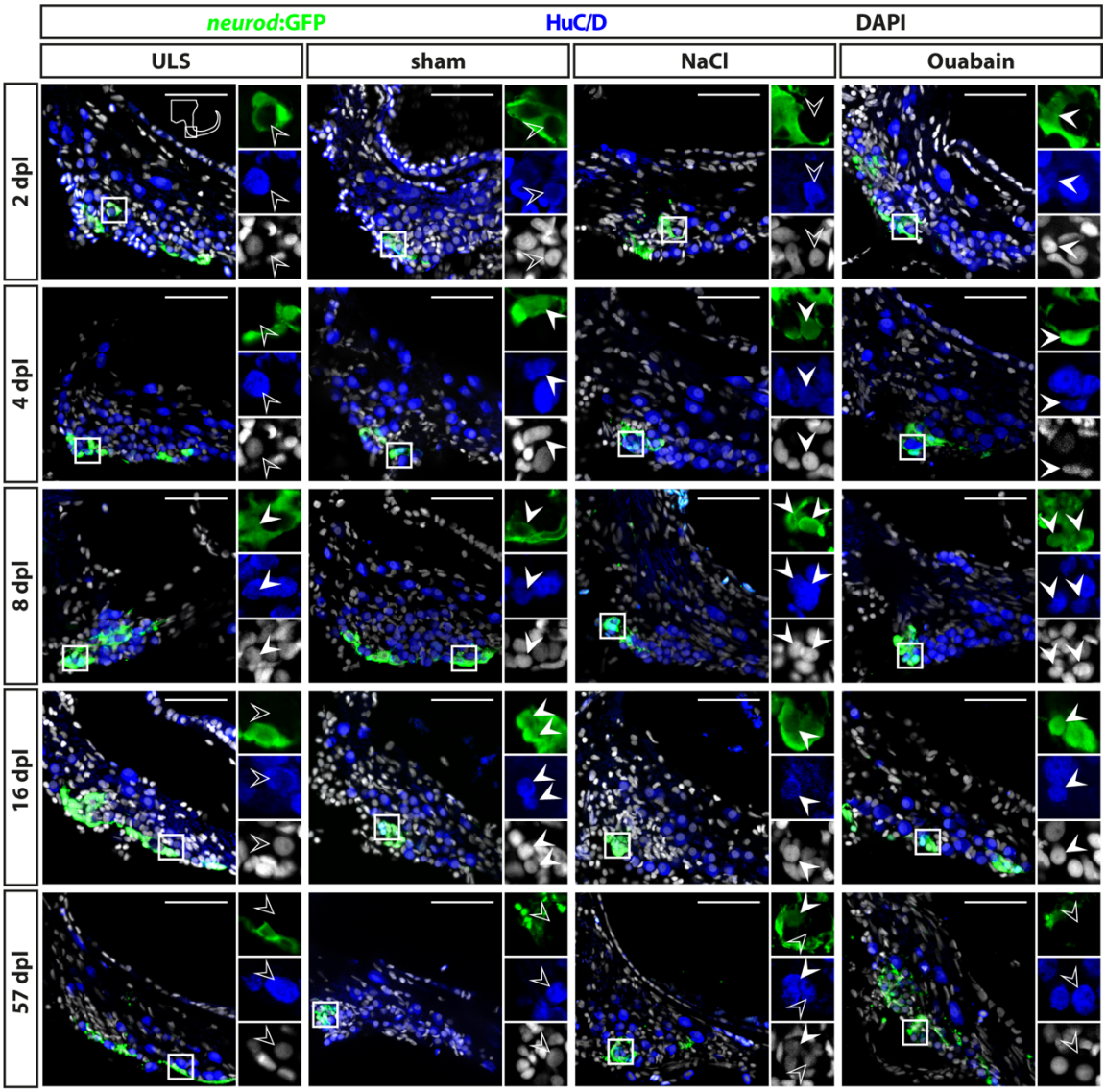

Figure 4.51 Generation of new sensory neurons from the *neurod*:GFP-positive progenitor pool upon lesion.
Short-term lineage tracing using the perdurance of GFP in the SAG of *neurod*:GFP transgenic animals. Immunohistochemistry against the neuronal marker HuC/D and GFP label newborn neurons in sham-treated, NaCl- and Ouabain-injected animals as well as the unlesioned side (ULS) of either sham-treated, NaCl- or Ouabain-injected animal at 2, 4, 8, 16 and 57 days post lesion (dpl). Shown are representative overviews of the neurogenic niche of the SAG as well as close-ups to visualize co-staining. At 4 dpl, several *neurod*:GFP/HuC/D-double positive cells can be found in the lesioned side independent of the type of lesion, whereas neurogenesis is almost not existing in the corresponding unlesioned side (upper row). At 8 and 16 dpl, neurogenesis was abundant in the lesioned sides and increased as well in the respective unlesioned sides at 8 dpl in sham-treated, NaCl-injected and at 16 dpl in Ouabain-injected animals (middle row). At 57 dpl, neurogenesis returned to low levels in the lesioned and unlesioned side with only a few newborn neurons present in the SAG (lower row). Scale bar: 50 µm, cross sections showing dorsal to the top and lateral to the right.

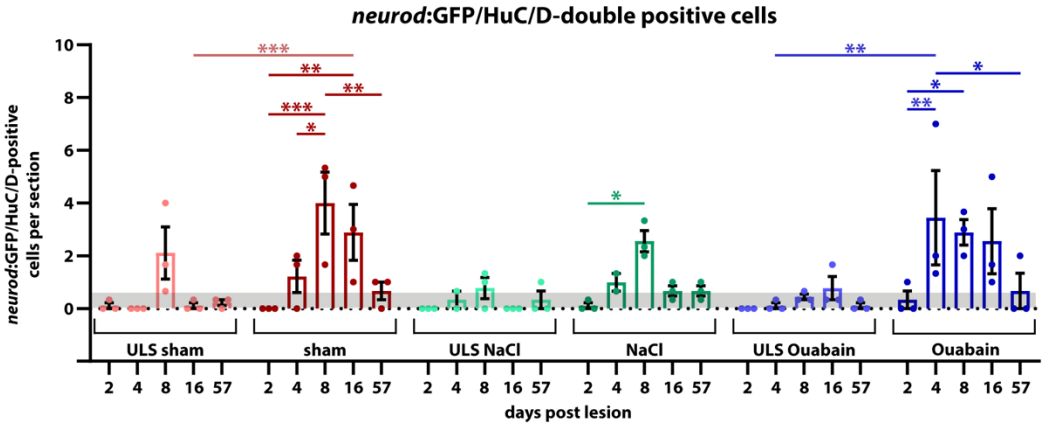

Figure 4.52 Quantification of reactive neurogenesis upon lesion.
Quantification of *neurod*:GFP/HuC/D-double positive cells per section at 2, 4, 8, 16 and 57 days post lesion. The number of *neurod*:GFP/HuC/D-double positive cells per sections revealed a significant increase in neurogenesis in the lesioned side in comparison to the homeostatic baseline (0,56 *neurod*:GFP/Huc/D-double positive cells per section) calculated from chapter 4.1.5 (grey box). The number of newborn neurons per section peaked at 4 dpl in Ouabain-injected SAGs and at 8 dpl in sham-treated as well as in NaCl-injected SAGs, respectively. At 57 dpl, neurogenesis returned to homeostatic levels in all three lesion conditions. Interestingly, neurogenesis rates in the SAGs of the respective unlesioned sides were also increased over time and even reached levels slightly above the homeostatic baseline at 8 dpl in sham-treated and NaCl-injected animals as well as at 16 dpl in Ouabain-injected animals. Baseline levels in neurogenesis in the respective unlesioned sides was reached again at 16 dpl and 57 dpl, respectively. Samples size n=3 (n=fish with 3 sections/SAG; exception: 4 dpl/NaCl: n=2); data is presented as mean±SEM. two-way ANOVA with Tukey's multiple comparisons test; ***$P \leq 0.001$; **$P \leq 0.01$; *$P \leq 0.05$.

4.3.7 Sensory neurons derived from reactive proliferating mature within 19 days post lesion.

To analyze whether newborn sensory neurons derive from progenitors that underwent reactive proliferation, I conducted a BrdU pulse chase experiment. To label a great amount of proliferating cells in sham-treated, NaCl-injected or Ouabain-injected neurod:GFP transgenic fish, lesioned animals were immersed in a BrdU solution from 2 to 3 dpl and from 4 to 5 dpl with a 24 hours resting period in between (Figure 4.53A). The previous BrdU pulse chase experiments of the adult homeostatic zebrafish SAG revealed that BrdU/neurod:GFP/HuC/D-triple positive newborn neurons are present at 14 days post BrdU pulse (4.1.6 4.1.7). Therefore, experimental animals were kept for additional 14 days after the second BrdU pulse, adding up to 19 dpl as the time point of analysis. Antibody staining against BrdU, HuC/D and GFP revealed that BrdU-positive cells were present in the neurogenic niche, but do not co-label with neurod:GFP and/or HuC/D in the unlesioned side. In contrast, BrdU/neurod:GFP-double positive neuronal progenitors, BrdU/neurod:GFP/HuC/D-triple positive newborn neurons and BrdU/HuC/D- double

positive neurons were found in the lesioned SAG, irrespective of the type of lesion (Figure 4.53B).

In summary, I show that the *neurod*:GFP-positive neuronal progenitor pool acts as a source of newborn neurons also during regeneration and that the neurogenesis rate is indeed transiently but significantly increased upon lesion. Moreover, I find that neurogenesis in the unlesioned side exceeds homeostatic levels, indicating a systemic effect caused by the unilateral lesion.

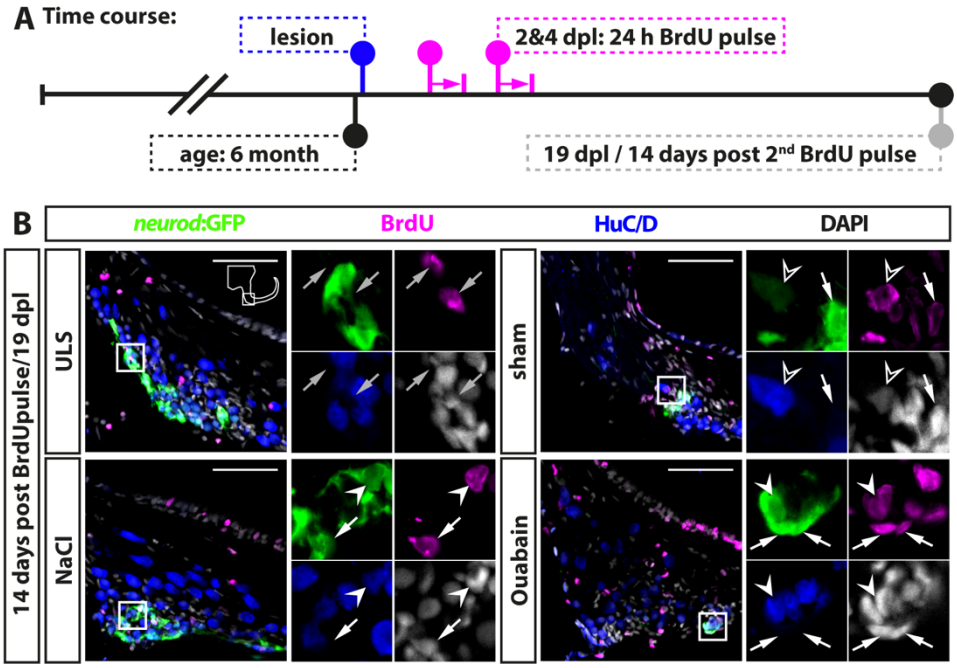

Figure 4.53 Sensory neurons derived from reactive proliferating mature within 19 days post lesion.
(**A**) Time course for BrdU pulse chase experiment. 6 months old *Tg(neurod:GFP)* zebrafish were lesioned, followed by two 24 hour long BrdU treatments at 2 and 4 days post lesion (dpl). Animals were sacrificed at 19 dpl corresponding to 14 days after the second BrdU treatment. (**B**) Antibody staining against the thymidine analogue BrdU, the neuronal marker HuC/D and *neurod*:GFP in the SAG of sham-treated, NaCl- and Ouabain-injected *neurod*:GFP animals 19 dpl / 14 days post BrdU pulse. In the SAG of the unlesioned side, BrdU-positive cells were found in close proximity to *neurod*:GFP-positive cells (grey arrow). In contrast, neurod:GFP/BrdU-double positive progenitors (arrow), *neurod*:GFP/BrdU/ HuC/D-triple positive newborn neurons (arrowhead) and BrdU/HuC/D-double positive neurons (open arrowhead) were present in the SAG of sham-treated, NaCl-and Ouabain-injected animals. Scale bars: 50 µm, cross sections showing dorsal to the top and lateral to the right.

4.3.8 Summary

This thesis presents the first lesion model to study the regenerative capacity of the adult zebrafish SAG. After lesion, first apoptotic mature sensory neurons appeared within hours and the SAG was infiltrated with immune cells that resided in the lesioned SAG for more than two weeks. Within the neurogenic niche, Neurod-positive progenitor cells were reactivated, started to proliferate and increased the neurogenesis rate above the homeostatic baseline. Interestingly, reactive proliferation and reactive neurogenesis showed similar temporal dynamics, indicating that the first wave of reactive neurogenesis is not dependent on previous proliferation of neuronal progenitor cells but rather relies on already existing neuronal progenitor cells in the neurogenic niche. A BrdU pulse chase experiment revealed that newborn neurons were differentiated from proliferating neuronal stem/progenitor cells within two weeks. Surprisingly, the unilateral lesion also induced the reactivation of the unlesioned SAG, suggesting a systemic response upon injury.

5. Discussion

According to the World Health Organization (WHO, 2023), over 5 % of the world's population suffer from disabling hearing loss. Sensorineural hearing loss accounts for the most cases and is caused by either the loss of sensory hair cells and/or their innervating sensory neurons in the inner ear. In mammals, including humans, the generation of sensory hair cells as well as sensory neurons are almost exclusively limited to embryonic stages, making this disability permanent and irreversible.

In contrast, other non-mammalian vertebrates such as fish, birds or reptiles, are capable of producing new hair cells throughout life and can even increase their production upon damage (reviewed in Rubel, Furrer and Stone, 2013). However, whether this holds true also for the innervating sensory neurons remains unknown.

In this thesis I used zebrafish as a model organism to study the vertebrate inner ear. It is known since decades, that hair cells in the zebrafish inner ear are produced throughout life (Higgs *et al.*, 2002). Additionally, zebrafish possess a remarkable regenerative capacity and can repair several organs and tissues upon lesion, such as neurons in the central nervous system (CNS) but also hair cells of the inner ear and lateral line (Kroehne *et al.*, 2011; Lush, Mark E, Piotrowski, 2013).

This study is the first to investigate (I) the presence of neurogenesis beyond larval stages during growth and homeostasis and (II) the regenerative capacity of the zebrafish statoacoustic ganglion (SAG), VIIIth cranial nerve of the peripheral nervous system (PNS). To this aim, I established (I) a pipeline to obtain single cells for in-depths transcriptome analysis and (II) the first lesion paradigm to study the loss of sensory neurons in the adult SAG and the resulting consequences in the zebrafish inner ear.

5.1 Characterization of the zebrafish SAG during growth and homeostasis focusing on juvenile and adult neurogenesis

5.1.1 Cellular composition and landmarks in the SAG

The foundation of this study was the thorough characterization of the anatomy and the cellular composition of the juvenile and adult SAG via immunohistochemical staining (IHC) on wild-type and transgenic zebrafish.

Morphologically, the SAG can be divided into an anterior and a posterior part in transversal cross-sections. The anterior part resides lateral of the brain whereas the posterior part resides ventral of the brain. Both parts, however, display the same cellular composition and landmarks (Figure 5.1).

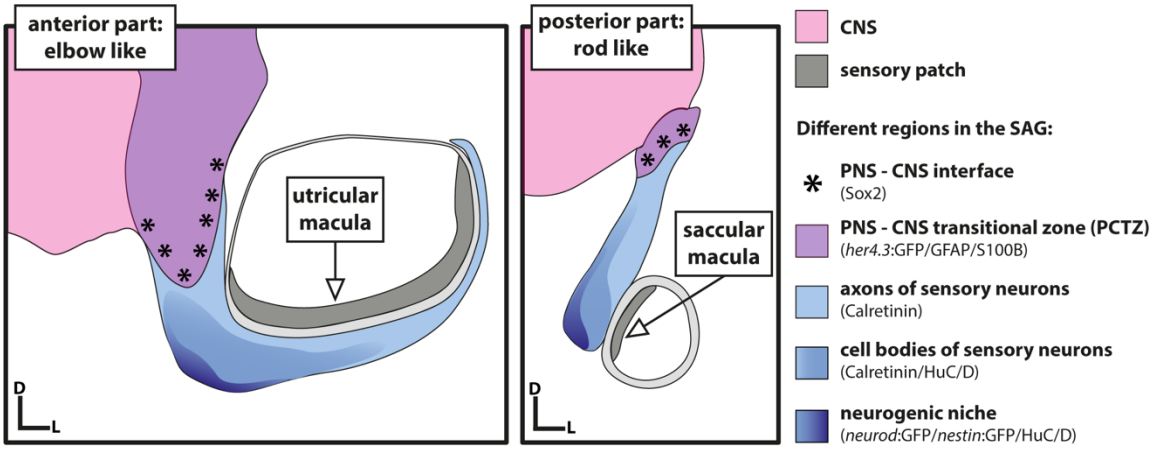

Figure 5.1 Cellular composition of the zebrafish SAG.
The SAG connects the sensory patches of the inner ear to the CNS and can be morphologically divided into an anterior elbow-shaped part and a posterior rod-shaped part. The peripheral-central nervous system transitional zone (PCTZ) is a strong landmark further dividing the SAG along the lateromedial axis into two parts: a lateral part corresponding to the PNS and characterized by weaker myelination and a lack of glia marker expression, and a medial part, corresponding to the CNS and characterized by a strong myelination pattern and expression of various glia markers. The anterior and the posterior part harbour a neurogenic niche at the ventromedial side consisting of Neurod/Nestin-double-positive neuronal progenitor cells. The cell bodies of the neurons are located dorsolaterally around the neurogenic niche. In the anterior part of the SAG, neuronal cell bodies and the neurogenic niche are found between the lateral and the medial part, whereas in the posterior part of the SAG, both are located in the medial part at the ventral tip. Neurons extend their axons in the medial part towards the CNS and their dendrites into the lateral part towards the sensory patches. D, dorsal; L, lateral.

The juvenile as well as the adult SAG harbors a neurogenic niche consisting of Neurod/Nestin-positive progenitor cells at the ventromedial side. Importantly, the neurogenic niche in the adult SAG is not a continuous band of cells but is rather composed of dispersed islets along the anteroposterior axis.

The cell bodies of the bipolar sensory neurons are located at the dorsolateral side of the neurogenic niche, with newborn neurons being in close proximity to the neurogenic niche and older neurons residing further dorsally. Mature neurons expand their dendrites laterally to innervate the sensory hair cells in the respective sensory patch. Medially, the axons of the mature neurons enter the CNS to project to the corresponding nuclei, thus crossing the peripheral-central nervous system transitional zone (PCTZ) (Figure 5.1).

The PCTZ is defined as the area where the axons of the PNS overlap with the CNS in the nerve roots of vertebrates and is characterized by a switch of the type of myelinating cells: oligodendrocytes in the CNS vs. Schwann cells in the PNS. The interface at the PCTZ is established by glia cells and oligodendrocytes on the side of the CNS and Schwann cells on the side of the PNS and prevents any cell or part of a cell to cross this boarder except the axons of the PNS neurons projecting to the

CNS (Toesca, 1996; Wang *et al.*, 2013). In line with this, I identified the PCTZ as a landmark in the zebrafish SAG which is characterized by a strong oligodendrocyte-mediated myelination pattern compared to the weaker, Schwann cell-mediated myelination pattern present in the lateral part of the SAG (see Figure 4.17). In addition, the PCTZ is marked by the presence of cells expressing glia markers such as GFAP, S100B and *her4.3*:GFP in the CNS. Interestingly, the neural progenitor marker Sox2 is expressed in cells at the interface from PNS to CNS, making it an additional marker for the zone. Mammals exhibit an exceptionally long CNS extension in the spiral ganglion of the cochlea in comparison to other nerves (Fraher and Delanty, 1987; Wang *et al.*, 2013). Similarly, in the zebrafish SAG, the PCTZ covers more than 100 µm of the medial part in the anterior SAG and reaches close to the neurogenic niche. Together, this data establishes two important landmarks for future studies of the zebrafish SAG: the neurogenic niche containing Neurod/Nestin-positive neuronal progenitors in the ventromedial part of the SAG which is not present/existing in mammals and the PCTZ marked by expression of glia marker as well as the presence of Sox2 expressing cells and the characteristic myelination pattern which is also described in mammals.

5.1.2 Neurod/Nestin-positive progenitor cells in the neurogenic niche act as a source for lifelong neurogenesis in the SAG

Neurogenesis from Neurod-positive progenitor cells in the SAG exists throughout life

The phenomenon of programmed cell death leading to a loss of 20-80 % of newly generated neurons is a physiological process during development and maturation of the vertebrate CNS and PNS (Oppenheim, 1991). Quantification of all HuC/D-positive neurons in the anterior SAG revealed that the overall number and the density of sensory neurons decreases as the SAG grows and increases in thickness (~20 % decrease on overall number of neurons from 2 to 8 months, Figure 4.3). This suggests that there is a surplus of neurons produced during juvenile stages (which is subsequently lost at later stages), indicating that cell elimination does also take place in the zebrafish SAG.

Interestingly, data obtained in this thesis shows that neurogenesis still occurs with a high rate at juvenile stages and is even present at low levels in the adult SAG. During vertebrate inner ear development, otic neurogenesis requires a sequential process including specification, delamination, proliferative expansion and differentiation of neuronal precursor cells to give rise to mature sensory neurons (Vemaraju *et al.*, 2012). Moreover, in vertebrates, expression of the bHLH gene *neurod* is essential for generating the pool of transient-amplifying progenitor cells which will eventually stop proliferating and start differentiating into mature neurons in (Korzh *et al.*, 1998; Kim *et al.*, 2001; Vemaraju *et al.*, 2012). However, whether *neurod* expressing neuronal progenitor cells in the SAG were still present

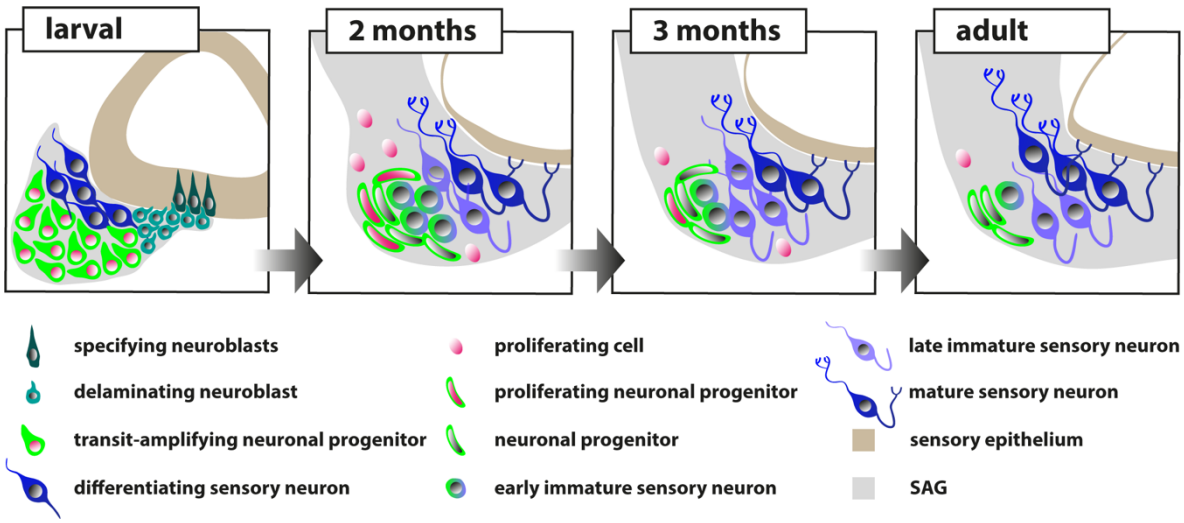

Figure 5.2 Neurod/Nestin-expressing neuronal progenitor cells act as a source for lifelong neurogenesis in the SAG.
Larval neurogenesis in the inner ear is a sequential process including specification, delamination, transient-amplification and differentiation (modified after Vemaraju *et al.*, 2012.). At juvenile stages (age 2 months), Neurod/Nestin-positive progenitor cells are not only present but also still proliferating and the neurogenesis rate is high. Over time the proliferation rate of neuronal progenitors decreases, resulting in a quiescent neurogenic niche regarding proliferation. In contrast, neurogenesis is not absent in the adult SAG but only significantly decreased to a low level. Interestingly, marker-negative cells surrounding the neurogenic niche are still proliferating and their offspring differentiate into new neuronal progenitors thus replenishing the pool of Neurod/Nestin positive cells in the adult SAG lifelong.

beyond larval stages and whether these cells could be a source of neurogenesis in the adult SAG was unknown.

Here, it was shown that the population of Neurod-positive progenitor cells persists throughout life, forming dispersed islets of neuronal progenitors in the anterior and posterior SAG. At juvenile stages, the neurogenic niche is still highly active and Neurod-positive cells proliferate and give rise to newborn neurons as the short-term lineage tracing experiment revealed. Moreover, quantification after BrdU treatment shows that the percentage of BrdU/*neurod*:GFP-positive cells does not change significantly from a 7 days chase to later time points, indicating that some of the proliferating *neurod*:GFP-positive cells remain in the transient-amplifying progenitor pool and do not initiate differentiation within 28 days after proliferation. Whether these cells belong to a subpopulation of progenitors retaining a proliferative potential while residing in the neurogenic niche and/or will eventually differentiate into new neurons at later time points is not yet clear. In contrast, the Neurod-positive progenitor pool turns quiescent in terms of proliferation at adulthood. Moreover, neurogenesis (*neurod*:GFP/HuC/D-positive cells) is reduced to extremely low levels. This indicates that neurogenesis from the *neurod*:GFP-positive progenitor pool in the adult SAG is independent of previous proliferation of these

cells. This hypothesis is further supported by the two different lineage-tracing approaches applied in the adult SAG. The short-term lineage tracing experiment based on GFP perdurance in HuC/D-positive neuronal offspring of *neurod*:GFP-positive progenitor cells revealed a low neurogenesis rate at adult stages (Figure 4.6). The long-term lineage tracing experiment using BrdU application to follow the progeny of proliferating cells in the adult SAG, however, showed that almost no newborn neurons were born after a 28 day-lasting trace of proliferating cells (Figure 4.10), suggesting that the neuronal progenitor cells differentiating into mature neurons were most likely not a recently (< 28 days) proliferating cell. Because of the low, yet constant, level of adult neurogenesis descending from the no longer proliferating, quiescent Neurod-positive progenitor cells, one would anticipate an exhaustion of this progenitor pool over time. However, I found that even aged fish still display the *neurod*:GFP-positive cell pool, implicating the presence of a replenishing source. Indeed, the BrdU pulse chase experiment in the adult SAG revealed a small population of proliferating but otherwise marker-negative cells which differentiate into *neurod*:GFP-positive progenitor cells within 7 days and also give rise to neurons at a low but steady-state level (Figure 4.10).

Altogether, this study is the first to show, that indeed, lifelong hair cell production in the zebrafish inner ear is accompanied by lifelong neurogenesis from a neurogenic niche consisting of *neurod*-expressing neuronal progenitor cells. These findings are in line with the production rate of hair cells reported for the inner ear of adult zebrafish and other teleost species. Studies on hair cell and ganglion cell generation in *Astronotus* have shown that the average ratio of hair cells to afferent ganglion cells increases from 30:1 in small/younger fish to 300:1 in larger/older fish (Popper and Hoxter, 1984). Quantification of saccular hair cells in zebrafish aged 2 to 20 months revealed an increase from 2800 hair cells in 6 months old zebrafish to almost 3600 hair cells in 10 months old zebrafish (Higgs *et al.*, 2002). The addition of ~800 hair cells within 4 months corresponds to a hair cell production rate in the magnitude of, on average, 6.5 hair cells per day within the whole saccule. As one sensory neuron innervates multiple hair cells, my experiments revealing a production rate of less than one sensory neuron per day deriving from proliferating neuronal stem/progenitor cells in the anterior part of the adult SAG fit perfectly well to the known literature.

The VI intermediate filament protein Nestin labels a subpopulation of Neurod-positive progenitor cells

The class VI intermediate filament protein Nestin was first described as a marker for neuroepithelial stem cells and is expressed among other tissues in the CNS and PNS in neural stem and progenitor cells (Frederikson and McKay, 1988; Lendahl, Zimmerman and McKay, 1990; Dahlstrand, Lardelli and Lendahl, 1995;

Bernal and Arranz, 2018). Several studies in rodents have shown, that Nestin-expressing cells are present in the spiral ganglion cell region as well as in other regions of the inner ear such as the organ of Corti during development and even persists - though reduced in number - to adulthood (Lopez *et al.*, 2004; Watanabe *et al.*, 2012; Chow *et al.*, 2015). Using a long-term lineage tracing approach I showed, that more than 50 % of the mature neurons in the adult SAG are the offspring of *nestin*-expressing neuronal progenitor cells present during otic development from 5 to 72 hpf (see 4.1.9). Similar to Neurod, Nestin expression does not ceases after otic development during larval stages but is still present in the neurogenic niche of juvenile and adult fish. In the neurogenic niche, analysis of double transgenic *neurod*:GFP/*nestin*:mCherry-T2a-CreER^{T2} fish indicated, that expression of Neurod and Nestin overlap almost completely (Figure 4.12). Together with the finding, that *nestin*-expressing cells in the juvenile SAG are proliferating and give rise to new neurons while no proliferating Nestin-positive cells were present in the adult SAG (similar to *neurod*-expressing cells) it can be concluded, that Nestin and Neurod mark the same cell population.

In contrast, the data obtained from the single-cell RNA sequencing of *pcna*:GFP-positive and *pcna*:GFP/*nestin*:mCherry-T2a-CreER^{T2}-double positive cells in the juvenile SAG clearly revealed that *nestin* is only expressed in a subpopulation of *neurod1*-positive progenitor cells (Figure 4.25). Besides two clusters containing immune cells (cluster 11 and 12), a cluster of endothelial cells and cells of lymphatic vessels (cluster 10), a cluster expressing markers assigned to the sensory epithelium (cluster 1) and two clusters containing myelinating cells and oligodendrocyte precursors (cluster 2 and 3, respectively), six clusters were found to be associated to the neuronal lineage of the SAG. Out of those six, two clusters were identified as "progenitor cells" based on their gene expression profile.

Interestingly, the progenitor cell clusters each expressed a set of genes that might indicate a different degree of maturity. Besides expressing several genes encoding for ribosomal proteins, the progenitor cells 1 cluster was characterized by the expression of genes from the *her*-family, such as *her4.2/4.3/4.4* and *her15.1/15.2* that are known to play a role in neuronal stem and progenitor cells. In contrast, the cluster of Neurod1-only expressing progenitor cells, progenitor cells 2, exclusively expressed markers associated with glutamatergic synapses such as *cbln12* (known to be co-expressed with Neurod1 in granule cells in zebrafish larvae; (Dohaku *et al.*, 2019)), *grin1b* (previous name *NMDAR1.2*, (Cox, Kucenas and Voigt, 2005)) and *sh3gl2a* (zfin.org). This suggests that this population of neuronal progenitor cells might have already matured further compared to the cluster of progenitor cells 1. In line with this hypothesis, few cells in the progenitor cells 1 cluster are still expressing proliferation markers such as *pcna*, *mki67* and *mcm5*, whereas cells form the progenitor cells 2 cluster were not expressing those markers. Furthermore, both progenitor cell populations express genes they share with the cluster of newborn neurons that the other progenitor cell population does not

express. In case of the progenitor cells 1 cluster these genes are for example the radial glia marker *vim*, a marker for the statoacoustic ganglion called *tlx2* (Hatano *et al.*, 1997) and *sfpq*, a gene known to be involved in CNS development (Lowery, Rubin and Sive, 2007), all genes associated with neuronal progenitor cells and neuronal development. In contrast, cells from cluster progenitor cells 2 expressed genes related to the function of mature neurons, such as *snap25a/b* associated with the neuronal SNARE complex mediating synaptic vesicle fusion (Oyler *et al.*, 1989), but also genes involved during neuronal development like *stmn4*, which is critical for maintenance of neural progenitor cells during zebrafish CNS development (Lin and Lee, 2016) and *r3hdm1*, expressed in mouse hair cells and associated with the function of hearing in mammals (Concas *et al.*, 2021) (for all genes see also zfin.org). However, further analysis of *r3hdm1* expression using *in situ* hybridization could not confirm *r3hdm1* as a marker to distinguish the *r3hdm1*-expressing population of progenitor cells 2 (Bachelor Thesis Daniel Scherer, 2021). FISH combined with antibody staining for *r3hdm*1, GFP and PCNA in juvenile transgenic *neurod*:GFP animals revealed a much broader expression of *r3hdm1* than expected: r*3hdm1* was found in a subset of *neurod*:GFP-positive neuronal progenitor cells but also in all HuC/D-positive newborn, differentiating and mature neurons in the juvenile SAG. In line with the *r3hdm1*-expression pattern in the transcriptome data, there were also *neurod*:GFP-positive neuronal progenitor cells not expressing *r3hdm1*, most probably relating to the cells from the cluster progenitor cells 1 that mostly do not express *r3hdm1*. Interestingly, in the transcriptome data set from the adult SAG, out of eight *r3hdm1* expressing cells only two cells were found in the cluster of newborn/differentiating neurons, whereas four cells also expressed hair cell markers such as *otofb*, *s100s* and *gpx2* (see below), correlating with the expression pattern of *r3hdm1* found in mice (Concas *et al.*, 2021).

Moreover, there were also differences in the expression of the neuronal markers *elavl3* and *elavl4*: both of these markers were expressed in newborn and differentiating neurons, *elavl3* (also known as HuC), however, was expressed at higher levels in NPC-1 cells compared to NPC-2, whereas it was the other way around for *elavl4* (also known as HuD).

One explanation for the presence of these two different progenitor cell populations in the transcriptome data could be a hierarchical order of neuronal progenitor cells in the neurogenic niche, where one of the progenitor cell populations gives rise to the other. The fact that there are only actively proliferating cells in the progenitor cells 1 cluster and not in the progenitor cells 2 cluster as well as the expression of radial glia markers in progenitor cells 1 vs. expression of more mature neuronal markers associated with synapses in progenitor cells 2 would argue in favor of progenitor cells 1 to be upstream of progenitor cells 2 in the neuronal stem/progenitor cell hierarchy. In contrast, the distribution of *neurod*:GFP-positive vs. *nestin*:mCherry-T2a-CreER^{T2}-positive progenitor cells found in IHC staining revealed *nestin*:mCherry-T2a-CreER^{T2}/HuC/D-double positive newborn neurons not

expressing *neurod*:GFP (Figure 4.12). Additionally, *neurod*:GFP-only expressing cells were found at the most ventromedial side of the SAG were usually the proliferating neuronal progenitor reside. These findings would rather suggest a reverse hierarchical order of Neurod-only positive progenitor cells standing above Neurod/Nestin-double positive progenitor cells.

Instead of one progenitor cluster being on top of the other in a hierarchical order, both progenitor cell clusters could also be aside of each other serving as neuronal progenitor cells for different types of neurons in the SAG. The auditory system of mammals for instant harbors to different types of spiral ganglion neurons (SGNs). The majority of neurons (90-95 %) belong to the afferent, bipolar type I SGNs, each dendrite only innervating one inner hair cell. The other 5-10 % of neurons are classified as afferent pseudo-unipolar type II SGNs, each innervating multiple outer hair cells (reviewed in Carricondo and Romero-Gómez, 2019)).

Recently, using single-cell RNA sequencing Petitpré et al. identified three subclasses of type I SGNs in the mouse cochlea that are already present at birth indicating that this neuronal diversity is independent of neuronal activity but rather established during neurogenesis (Petitpré *et al.*, 2018). In a study for candidate genes for hearing loss, Nascimento et al. recently showed that the *Cnrip1* genes is expressed at different levels in type I and type II SGNs in mice, with higher expression levels in type II SGNs compared to type I SGNs (Nascimento *et al.*, 2022). In the same study, the authors also re-analyzed published transcriptome data and used RT-qPCR to investigate expression patterns of the zebrafish homolog genes *cnrip1a* and *cnrip1b* in several tissues. They found, that in contrast to mice, zebrafish *cnrip1a* is expressed in hair cells and sensory epithelium of the lagena and utricle as well as the brain, further recapitulating their finding with *in situ* hybridization on 5 dpf and 30 dpf old zebrafish. Due to their inability to dissect the anatomically complex structured SAG, they could not analyze the expression of *cnrip1a* in the SAG. Interestingly, in line with the expression pattern found in mice, analyzing the transcriptome data of the juvenile SAG obtained in this thesis revealed that only a fraction of cells in the cluster defined as newborn and differentiating neurons expressed *cnrip1a*. However, the question whether there are indeed different types of neurons in the zebrafish SAG similar to type I and type II SGNs found in mammals cannot be answered with the sorting strategy and subsequent scRNAseq of cells from the juvenile SAG used in this study and remains subject for further investigations.

Identification of tubb5 and gap43 as novel marker for neuronal progenitor cells and newborn neurons

The transcriptome data of the juvenile SAG suggest *tubb5*, a marker known to be expressed in neuronal tissue during vertebrate CNS and PNS development

(Breuss *et al.*, 2012; Baraban *et al.*, 2013), to be another early neuronal marker for newborn neurons in the SAG. Additionally, Lange et al. recently identified *tubb5* as a marker for newborn neurons in the telencephalon of adult zebrafish (Lange *et al.*, 2020). In contrast to *r3hdm1*, it was not expressed in the progenitor cells 2 cluster but in the progenitor cells 2 cluster and at high levels in the cluster of newborn neurons. Further analysis using *in situ* hybridization confirmed its expression in non-proliferating, *neurod*:GFP-expressing neuronal progenitor cells in the neurogenic niche (Lab Rotation Project Nora Bölicke, 2021).

Another novel marker for newborn neurons identified in the transcriptome data set of the juvenile SAG was *gap43*, which is known to be expressed in post-mitotic neurons during axon elongation (Biffo *et al.*, 1990). Combining antibody staining for GFP, the proliferation marker PCNA and the neuronal marker HuC/D on section from juvenile, transgenic *gap43*:GFP animals revealed the expression of *gap43*:GFP/HuC/D-double positive newborn neurons and their axonal projections in the area of the neurogenic niche in the medial part of the SAG (Figure 4.27B). In contrast to the finding of *gap43* being expressed in post-mitotic neurons by Biffo et al., a fraction of *gap43*:GFP-positive cells were also PCNA-positive. Surprisingly, in one individual one cell was found triple-positive for *gap43*:GFP, PCNA and HuC/D, suggesting Gap43 as a marker for neuronal progenitor cells still proliferating as well as newborn neurons.

The applied sorting-strategy using double transgenic pcna:GFP/nestin:mCherry-T2a-CreER^{T2} line does not allow to analyze neuronal progenitor cells in the adult SAG

To analyze the transcriptome of the adult SAG, the sorting strategy used before based on double transgenic *pcna*:GFP/*nestin*:mCherry-T2a-CreER^{T2} line was modified. To obtain the transcriptomic profile of newborn neurons derived from non-proliferating neuronal progenitor cells, *nestin*:mCherry-T2a-CreER^{T2}-only positive cells were collected additionally to *pcna*:GFP/*nestin*:mCherry-T2a-CreER^{T2}-double positive and *pcna*:GFP-only positive cells.

In contrast to the transcriptome data of the juvenile SAG, less than 16 % of the analyzed cells in the adult transcriptome data could be assigned to potentially be part of the neuronal lineage. Those cells were distributed between two clusters, one classified as the stem-cell like 1, the other as the cluster of newborn/differentiating neurons. A subcluster characterized by the expression of *her*-genes also co-expressed *otog* as well as *otogl,* two genes associated with otolith formation, identifying it as a cluster of sensory/hair cell progenitor cells instead of neuronal progenitor cells. Even though 156 cells were sorted based on the presence of the fluorophore mCherry driven by the *nestin*-promotor, only 2 of these cells, both located in the cluster of newborn/differentiating neurons, actually expressed *nestin*.

Similar, there was also no cluster of *neurod1*-expressing neuronal progenitor cells. Only 9 cells out of all 216 analyzed cells expressed *neurod1*, all of them located in different clusters. Even though I proofed the existence of the neuronal progenitor cell population in the adult SAG, no distinct neuronal progenitor cell cluster was found in the transcriptome data set from the adult SAG, making it impossible to compare the juvenile neuronal progenitor cell pool to the adult. Besides three (sub)clusters identified as different types of immune cells (immune cells 1: neutrophiles; immune cells 2: dendritic cells; immune cells 3 macrophages) one cluster identified as endothelial cells/lymphatic vessels (cluster 5) and one subcluster containing myelinating cells (subcluster 4.1), the other four clusters were surprisingly assigned to the sensory lineage. Two of the clusters were expressing markers of the sensory epithelium, one (as mentioned above) was identified as sensory progenitor cells and the last cluster was identified as a cluster of hair cells expressing typical hair cell markers such as *otofb* (Chatterjee *et al.*, 2015), *s100s* (Kraemer, Saraiva and Korsching, 2008) and *gpx2* (Erickson and Nicolson, 2015). The majority of hair cells was sorted as "*nestin*:mCherry-T2a-CreER^{T2}-positive cells", indicating that the chosen double transgenic lines and the sorting strategy was not suitable to analyze the neurogenic niche focusing on neuronal stem and progenitor cells in the adult SAG. To improve the characterization of the neurogenic niche and to identify differences in the transcriptomic profile of the actively proliferating neuronal progenitor cells in the juvenile SAG und the quiescent, non-proliferating neuronal progenitor cells in the adult SAG, a second set of transcriptome data using transgenic *neurod*:GFP fish to label all neuronal progenitor cells in the juvenile and adult SAG is currently work in progress. Another ongoing approach is the generation and analysis of a single-cell transcriptome atlas of the entire adult zebrafish to capture every cell population in the SAG and hopefully identify potential neuronal stem cell markers and investigate whether the SAG harbors different types of sensory neurons.

Taken together, this study is the first to show the presence of a neurogenic niche in the zebrafish SAG that switches from a high neurogenesis rate at juvenile stages to a low-level production of neurons in the adult SAG. At juvenile stages, two subpopulations of neuronal progenitors could be distinguished using single-cell RNA sequencing, one co-expressing *nestin* and *neurod1*, the other only expressing *neurod1*. Neuronal progenitors in the juvenile SAG are still highly proliferating whereas neuronal progenitors in the adult SAG turn to a quiescent, non-proliferative state. Interestingly, the number of neuronal progenitor cells remains constant throughout life and proliferating, marker-negative cells differentiate into new neuronal progenitor cells at adult stages, indicating the presence of a so fare uncharacterized population of putative stem cell-like cells in the SAG replenishing the pool of neuronal progenitor cells.

5.1.3 Finding the presumptive stem cell-like cell population maintaining the pool of neuronal progenitor cells

It is not yet clear, whether neurogenesis exclusively occurs via the Neurod/Nestin-positive progenitor pool or if alternative mechanisms such as proliferation of stem/progenitor cells followed by direct differentiation into mature neurons without expression of Neurod or Nestin as an intermediate progenitor might also play a role in the SAG. Additionally, this study aimed to unravel the identity of the postulated yet uncharacterized stem cell-like cells population replenishing the neuronal progenitor cell pool. To this aim, known markers for neuronal stem and progenitor cells were analyzed for their presence in the SAG using IHC. Moreover, I used the two generated transcriptome data set of the neurogenic niche from juvenile and adult SAG to identify (novel) marker genes for the presumptive neuronal stem cell-like cells.

fabp7a/sox2 co-expressing cells might be a zebrafish equivalent of boundary cap cells found in other vertebrate species

In the zebrafish telencephalon, GFAP/S100B/Her4.3-positive radial glia cells serve as neuronal progenitors (Ganz *et al.*, 2010; Chapouton *et al.*, 2011). However, analysis in the juvenile and adult SAG using IHC revealed the expression of these glia markers in the PCTZ, hence in the CNS. Sorting for *pcna*:GFP-positive cells and their offspring carrying the inherited fluorescent protein for transcriptome analysis of the neurogenic niche in juvenile SAG also revealed a cluster of cells (cluster 6, stem cell-like 2) expressing *her4.2/her4.3* and *s100b* as well as other radial glia marker such as *fabp7a* and *cx43* (Kunze *et al.*, 2009; Ito *et al.*, 2010). *s100b* as well as *fabp7a* were also expressed by the cluster of oligodendrocyte precursor cells, annotated based on the expressing of oligodendrocyte precursor cell marker such as *olig1*, *olig2*, *nkx2.2a* and *sox10* (Ackerman and Monk, 2016). Considering the position of where the SAG was cut from the brain, that was approx. 100-300 µm mediodorsally from the CNS-PNS interface, these two clusters most likely derive from the PCTZ, where oligodendrocytes from the CNS myelinate the axons of the sensory neurons. *in situ* hybridization in the juvenile SAG confirmed the expression of *fabp7a* in the PCTZ (Lab Rotation Project Nora Bölicke, 2021). Additionally, *fabp7a* was also found to be expressed in *neurod*:GFP-positive neuronal progenitor cells in the ventromedial side of the juvenile SAG, indicating that *fabp7a* might also play a role in the neurogenic niche and as a potential stem cell marker. The transcriptome data of the adult SAG picked up three cells expressing *fabp7a*, from which two also expressed several other markers of the stem cell-like 2 cluster of the juvenile SAG data set and additionally clustered together with this cluster in the combined analysis. However, further investigations including *in situ* hybridization

against *fabp7a* combined with staining against PCNA labeling proliferating cells and BrdU lineage tracing experiments in the adult SAG are necessary to elucidate the role of *fabp7a* in the SAG.

Another analyzed potential marker for the neuronal stem cells in the SAG was Sox2. In addition to the Sox2-expressing cells in the sensory patch, Sox2-expressing cells in the SAG are (similar to the expression pattern of the glia markers GFAP/S100B/Her4.3) located in the PCTZ, remarkably only at the CNS-PNS interface, turning it into another useful marker for the PCTZ. Surprisingly, this distribution of Sox2 along the CNS-PNS interface in the SAG is in contrast to Sox2 expression in neonatal mice, in which Sox2-expressing glia cells are distributed evenly within the spiral ganglion and preserve a high potency of neuronal differentiation (Arnold *et al.*, 2011; Meas, C.-L. Zhang and Dabdoub, 2018; Noda *et al.*, 2018; He *et al.*, 2021). In line with the expression pattern detected with a Sox2 antibody, *sox2* expressing cells are found in the stem cell-like 2 cluster in the transcriptome data of the juvenile SAG, co-expressing the radial glia markers *her4.2/her4.3*, *s100b* and also *fabp7a*. The transcriptome data set of the adult SAG contained three Sox2-expressing cells, one co-expressing radial glia markers, the other two co-expressing hair cell markers.

Interestingly, in cranial and dorsal root ganglia of birds and mammals, a neural-crest-derived population called boundary cap cells is involved in CNS-PNS boundary formation and is transiently found at the peripheral nerve entry/exit points during development (Niederländer and Lumsden, 1996; Maro *et al.*, 2004). It has been shown in various studies that boundary cap cells are capable of differentiating into glia cells and sensory neurons of the PNS and serve as a multitask stem cell-like cell population of the developing PNS, giving rise to neuronal and non-neuronal cell types (Maro *et al.*, 2004; Hjerling-Leffler *et al.*, 2005; Gresset *et al.*, 2015). Additionally, boundary cap cells can even be redirected into CNS lineages, indicating their differentiation plasticity beyond exclusively giving rise to cells from the PNS lineage (Zujovic *et al.*, 2011). One marker for neural-crest-derived cells that has also been used to label boundary cap cells, is cadherin-7 (Nakagawa and Takeichi, 1995; Niederländer and Lumsden, 1996). The two ortholog zebrafish genes *cdh7a* and *cdh7b* were found to be expressed in cells of the stem cell-like 2 cluster in the transcriptome data obtained from the juvenile SAG, co-expressing *sox2, s100b*, *her4.2/her4.3* and *fabp7a,* suggesting that the *sox2*-positive cells in the SAG might be the zebrafish equivalent of boundary cap cells found in the PCTZ of other vertebrates. However, further research is needed to confirm Sox2-expressing cells as boundary cap cells and investigate the capacity of Sox2-positive cells to serve as neuronal stem and/or progenitor cells for sensory neurons in the SAG. Lineage tracing experiments for example would allow to trace the progeny of Sox2-expressing cells in the SAG to investigate whether Sox2-positive cells are indeed replenishing the neurogenic niche and/or give rise to sensory neurons.

rbp4 as a promising marker for the presumptive stem cell-like cell population maintaining the neuronal progenitor cell pool in the SAG

Besides the potential stem cell-like cluster 2 found in the juvenile transcriptome data set, the juvenile and adult transcriptome data set revealed the presence of another potential stem cell cluster named stem cell-like cluster 1. This cluster in the juvenile and adult SAG was characterized by the expression of *socs3a*, known as a key regulator of hair cell regeneration (Liang *et al.*, 2012), *sdc4*, encoding syndecan 4 associated with modulating neural stem cell proliferation (Luo *et al.*, 2016) and *rbp4*, encoding for the primary carrier protein of vitamin A also known as retinol (Rask *et al.*, 1979). Rbp4 is primarily known to be expressed in the liver and plays an important role in retinoic acid signaling pathways (Blaner, 1989; Alapatt *et al.*, 2013). It forms a complex with retinol and enables the transport of retinol from the liver through the bloodstream to it target tissues, where the complex binds to tissue specific receptors to facilitate the uptake of retinol into the cell, where retinol is converted into at least two critical metabolites, all-*trans* retinoic acid and 11-*cis* retinaldehyde (Gudas, 1994; Chambon, 1996; Kiser and Palczewski, 2016). Retinoic acid signaling plays a crucial role in neurogenesis (Maden, 2002). In zebrafish and chick, Rbp4 is found in cerebrospinal fluid during embryonic development and promotes embryonic neuroepithelial survival (Alonso *et al.*, 2011, 2014; Chang, Lehtinen and Sive, 2015). Additionally, experiments on explanted chick neuroepithelium revealed that retinoic acid signaling promotes neurogenesis (Alonso *et al.*, 2011, 2014). In context of regeneration, the retinoic acid pathway was also found to be required for hair cell regeneration in the zebrafish inner ear and lateral line (Rubbini *et al.*, 2015). Analysis of the expression of genes involved in retinoic acid signaling such as Aldh1, catalyzing the synthesis of retinoic acid from retinaldehyde and Cyp26, involved in the degradation of retinoic acid, in the juvenile SAG revealed the presence of few cells co-expressing *rbp4* and *aldh1a2* and *aldh1a3* and the expression of *cyp26b1* on the cluster of newborn neurons (Figure S.11), indicating a potential role of retinoic acid signaling in mediating neurogenesis in the SAG (Parés *et al.*, 2008; Xi, Yue and Yang, 2015; Hawkins and Wingert, 2023).

Verification of the expression of *rbp4* in the SAG of 3 months old fish via *in situ* hybridization done by Daniel Scherer revealed that *rbp4* is expressed medially of *neurod*-expressing progenitor cells in a small cell population, infrequently also containing proliferating cells (Bachelor Thesis Daniel Scherer, 2021). The close proximity of the *rbp4* expressing cells to the *neurod*-expressing progenitor cells as well their ability to proliferate makes *rbp4* a promising marker for the presumptive neuronal stem cell-like cell population. However, further studies are needed to verify *rbp4*-positive cells as the neuronal stem cells maintaining the neuronal progenitor pool in the SAG. CRISPR-Cas9-mediated generation of transgenic *rbp4* reporter lines would allow labeling of *rbp4* expressing cells and – based on fluorophore perdurance – also their recent progeny to further confirm

their location within the SAG (Hwang *et al.*, 2013). Additionally, similar to the sorting strategy used in this thesis, a *rbp4* reporter line could be used for transcriptome analysis via single-cell RNA sequencing to prove that *rbp4* expressing cells differentiate into *neurod*-expressing, neuronal progenitor cells. Generation of a *rbp4*-Cre-driver line would additionally allow to perform lineage tracing experiments based on the Cre/loxP system; here the ligand inducible recombinase CreER^{T2} would be expressed under the control of the *rbp4* promotor. Crossed to a Cre-dependent reporter line (e.g. *Tg(hsp70l:loxP-DsRed2-loxP-nlsEGFP)* line, the *rbp4*-CreER^{T2} driver line would induce the recombination of the reporter line hence excising the DsRed2 fluorophore upon application of the ligand (here tamoxifen), resulting in labeling all progeny of *rbp4*-expressing cells with EGFP (Hans *et al.*, 2011).

In summary, this thesis revealed three promising candidate markers for the postulated neuronal stem cell niche in the SAG: *rbp4* and *fabp7a/sox2*. Future studies will focus on verifying these markers to identify the neuronal stem cell-like cell population and enable further studies for in-depth characterization of the different cell types involved in neurogenesis in the SAG. Additionally, future work will also focus on the signaling pathways governing neurogenesis and enabling the switch from a highly active neurogenic niche in the juvenile to an almost quiescent neurogenic niche in the adult SAG.

5.2 Regenerative capacity of the adult zebrafish SAG

Lifelong production as well as regeneration of hair cells is known to occur in various vertebrate species, except mammals (reviewed by Rubel, Furrer and Stone, 2013). In zebrafish, studies on hair cell regeneration, in particular on hair cells in neuromasts of the lateral line, have been carried out confirming the regenerative capacity of hair cells after injury. This raises the question of whether neurons, which can undergo secondary degeneration after hair cell loss or be injured directly by various other factors such as noise, ototoxic drugs or infections, are also capable of regeneration. In the adult zebrafish, neurons in the CNS displays robust regeneration after brain injury and light-induced lesion of the retina (Kroehne *et al.*, 2011; Weber *et al.*, 2013; Kaslin *et al.*, 2017). In general, regeneration requires the maintenance of the neurogenic niche into adulthood. In the zebrafish cerebellum, the stem cell niche arises during embryonic development from the rhombic lip and consists of two distinct populations with either radial glia or neuro-epithelial-like identity (Kaslin *et al.*, 2009). However, only the neuro-epithelial-like stem cell pool persists throughout life whereas the radial glia stem cells are terminated during juvenile stages. Consequently, neuronal cell lineages of the epithelial-like stem cell pool are replaced but cell lineages of the cerebellar radial glia do not regenerate (Kaslin *et al.*, 2017). In line with adult neurogenesis from neuronal stem cells in the zebrafish CNS, the experiments in this thesis revealed the presence of a neurogenic

niche that is not terminated but maintained throughout life. Remarkably, the neurogenic niche is highly active in the juvenile SAG but turns to a quiescent state regarding proliferation of neuronal progenitor cells in the adult SAG and produces only few newborn neurons at adulthood. To investigate whether this neurogenic niche is capable to increase its activity regarding proliferation and neurogenesis to cope with a loss of mature sensory neurons upon lesion in the adult SAG was the second aim of this study.

5.2.1 Establishment of a suitable lesion model to study neuronal regeneration in the adult zebrafish SAG

The vertebrate PNS has a remarkable capacity to regenerate axonal projections after nerve injury. Upon injury, peripheral axons form motile-growth-cone structures enabling axonal regrowth to establish neuronal connection with the target cells (as reviewed in He and Jin, 2016). In zebrafish, axonal regeneration also occurs in the adult CNS, for example after spinal cord injury (as reviewed in Ghosh and Hui, 2018; Tsata and Wehner, 2021). In contrast, neurons in the mammalian CNS exhibit axonal degradation and the formation of retraction bulbs inhibits axonal regrowth and re-innervation upon injury (Ertürk *et al.*, 2007). The aim of this thesis was to analyze neuronal regeneration in the inner ear beyond axonal regeneration, investigating the potential of the zebrafish SAG to replace entire mature neurons upon lesion. Therefore, the first goal of this thesis was to establish a suitable lesion paradigm to ablate mature neurons while sparing other cell types of the inner ear and especially cells in the neurogenic niche.

In various mammalian species including rat, mice and gerbil, a well-studied model of auditory neuropathy is based on the application of the neurotoxin Ouabain, a potent inhibitor of the Na^+/K^+-ATPase pump, to the round window (Schmiedt *et al.*, 2002; Lang, Schulte and Schmiedt, 2005; Lang *et al.*, 2011; Fu *et al.*, 2012; Yuan *et al.*, 2014).

The repeated application of Ouabain is highly specific in inducing massive degeneration of type-I spiral ganglion neurons while preserving the number as well as the function of hair cells (Schmiedt *et al.*, 2002; Lang, Schulte and Schmiedt, 2005). Besides the appearance of ectopic neuronal processes forming non-functional, supranuclear contacts with inner hair cells, no visible sign of regeneration in terms of newly formed synapses via branching of surviving neurons, axonal regrowth or replacement of lost spiral ganglion cells occur in mammals (Yuan *et al.*, 2014).

In zebrafish, intravitreal injection of the neurotoxin Ouabain is also a well-established lesion model to study retina regeneration, enabling to ablate various retinal cell types in a dose-dependent manner (Fimbel *et al.*, 2007). Due to the anatomical location of the inner ear within the brain, a non-invasive application of Ouabain was not possible and a suitable side to inject the solution into the inner ear

had to be identified. Experiments using a CellTracker Dye confirmed the lesion protocol as eligible for targeting the SAG with minimal damage to the surrounding tissue. The first step of the protocol was to carefully create an opening the skull with a needle to, in the second step, enable insertion of a Hamilton syringe for injection. To then analyze the regenerative capacity of the adult SAG, lesions were applied unilaterally into the right otic capsule to use the unlesioned left SAG as an internal control. Surprisingly, the regenerative response in the SAG was similar under all tested conditions (sham treatment, NaCl or Ouabain injection), indicating that the chosen procedure for neurotoxin injection by inserting a syringe into the otic capsule harms the SAG even without injecting a fluid. Studies in the mammalian inner ear suggest an intoxication of sensory and neural structures caused by changes in K^+ levels through endolymph leakage (Zenner *et al.*, 1994; Claußen, Schulze and Nothwang, 2020). Additionally, a temporal and reversible mechanical lesion of hair cells through overexposure to intense sound can lead to an acute loss of afferent nerve terminals and cochlear nerve-degeneration in mice (Kujawa and Liberman, 2009). Inserting a Hamilton syringe into the otic capsule is most likely causing a damage to the semicircular canals and/or the thin epithelium surrounding the utricular macula which together form an enclosed cavity, thereby leading to the leakage of endolymph and a potential damage to hair cells and the sensory neurons. A mechanical damage of the hair cells and/or the sensory neurons via increasing the pressure inside the otic capsule, especially when injecting a fluid, might also be a cause of the damage seen in all three experimental conditions.

Mature sensory neurons in the adult SAG die within hours after lesion

As mentioned above, the prerequisite for a lesion paradigm to be suitable for this study was the ablation of mature neurons in the SAG upon lesion. Analysis of the *ubiq*:secAnnexinV-mVenus line at 12 hours post lesion showed a strong mVenus-signal in the peripheral dendrites of sensory neurons in the most lateral SAG close to the entrance hole of the Hamilton syringe. Besides this sign of axonal degeneration in the dendrites of sensory neurons, no mVenus-signal was detected in the cell bodies of sensory neurons which would have indicated cell death of sensory neurons upon lesion.

Furthermore, TUNEL-assay revealed the presence of apoptotic sensory neurons within hours after the lesion procedure with a peak of apoptotic neurons at 12 hours post lesion after sham treatment, NaCl- and Ouabain injections (Figure 5.3A), confirming the suitability of the established lesion paradigm.

Massive leukocyte infiltration persists weeks after lesion

It has been shown in the zebrafish central nervous system that acute inflammation plays an important role for the proper induction of regenerative neurogenesis from neural stem cells (Kyritsis *et al.*, 2012; Tsarouchas *et al.*, 2018; Silva *et al.*, 2020). In the lesion paradigm established for this study, injury caused a massive infiltration of leukocytes in the SAG, which accumulated in the SAG and were still present more than 16 days post lesion, which constituted the end of the analyzed time course (Figure 5.3B). This is in contrast to the temporal dynamics of the immune response seen in the central nervous system, where the number of infiltrated immune cells following injury is decreased within days (Kyritsis *et al.*, 2012).

5.2.2 Reactivation of the neurogenic niche upon lesion results in reactive proliferation and reactive neurogenesis

The main question of the regeneration-related study was to investigate whether death of sensory neurons in the SAG is followed by a regenerative response of the neurogenic niche. Indeed, upon a unilateral applied traumatic lesion using (I) sham treatment, (II) NaCl or (III) Ouabain injections into the otic capsule, the neurogenic niche is reactivated to compensate the loss of sensory neurons. Reactive proliferation of marker-negative cells and also neuronal progenitor cells occurred as early as 2 days post lesion and approx. 4 days post lesion, respectively, and continued over the next weeks (Figure 5.3A). Similarly, newborn neurons are produced by reactive neurogenesis from neuronal progenitor cells, which exceeded the homeostatic baseline neurogenesis at 4 days post lesion. BrdU pulse chase experiments revealed, that newborn neurons differentiated within two weeks from proliferating stem/progenitor cells. Surprisingly, also the unlesioned SAG, which was serving as an internal control, showed reactive proliferation including proliferation of Neurod-positive progenitor cells as well as reactive neurogenesis exceeding the homeostatic baseline upon lesion under all three conditions. Hence, this indicates that the unilateral damage of the SAG induces a systemic response activating also the neurogenic niche of the non-lesioned SAG.

Similar to the zebrafish CNS, the adult SAG exhibits a regenerative response consisting of reactive proliferation and reactive neurogenesis. Upon lesion of the zebrafish retina, quiescent Müller glia re-enter the cell cycle resulting in the production of multipotent progenitors that differentiate into all retinal cell types replacing the lost cells (Lenkowski and Raymond, 2014). Similarly, radial glia serve as neuronal stem cells in the zebrafish forebrain and show increased production of neuronal progenitors following injury which then can differentiate into neurons (Kroehne *et al.*, 2011). In contrast to these examples where reactive proliferation and reactive neurogenesis rather occur sequentially, reactive proliferation and reactive

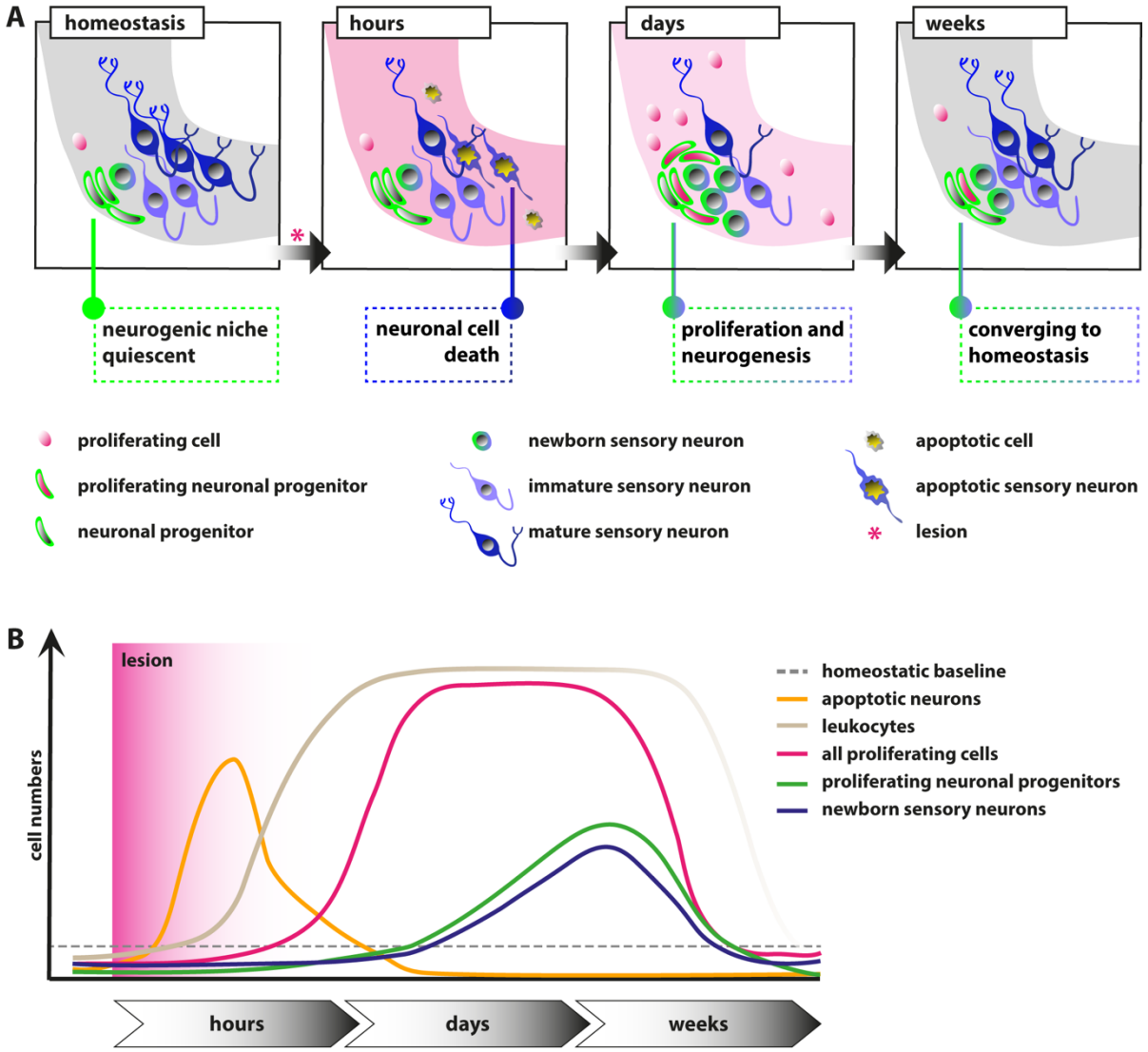

Figure 5.3 Temporal dynamics of the regenerative response in the adult zebrafish SAG upon lesion.

(A) Scheme depicting the cellular events within the neurogenic niche. During homeostasis, the neurogenic niche of the adult zebrafish SAG is quiescent in regard to proliferation and shows only very rare neurogenesis. Upon lesion, mature sensory neurons as well as other marker-negative cells undergo apoptosis within several hours. Within days, reactive proliferation of marker-negative and neuronal progenitor cells is observed accompanied by reactive neurogenesis from the neuronal progenitor pool. Reactive proliferation and reactive neurogenesis continue over the next weeks until previous homeostatic levels are reached. (**B**) Scheme of the temporal order of events. During homeostasis in the adult SAG, proliferating marker-negative cells, leucocytes and neurogenesis are present at basal levels, whereas proliferating neuronal progenitors and apoptotic cells are absent. Upon lesion, a strong increase in the number of apoptotic cells and in particular apoptotic sensory neurons is observed which is also resolved rapidly. Also within hours, a massive accumulation of leukocytes occurs which persists for several weeks. Within days, the number of proliferating cells increases significantly within the neurogenic niche of the SAG and remains high for a couple of weeks until it returns to lower levels. Following the general gain in proliferation, the number of proliferating neuronal progenitors is also significantly increased for approx. 2-3 weeks until it returns to baseline levels. With the same temporal dynamics, production of newborn neurons increases and remains high for approx. 2-3 weeks until it returns to homeostatic levels.

neurogenesis showed similar temporal dynamics in the regenerative response of the adult SAG: both peaked at around 8 days post lesion before returning to (almost) homeostatic condition weeks after the lesion (Figure 5.3B).

This finding suggests that the initial reactive neurogenesis is not dependent on previous reactive proliferation of stem/progenitor cells but rather driven by the existing Neurod-positive progenitor pool, which is subsequently replenished by reactive proliferation of Neurod-positive progenitor cells as well as potentially by the presumptive marker-negative stem cells.

Surprisingly, there were no fundamental differences regarding the amount of apoptotic sensory neurons, the infiltration of the SAG with leukocytes, reactive proliferation or reactive neurogenesis in the three lesion types with two exceptions: (I) an increased level of proliferation in ouabain-injected SAGs in comparison with sham-treated SAGs at 4 days post lesion and (II) a significant lower amount of proliferating Neurod-positive progenitor cells in NaCl-injected SAGs compared to sham-treated and Ouabain-injected SAGs at 8 days post lesion. Hence, the presented lesion paradigm does not rely on the injection of Ouabain, but rather on a mechanically induced damage. A possible explanation for this is that either the chosen Ouabain concentration was too low to ablate high numbers of sensory neurons in the adult SAG or that sensory neurons are not or less susceptible to Ouabain-induced damage. From regeneration studies in the zebrafish retina it is known, that the neurotoxin Ouabain ablates retinal neurons in a dose-dependent manner: in lower concentrations, intravitreal Ouabain injections rapidly damage the ganglion cell layer and inner nuclear layer whereas higher concentrations additionally also ablate photoreceptors, indicating a different sensitivity of different neurons to exposure of Ouabain (Fimbel *et al.*, 2007). Additionally, studies using Ouabain as an auditory neuropathy model in gerbils revealed that Ouabain exclusively induces apoptotic cell death in type I spiral ganglion neurons and not in type II spiral ganglion neurons (Lang, Schulte and Schmiedt, 2005). Therefore, it might be useful for future experiments to either increase the Ouabain concentration or to test other neurotoxins for their potential to specifically ablate mature sensory neurons in the adult SAG and induce a stronger and more specific lesion response.

5.2.3 Future goal: investigating underlying mediators of regenerative response

Although the study presented here shows that this lesion paradigm elicits a strong regeneration response within the adult zebrafish SAG, the underlying mechanism remains unclear. The neuronal loss upon lesion might represent a direct and local effect on the cell cycle status of presumptive stem cells and Neurod-positive progenitors. In this respect, it has been reported that dying retinal neurons produce Tumor necrosis factor α, a secreted cytokine that is necessary and sufficient for

retinal stem cells to initiate cell cycle re-entry during zebrafish retina regeneration (Nelson *et al.*, 2013). Similarly, expression of many other mitogens from local sources has been described to induce proliferation of former quiescent stem cells during regeneration (Fuchs and Steller, 2016). Trauma to the sensory patches after insertion of the Hamilton syringe into the otic capsule, which generates an opening in the usually enclosed inner ear, might provide an additional local cue in the lesion paradigm because strong re-formation of sensory hair cells accompanied neuronal regeneration.

However, in addition to local cues, systemic cues must play an important role because of the observed reactive proliferation and reactive neurogenesis in the unlesioned side following a unilateral lesion, especially following Ouabain injections. In this aspect, various systemic effects, including steroids such as estrogen or thyroid hormone, as well as peptide hormones, such as insulin or leptin, have been shown to act as mediators of complex tissue regeneration (Losner, Courtemanche and Whited, 2021). With respect to leptin function, epigenetic profiling provided even evidence for regeneration-dependent enhancer elements in the regeneration-competent zebrafish that are also able to control expression in transgenic mice in a lesion-dependent context (Kang *et al.*, 2016).

Another systemic response, that elicits its effect locally, constitutes the immune system. In particular, the cellular and molecular events during spinal cord regeneration have been dissected in great detail (Tsata and Wehner, 2021). Upon injury, peripheral neutrophils invade the lesion side immediately followed by macrophages, which play a pivotal role in the subsequent functional regeneration, by producing Tumor necrosis factor α and controlling Interleukin-1 ß-mediated inflammation (Tsarouchas *et al.*, 2018). Similarly, T-cells rapidly infiltrate the damaged spinal cord and stimulate regenerative precursor cell proliferation by producing pro-regenerative factors (Hui *et al.*, 2017). It will be interesting to see if the very same or different mechanisms promote neuronal regeneration in the regenerating adult zebrafish SAG, since the accumulation of immune cells in the SAG persists beyond weeks, while immune cells in the CNS are cleared within days after lesion.

5.2.4 Generation of more precise lesion paradigms for future studies

The novel lesion paradigm presented in this study is the first to show that the neurogenic niche within the adult zebrafish SAG displays a strong regeneration response upon injury, which provides a first entry point to address the underlying cellular and molecular events. The lesion procedure allowed to ablate mature sensory neurons without (in most cases) damaging the structure of the SAG itself. However, as mentioned above the applied injection strategy most likely mechanically damages the semicircular canal and/or the utricle directly or via an

increased pressure during fluid injection and can also lead to a massive hemorrhage in the otic capsule, all adding to a multifactorial-induced trauma of the SAG and the sensory tissue. Therefore, the establishment of alternative lesion paradigms would be beneficial to understand regeneration of the SAG in-depth. For instance, in addition to mechanical lesions and the application of neurotoxins, several other injury models are available to address regeneration of the adult retina, including intense light to ablate photoreceptor or pharmacogenetic approaches (Fimbel *et al.*, 2007; Montgomery, Parsons and Hyde, 2010; Weber *et al.*, 2013). In particular, the latter provides a conditional and unique platform for the precise and targeted ablation of cells in a tissue- or cell type-specific manner. Commonly, the nitroreductase/metronidazole system is used in which the bacterial nitroreductase is expressed by a tissue- or cell type-specific transgene to convert the prodrug metronidazole into a cytotoxic DNA cross-linking agent thus inducing apoptosis of the nitroreductase-expressing cell (Curado *et al.*, 2007). Similarly, when using the human diphtheria toxin receptor/diphtheria toxin system, cells specifically expressing the human diphtheria toxin receptor undergo apoptosis after application of diphtheria toxin to the organism (Jimenez *et al.*, 2021). Both pharmacogenetic approaches offer the unique possibility to generate a sterile lesion without harming the surrounding tissue by the lesion procedure. However, to allow for a tissue- and/or cell-type specific ablation using these systems, the knowledge of tissue- and cell-type specific markers is a prerequisite. In case of the SAG, further research would be necessary to find a suitable transgene allowing the expression of Nitroreductase or the human diphtheria toxin receptor exclusively in the neurons of the SAG. Nevertheless, the transgenic hair cell ablation line generated by Jimenez et al., based on the expression of the human diphtheria toxin receptor specifically in hair cells, might still serve as a valuable tool to study the regenerative capacity of the SAG (Jimenez *et al.*, 2021). Therefore, multiple rounds of diphtheria toxin applications could be applied to ablate hair cells permanently or at least for a longer period of time to investigate whether the loss of hair cells induces a secondary loss of sensory neurons followed by a regenerative response of the SAG.

In humans, sensorineural hearing loss is also induced via ototoxic drugs such as aminoglycoside antibiotics, like kanamycin and gentamycin, platinum-containing chemotherapeutics such as cisplatin, but also common pain relief medication such as ibuprofen and aspirin (Sugawara, Corfas and Liberman, 2005; Rybak *et al.*, 2007; Kyle, Wang and Shin, 2015). These drugs either have a direct neurotoxic effect on sensory neurons or induce damage to the hair cells and/or supporting cells subsequently inducing the secondary loss of sensory neurons (Zilberstein, Liberman and Corfas, 2012). The latter can be caused by for example a lack of sensory input, neurotrophic support or neurotoxicity caused by high concentration of glutamate released by dying hair cells (Spoendlin, 1984; Matsuda *et al.*, 1999). Therefore, the systemic application of these ototoxic drug would also be an interesting lesion paradigm to consider, since it would not only enable to investigate the regenerative

response of the zebrafish SAG as such, but also offers the possibility to study the pathology of ototoxic drug-induced hearing loss and to search for a potential strategy to protect the inner ear.

6. Conclusion & Outlook

This thesis provides the first in-depth characterization of the juvenile and adult zebrafish SAG, discovering the presence of neurogenesis beyond larval stages. Neurogenesis occurs from a lifelong maintained neurogenic niche that is highly active in the juvenile SAG but turns quiescent so that it only comprises of non-proliferating neuronal progenitor cells rarely differentiating into new neurons at adulthood. Additionally, the lesion paradigm established here reveals the regenerative capacity of the adult zebrafish SAG. Upon traumatic injury and subsequent loss of mature neurons, reactive proliferation as well as reactive neurogenesis occurs in the neurogenic niche to replace lost neurons. Understanding neurogenesis in the adult zebrafish SAG during homeostasis and regeneration is of particular importance because it can provide significant insights into the cellular properties of stem and progenitor cells in the vertebrate inner ear. This knowledge will help to develop cell-based therapies using transplantation approaches and identify mechanisms to induce reprogramming of endogenous cells to rekindle the regenerative potential in the mammalian inner ear.

Besides studies showing the potential of embryonic stem cells or induced pluripotent stem cells to act as a source for new sensory neurons upon transplantation (Coleman *et al.*, 2006; Nishimura *et al.*, 2009), approaches targeting resident cells within the auditory system *in vivo* for direct reprogramming to produce new neurons are considered a promising way to cure hearing loss (Meas, C. L. Zhang and Dabdoub, 2018). Noda et al. have shown that glia cells of the VIIIth cranial ganglion that have been reprogrammed *in vitro* into neuron-like cells display a transcriptome profile resembling that of endogenous inner ear neurons (Noda *et al.*, 2018). Although the results indicate that reprogramming of glia represents a viable strategy, a valid alternative might be to target residential progenitor-like cells to re-initiate proliferation and differentiation. As this thesis has shown, Nestin is expressed in a subpopulation of progenitor cells within the neurogenic niche that actively proliferates and gives rise to new neurons in the juvenile SAG. During adulthood however, these Nestin-positive progenitor cells turn into a quiescent state in regard to proliferation and only rarely give rise to new neurons in the adult zebrafish SAG. Interestingly, the analysis of *nestin*:GFP transgenic mice revealed a reduced but persisting population of *nestin*-expressing cells in the VIIIth cranial ganglion, indicating the presence of progenitor-like cells also in the mammalian auditory system (Chow *et al.*, 2016). Furthermore, additional studies have revealed, that the postnatal mammalian inner ear still contains stem and progenitor cells. These were able to proliferate and dependent on their origin differentiate into hair cells or sensory neurons *in vitro* which might be a suitable target to induce neurogenesis in the adult mammalian inner ear (Li, Liu and Heller, 2003; Oshima *et al.*, 2007; Diensthuber *et al.*, 2014). However, even if reprogramming of inner ear glia or the reactivation of progenitor-like cells successfully gives rise to new neurons,

the necessary cellular properties to ensure their functional integration remains unclear. To unravel the cellular and molecular properties of sensory and neuronal progenitor cells, the comparison of species such as zebrafish, which exhibit a lifelong production of hair cells and sensory neurons and possess the ability to replace these cells upon loss, with regeneration-incompetent organisms can offer new insights into the underlying mechanisms of adult neurogenesis and regeneration in the inner ear.

It will now be crucial to identify the nature of the presumptive stem cell-like cells and their progenitors as well as the underlying genes and pathways that are active during homeostasis and regeneration. To this end, single-cell RNA sequencing (scRNAseq) will represent the method of choice. The advent of high-throughput, cost-effective droplet-based scRNAseq allows the assembly of transcriptomic atlases of whole organs including the inner ear (Wu *et al.*, 2021; Yamamoto *et al.*, 2021). As this thesis showed, scRNAseq is also applicable to the juvenile and adult SAG. Importantly, in addition to scRNAseq data from homeostatic tissues, the transcriptional changes following trauma will be of high importance as recently pioneered by Milon and others (Milon *et al.*, 2021). The comprehensive information gained from these datasets enables to unravel the cellular composition of the entire tissue and the transcriptomic state of all cell populations within. Moreover, computational algorithms are available that infer a pseudo-temporal ordering of cells based on comparative transcriptomic profiling, allowing to derive differentiation trajectories from stem cell or progenitor populations toward differentiated somatic cells in a given tissue or organism (Plass *et al.*, 2018). Once established, interspecies comparisons of scRNAseq datasets from regeneration-competent as well as regeneration-incompetent organisms will identify specific modules of regeneration as well as potential mammalian-specific roadblocks. The employment of recently established conditional gene-targeting approaches, including traditional loxP-flanked alleles or more recent CRISPR/Cas9-based strategies (Hoshijima, Jurynec and Grunwald, 2016; Burg *et al.*, 2018; Wu and Wang, 2020; Hans *et al.*, 2021), will enable the rapid genetic analysis of identified pathways to develop new therapeutical strategies and ultimately cure sensorineural hearing loss in the future.

Supplements

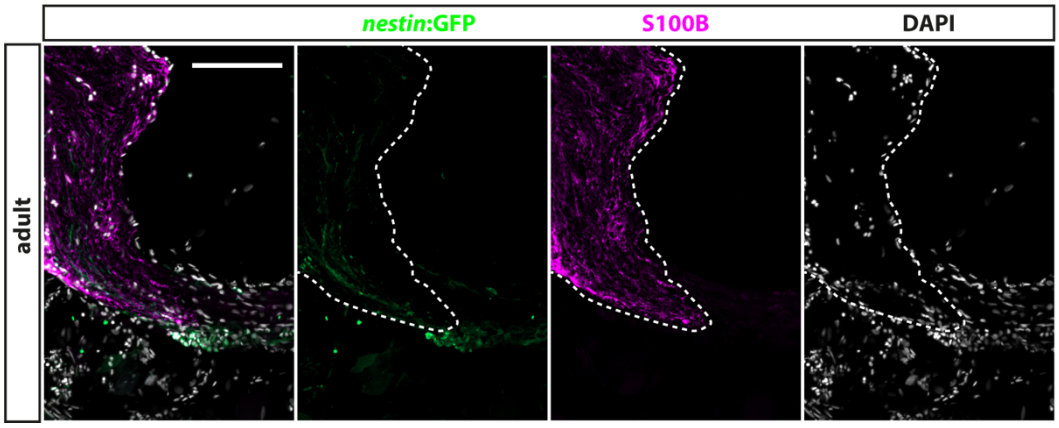

Figure S.1 Expression of glia marker S100B shows similar expression pattern to GFAP.
Antibody staining against the glia marker S100B in adult *nestin*:GFP fish revealed expression of S100B in the medial part of the SAG similar to the GFAP expression pattern (dashed line; see also Figure 4.15); S100B expression was found close-by but not overlapping with the neurogenic niche, here marked by *nestin*:GFP. Scale bar: 50 µm; cross sections showing dorsal to the top and lateral to the right.

Figure S.2 Heatmap showing the expression of selected marker genes in all cell clusters from the transcriptome data set obtained from the juvenile SAG.
Plotted genes contain a mix of genes selected from the list of the top 25 differentially expressed genes as well as known cell type specific marker genes.

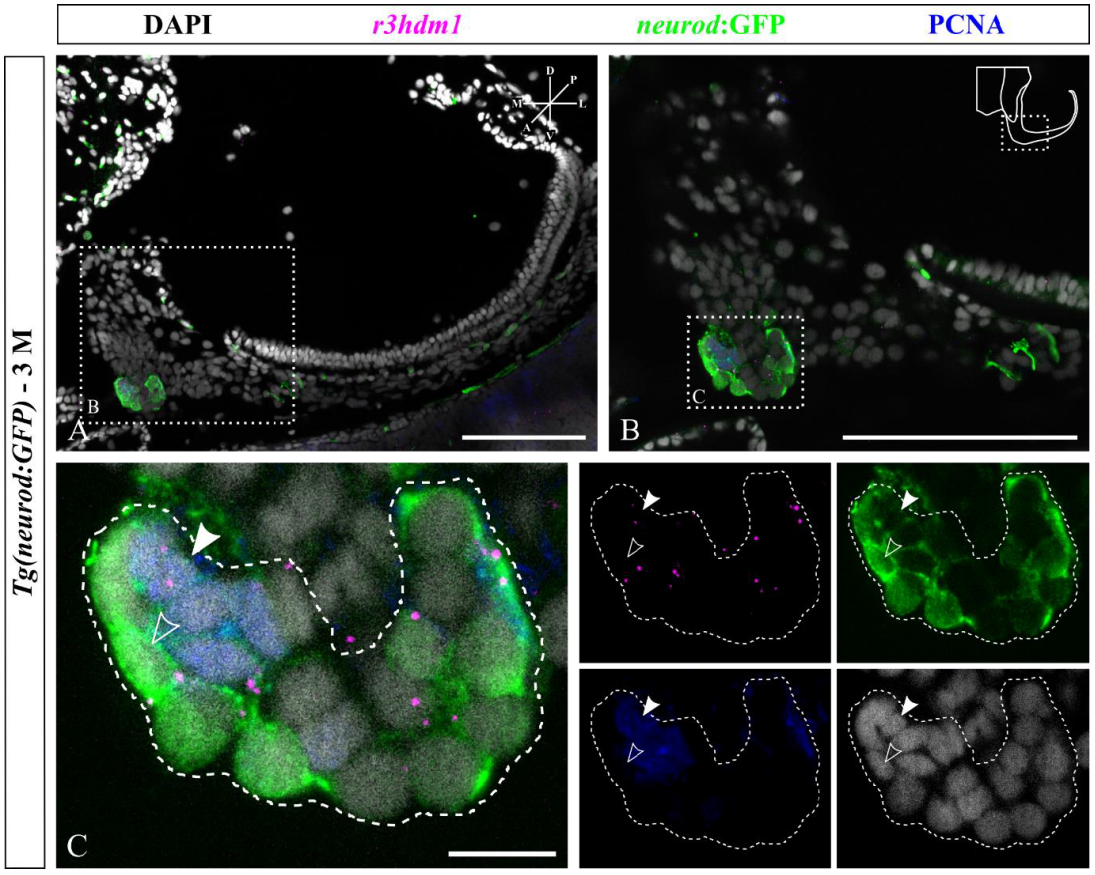

Figure S.3 *r3hdm1* expression can be observed in proliferating and non-proliferating cells of the neurogenic niche in the juvenile SAG.
Combined FISH and antibody staining for *r3hdm1*, GFP and proliferation marker PCNA in the SAG of juvenile *neurod*:GFP fish (3 months). Within the neurogenic niche (encircled by dashed line), expression of *r3hdm1* was colocalizing with *neurod*:GFP in proliferating cells (arrowhead) as well as non-proliferating cells (open arrowhead). Scale bar: 100 µm (**A**,**B**), 10 µm (**C**); cross sections showing dorsal to the top and lateral to the right. Experiment performed by Daniel Scherer.

(from: Daniel Scherer, Bachelor thesis, 2021)

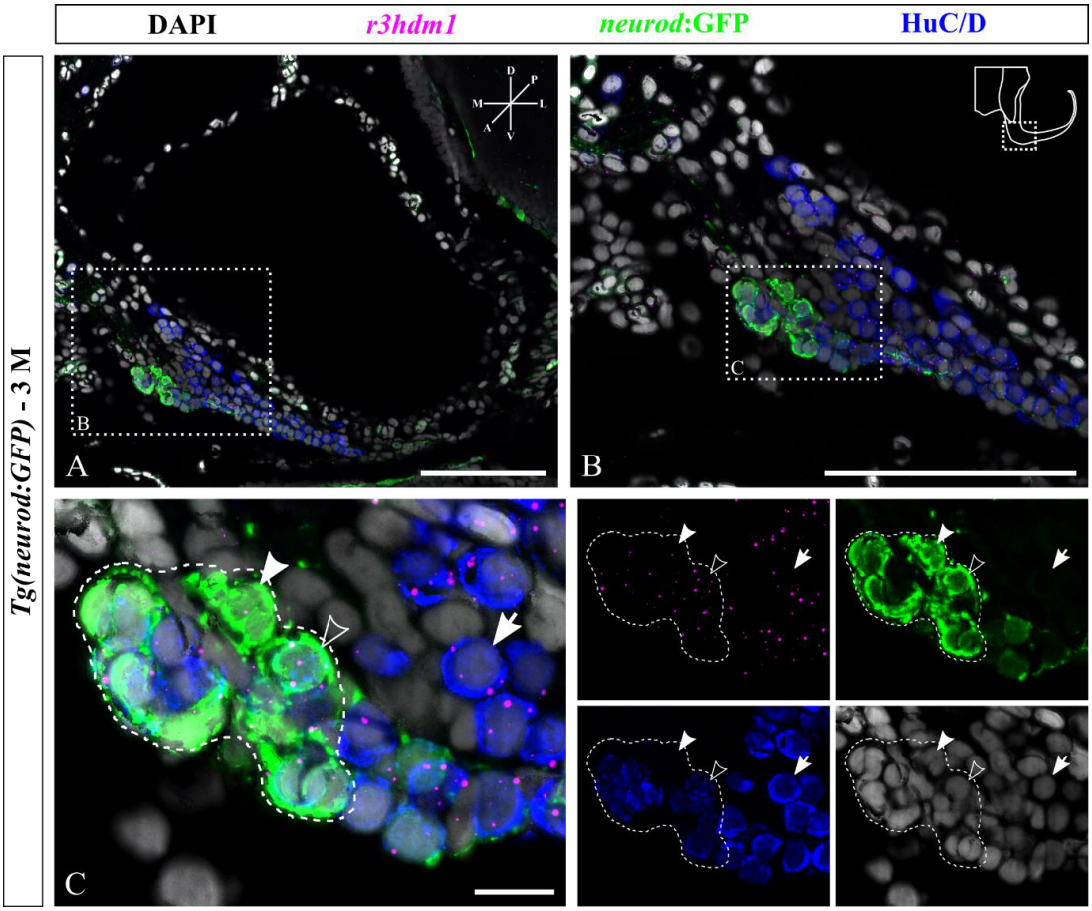

Figure S.4 *r3hdm1* is expressed in cells of the neurogenic niche as well as in mature neurons in the juvenile SAG.
Combined FISH and antibody staining for *r3hdm1*, GFP and neuronal marker HuC/D in the SAG of juvenile *neurod*:GFP fish (3 months). Within the neurogenic niche (encircled by dashed line), expression of *r3hdm1* was found in *neurod*:GFP-only positive neuronal progenitor cells (arrowhead), HuC/D-positive neurons (arrow) and *neurod*:GFP/HuC/D-double positive cells (open arrowhead), hence labeling cells in the neurogenic niche as well as mature neurons. Scale bar: 100 µm (**A**,**B**), 10 µm (**C**); cross sections showing dorsal to the top and lateral to the right. Experiment done by Daniel Scherer.
(from: Daniel Scherer, Bachelor thesis, 2021)

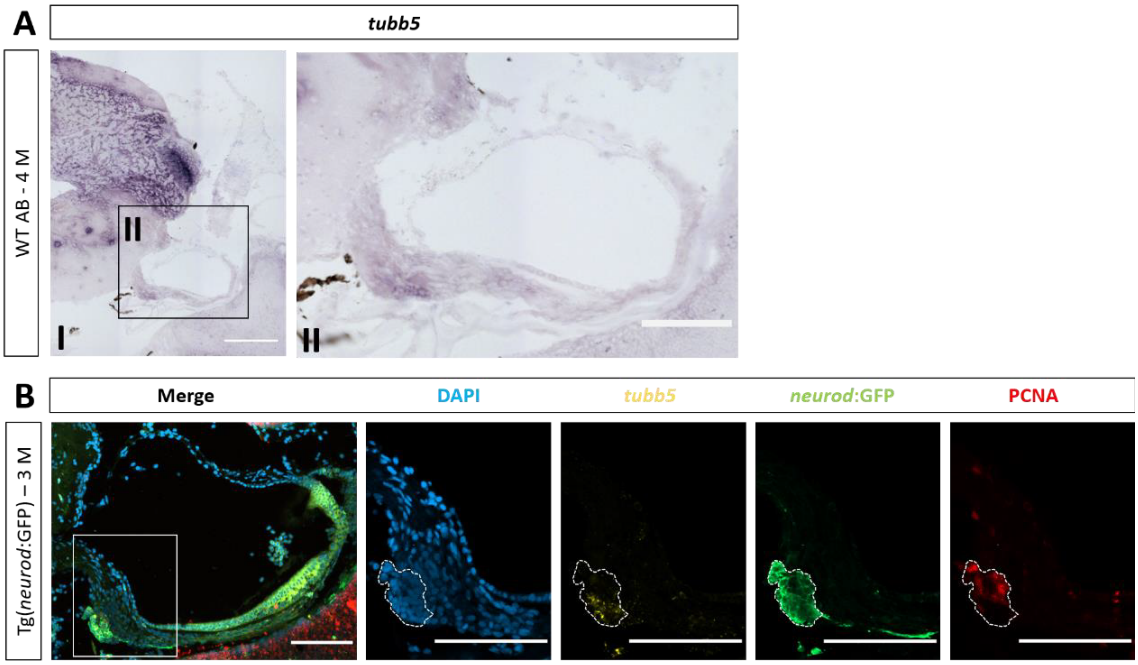

Figure S.5 Expression of *tubb5* is confined to the *neurod*:GFP-positive neurogenic niche.
(**A**) Chromogenic ISH for *tubb5* in WT AB zebrafish (4 months) shows *tubb5* expression in the area of the neurogenic niche. (**B**) Combined FISH and antibody staining for GFP and PCNA in the SAG of juvenile transgenic *neurod*:GFP fish (3 months) reveals expression of *tubb5* in non-proliferating, *neurod*:GFP-positive progenitor cells (encircled by dotted line). Scale bar: 200 µm (**A**,**I**), 100 µm (**A**,**II**;**B**); cross sections showing dorsal to the top and lateral to the right. Experiments done by Nora Bölicke.

(from: Nora Bölicke, lab rotation report, 2021)

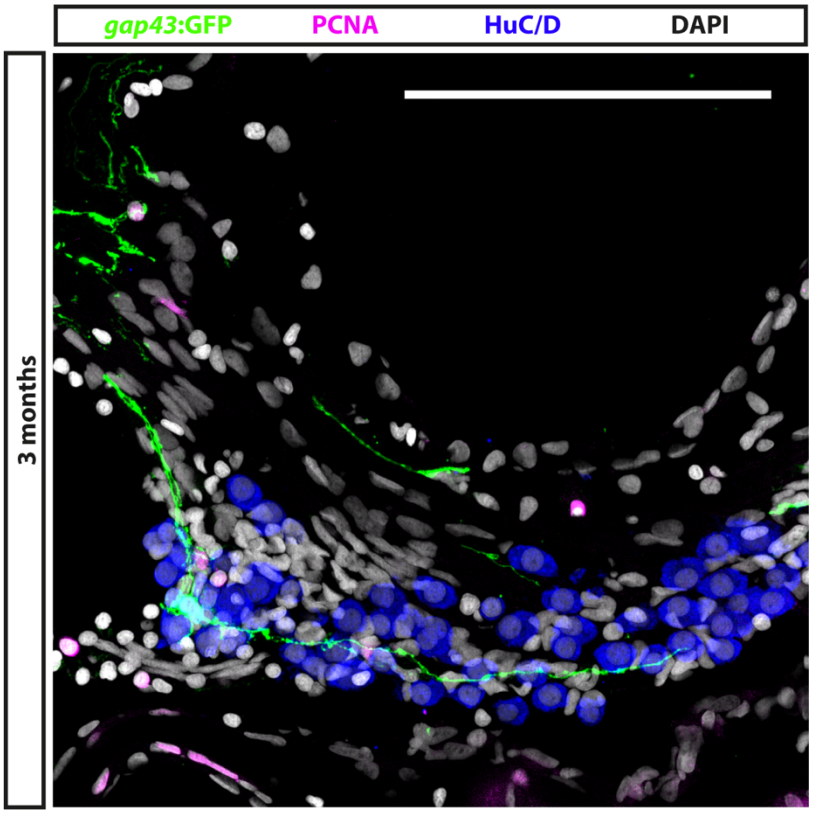

Figure S.6 *gap43*:GFP labels axonal projections of newborn neuron.
Antibody staining for GFP, PCNA and HuC/D in the juvenile SAG of transgenic *gap43*:GFP fish. *gap43*:GFP is expressed in newborn neurons labeling the neuronal cell body as well as the axons. Scale bar: 100 µm; cross sections showing dorsal to the top and laterak to the right.

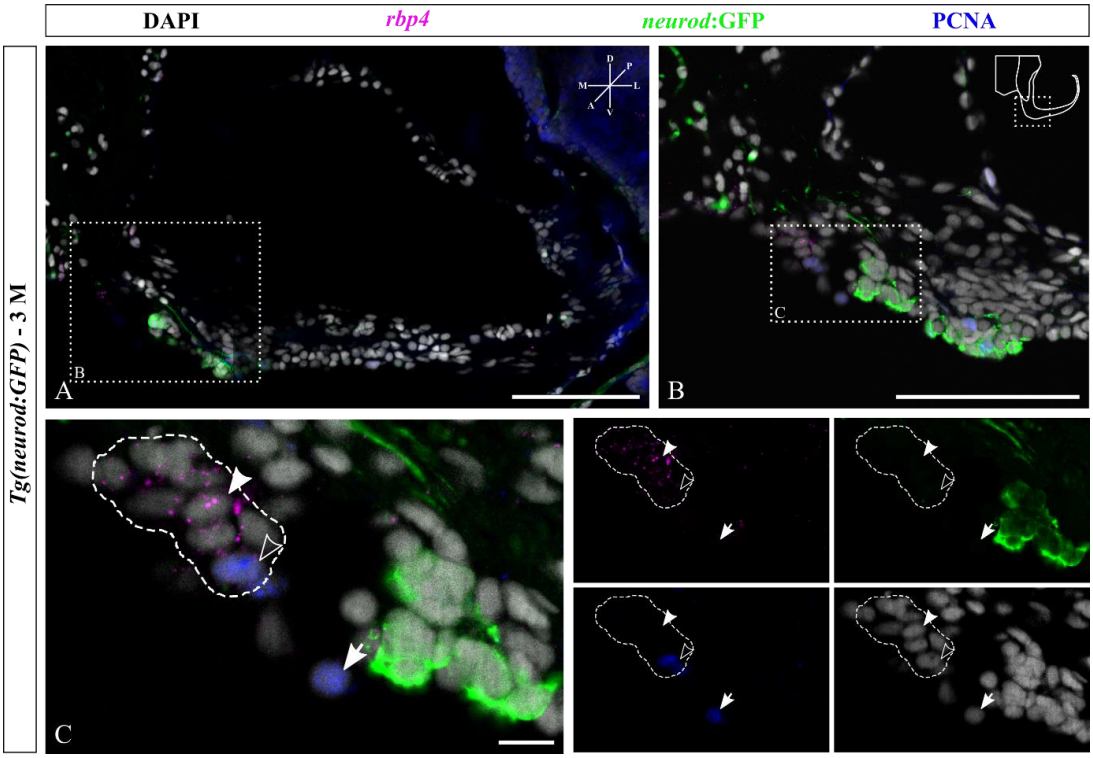

Figure S.7 Expression of rbp4 in a small cell population medial to the neurogenic niche.

Combined FISH and antibody staining for *rbp4*, GFP and PCNA in juvenile *neurod*:GFP fish (3 months). A small population of *rbp4*-expressing cells (encircled by dashed line) were found medial to the *neurod*:GFP-positive neurogenic niche. The majority of *rbp4*-expressing cells were not co-labeled with PCNA (arrowhead) hence not proliferating, but a minority of *rbp4*-expressing cells were also found to be PCNA-positive (open arrowhead). Additionally, proliferating cells not expressing *rbp4* were also present in close proximity to the neurogenic niche (arrow). Scale bar: 100 µm (**A**,**B**), 10 µm (**C**); cross sections showing dorsal to the top and lateral to the right. Experiment done by Daniel Scherer.

(from: Daniel Scherer, Bachelor thesis, 2021)

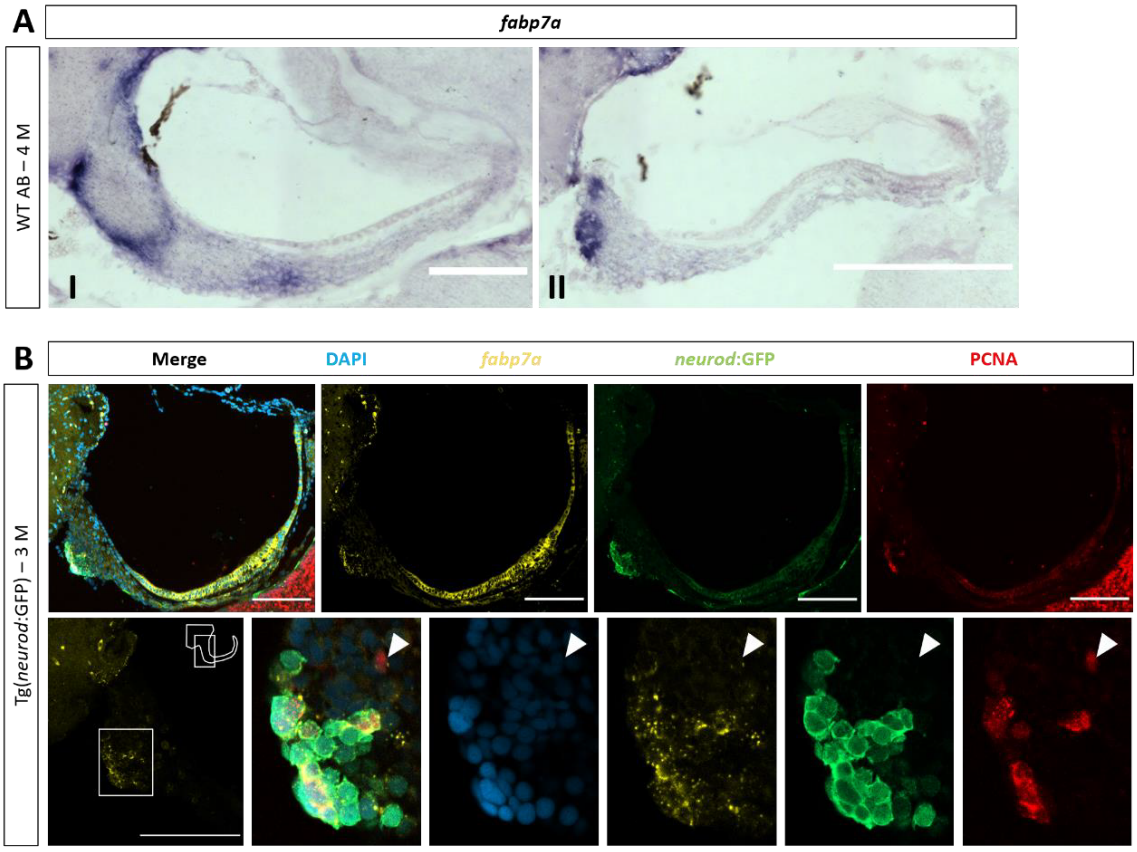

Figure S.8 fabp7a is expressed in the PCTZ and throughout the neurogenic niche in the juvenile SAG.
(**A**) Chromogenic ISH for *fabp7a* in WT AB zebrafish (4 months) shows expression of fabp7a in the PCTZ and the area of the neurogenic niche in the ventromedial part of the SAG. (**B**) Combined FISH and antibody staining for *fabp7a*, GFP and PCNA in juvenile, transgenic neurod:GFP fish (3 months). *fabp7a* is broadly expressed in *neurod*:GFP-positive progenitor cells and in newborn neurons close by (identifiable by their round nuclei). Additionally, proliferating, PCNA/*fabp7a* double positive cells (arrowhead) are found dorsally near the neurod:GFP-positive neuronal progenitor cells. Scale bar: 100 µm (**A**,**I**/**B**), 200 µm (**A**,**II**); cross sections showing dorsal to the top and lateral to the right. Experiments done by Nora Bölicke.

(modified from: Nora Bölicke, lab rotation report, 2021)

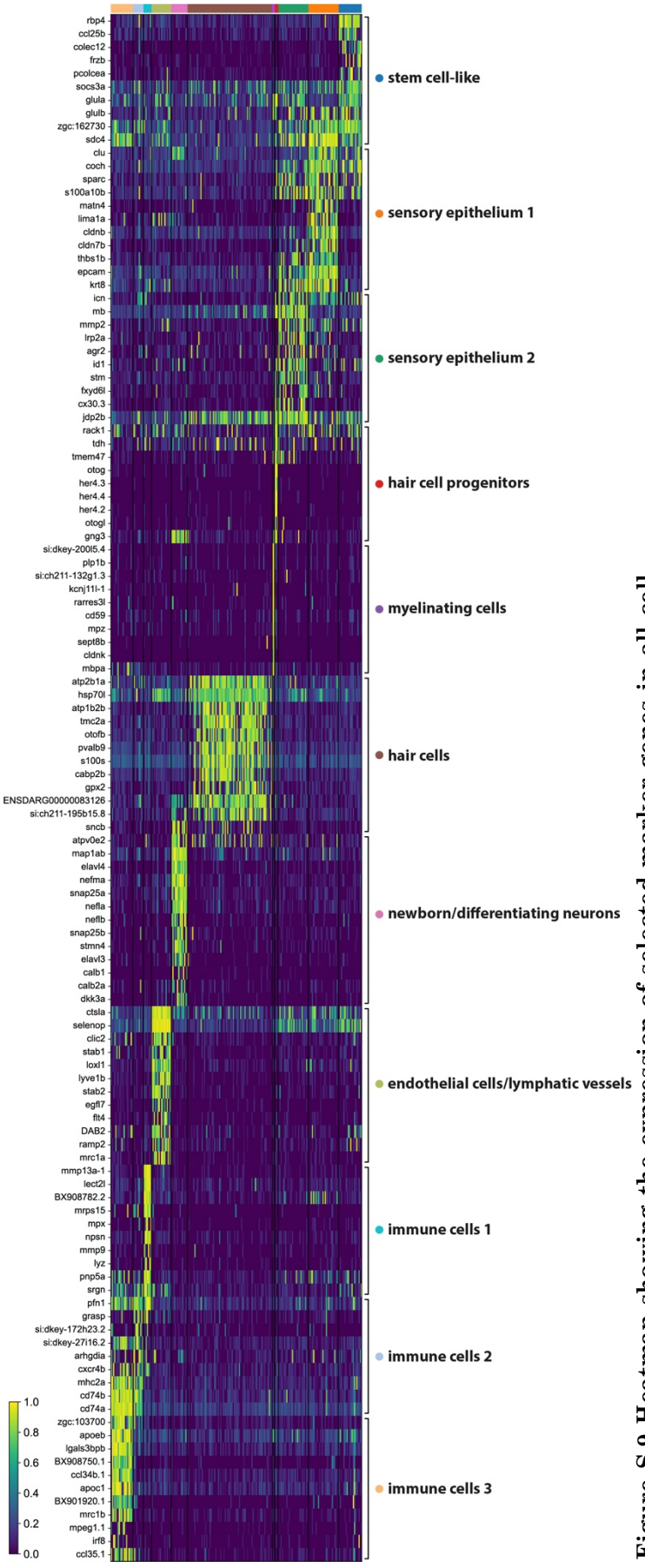

Figure S.9 Heatmap showing the expression of selected marker genes in all cell clusters from the transcriptome data set obtained from the adult SAG. Plotted genes contain a mix of genes selected from the list of the top 25 differentially expressed genes as well as known cell type specific marker genes.

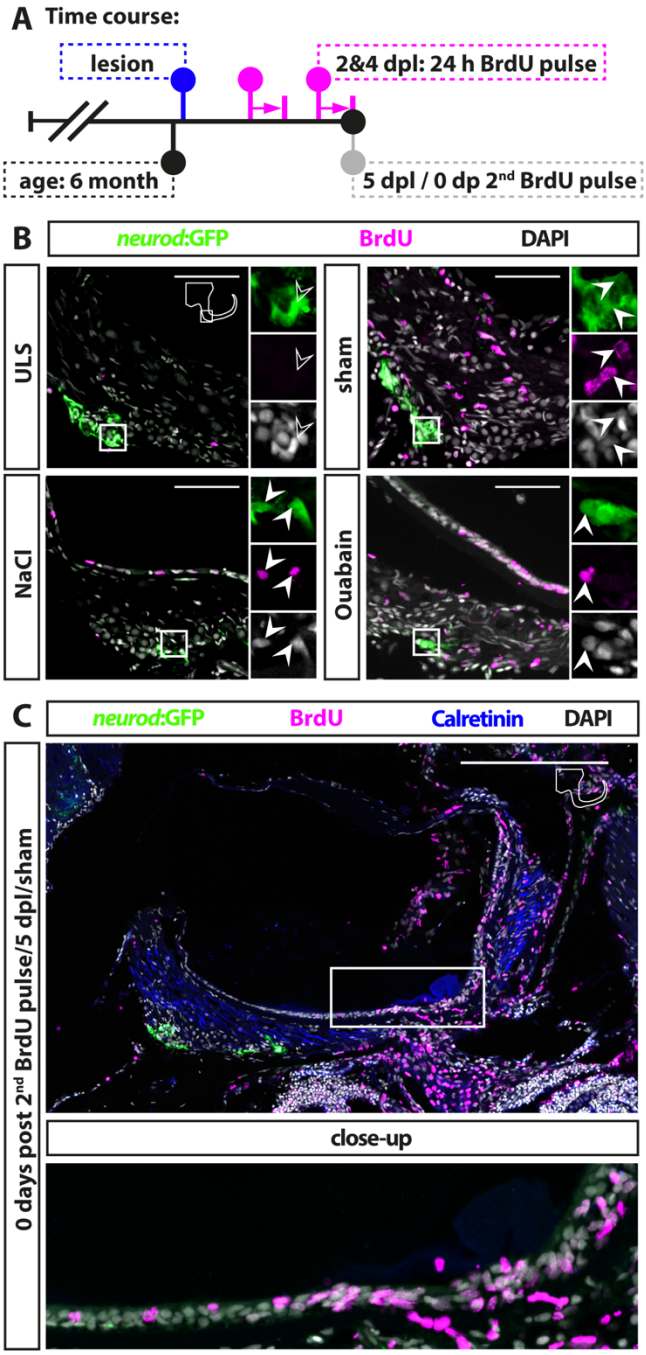

Figure S.10 Reactive proliferation in the neurogenic niche and the utricular macula.

(**A**) Time course for BrdU pulse chase experiment. 6 months old *Tg(neurod:GFP)* zebrafish were lesioned, followed by two 24 hour long BrdU treatments at 2 and 4 days post lesion (dpl). Animals were sacrificed at immediately after the second BrdU treatment (0 days post 2nd BrdU pulse (dpp)). (**B**) Antibody staining against the BrdU and *neurod*:GFP in the SAG of sham-treated, NaCl- and Ouabain-injected *neurod*:GFP animals 5 dpl/0 dpp. In the SAG of the unlesioned side, BrdU-positive cells were found in in the SAG outside of the *neurod*:GFP-positive cell population. In contrast, n*eurod*:GFP/BrdU-double positive progenitors (arrow) were present in the SAG of sham-treated, NaCl-and Ouabain-injected animals. (**C**) Antibody staining against the BrdU, *neurod*:GFP and the neuronal marker Calretinin in the lesioned SAG 5 dpl/0 dpp. Representative image depicts massive reactive proliferation in lateral area of the utricular macula upon lesion. Scale bars: (**B**) 50 µm, (**C**) 200 µm, cross sections showing dorsal to the top and lateral to the right.

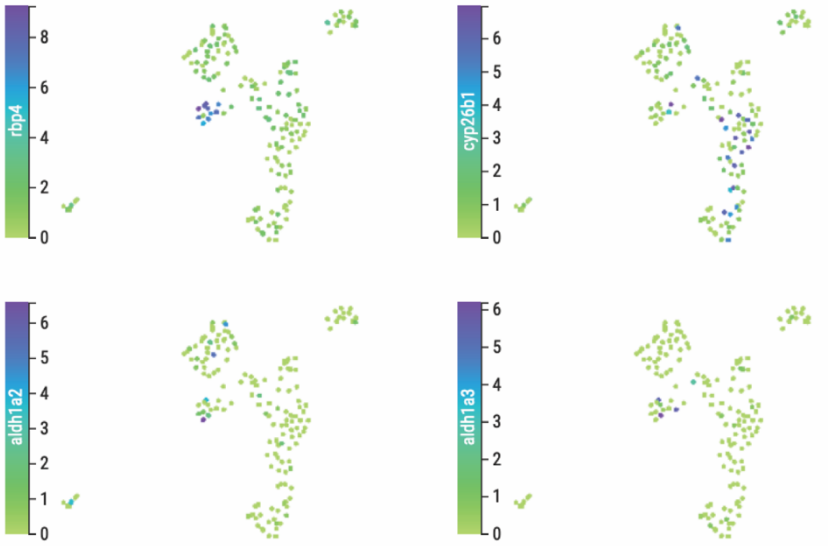

Figure S.11 Expression of *rbp4*, *cyp26b1*, *aldh1a2* and *aldh1a3* in the transcriptome obtained from cells in the juvenile SAG.
The stem cell-like cluster 1 is characterized by the expression of the *retinol binding protein 4* (*rbp4*), which forms a complex with retinol and enables it transportation to and uptake by target cells. Retinoic acid is synthesized from retinol by the enzymes Aldh1a2 and Aldh1a3 (expressed in a few cells in the cluster of rbp4 expressing stem cell-like 1) and its degradation is catalyzed by Cyp26 (expressed in the cluster of newborn neurons).

References

Abbas, L. and Rivolta, M. N. (2015) 'Aminoglycoside ototoxicity and hair cell ablation in the adult gerbil: A simple model to study hair cell loss and regeneration', *Hearing Research*, 325, pp. 12–26. doi: 10.1016/j.heares.2015.03.002.

Ackerman, S. D. and Monk, K. R. (2016) 'The scales and tales of myelination: using zebrafish and mouse to study myelinating glia', *Brain Research*, 1641, pp. 79–91. doi: 10.1016/j.brainres.2015.10.011.

Alapatt, P. *et al.* (2013) 'Liver Retinol Transporter and Receptor for Serum Retinol-binding Protein (RBP4) *', 288(2), pp. 1250–1265. doi: 10.1074/jbc.M112.369132.

Alonso, M. I. *et al.* (2011) 'Cerebrospinal Fluid Control of Neurogenesis Induced by Retinoic Acid During Early Brain Development'. doi: 10.1002/dvdy.22657.

Alonso, M. I. *et al.* (2014) 'Developmental Biology Retinoic Acid , under Cerebrospinal Fluid Control ', pp. 72–83. doi: 10.3390/jdb2020072.

Andermann, P., Ungos, J. and Raible, D. W. (2002) 'Neurogenin1 Defines Zebrafish Cranial Sensory Ganglia Precursors', *Developmental Biology*, 251(1), pp. 45–58. doi: 10.1006/dbio.2002.0820.

Arnold, K. *et al.* (2011) 'Article Sox2 + Adult Stem and Progenitor Cells Are Important for Tissue Regeneration and Survival of Mice', *Stem Cell*, 9(4), pp. 317–329. doi: 10.1016/j.stem.2011.09.001.

Ashmore, J. (2008) 'Cochlear outer hair cell motility', *Physiological Reviews*, 88(1), pp. 173–210. doi: 10.1152/physrev.00044.2006.

Ashmore, J. *et al.* (2010) 'The remarkable cochlear amplifier', *Hearing Research*, 266(1–2), pp. 1–17. doi: 10.1016/j.heares.2010.05.001.

Bang, P. I., Sewell, W. F. and Malicki, J. J. (2001) 'Morphology and cell type heterogeneities of the inner ear epithelia in adult and juvenile zebrafish (Danio rerio)', *Journal of Comparative Neurology*, 438(2), pp. 173–190. doi: 10.1002/cne.1308.

Baraban, M. *et al.* (2013) 'Zebrafish embryonic neurons transport messenger RNA to axons and growth cones In Vivo', *Journal of Neuroscience*, 33(40), pp. 15726–15734. doi: 10.1523/JNEUROSCI.1510-13.2013.

Barald, K. F. and Kelley, M. W. (2004) 'From placode to polarization: New tunes in inner ear development', *Development*, 131(17), pp. 4119–4130. doi: 10.1242/dev.01339.

Berger, G. *et al.* (1997) 'Patterns of hearing loss in non-explosive blast injury of the ear', *Journal of Laryngology and Otology*, 111(12), pp. 1137–1141. doi: 10.1017/S0022215100139544.

Bermingham, N. a *et al.* (1999) 'Math1: an essential gene for the generation of inner ear hair cells.', *Science (New York, N.Y.)*, 284(5421), pp. 1837–1841. doi: 10.1126/science.284.5421.1837.

Bernal, A. and Arranz, L. (2018) 'Nestin - expressing progenitor cells : function , identity and therapeutic implications', *Cellular and Molecular Life Sciences*, 75(12), pp. 2177–2195. doi: 10.1007/s00018-018-2794-z.

Bever, M. M. and Fekete, D. M. (2002) 'Atlas of the developing inner ear in zebrafish', *Developmental dynamics : an official publication of the American Association of Anatomists*, 223(4), pp. 536–543. doi: 10.1002/DVDY.10062.

Bianchi, M. G. *et al.* (2014) 'Changes in the expression of the glutamate transporter EAAT3/EAAC1 in health and disease', *Cellular and Molecular Life Sciences*, 71(11), pp. 2001–2015. doi: 10.1007/s00018-013-1484-0.

Bideau, L. *et al.* (2021) 'Animal regeneration in the era of transcriptomics', *Cellular and Molecular Life Sciences*, 78(8), pp. 3941–3956. doi: 10.1007/s00018-021-03760-7.

Biffo, S. *et al.* (1990) 'B-50/GAP43 Expression Correlates with Process Outgrowth in the Embryonic Mouse Nervous System', *European Journal of Neuroscience*, 2(6), pp. 487–499. doi: 10.1111/j.1460-9568.1990.tb00440.x.

Blaner, W. S. (1989) 'Retinol-binding protein: The serum transport protein for vitamin a', *Endocrine Reviews*, 10(3), pp. 308–316. doi: 10.1210/edrv-10-3-308.

Bölicke, N. (2021) 'Characterization of cell populations in the Zebrafish statoacoustic ganglion', *Lab rotation report "Model Organism"*

Bohne, B. a and Harding, G. W. (2000) 'Degeneration in the cochlea after noise damage: primary versus secondary events.', *The American journal of otology*, 21(4), pp. 505–509.

Bojrab, D. *et al.* (2017) 'Expression of Oligodendrocyte Marker during Peripheral-Central Transitional Zone Formation of the Postnatal Mouse Cochlear Nerve', *Otolaryngology - Head and Neck Surgery (United States)*, pp. 488–492. doi: 10.1177/0194599817718806.

Brand, M., Granato, M. and Nüsslein-Volhard, C. (2002) 'Keeping and raising zebrafish', *Zebrafish (2002)*.

Brandt, T. and DIeterich, M. (2017) 'The dizzy patient: Don't forget disorders of the central vestibular system', *Nature Reviews Neurology*, 13(6), pp. 352–362. doi: 10.1038/nrneurol.2017.58.

Breuss, M. *et al.* (2012) 'Mutations in the ß-Tubulin Gene TUBB5 Cause Microcephaly with Structural Brain Abnormalities', *Cell Reports*, 2(6), pp. 1554–1562. doi: 10.1016/j.celrep.2012.11.017.

Buffo, A. *et al.* (2008) 'Origin and progeny of reactive gliosis: A source of multipotent cells in the injured brain', *Proceedings of the National Academy of Sciences of the United States of America*, 105(9), pp. 3581–3586. doi: 10.1073/pnas.0709002105.

Burg, L. *et al.* (2018) 'Conditional mutagenesis by oligonucleotide-mediated integration of loxP sites in zebrafish', *PLoS Genetics*, 14(11), pp. 1–26. doi: 10.1371/journal.pgen.1007754.

Burns, J. C. and Corwin, J. T. (2013) 'A historical to present-day account of efforts to answer the question: "What puts the brakes on mammalian hair cell

regeneration?'", *Hearing Research*, 297, pp. 52–67. doi: 10.1016/j.heares.2013.01.005.

Campbell, K. R. and Yau, C. (2018) 'Uncovering pseudotemporal trajectories with covariates from single cell and bulk expression data', *Nature Communications*, 9(1). doi: 10.1038/s41467-018-04696-6.

Carricondo, F. and Romero-Gómez, B. (2019) 'The Cochlear Spiral Ganglion Neurons: The Auditory Portion of the VIII Nerve', *Anatomical Record*, 302(3), pp. 463–471. doi: 10.1002/ar.23815.

Celotto, L. (2022) 'Deciphering the transcriptional states of Müller glia and their progeny in the regenerating zebrafish retina'.

Chambon, P. (1996) 'A decade receptors biology of retinoic acid', *The FASEB Journal*, 10(9). doi: 10.1096/fasebj.10.9.8801176.

Chang, J. T., Lehtinen, M. K. and Sive, H. (2015) 'Zebrafish Cerebrospinal Fluid Mediates Cell Survival through a Retinoid Signaling Pathway', *Developmental Neurobiology*, 76(1), pp. 75–92.

Chang, S. Y. *et al.* (2021) 'Distribution and Afferent Effects of Transplanted mESCs on Cochlea in Acute and Chronic Neural Hearing Loss Models', *BioMed Research International*, 2021. doi: 10.1155/2021/4956404.

Chapouton, P. *et al.* (2006) 'Her5 Expression Reveals a Pool of Neural Stem Cells in the Adult Zebrafish Midbrain.', *Development (Cambridge, England)*, 133(21), pp. 4293–4303. doi: 10.1242/dev.02573.

Chapouton, P. *et al.* (2011) 'Expression of Hairy/enhancer of split genes in neural progenitors and neurogenesis domains of the adult zebrafish brain', *Journal of Comparative Neurology*, 519(9), pp. 1748–1769. doi: 10.1002/cne.22599.

Chatterjee, P. *et al.* (2015) 'Otoferlin Deficiency in Zebrafish Results in Defects in Balance and Hearing: Rescue of the Balance and Hearing Phenotype with Full-Length and Truncated Forms of Mouse Otoferlin', *Molecular and Cellular Biology*, 35(6), pp. 1043–1054. doi: 10.1128/mcb.01439-14.

Chen, G., Ning, B. and Shi, T. (2019) 'Single-cell RNA-seq technologies and related computational data analysis', *Frontiers in Genetics*, 10(APR), pp. 1–13. doi: 10.3389/fgene.2019.00317.

Chern, A. and Golub, J. S. (2019) 'Age-related Hearing Loss and Dementia', *Alzheimer Disease and Associated Disorders*, 33(3), pp. 285–290. doi: 10.1097/WAD.0000000000000325.

Chow, C. L. *et al.* (2015) 'Characterization of a unique cell population marked by transgene expression in the adult cochlea of nestin-CreERT2/tdTomato-reporter mice', *Journal of Comparative Neurology*, pp. 1474–1487. doi: 10.1002/cne.23747.

Chow, C. L. *et al.* (2016) 'Evaluation of Nestin Expression in the Developing and Adult Mouse Inner Ear', *Stem Cells and Development*, 25(19), pp. 1419–1432. doi: 10.1089/scd.2016.0176.

Claußen, M., Schulze, J. and Nothwang, H. G. (2020) 'Loss of inner hair cell ribbon synapses and auditory nerve fiber regression in Cldn14 knockout mice', *Hearing Research*, 391, p. 107950. doi: 10.1016/j.heares.2020.107950.

Clifford, R. E., Hertzano, R. and Ohlemiller, K. K. (2019) ' Untangling the genomics of noise-induced hearing loss and tinnitus: Contributions of Mus musculus and Homo sapiens ', *The Journal of the Acoustical Society of America*, 146(5), pp. 4007–4019. doi: 10.1121/1.5132552.

Coleman, B. *et al.* (2006) 'Fate of embryonic stem cells transplanted into the deafened mammalian cochlea', *Cell Transplantation*, 15(5), pp. 369–380. doi: 10.3727/000000006783981819.

Concas, M. P. *et al.* (2021) 'Hearing function: Identification of new candidate genes further explaining the complexity of this sensory ability', *Genes*, 12(8), pp. 1–15. doi: 10.3390/genes12081228.

Corwin, J. T. and Cotanche, D. A. (1988) 'Regeneration of Sensory Hair Cells After Acoustic Trauma', 240(December 1987), pp. 0–2.

Cox, J. A., Kucenas, S. and Voigt, M. M. (2005) 'Molecular characterization and embryonic expression of the family of N-methyl-D-aspartate receptor subunit genes in the zebrafish', *Developmental Dynamics*, 234(3), pp. 756–766. doi: 10.1002/dvdy.20532.

Cullen, K. E. (2019) 'Vestibular processing during natural self-motion: implications for perception and action', *Nature Reviews Neuroscience*, 20(6), pp. 346–363. doi: 10.1038/s41583-019-0153-1.

Curado, S. *et al.* (2007) 'Conditional targeted cell ablation in zebrafish: A new tool for regeneration studies', *Developmental Dynamics*, 236(4), pp. 1025–1035. doi: 10.1002/dvdy.21100.

Dahlstrand, J., Lardelli, M. and Lendahl, U. (1995) 'Nestin mRNA expression correlates with the central nervous system progenitor cell state in many, but not all, regions of developing central nervous system', *Developmental Brain Research*, 84(1), pp. 109–129. doi: 10.1016/0165-3806(94)00162-S.

Di, Q. *et al.* (2017) 'Zebrafish nephrosin helps host defence against Escherichia coli infection', *Open Biology*, 7(8). doi: 10.1098/rsob.170040.

Diensthuber, M. *et al.* (2014) 'Spiral ganglion stem cells can be propagated and differentiated into neurons and glia.', *BioResearch open access*, 3(3), pp. 88–97. doi: 10.1089/biores.2014.0016.

Dillard, L. K. *et al.* (2022) 'Prevalence and global estimates of unsafe listening practices in adolescents and young adults: a systematic review and meta-analysis', *BMJ Global Health*, 7(11), pp. 1–11. doi: 10.1136/bmjgh-2022-010501.

Doğanli, C. *et al.* (2013) 'α3Na+/K+-ATPase deficiency causes brain ventricle dilation and abrupt embryonic motility in zebrafish', *Journal of Biological Chemistry*, 288(13), pp. 8862–8874. doi: 10.1074/jbc.M112.421529.

Dohaku, R. *et al.* (2019) 'Tracing of afferent connections in the zebrafish cerebellum using recombinant rabies virus', *Frontiers in Neural Circuits*, 13(April), pp. 1–15. doi: 10.3389/fncir.2019.00030.

ELDREDGE, D. H., COVELL, W. P. and GANNON, R. P. (1959) 'Acoustic trauma following intermittent exposure to tones.', *Transactions of the American Otological Society*, 47(March), pp. 94–105.

Erickson, T. and Nicolson, T. (2015) 'Identification of sensory hair-cell transcripts by thiouracil-tagging in zebrafish', *BMC Genomics*, 16(1), pp. 1–10. doi: 10.1186/s12864-015-2072-5.

Ertürk, A. *et al.* (2007) 'Disorganized microtubules underlie the formation of retraction bulbs and the failure of axonal regeneration', *Journal of Neuroscience*, 27(34), pp. 9169–9180. doi: 10.1523/JNEUROSCI.0612-07.2007.

Escabi, C. D. *et al.* (2019) 'The rat animal model for noise-induced hearing loss', *The Journal of the Acoustical Society of America*, 146(5), pp. 3692–3709. doi: 10.1121/1.5132553.

Fay, R. R. and Popper, A. N. (2000) 'Evolution of hearing in vertebrates: The inner ears and processing', *Hearing Research*, 149(1–2), pp. 1–10. doi: 10.1016/S0378-5955(00)00168-4.

Fimbel, S. M. *et al.* (2007) 'Regeneration of inner retinal neurons after intravitreal injection of ouabain in zebrafish', *Journal of Neuroscience*, 27(7), pp. 1712–1724. doi: 10.1523/JNEUROSCI.5317-06.2007.

Fraher, J. P. (1999) 'The transitional zone and CNS regeneration', *Journal of Anatomy*, pp. 161–182. doi: 10.1017/S002187829800449X.

Fraher, J. P. and Delanty, F. J. (1987) 'The development of the central-peripheral transitional zone of the rat cochlear nerve. A light microscopic study', *J Anat*, 155, pp. 109–118.

Fraher, J. P., Smiddy, P. F. and O'Sullican, V. R. (1988) 'Central-Peripheral Transitional Regions of Cranial Nerves. Oculomotor nerve.', *Journal of Anatomy*, 161, pp. 103–113.

Frederikson, K. and McKay, R. D. G. (1988) 'Proliferation and differentiation of rat neuroepithelial precursor cells in vivo', *Journal of Neuroscience*, 8(4), pp. 1144–1151. doi: 10.1523/jneurosci.08-04-01144.1988.

Fritzsch, B. (2013) 'Development of inner ear afferent connections: forming primary neurons and connecting them to the developing sensory epithelia', 18(9), pp. 1199–1216. doi: 10.1016/j.micinf.2011.07.011.Innate.

Fritzsch, B. and Beisel, K. W. (2001) 'Evolution and development of the vertebrate ear', *Brain Research Bulletin*, 55(6), pp. 711–721. doi: 10.1016/S0361-9230(01)00558-5.

Fu, Y. *et al.* (2012) 'Ouabain-induced cochlear degeneration in rat', *Neurotoxicity Research*, 22(2), pp. 158–169. doi: 10.1007/s12640-012-9320-0.

Fuchs, Y. and Steller, H. (2016) 'Live to die another way: modes of programmed cell death and the signals emanating from dying cells', *Physiology & behavior*, 176(1), pp. 139–148. doi: 10.1038/nrm3999.Live.

Ganz, J. *et al.* (2010) 'Heterogeneity and Fgf dependence of adult neural progenitors in the zebrafish telencephalon', *Glia*, 58(May), pp. 1345–1363. doi: 10.1002/glia.21012.

Gemberling, M. *et al.* (2013) 'The zebrafish as a model for complex tissue regeneration', *Trends in Genetics*, 29(11), pp. 611–620. doi: 10.1016/j.tig.2013.07.003.

Ghosh, S. and Hui, S. P. (2018) 'Axonal regeneration in zebrafish spinal cord', *Regeneration*, 5(1), pp. 43–60. doi: 10.1002/reg2.99.

Gibaja, A. *et al.* (2022) 'Kanamycin and Cisplatin Ototoxicity: Differences in Patterns of Oxidative Stress, Antioxidant Enzyme Expression and Hair Cell Loss in the Cochlea', *Antioxidants*, 11(9). doi: 10.3390/antiox11091759.

Goman, A. M. and Lin, F. R. (2016) 'Prevalence of hearing loss by severity in the United States', *American Journal of Public Health*, 106(10), pp. 1820–1822. doi: 10.2105/AJPH.2016.303299.

Grandel, H. *et al.* (2006) 'Neural stem cells and neurogenesis in the adult zebrafish brain: Origin, proliferation dynamics, migration and cell fate', *Developmental Biology*, 295(1), pp. 263–277. doi: 10.1016/j.ydbio.2006.03.040.

Gresset, A. *et al.* (2015) 'Boundary Caps Give Rise to Neurogenic Stem Cells and Terminal Glia in the Skin', *Stem Cell Reports*, 5(2), pp. 278–290. doi: 10.1016/j.stemcr.2015.06.005.

Gudas, L. J. (1994) 'Retinoids and vertebrate development.', *Journal of Biological Chemistry*, 269(22), pp. 15399–15402. doi: 10.1016/S0021-9258(17)40689-2.

Haddon, C. and Lewis, J. (1996) 'Early ear development in the embryo of the zebrafish, Danio rerio', *Journal of Comparative Neurology*, 365, pp. 113–128. doi: 10.1002/(SICI)1096-9861(19960129)365:1<113::AID-CNE9>3.0.CO;2-6.

Hagey, D. W. *et al.* (2018) 'SOX2 regulates common and specific stem cell features in the CNS and endoderm derived organs', *PLoS Genetics*, 14(2), pp. 1–20. doi: 10.1371/journal.pgen.1007224.

Ham, T. J. *et al.* (2010) 'Live imaging of apoptotic cells in zebrafish', *The FASEB Journal*, 24(11), pp. 4336–4342. doi: 10.1096/fj.10-161018.

Han, C. and Someya, S. (2013) 'Mouse models of age-related mitochondrial neurosensory hearing loss', *Molecular and Cellular Neuroscience*, 55, pp. 95–100. doi: 10.1016/j.mcn.2012.07.004.

Han, Y. *et al.* (2011) 'Grhl2 deficiency impairs otic development and hearing ability in a zebrafish model of the progressive dominant hearing loss DFNA28', *Human Molecular Genetics*, 20(16), pp. 3213–3226. doi: 10.1093/hmg/ddr234.

Hans, S. *et al.* (2011) 'Generation of a non-leaky heat shock-inducible Cre line for conditional Cre/lox strategies in zebrafish', *Developmental Dynamics*, 240(1), pp. 108–115. doi: 10.1002/dvdy.22497.

Hans, S. *et al.* (2021) 'Cre-Controlled CRISPR mutagenesis provides fast and easy conditional gene inactivation in zebrafish', *Nature Communications*, 12(1), pp. 1–12. doi: 10.1038/s41467-021-21427-6.

Hans, S. and Campos-Ortega, J. a (2002) 'On the organisation of the regulatory region of the zebrafish deltaD gene.', *Development (Cambridge, England)*, 129, pp. 4773–4784.

Hatano, M. *et al.* (1997) 'Ncx, a Hox11 related gene, is expressed in a variety of tissues derived from neural crest cells', *Anatomy and Embryology*, 195(5), pp. 419–425. doi: 10.1007/s004290050061.

Hawkins, M. R. and Wingert, R. A. (2023) 'Zebrafish as a Model to Study Retinoic Acid Signaling in Development and Disease', *Biomedicines*, 11(4). doi: 10.3390/biomedicines11041180.

He, Z. *et al.* (2021) 'Stem Cell-Based Therapies in Hearing Loss', *Frontiers in Cell and Developmental Biology*. doi: 10.3389/fcell.2021.730042.

He, Z. and Jin, Y. (2016) 'Intrinsic Control of Axon Regeneration', *Neuron*, 90(3), pp. 437–451. doi: 10.1016/j.neuron.2016.04.022.

Herring, C. A. *et al.* (2018) 'Single-Cell Computational Strategies for Lineage Reconstruction in Tissue Systems', *Cmgh*, 5(4), pp. 539–548. doi: 10.1016/j.jcmgh.2018.01.023.

Higgs, D. M. *et al.* (2002) 'Age- and size-related changes in the inner ear and hearing ability of the adult zebrafish (Danio rerio)', *JARO - Journal of the Association for Research in Otolaryngology*, 3(2), pp. 174–184. doi: 10.1007/s101620020035.

Hjerling-Leffler, J. *et al.* (2005) 'The boundary cap: A source of neural crest stem cells that generate multipe sensory neuron subtypes', *Development*, 132(11), pp. 2623–2632. doi: 10.1242/dev.01852.

Hoshijima, K., Jurynec, M. J. and Grunwald, D. J. (2016) 'Precise Editing of the Zebrafish Genome Made Simple and Efficient', *Developmental Cell*, 36(6), pp. 654–667. doi: 10.1016/j.devcel.2016.02.015.

Hu, Z. *et al.* (2014) 'The Astroglial Reaction along the Mouse Cochlear Nerve following Inner Ear Damage', *Otolaryngology-Head and Neck Surgery*, 150(1), pp. 121–125. doi: 10.1177/0194599813512097.

Hu, Z. *et al.* (2021) 'Generation of a Spiral Ganglion Neuron Degeneration Mouse Model', *Frontiers in Cell and Developmental Biology*, 9(October), pp. 1–10. doi: 10.3389/fcell.2021.761847.

Huang, Y. *et al.* (2019) 'Ikzf1 regulates embryonic T lymphopoiesis via Ccr9 and Irf4 in zebrafish', *Journal of Biological Chemistry*, 294(44), pp. 16152–16163. doi: 10.1074/jbc.RA119.009883.

Hui, S. P. *et al.* (2017) 'Zebrafish Regulatory T Cells Mediate Organ-Specific Regenerative Programs', *Developmental Cell*, 43(6), pp. 659-672.e5. doi: 10.1016/j.devcel.2017.11.010.

Hwang, W. Y. *et al.* (2013) 'Efficient genome editing in zebrafish using a CRISPR-Cas system', *Nature Biotechnology*, 31(3), pp. 227–229. doi: 10.1038/nbt.2501.

Ito, Y. *et al.* (2010) 'Characterization of neural stem cells and their progeny in the adult zebrafish optic tectum', *Developmental Biology*, 342(1), pp. 26–38. doi: 10.1016/j.ydbio.2010.03.008.

Jahan, I. *et al.* (2015) 'The quest for restoring hearing: Understanding ear development more completely', *BioEssays*, p. n/a-n/a. doi: 10.1002/bies.201500044.

Jimenez, E. *et al.* (2021) 'Vestibular and Auditory Hair Cell Regeneration Following Targeted Ablation of Hair Cells With Diphtheria Toxin in Zebrafish', *Frontiers in Cellular Neuroscience*, 15.

Julier, Z. *et al.* (2017) 'Promoting tissue regeneration by modulating the immune system', *Acta Biomaterialia*, 53(June), pp. 13–28. doi: 10.1016/j.actbio.2017.01.056.

Kang, J. *et al.* (2016) 'Modulation of tissue repair by regeneration enhancer elements', *Nature*, 532(7598), pp. 201–206. doi: 10.1038/nature17644.

Kaslin, J. *et al.* (2009) 'Stem cells in the adult zebrafish cerebellum: initiation and maintenance of a novel stem cell niche.', *The Journal of neuroscience : the official journal of the Society for Neuroscience*, 29(19), pp. 6142–6153. doi: 10.1523/JNEUROSCI.0072-09.2009.

Kaslin, J. *et al.* (2017) 'Correction: Distinct roles of neuroepithelial-like and radial glia-like progenitor cells in cerebellar regeneration', *Development*, 144(18), pp. 3388–3388. doi: 10.1242/dev.158600.

Kenis, H. *et al.* (2005) 'Annexin A5 inhibits engulfment through internalization of PS-expressing cell membrane patches', *Experimental Cell Research*, 312(6), pp. 719–726. doi: 10.1016/j.yexcr.2005.11.023.

Kiernan, A. E. *et al.* (2005) 'Sox2 is required for sensory organ development in the mammalian inner ear.', *Nature*, 434(7036), pp. 1031–1035. doi: 10.1038/nature03487.

Kim, H. *et al.* (2018) 'Mouse Cre-LoxP system: general principles to determine tissue-specific roles of target genes', *Laboratory Animal Research*, 34(4), p. 147. doi: 10.5625/lar.2018.34.4.147.

Kim, W. Y. *et al.* (2001) 'NeuroD-null mice are deaf due to a severe loss of the inner ear sensory neurons during development', *Development*, 128(3), pp. 417–426. doi: 10.1242/DEV.128.3.417.

Kiser, P. D. and Palczewski, K. (2016) 'Retinoids and Retinal Diseases', *Annual review of vision science*, 2:197-234. doi: 10.1146/annurev-vision-111815-114407.

Kizil, C. *et al.* (2012) 'Regenerative Neurogenesis from Neural Progenitor Cells Requires Injury-Induced Expression of Gata3', *Developmental Cell*, 23(6), pp. 1230–1237. doi: 10.1016/j.devcel.2012.10.014.

Knopf, F. *et al.* (2011) 'Bone Regenerates via Dedifferentiation of Osteoblasts in the Zebrafish Fin', *Developmental Cell*, 20(5), pp. 713–724. doi: 10.1016/j.devcel.2011.04.014.

Kobak, D. and Berens, P. (2019) 'The art of using t-SNE for single-cell transcriptomics', *Nature Communications*, 10(1). doi: 10.1038/s41467-019-13056-x.

Korzh, V. *et al.* (1998) 'Expression of zebrafish bHLH genes ngn1 and nrd defines distinct stages of neural differentiation', *Developmental Dynamics*, 213(1), pp. 92–104. doi: 10.1002/(SICI)1097-0177(199809)213:1<92::AID-AJA9>3.0.CO;2-T.

Kozlowski, L. *et al.* (2017) 'Satisfaction of Elderly Hearing Aid Users', *International Archives of Otorhinolaryngology*, 21(1), pp. 92–96. doi: 10.1055/s-0036-1579744.

Kraemer, A. M., Saraiva, L. R. and Korsching, S. I. (2008) 'Structural and functional diversification in the teleost S100 family of calcium-binding proteins',

BMC Evolutionary Biology, 8(1), pp. 1–23. doi: 10.1186/1471-2148-8-48.

Kroehne, V. *et al.* (2011) 'Regeneration of the adult zebrafish brain from neurogenic radial glia-type progenitors', *Development*, 138, pp. 4831–4841. doi: 10.1242/dev.072587.

Kuan, S. W. *et al.* (2009) 'Identification of vasculature-specific genes by microarray analysis of Etsrp/Etv2 overexpressing zebrafish embryos', *Developmental Dynamics*, 238(7), pp. 1836–1850. doi: 10.1002/dvdy.21990.

Kujawa, S. G. and Liberman, M. C. (2006) 'Acceleration of age-related hearing loss by early noise exposure: Evidence of a misspent youth', *Journal of Neuroscience*, 26(7), pp. 2115–2123. doi: 10.1523/JNEUROSCI.4985-05.2006.

Kujawa, S. G. and Liberman, M. C. (2009) 'Adding insult to injury: Cochlear nerve degeneration after "temporary" noise-induced hearing loss', *Journal of Neuroscience*, 29(45), pp. 14077–14085. doi: 10.1523/JNEUROSCI.2845-09.2009.

Kunze, A. *et al.* (2009) 'Connexin expression by radial glia-like cells is required for neurogenesis in the adult dentate gyrus', *Proceedings of the National Academy of Sciences of the United States of America*, 106(27), pp. 11336–11341. doi: 10.1073/pnas.0813160106.

Kyle, M. E., Wang, J. C. and Shin, J. J. (2015) 'Impact of Nonaspirin Nonsteroidal Anti-inflammatory Agents and Acetaminophen on Sensorineural Hearing Loss: A Systematic Review', *Otolaryngology-Head and Neck Surgery*, 152(3), pp. 393–409. doi: 10.1177/0194599814564533.

Kyritsis, N. *et al.* (2012) 'Acute inflammation initiates the regenerative response in the adult zebrafish brain.', *Science (New York, N.Y.)*, 338(6112), pp. 1353–6. doi: 10.1126/science.1228773.

Lahne, M. *et al.* (2021) 'The Regenerating Adult Zebrafish Retina Recapitulates Developmental Fate Specification Programs', *Frontiers in Cell and Developmental Biology*, 8(February). doi: 10.3389/fcell.2020.617923.

Lam, E. Y. N. *et al.* (2009) 'Zebrafish runx1 promoter-EGFP transgenics mark discrete sites of definitive blood progenitors', *Blood*, 113(6), pp. 1241–1249. doi: 10.1182/blood-2008-04-149898.

Lang, H. *et al.* (2011) 'Sox2 up-regulation and glial cell proliferation following degeneration of spiral ganglion neurons in the adult mouse inner ear', *JARO - Journal of the Association for Research in Otolaryngology*, 12(2), pp. 151–171. doi: 10.1007/s10162-010-0244-1.

Lang, H., Schulte, B. A. and Schmiedt, R. A. (2005) 'Ouabain induces apoptotic cell death in type I spiral ganglion neurons, but not type II neurons', *JARO - Journal of the Association for Research in Otolaryngology*, 6(1), pp. 63–74. doi: 10.1007/s10162-004-5021-6.

Lange, C. *et al.* (2020) 'Single cell sequencing of radial glia progeny reveals the diversity of newborn neurons in the adult zebrafish brain', *Development (Cambridge)*, 147(1). doi: 10.1242/dev.185595.

Le, T. N. *et al.* (2017) 'Current insights in noise-induced hearing loss: a literature review of the underlying mechanism, pathophysiology, asymmetry, and

management options', *Journal of Otolaryngology - Head and Neck Surgery*, 46(1), pp. 1–15. doi: 10.1186/s40463-017-0219-x.

Leach, L. L. *et al.* (2021) 'The immune response is a critical regulator of zebrafish retinal pigment epithelium regeneration', *Proceedings of the National Academy of Sciences of the United States of America*, 118(21). doi: 10.1073/pnas.2017198118.

Leitner, M. G. (2014) 'Zebrafish in auditory research: Are fish better than mice?', *Journal of Physiology*, 592(21), pp. 4611–4612. doi: 10.1113/jphysiol.2014.280438.

Lendahl, U., Zimmerman, L. B. and McKay, R. D. G. (1990) 'CNS stem cells express a new class of intermediate filament protein', *Cell*, 60(4), pp. 585–595. doi: 10.1016/0092-8674(90)90662-X.

Lenkowski, J. R. and Raymond, P. A. (2014) 'Müller glia: Stem cells for generation and regeneration of retinal neurons in teleost fish', *Progress in Retinal and Eye Research*, 40(January), pp. 94–123. doi: 10.1016/j.preteyeres.2013.12.007.

Li, H. *et al.* (2003) 'Generation of hair cells by stepwise differentiation of embryonic stem cells.', *Proceedings of the National Academy of Sciences of the United States of America*, 100(23), pp. 13495–500. doi: 10.1073/pnas.2334503100.

Li, H., Liu, H. and Heller, S. (2003) 'Pluripotent stem cells from the adult mouse inner ear', *Nat Med*, 9(10), pp. 1293–1299. doi: 10.1038/nm925\rnm925 [pii].

Liang, J. *et al.* (2012) 'The stat3/socs3a pathway is a key regulator of hair cell regeneration in zebrafish stat3/socs3a pathway: Regulator of hair cell regeneration', *Journal of Neuroscience*, 32(31), pp. 10662–10673. doi: 10.1523/JNEUROSCI.5785-10.2012.

Lin, F. R. *et al.* (2013) 'Hearing loss and cognitive decline in older adults', *JAMA Internal Medicine*, 173(4), pp. 293–299. doi: 10.1001/jamainternmed.2013.1868.

Lin, M. J. and Lee, S. J. (2016) 'Stathmin-like 4 is critical for the maintenance of neural progenitor cells in dorsal midbrain of zebrafish larvae', *Scientific Reports*, 6(May), pp. 1–15. doi: 10.1038/srep36188.

Lin, X. *et al.* (2021) 'Experimental animal models of drug-induced sensorineural hearing loss: a narrative review', *Annals of Translational Medicine*, 9(17), pp. 1393–1393. doi: 10.21037/atm-21-2508.

Lindsten, T. *et al.* (2000) 'The Combined Functions of Proapoptotic Bcl-2 Family Members Bak and Bax Are Essential for Normal Development of Multiple Tissues cells within both the central nervous and hematopoi-etic systems. Thus, Bax and Bak have overlapping roles in the regulation o', *Molecular Cell*, 6, pp. 1389–1399.

Liu, D. *et al.* (2003) 'Fgf3 and Fgf8 dependent and independent transcription factors are required for otic placode specification.', *Development (Cambridge, England)*, 130(10), pp. 2213–2224. doi: 10.1242/dev.00445.

Livingston, G. *et al.* (2017) 'Dementia prevention, intervention, and care', *The Lancet*, 390(10113), pp. 2673–2734. doi: 10.1016/S0140-6736(17)31363-6.

Lopez, I. A. *et al.* (2004) 'Stem/progenitor cells in the postnatal inner ear of the GFP-nestin transgenic mouse', *International Journal of Developmental Neuroscience*, 22(4), pp. 205–213. doi: 10.1016/j.ijdevneu.2004.04.006.

Losner, J., Courtemanche, K. and Whited, J. L. (2021) 'A cross-species analysis of systemic mediators of repair and complex tissue regeneration', *npj Regenerative Medicine*, 6(1), pp. 1–11. doi: 10.1038/s41536-021-00130-6.

Lowery, L. A., Rubin, J. and Sive, H. (2007) 'Whitesnake/sfpq is required for cell survival and neuronal development in the zebrafish', *Developmental Dynamics*, 236(5), pp. 1347–1357. doi: 10.1002/dvdy.21132.

Lu, Z. and Desmidt, A. A. (2013) 'Early Development of Hearing in Zebrafish', *JARO: Journal of the Association for Research in Otolaryngology*, 14(4), p. 509. doi: 10.1007/S10162-013-0386-Z.

Lübke, L. *et al.* (2022) 'mdka Expression Is Associated with Quiescent Neural Stem Cells during Constitutive and Reactive Neurogenesis in the Adult Zebrafish Telencephalon', *Brain Sciences*, 12(2). doi: 10.3390/brainsci12020284.

Luecken, M. D. and Theis, F. J. (2019) 'Current best practices in single-cell RNA-seq analysis: a tutorial', *Molecular Systems Biology*, 15(6). doi: 10.15252/msb.20188746.

Lundberg, Y. W. *et al.* (2015) 'Mechanisms of otoconia and otolith development', *Developmental Dynamics*, 244(3), pp. 239–253. doi: 10.1002/dvdy.24195.

Luo, N. *et al.* (2016) 'Syndecan-4 modulates the proliferation of neural cells and the formation of CaP axons during zebrafish embryonic neurogenesis', *Scientific Reports*. doi: 10.1038/srep25300.

Lush, Mark E, Piotrowski, T. (2013) 'SENSORY HAIR CELL REGENERATION IN THE ZEBRAFISH LATERAL LINE', 18(9), pp. 1199–1216. doi: 10.1016/j.micinf.2011.07.011.Innate.

Ma, Q. *et al.* (1998) 'Neurogenin1 Is Essential for the Determination of Neuronal Precursors for Proximal Cranial Sensory Ganglia', *Neuron*, 20(3), pp. 469–482. doi: 10.1016/S0896-6273(00)80988-5.

Mackenzie, S. M. and Raible, D. W. (2012) 'Proliferative Regeneration of Zebrafish Lateral Line Hair Cells after Different Ototoxic Insults', *PLoS ONE*, 7(10), pp. 1–8. doi: 10.1371/journal.pone.0047257.

Maden, M. (2002) 'Retinoid signalling in the development of the central nervous system', *Nature Reviews Neuroscience*, 3(11), pp. 843–853. doi: 10.1038/nrn963.

Maden, M. (2018) 'The evolution of regeneration – Where does that leave mammals?', *International Journal of Developmental Biology*, 62(6–8), pp. 369–372. doi: 10.1387/ijdb.180031mm.

Mahler, J. and Driever, W. (2007) 'Expression of the zebrafish intermediate neurofilament Nestin in the developing nervous system and in neural proliferation zones at postembryonic stages', *BMC Developmental Biology*, 7, pp. 1–11. doi: 10.1186/1471-213X-7-89.

Mallo, M. (2001) 'Formation of the middle ear: Recent progress on the developmental and molecular mechanisms', *Developmental Biology*, 231(2), pp. 410–419. doi: 10.1006/dbio.2001.0154.

La Manno, G. *et al.* (2018) 'RNA velocity of single cells', *Nature*, 560(7719), pp. 494–498. doi: 10.1038/s41586-018-0414-6.

Maro, G. S. *et al.* (2004) 'Neural crest boundary cap cells constitute a source of neuronal and glial cells of the PNS', *Nature Neuroscience*, 7(9), pp. 930–938. doi: 10.1038/nn1299.

Marques, I. J., Lupi, E. and Mercader, N. (2019) 'Model systems for regeneration: Zebrafish', *Development (Cambridge)*, 146(18). doi: 10.1242/dev.167692.

Martinou, J. C. *et al.* (1994) 'Overexpression of BCL-2 in transgenic mice protects neurons from naturally occurring cell death and experimental ischemia', *Neuron*, 13(4), pp. 1017–1030. doi: 10.1016/0896-6273(94)90266-6.

Matsuda, K. *et al.* (1999) 'Increase in glutamate-aspartate transporter (GLAST) mRNA during kanamycin-induced cochlear insult in rats', *Hearing Research*, 133(1–2), pp. 10–16. doi: 10.1016/S0378-5955(99)00050-7.

Maxwell Cowan, W. *et al.* (1984) 'Regressive events in neurogenesis', *Science*, 225(4668), pp. 1258–1265. doi: 10.1126/science.6474175.

McInnes, L. *et al.* (2018) 'UMAP: Uniform Manifold Approximation and Projection', *Journal of Open Source Software*, 3(29), p. 861. doi: 10.21105/joss.00861.

Meas, S. J., Zhang, C.-L. and Dabdoub, A. (2018) 'Reprogramming Glia Into Neurons in the Peripheral Auditory System as a Solution for Sensorineural Hearing Loss: Lessons From the Central Nervous System', *Frontiers in Molecular Neuroscience*, 11(March), pp. 1–12. doi: 10.3389/fnmol.2018.00077.

Meas, S. J., Zhang, C. L. and Dabdoub, A. (2018) 'Reprogramming glia into neurons in the peripheral auditory system as a solution for sensorineural hearing loss: Lessons from the central nervous system', *Frontiers in Molecular Neuroscience*, 11(March), pp. 1–12. doi: 10.3389/fnmol.2018.00077.

Milon, B. *et al.* (2021) 'A cell-type-specific atlas of the inner ear transcriptional response to acoustic trauma', *Cell reports*, 36(13), p. 109758. doi: 10.1016/j.celrep.2021.109758.

Montgomery, J. E., Parsons, M. J. and Hyde, D. R. (2010) 'A novel model of retinal ablation demonstrates that the extent of rod cell death regulates the origin of the regenerated zebrafish rod photoreceptors', *Journal of Comparative Neurology*, 518(6), pp. 800–814. doi: 10.1002/cne.22243.

Morsch, M. *et al.* (2015) 'In vivo characterization of microglial engulfment of dying neurons in the zebrafish spinal cord', *Frontiers in Cellular Neuroscience*, 9(August), pp. 1–11. doi: 10.3389/fncel.2015.00321.

Münzel, E. J. *et al.* (2012) 'Claudin k is specifically expressed in cells that form myelin during development of the nervous system and regeneration of the optic nerve in adult zebrafish', *Glia*, 60(2), pp. 253–270. doi: 10.1002/glia.21260.

Murayama, E. *et al.* (2005) 'Otolith matrix proteins OMP-1 and Otolin-1 are

necessary for normal otolith growth and their correct anchoring onto the sensory maculae', *Mechanisms of Development*, 122(6), pp. 791–803. doi: 10.1016/j.mod.2005.03.002.

Nakagawa, S. and Takeichi, M. (1995) 'Neural crest cell-cell adhesion controlled by sequential and subpopulation-specific expression of novel cadherins', *Development*, 121(5), pp. 1321–1332. doi: 10.1242/dev.121.5.1321.

Nakaya, N., Sultana, A. and Tomarev, S. I. (2017) 'Impaired AMPA receptor trafficking by a double knockout of zebrafish olfactomedin1a/b', *Journal of Neurochemistry*, 143(6), pp. 635–644. doi: 10.1111/jnc.14231.

Nascimento, L. R. do *et al.* (2022) 'New Insights into the Identity of the DFNA58 Gene', *Genes*, 13(12). doi: 10.3390/genes13122274.

Nelson, C. M. *et al.* (2013) 'Tumor necrosis factor-alpha is produced by dying retinal neurons and is required for Müller glia proliferation during zebrafish retinal regeneration', *Journal of Neuroscience*, 33(15), pp. 6524–6539. doi: 10.1523/JNEUROSCI.3838-12.2013.

Niederländer, C. and Lumsden, A. (1996) 'Late emigrating neural crest cells migrate specifically to the exit points of cranial branchiomotor nerves', 2374, pp. 2367–2374.

Nishimura, K. *et al.* (2009) 'Transplantation of mouse induced pluripotent stem cells into the cochlea', *NeuroReport*, 20(14), pp. 1250–1254. doi: 10.1097/WNR.0b013e32832ff287.

Noda, T. *et al.* (2018) 'Direct Reprogramming of Spiral Ganglion Non-neuronal Cells into Neurons: Toward Ameliorating Sensorineural Hearing Loss by Gene Therapy', *Frontiers in Cell and Developmental Biology*, 6(February), pp. 1–14. doi: 10.3389/fcell.2018.00016.

Nouvian, R. *et al.* (2006) 'Structure and function of the hair cell ribbon synapse', *Journal of Membrane Biology*, 209(2–3), pp. 153–165. doi: 10.1007/s00232-005-0854-4.

Obholzer, N. *et al.* (2008) 'Vesicular Glutamate Transporter 3 Is Required for Synaptic Transmission in Zebrafish Hair Cells', *Journal of Neuroscience*, 28(9), pp. 2110–2118. doi: 10.1523/JNEUROSCI.5230-07.2008.

Oppenheim (1991) 'Cell death during development of the nervous system', *Annual Review of Neuroscience*, 14:453-501, pp. 453–501.

Oshima, K. *et al.* (2007) 'Differential distribution of stem cells in the auditory and vestibular organs of the inner ear', *JARO - Journal of the Association for Research in Otolaryngology*, 8(1), pp. 18–31. doi: 10.1007/s10162-006-0058-3.

Oyler, G. A. *et al.* (1989) 'The identification of a novel synaptosomal-associated protein, SNAP-25, differentially expressed by neuronal subpopulations', *Journal of Cell Biology*, 109(6 I), pp. 3039–3052. doi: 10.1083/jcb.109.6.3039.

Pan, H. *et al.* (2017) 'Auditory Neuropathy after Damage to Cochlear Spiral Ganglion Neurons in Mice Resulting from Conditional Expression of Diphtheria Toxin Receptors', *Scientific Reports*, 7(1), pp. 1–9. doi: 10.1038/s41598-017-06600-6.

Parés, X. *et al.* (2008) 'Medium- and short-chain dehydrogenase/reductase

gene and protein families: Medium-chain and short-chain dehydrogenases/reductases in retinoid metabolism', *Cellular and Molecular Life Sciences*, 65(24), pp. 3936–3949. doi: 10.1007/s00018-008-8591-3.

Park, H. C. *et al.* (2000) 'Analysis of upstream elements in the HuC promoter leads to the establishment of transgenic Zebrafish with fluorescent neurons', *Developmental Biology*, 227(2), pp. 279–293. doi: 10.1006/dbio.2000.9898.

Pavlinkova, G. (2021) 'Molecular aspects of the development and function of auditory neurons', *International Journal of Molecular Sciences*, 22(1), pp. 1–13. doi: 10.3390/ijms22010131.

Pearson, K. (1901) ' LIII. On lines and planes of closest fit to systems of points in space ', *The London, Edinburgh, and Dublin Philosophical Magazine and Journal of Science*, 2(11), pp. 559–572. doi: 10.1080/14786440109462720.

Petitpré, C. *et al.* (2018) 'Neuronal heterogeneity and stereotyped connectivity in the auditory afferent system', *Nature Communications*, 9(1). doi: 10.1038/s41467-018-06033-3.

Pinzon-Olejua, A. *et al.* (2017) 'Cre-inducible site-specific recombination in zebrafish oligodendrocytes', *Developmental Dynamics*, 246(1), pp. 41–49. doi: 10.1002/dvdy.24458.

Plass, M. *et al.* (2018) 'Cell type atlas and lineage tree of a whole complex animal by single-cell transcriptomics', *Science*, 360(6391). doi: 10.1126/science.aaq1723.

Popper, A. N. and Hoxter, B. (1984) 'Growth of a fish ear: 1. Quantitative analysis of hair cell and ganglion cell proliferation', *Hearing Research*, 15(2), pp. 133–142. doi: 10.1016/0378-5955(84)90044-3.

Puligilla, C. *et al.* (2010) 'Sox2 induces neuronal formation in the developing mammalian cochlea', *Journal of Neuroscience*, 30(2), pp. 714–722. doi: 10.1523/JNEUROSCI.3852-09.2010.

Qiu, X. and Müller, U. (2018) 'Mechanically gated ion channels in mammalian hair cells', *Frontiers in Cellular Neuroscience*, 12(April), pp. 1–10. doi: 10.3389/fncel.2018.00100.

Ramírez-Camacho, R. *et al.* (2006) 'Central role of supporting cells in cochlear homeostasis and pathology', *Medical Hypotheses*, 67(3), pp. 550–555. doi: 10.1016/j.mehy.2006.02.044.

Rask, L. *et al.* (1979) 'The primary structure of the human retinol-binding protein', 104(1), pp. 55–58.

Raymond, P. A. *et al.* (2006) 'Molecular characterization of retinal stem cells and their niches in adult zebrafish', *BMC Developmental Biology*, 6, pp. 1–17. doi: 10.1186/1471-213X-6-36.

Reimer, M. M. *et al.* (2008) 'Motor neuron regeneration in adult zebrafish', *Journal of Neuroscience*, 28(34), pp. 8510–8516. doi: 10.1523/JNEUROSCI.1189-08.2008.

Reyes, J. H. *et al.* (2008) 'Glutamatergic neuronal differentiation of mouse embryonic stem cells after transient expression of neurogenin 1 and treatment with

BDNF and GDNF: In vitro and in vivo studies', *Journal of Neuroscience*, 28(48), pp. 12622–12631. doi: 10.1523/JNEUROSCI.0563-08.2008.

Rougeot, J. *et al.* (2019) 'RNAseq profiling of leukocyte populations in zebrafish larvae reveals a cxcl11 chemokine gene as a marker of macrophage polarization during mycobacterial infection', *Frontiers in Immunology*, 10(MAR), pp. 1–17. doi: 10.3389/fimmu.2019.00832.

Royl, G. *et al.* (2010) 'Neurologische leitsymptome in einer notaufnahme', *Nervenarzt*, 81(10), pp. 1226–1230. doi: 10.1007/s00115-010-3020-x.

Rubbini, D. *et al.* (2015) 'Retinoic Acid Signaling Mediates Hair Cell Regeneration by Repressing p27kip and sox2 in Supporting Cells.', *The Journal of neuroscience : the official journal of the Society for Neuroscience*, 35(47), pp. 15752–66. doi: 10.1523/JNEUROSCI.1099-15.2015.

Rubel, E. W., Furrer, S. A. and Stone, J. S. (2013) 'A brief history of hair cell regeneration research and speculations on the future', *Hearing Research*, 297, pp. 42–51. doi: 10.1016/j.heares.2012.12.014.

Ryals, B. M. and Westbrook, E. W. (1990) 'Hair cell regeneration in senescent quail', *Hearing Research*, 50(1–2), pp. 87–96. doi: 10.1016/0378-5955(90)90035-N.

Rybak, L. P. *et al.* (2007) 'Mechanisms of cisplatin-induced ototoxicity and prevention', *Hearing Research*, 226(1–2), pp. 157–167. doi: 10.1016/j.heares.2006.09.015.

Santi, P. A. *et al.* (2009) 'Thin-sheet laser imaging microscopy for optical sectioning of thick tissues', *BioTechniques*, 46(4), pp. 287–294. doi: 10.2144/000113087.

Sapède, D. and Pujades, C. (2010a) 'Hedgehog signaling governs the development of otic sensory epithelium and its associated innervation in zebrafish.', *The Journal of neuroscience : the official journal of the Society for Neuroscience*, 30(10), pp. 3612–3623. doi: 10.1523/JNEUROSCI.5109-09.2010.

Sapède, D. and Pujades, C. (2010b) 'Hedgehog signaling governs the development of otic sensory epithelium and its associated innervation in zebrafish', *Journal of Neuroscience*, 30(10), pp. 3612–3623. doi: 10.1523/JNEUROSCI.5109-09.2010.

Schacht, J., Talaska, A. E. and Rybak, L. P. (2012) 'Cisplatin and Aminoglycoside Antibiotics: Hearing Loss and Its Prevention', *Anatomical Record*, 295(11), pp. 1837–1850. doi: 10.1002/ar.22578.

Scherer, D. (2021) 'Validation of single cell RNA sequencing data to identify different cell populations in the zebrafish statoacoustic ganglion', *Bachelor Thesis*

Schmiedt, R. A. *et al.* (2002) 'Ouabain application to the round window of the gerbil cochlea: A model of auditory neuropathy and apoptosis', *JARO - Journal of the Association for Research in Otolaryngology*, 3(3), pp. 223–233. doi: 10.1007/s101620020017.

Schriner, S. E. *et al.* (2005) 'Medecine: Extension of murine life span by overexpression of catalase targeted to mitochondria', *Science*, 308(5730), pp. 1909–1911. doi: 10.1126/science.1106653.

Schuck, Julie B, Smith, M. E. (2009) 'Cell proliferation follows acoustically-induced hair cell bundle loss in the zebrafish saccule', 42(2), pp. 157–162. doi: 10.1037/a0030561.Striving.

Schwander, M., Kachar, B. and Müller, U. (2010) 'The cell biology of hearing', *Journal of Cell Biology*, 190(1), pp. 9–20. doi: 10.1083/jcb.201001138.

Schwarzer, S. *et al.* (2020) 'Neurogenesis in the inner ear: The zebrafish statoacoustic ganglion provides new neurons from a Neurod/Nestin-positive progenitor pool well into adulthood', *Development (Cambridge)*, 147(7). doi: 10.1242/dev.176750.

Shen, Y. C. *et al.* (2012) 'The cytokine macrophage migration inhibitory factor (MIF) acts as a neurotrophin in the developing inner ear of the zebrafish, Danio rerio', *Developmental Biology*, 363(1), pp. 84–94. doi: 10.1016/j.ydbio.2011.12.023.

Sherpa, T. *et al.* (2007) 'Ganglion Cell Regeneration Following Whole-Retina Destruction in Zebrafish', pp. 166–181. doi: 10.1002/dneu.

Sherpa, T. *et al.* (2008) 'Ganglion Cell Regeneration Following Whole-Retina Destruction in Zebrafish', *Zebrafish*, 68(November 2007), pp. 166–181. doi: 10.1002/dneu.20568.Ganglion.

Shi, F. *et al.* (2007) 'BMP4 induction of sensory neurons from human embryonic stem cells and reinnervation of sensory epithelium', *European Journal of Neuroscience*, 26(11), pp. 3016–3023. doi: 10.1111/j.1460-9568.2007.05909.x.

Shi, F. and Edge, A. S. B. (2013) 'Prospects for replacement of auditory neurons by stem cells', *Hearing Research*, 297, pp. 106–112. doi: 10.1016/j.heares.2013.01.017.

Shin, J., Chen, J. and Solnica-Krezel, L. (2014) 'Efficient homologous recombination-mediated genome engineering in zebrafish using TALE nucleases', *Development (Cambridge, England)*, 141(19), pp. 3807–3818. doi: 10.1242/dev.108019.

Silva, N. J. *et al.* (2020) 'Inflammation and matrix metalloproteinase 9 (Mmp-9) regulate photoreceptor regeneration in adult zebrafish', *Glia*, 68(7), pp. 1445–1465. doi: 10.1002/glia.23792.

Slanchev, K. *et al.* (2009) 'The epithelial cell adhesion molecule EpCAM is required for epithelial morphogenesis and integrity during zebrafish epiboly and skin development', *PLoS Genetics*, 5(7). doi: 10.1371/journal.pgen.1000563.

Söllner, C. *et al.* (2003) 'Control of crystal size and lattice formation by starmaker in otolith biomineralization.', *Science (New York, N.Y.)*, 302(5643), pp. 282–286. doi: 10.1126/science.1088443.

Spoendlin, H. (1984) 'Factors inducing retrograde degeneration of the cochlear nerve . PubMed Commons', *Ann Otol Rhinol Laryngol Suppl. 1984 Jul-Aug;112:76-82.*, p. 6431887.

Steevens, A. R. *et al.* (2017) 'SOX2 is required for inner ear neurogenesis', *Scientific Reports*, 7(1), pp. 1–11. doi: 10.1038/s41598-017-04315-2.

Stoll, S. J., Bartsch, S. and Kroll, J. (2013) 'HOXC9 Regulates Formation of Parachordal Lymphangioplasts and the Thoracic Duct in Zebrafish via Stabilin 2',

PLoS ONE, 8(3). doi: 10.1371/journal.pone.0058311.

Stone, J. S. and Cotanche, D. A. (2007) 'Hair cell regeneration in the avian auditory epithelium', *International Journal of Developmental Biology*, 51(6–7), pp. 633–647. doi: 10.1387/ijdb.072408js.

Stone, J. S. and Rubel, E. W. (2000) 'Temporal , Spatial , and Morphologic Features of Hair Cell Regeneration in the Avian Basilar Papilla', 16(July 1999), pp. 1–16.

Sugawara, M., Corfas, G. and Liberman, M. C. (2005) 'Influence of supporting cells on neuronal degeneration after hair cell loss', *JARO - Journal of the Association for Research in Otolaryngology*, 6(2), pp. 136–147. doi: 10.1007/s10162-004-5050-1.

Suzuki, M., Ushio, M. and Yamasoba, T. (2008) 'Time course of apoptotic cell death in guinea pig cochlea following intratympanic gentamicin application', *Acta Oto-Laryngologica*, 128(7), pp. 724–731. doi: 10.1080/00016480701714244.

Tanoshima, R. *et al.* (2019) 'Analyses of Adverse Drug Reactions–Nationwide Active Surveillance Network: Canadian Pharmacogenomics Network for Drug Safety Database', *Journal of Clinical Pharmacology*, 59(3), pp. 356–363. doi: 10.1002/jcph.1336.

Thompson, T. L. and Amedee, R. (2009) 'Vertigo: A review of common peripheral and central vestibular disorders', *Ochsner Journal*, 9(1), pp. 20–26.

Toesca, A. (1996) 'Central and peripheral myelin in the rat cochlear and vestibular nerves', *Neuroscience Letters*, 221(1), pp. 21–24. doi: 10.1016/S0304-3940(96)13273-0.

Trapnell, C. *et al.* (2014) 'The dynamics and regulators of cell fate decisions are revealed by pseudotemporal ordering of single cells', *Nature Biotechnology*, pp. 381–386. doi: 10.1038/nbt.2859.

Trevarrow, B., Marks, D. L. and Kimmel, C. B. (1990) 'Organization of hindbrain segments in the zebrafish embryo', *Neuron*, 4(5), pp. 669–679. doi: 10.1016/0896-6273(90)90194-K.

Trevino, M. *et al.* (2019) 'The chinchilla animal model for hearing science and noise-induced hearing loss', *The Journal of the Acoustical Society of America*, 146(5), pp. 3710–3732. doi: 10.1121/1.5132950.

Tsarouchas, T. M. *et al.* (2018) 'Dynamic control of proinflammatory cytokines Il-1ß and Tnf-α by macrophages in zebrafish spinal cord regeneration', *Nature Communications*, 9(1). doi: 10.1038/s41467-018-07036-w.

Tsata, V. and Wehner, D. (2021) 'Know How to Regrow - Axon Regeneration in the Zebrafish Spinal Cord', *Cells*, 10(6):1404.

Usami, S. I. *et al.* (2003) 'Mutations in the COCH gene are a frequent cause of autosomal dominant progressive cochleo-vestibular dysfunction, but not of Meniere's disease', *European Journal of Human Genetics*, 11(10), pp. 744–748. doi: 10.1038/sj.ejhg.5201043.

Valente, R. C. *et al.* (2003) 'Mechanisms of ouabain toxicity', (1).

Varga, M. (2018) 'The doctor of delayed publications: The remarkable life of

George Streisinger (1927-1984)', *Zebrafish*, 15(3), pp. 314–319. doi: 10.1089/zeb.2017.1531.

Vemaraju, S. *et al.* (2012) 'A Spatial and Temporal Gradient of Fgf Differentially Regulates Distinct Stages of Neural Development in the Zebrafish Inner Ear', *PLoS Genetics*, 8(11). doi: 10.1371/journal.pgen.1003068.

Wakizono, T. *et al.* (2021) 'Growth factors with valproic acid restore injury-impaired hearing by promoting neuronal regeneration', *JCI Insight*, 6(22), pp. 1–12. doi: 10.1172/jci.insight.139171.

Wan, G., Corfas, G. and Stone, J. S. (2013) 'Inner ear supporting cells: Rethinking the silent majority', *Seminars in Cell and Developmental Biology*. doi: 10.1016/j.semcdb.2013.03.009.

Wang, J. *et al.* (2013) 'Myelination of the postnatal mouse cochlear nerve at the peripheral-central nervous system transitional zone', *Frontiers in Pediatrics*, 1(DEC), pp. 5–8. doi: 10.3389/fped.2013.00043.

Wang, J., Ding, D. and Salvi, R. J. (2003) 'Carboplatin-induced early cochlear lesion in chinchillas', *Hearing Research*, 181(1–2), pp. 65–72. doi: 10.1016/S0378-5955(03)00176-X.

Wang, X. *et al.* (2021) 'Direct Comparative Analyses of 10X Genomics Chromium and Smart-seq2', *Genomics, Proteomics and Bioinformatics*, 19(2), pp. 253–266. doi: 10.1016/j.gpb.2020.02.005.

Wang, Y. *et al.* (2015) 'Establishment of a model of cochlear lesions in rats to study potential gene therapy for sensorineural hearing loss', *International Journal of Pediatric Otorhinolaryngology*, 79(12), pp. 2147–2154. doi: 10.1016/j.ijporl.2015.09.037.

Watanabe, R. *et al.* (2012) 'Nestin-expressing cells in the developing, mature and noise-exposed cochlear epithelium', *Molecular and Cellular Neuroscience*, 49(2), pp. 104–109. doi: 10.1016/j.mcn.2011.11.001.

Waterman, R. E. and Bell, D. H. (1984) 'Epithelial fusion during early semicircular canal formation in the embryonic zebrafish, Brachydanio rerio', *The Anatomical Record*, 210(1), pp. 101–114. doi: 10.1002/AR.1092100113.

Wayne, R. V. and Johnsrude, I. S. (2015) 'A review of causal mechanisms underlying the link between age-related hearing loss and cognitive decline', *Ageing Research Reviews*, 23, pp. 154–166. doi: 10.1016/j.arr.2015.06.002.

Weber, A. *et al.* (2013) 'Characterization of light lesion paradigms and optical coherence tomography as tools to study adult retina regeneration in zebrafish', *PLoS ONE*, 8(11). doi: 10.1371/journal.pone.0080483.

Whitfield, T. T. (2002) 'Zebrafish as a model for hearing and deafness', *Journal of Neurobiology*, 53(2), pp. 157–171. doi: 10.1002/neu.10123.

Whitfield, T. T. (2015) 'ScienceDirect Development of the inner ear', *Current Opinion in Genetics & Development*, 32, pp. 112–118. doi: 10.1016/j.gde.2015.02.006.

Wiese, C. *et al.* (2004) 'Nestin expression - A property of multi-lineage progenitor cells?', *Cellular and Molecular Life Sciences*, 61(19–20), pp. 2510–2522. doi: 10.1007/s00018-004-4144-6.

Willenborg, S. *et al.* (2022) 'Isolation of macrophages from mouse skin wounds for single-cell RNA sequencing', *STAR Protocols*, 3(2), p. 101337. doi: 10.1016/j.xpro.2022.101337.

Willett, C. E. *et al.* (1997) 'Expression of zebrafish rag genes during early development identifies the thymus', *Developmental Biology*, 182(2), pp. 331–341. doi: 10.1006/dbio.1996.8446.

Wolf, F. A., Angerer, P. and Theis, F. J. (2018) 'Scanpy: large-scale single-cell gene expression data analysis', *Genome Biology*, 19:15. doi: 10.1111/1462-2920.13787.

Wright, T. (2015) 'Ear wax', *BMJ clinical evidence*, 2015(July 2014), pp. 1–24.

Wu, M. *et al.* (2021) 'Single-Cell Sequencing Applications in the Inner Ear', *Frontiers in Cell and Developmental Biology*, 9(February), pp. 1–12. doi: 10.3389/fcell.2021.637779.

Wu, S. *et al.* (2020) 'Two phenotypically and functionally distinct microglial populations in adult zebrafish', *Science Advances*, 6(47), pp. 21–25. doi: 10.1126/sciadv.abd1160.

Wu, T. D. and Nacu, S. (2010) 'Fast and SNP-tolerant detection of complex variants and splicing in short reads', *Bioinformatics*, 26(7), pp. 873–881. doi: 10.1093/bioinformatics/btq057.

Wu, Y. C. and Wang, I. J. (2020) 'Heat-shock-induced tyrosinase gene ablation with CRISPR in zebrafish', *Molecular Genetics and Genomics*, 295(4), pp. 911–922. doi: 10.1007/s00438-020-01681-x.

Xi, J., Yue, J. and Yang, Z. (2015) 'Expression profles of retinoic acid synthetases ALDH1As and metabolic enzymes CYP26s in adult and embryonic zebrafsh (Danio rerio)', *Genetics and Molecular Research*, 14(2), pp. 3948–3956. doi: 10.4238/2015.April.27.9.

Xiao, T. *et al.* (2005) 'A GFP-based genetic screen reveals mutations that disrupt the architecture of the zebrafish retinotectal projection', *Development*, 132(13), pp. 2955–2967. doi: 10.1242/dev.01861.

Yamamoto, R. *et al.* (2021) 'In silico analysis of inner ear development using public whole embryonic body single-cell RNA-sequencing data', *Developmental Biology*, 469(June 2020), pp. 160–171. doi: 10.1016/j.ydbio.2020.10.009.

Yeo, S. Y. *et al.* (2007) 'Fluorescent protein expression driven by her4 regulatory elements reveals the spatiotemporal pattern of Notch signaling in the nervous system of zebrafish embryos', *Developmental Biology*, 301(2), pp. 555–567. doi: 10.1016/j.ydbio.2006.10.020.

Yuan, Y. *et al.* (2014) 'Ouabain-induced cochlear nerve degeneration: Synaptic loss and plasticity in a mouse model of auditory neuropathy', *JARO - Journal of the Association for Research in Otolaryngology*, 15(1), pp. 31–43. doi: 10.1007/s10162-013-0419-7.

Zahnert, T. (2011) 'Differenzialdiagnose der schwerhörigkeit', *Deutsches Arzteblatt*, 108(25), pp. 433–444. doi: 10.3238/arztebl.2011.0433.

Zenner, H. P. *et al.* (1994) 'Transitory endolymph leakage induced hearing

loss and tinnitus: depolarization, biphasic shortening and loss of electromotility of outer hair cells', *European Archives of Oto-Rhino-Laryngology*, 251(3), pp. 143–153. doi: 10.1007/BF00181826.

Zilberstein, Y., Liberman, M. C. and Corfas, G. (2012) 'Inner Hair Cells Are Not Required for Survival of Spiral Ganglion Neurons in the Adult Cochlea', *Journal of Neuroscience*, 32(2), pp. 405–410. doi: 10.1523/JNEUROSCI.4678-11.2012.

Zujovic, V. *et al.* (2011) 'Boundary cap cells are peripheral nervous system stem cells that can be redirected into central nervous system lineages', *Proceedings of the National Academy of Sciences of the United States of America*, 108(26), pp. 10714–10719. doi: 10.1073/pnas.1018687108.

Acknowledgement

After a long, exciting and productive time my PhD is finally coming to an end and it is time to acknowledge all the people who helped and supported me throughout these years.

First and foremost, I would like to thank Stefan Hans for offering me this interesting and engaging project and for supporting me all the years even though I abandoned you twice to start and expand my own family. Thank you for creating a work environment with the perfect balance of supervision and independency. You were always open for discussions when I needed it but also allowed me to develop the project further on my own ideas. Despite having quite different working styles, I always felt that we were a great team and managed to achieve quite a bit in the end. Other students thank you for always having an open door for them – I am grateful that I even had the key to that door for years and will truly miss sharing the office with you (maybe even the "Do you know where Stefan is?" -part)…

I am extremely grateful to Michael Brand for hosting me in his lab all the years, providing me with great feedback and support as a supervisor and member of my thesis advisory committee. I always felt lucky to be a part of the Brand Lab. Furthermore, I would like to thank Marius Ader and Michell Reimer as the additional two members of my thesis advisory committee for their valuable in-put and suggestions especially in the first years of my PhD. I would like to express my gratitude to Cristina Pujades as the second reviewer of my thesis.

No PhD work would have been possible without the help, guidance, patience and support of wonderful technicians: Anja Machate, Michaela Geffarth, Sandra Spieß and Daniela Zöller, thank you for always helping out, organizing the lab and creating such a great working atmosphere.

Additionally, I thank all members of the CRTD and BIOTEC Fish Facility and especially Marika Fischer and Judith Konantz not only for all their effort and help in the fish room but also for all the nice chats.

Moreover, I am grateful to all members of the Histology Facility, Light Microscopy Facility (thank you Ruth Hans and Hella Hartmann for always being reachable over phone for "emergency" help), Flow Cytometry Facility of the CMCB, and the DRESDEN-concept Genome Center (I promise you, Fabian Rost, that I'll not ask for yet another color-modified UMAP!) for all their help, support and expertise.

In more than eight years the lab and also the 3rd floor saw a lot of people coming and leaving – I would like to thank all past and present members from the brand lab, especially Oliver Bludau, Anke Weber, Avinash Chekuru, Jan-Martin Pidun-Odelga for all the help in the lab and making the start of the PhD fun and easy.

I'll be there for you – when the rain starts to pour…

During all these years, I did not only met colleagues, I also met friends. Thank you, Karina, for being the first to welcome me in the lab, take me out to lunch breaks and showing me how the lab works. Many thanks go to Conny, Nicole and the whole campua-coffee gang for all the great coffee breaks in the CRTD backyard. And thank you, Laura, for all the fun and deep talks – lunch as usual, coffee afterwards, you pick me up?

I am so glad that I met you, Heidi, Jule, Vicky and Basti (and Ami & Jonah) during my time as a PhD. Thank you for all the great moments, coffee breaks, laughs and talks inside and outside the lab. Know that I am the only one left, it is definitely time for me to also move on…

A hearty c – c – c goes all the way to Greece. I have never been as excited in the lab like as I was the day in January, when I was staring out of the window, waiting for you to slowly walk all the way from the tram stop to the CRTD so that we could finally hug again after more than three years. Vania, we are THE best. You miss me, don't you?

I'll be there for you – like I've been there before…

A big thanks to all my friends inside and outside of Dresden. Christopher and Aleksandra, I'll never cooked more delicious food than at our epic cooking evenings. Thank you, Anja, Simon and Isabella, for all the outdoor trips, game evenings and family dates – we will so miss you! Thanks to the old Bachelor gang From Mainz, finally I also did it: I finished my PhD!

I'll be there for you – 'cause you're there for me too!

Last but not least I want to thank my closest friend and family. Nadine, if fortune wouldn't have had us team up in the second semester of the bachelor study, life would have been for sure a different one. No one gets me like you do and although we see each other in person for less than 100 hours per year, I know you are always there.

A big and hearty thank you to my parents, my brother and my grandma for all the love, support and encouragement in my life.

John, Kalotta and Frido – I know you had to do without me a lot lately, but now comes the time for an exciting new adventure for the four of us and I can not wait for it to start. I love you, my three Köllnerchens.

„…und, …hmm…DAS WAR'S!"

Erklärung entsprechend §5.5 der Promotionsordnung

Selbstständigkeitserklärung

Hiermit versichere ich, Simone Schwarzer, geboren am 03.10.1989 in Osterode am Harz, dass ich die vorliegende Arbeit ohne unzulässige Hilfe Dritter und ohne Benutzung anderer als der angegebenen Hilfsmittel angefertigt habe; die aus fremden Quellen direkt oder indirekt übernommenen Gedanken sind als solche kenntlich gemacht. Die Arbeit wurde bisher weder im Inland noch im Ausland in gleicher oder ähnlicher Form einer anderen Prüfungsbehörde vorgelegt.

Die Dissertation wurde von Prof. Dr. rer. nat. habil. Michael Brand, Professur für Molekulare Entwicklungsgenetik, Center for Molecular and Celullar Bioengineering (CMCB), DFG Forschungszentrum für Regenerative Therapien TU Dresden (CRTD), betreut und im Zeitraum von Februar 2015 bis Mai 2023 angefertigt.

Erklärung zur Anerkennung der Promotionsordnung

Ich erkläre hiermit, dass keine früheren erfolglosen Promotionsverfahren stattgefunden haben.

Ich erkläre hiermit, dass ich die Promotionsordnung der Technischen Universität Dresden, Bereich Mathematik und Naturwissenschaften von 23.02.2011 anerkenne.

Ort, Datum Unterschrift